THE UNIVERSITY
of EDINBURGH

This thesis has been submitted in fulfilment of the requirements for a postgraduate degree (e.g. PhD, MPhil, DClinPsychol) at the University of Edinburgh. Please note the following terms and conditions of use:

This work is protected by copyright and other intellectual property rights, which are retained by the thesis author, unless otherwise stated.
A copy can be downloaded for personal non-commercial research or study, without prior permission or charge.
This thesis cannot be reproduced or quoted extensively from without first obtaining permission in writing from the author.
The content must not be changed in any way or sold commercially in any format or medium without the formal permission of the author.
When referring to this work, full bibliographic details including the author, title, awarding institution and date of the thesis must be given.

Novel Applications of Positron Emission Tomography in the Non-invasive Assessment of Cardiovascular Disease

Dr. William Stephen Arthur Jenkins

BSc MBChB MRCP

A thesis presented for the degree of Doctor of Philosophy

University of Edinburgh

2017

To Sam, Mum, Dad, and Tiffer

Table of Contents

Index of Figures

Index of Tables

Declaration

This thesis represents research undertaken at the British Heart Foundation Centre for Cardiovascular Science, University of Edinburgh, and the Edinburgh Heart Centre. The studies described in this thesis were funded by the British Heart Foundation (SS/CH/09/002/2636, FS/12/84/29814, FS/10/026). I was personally involved in the formulation, conduct and data-analysis of the studies. In keeping with the continuous and collaborative nature of research, the initial patient recruitment and baseline assessments of the 'Ring of Fire' PET/CT study of aortic stenosis were performed by my supervisor and mentor, Dr. Marc Dweck (chapter 3 and 4), while the carotid artery specimens examined in chapter 6 were provided by Dr. Alex Vesey. Chapters 3, 4, 5 and 6, and portions of chapter 1, have been either published in peer-reviewed journals or are currently under review. The thesis has not been accepted in any previous applications for a degree, and all sources of information have been acknowledged. All studies were undertaken in accordance with the regulations of the regional Ethics Board within NHS Lothian and with the declaration of Helsinki of the World Medical Association.

WILLIAM STEPHEN ARTHUR JENKINS **1ST JULY 2017**

Acknowledgements

I would like to express my deepest gratitude to my supervisor and mentor Professor David Newby at the University of Edinburgh for his unerring and ongoing support and guidance. The entirety of this thesis would not have been possible without his insight, forethought and motivation. Through years of devotion to the expansion of medical research, he has shaped and continues to cultivate an infrastructure within which even the most inexperienced researchers can learn, collaborate, educate and ultimately flourish. Leading by example, he has been a source of inspiration for me and my peers, and there are very few seemingly-insurmountable problems that cannot be resolved by a 7.30am discussion with Dave.

I would also like to thank my secondary supervisor and mentor Dr. Marc Dweck. Despite his trajectory as a rising star in academia, he provided me with the daily support, clinical acumen, knowledge and inspiration that was required during my PhD program and beyond. He has become a close friend throughout this period, and continues to support me during my cardiology training. His creativity, tenacity and enthusiasm for research is infectious, and it has been a great honour to work with him.

I would like to acknowledge the British Heart Foundation for supporting the studies through research grants. Without their generosity, and the munificence of those that support it, this thesis and material would not have been possible. The staff in the Queens Medical Research Institute histology and tissue processing department, in particular Mike Miller and Lindsey Boswell, provided extensive assistance and

instruction on the acquisition and analysis of our histological specimens. The team of radiographers in the Clinical Research Imaging Centre were responsible for the acquisition of all PET/CT and MRI scans and I would like to acknowledge their contribution particularly. Similarly, I would like to acknowledge the help and support offered from others supporting my research and education, including Dr. James Rudd at the University of Cambridge, Dr. Maurice Sarano at Mayo Clinic, Minnesota, and Dr. Saeed Mirsadraee, Professor Edwin van Beek and staff members at the Clinical Research Facility at the University of Edinburgh.

I would like to extend a special thanks to my colleagues within 'the barn'. It was good fortune to have shared a working space with such a varied collection of clinical specialists, providing an environment in which debate, discussion, advice, help and collaboration were the norm. They provided a sanctuary of personal support, particularly Alex Vesey, without whom I could not have completed the research, but also , Anoop, Nik, Tim, Andrew, Colin and several others.

Finally, I would like to thank those closest to me for their invaluable support and guidance. My family and close friends shouldered numerous burdens supporting me thought this period, and I will be forever grateful for this. My parents are my primary inspiration for what one should seek to extract from life, and they continue to provide the bedrock upon which I build. Finally, I would like to thank my wife Samantha; a new chapter, and without doubt the most exciting one yet.

Abbreviations

18F-FDG	18F-fluorodeoxyglucose
18F-NaF	18F-Fluoride
AS	Aortic stenosis
AV	Aortic valve
AVC	Aortic valve calcification
AVR	Aortic valve replacement
CAVD	Calcific aortic valve disease
CT	Computed tomography
ECM	Extracellular matrix
LV	Left ventricle
LVOT	Left ventricular outflow tract
MI	Myocardial infarction
MRI	Magnetic Resonance Imaging
PET	Positron emission tomography
ROI	Region of interest
SMA	Smooth muscle actin
SMC	Smooth muscle cells
SPECT	Single-photon emission computed tomography
SUV	Standardised uptake valve
SVC	Superior vena cava
TAC	Time/activity curve

Abstract

Introduction.

Fused Positron Emission Tomography and Computed Tomography (PET/CT) is an emerging investigative tool in cardiovascular disease that provides an imaging-based quantification of pathophysiological processes of interest. The purpose of this thesis was to study the application of PET to identify fundamental pathophysiological processes driving 3 forms of cardiovascular disease: aortic stenosis, myocardial infarction, and atherosclerosis.

Methods.

Aortic Stenosis. Patients with a spectrum of calcific aortic valve disease (n=121) who underwent PET-CT imaging for the identification of valvular calcification (18F-fluoride) and inflammation (18F-fluorodeoxyglucose, 18F-FDG) underwent serial imaging and clinical follow-up over 2 years. Baseline imaging findings were compared with echocardiographic and CT markers of disease progression and clinical outcome.

Myocardial Infarction. Patients underwent PET-CT imaging with 18F-fluciclatide (a novel αvβ3-selective radiotracer highlighting active angiogenesis, inflammation and fibrosis) after ST-segment elevation MI (n=21), alongside stable patients with chronic total occlusion (CTO) of a major coronary vessel (n=7), and healthy volunteers (n=9). Myocardial radiotracer uptake was compared with clinical and cardiac magnetic resonance imaging (CMR) markers of infarction and remodeling.

Atherosclerosis. Patients with a spectrum of atherosclerotic disease categorized as stable or unstable (recent MI) underwent PET/CT imaging with 18F-fluciclatide (n=46). Thoracic aortic 18F-fluciclatide uptake was compared with aortic atherosclerotic burden quantified by CT plaque thickness, plaque volume and calcium scoring.

Histological validation. Tissue from the aortic valve, myocardium and carotid arteries of study subjects was acquired and examined *ex vivo* using histology and autoradiography.

Results.

Aortic Stenosis. Baseline valvular 18F-fluoride uptake correlated strongly with the rate of progression in AVC ($r=0.80$, $p<0.001$) and with haemodynamic progression (mean aortic valve gradient $r=0.32$, $p=0.001$). It emerged as independently associated with clinical outcome after age and sex-adjustment (HR 1.55 [1.33-1.81], $p<0.001$). 18F-FDG demonstrated moderate correlations with disease progression as assessed by CT ($r=0.43$, $p=0.001$) and echocardiography (18F-FDG $r=0.30$, $p=0.001$), and was associated with clinical outcomes independent of age and sex (HR 1.35 [1.16-1.58], $p<0.001$). Valvular 18F-fluoride uptake correlated with immunohistochemical markers of calcification activity. There was no correlation between 18F-FDG uptake and inflammation.

Myocardial Infarction. 18F-Fluciclatide binding was demonstrated in *ex vivo* peri-infarct myocardium and uptake was increased *in vivo* at sites of acute infarction

compared to remote myocardium (tissue-to-background ratio (TBRmean) 1.34±0.22 vs 0.85±0.17 respectively, p<0.001) and myocardium of healthy volunteers (TBRmean 1.34±0.22 vs 0.70±0.03; p<0.001). There was no 18F-fluciclatide uptake at sites of established prior infarction in patients with CTO, with myocardial activity similar to healthy volunteers (TBRmean 0.71±0.06 vs. 0.70±0.03,p=0.83). 18F-Fluciclatide uptake occurred at sites of regional wall hypokinesia (wall motion index ≥1 vs 0; TBRmean 0.93±0.31 vs 0.80±0.26 respectively, p<0.001), was increased in segments displaying functional recovery (TBRmean 0.95±0.33 vs 0.81±0.27, p=0.002) and associated with increase in probability of regional recovery.

Atherosclerosis. 18F-Fluciclatide vascular binding *ex vivo* co-localised with regions of increased $\alpha_v\beta_3$ integrin expression, and markers of inflammation and angiogenesis. 18F-Fluciclatide uptake *in vivo* correlated with measures of aortic atherosclerotic burden: plaque thickness (r=0.57, p=0.001), total plaque volume (r=0.56, p=0.001) and the CT aortic calcium score (r=0.37, p=0.01). Patients with recent MI had greater aortic 18F-fluciclatide uptake than those with stable disease (TBR_{max} 1.33 vs 1.21, p=0.01).

Conclusions.

In a range of cardiovascular diseases, PET-CT can provide insights into key pathophysiological processes, guide patient risk stratification and prognosis, and identify important biomarkers of disease activity that can be used for the development of future therapeutic interventions.

Lay Summary

Positron emission tomography (PET) is a nuclear medicine medical scanning technology that produces a 3-D image of disease processes occurring within the body. The technique enables us to measure the activity of these processes, identifying potentially important disease changes earlier than they might be seen on more common imaging techniques such as computed tomography (CT), and at a stage where treatment may be targeted more effectively. Within this thesis we explore new techniques for combined PET/CT imaging in cardiovascular disease.

Firstly, we have used PET/CT imaging to assess a common heart valve condition called 'aortic stenosis'. The aortic valve allows blood to exit the heart, and through a process involving inflammation and progressive calcium formation (calcification), the valve may become narrowed and cause an obstruction to blood flow. We used PET/CT imaging to successfully identify inflammation and calcification as it occurs within the heart valve. Over time, we determined that patients with more inflammation and calcification activity visible in their aortic valve on PET scanning were more likely to require an operation to replace the valve, or to die. This technique therefore may enable us to identify patients at greater risk, potentially offering us a way to direct treatment towards high-risk individuals and monitor the effectiveness of their treatment.

Secondly, we have used a new type of PET/CT imaging to assess the repair mechanisms that occur within the heart muscle after a heart attack. The healing processes following a heart attack are complex, and in some patients over time there

may be a deterioration in heart structure and function rather than an improvement. These patients are at risk of developing 'heart failure' and would benefit from more intensive medication and monitoring. Using PET scanning to identify the formation of microscopic blood vessels and scar tissue within the heart, we have developed a technique where we can visualise heart muscle repair activity as it occurs. Furthermore, the areas of heart muscle damage that displayed higher activity on their PET scan demonstrated greater functional improvement. This technology potentially provides a means of identifying those patients who may be at risk of 'dysfunctional' repair processes and 'heart failure'.

Finally, we have demonstrated that this method of visualising the formation of new microscopic blood vessels using PET scanning may also be used to highlight areas of narrowing within the blood vessels that are a sign of heart disease, potentially allowing us to identify those patients who may be at an increased risk of a heart attack or stroke.

In summary, these novel uses of PET imaging provide a way to recognise forms of early heart disease, potentially providing a way to treat and monitor heart disease in a manner that is tailored to the individual patient. However, further work is now required prior to its routine use in the hospital setting.

Chapter 1.

Positron Emission Tomography: Novel approaches in cardiovascular imaging

Excerpts from this chapter have been published in the review article by Jenkins WS, Chin C, Rudd JH, Newby DE and Dweck MR. What can we learn about valvular heart disease from PET/CT? *Future Cardiol.* 2013 Sep;9(5):657-67.

1.1. Overview

Cardiovascular disease represents the primary cause of morbidity and mortality worldwide.(1) With an aging population, this burden of disease is set to increase. To address this, we require a thorough understanding of cardiovascular disease physiology, isolating relevant pathological processes, understanding their relevance in cardiovascular physiology, and determining the consequence of modifying those processes *in vivo*.

It is increasingly appreciated that despite diversity in the clinical presentations of cardiovascular disease, there exists significant overlap in the pathophysiological mechanisms that initiate and propagate these disease states, with implications on clinical investigation and therapeutic targets. Aortic Stenosis, atherosclerosis and adverse myocardial remodeling are 3 cardiovascular diseases accountable for a significant proportion of cardiovascular disease burden. Phenotypically, each disease differs in its clinical presentation; historically this has ensured distinct management considerations. However, there are several key pathophysiological processes that are relevant within each condition to varying degrees, including calcification, inflammation, fibrosis and angiogenesis.

Here, we assess the application of novel non-invasive imaging methods to quantify these processes. Specifically we have employed Computed Tomography (CT) and combined Positron Emission Tomography - Computed Tomography (PET-CT) in aortic stenosis, adverse myocardial remodeling and atherosclerosis. Combined

PET/CT is a novel non-invasive imaging technique that allows the identification and quantification of specific physiological and pathophysiological processes occurring within the body, with a spatial resolution of between 4 and 6 mm. Its clinical use in cardiovascular disease has previously been limited to myocardial perfusion imaging, but with an appropriate radiotracer in theory the activity of any pathological process can be studied, and PET/CT has provided novel pathological insights into atherosclerosis, myocardial infarction and valvular heart disease.(2-6)

The purpose of this thesis was to examine the utility of novel PET radiotracers in assessing common pathophysiological processes that drive aortic stenosis, adverse myocardial remodeling and atherosclerosis, gaining unique insight into these disease states with potential diagnostic and prognostic implications.

1.2 Positron Emission Tomography

1.2.1. The Physics of Positron Emission Tomography

Positron emission tomography (PET) is a non-invasive imaging technique that permits the identification and quantitation of active biochemical processes as they occur within the body. The positron is the anti-particle of the electron and is released by unstable positron-emitting nuclei, such as 18F-fluoride, 15O-oxygen or 11C-carbon, following radioactive decay of a proton to a neutron (beta decay).(7) The positron travels a short distance (millimeters) before colliding with an electron. This collision results in annihilation of both particles and the release of two photons that travel at almost 180º degrees to one another with a fixed energy of 511 keV (Figure 1.1).

These fixed diverging photons provide the foundation of PET imaging, and may be detected using a ring of photon detectors that surround the patient. On the basis that two 511 keV photons detected in close temporal proximity by two opposing detectors are likely to have originated from an event somewhere along a straight line of response between them (the *line of coincidence*), a 3-dimensional (3D) PET image may be reconstructed using a summation of the detection events over a fixed period of scanning, and the computation of origins to these collisions (Figure 1.1).(7)

PET tracers consist of a positron emitter combined to a molecular vehicle designed to interrogate a specific pathophysiological process of interest. 18F-Fluoride is the most commonly used positron emitter, as its relatively long half-life permits commercial

production and distribution. These tracers are injected into the patient and accumulate in areas where activity of that process is increased. The PET scanner detects the emitted radiation and constructs a map of tracer uptake. Given the short distance travelled by the positron before annihilation, PET images tend to lack spatial resolution compared to CT or MR datasets**.** Therefore, PET imaging is often performed using a combined scanner, incorporating both PET and CT within the same gantry. Patients lie in the same position for both scans, which allows the PET and CT scans to be superimposed upon one another. This serves two purposes. First, the CT can be used to perform accurate attenuation correction of PET data. As photons emerge from the body their path is slowed or indeed blocked by the surrounding tissue, which will distort the activity detected by the scanner and the resultant image. Information from CT can be used to measure the relative densities of the tissues in the body and correct for this effect, providing a more accurate, map of tracer accumulation. Second, co-registration of the PET and CT images allows the more precise localisation of tracer uptake within the body.(8) Radiation exposure is increased on account of performing both scans but remains modest, amounting to around 5 millisieverts using conventional tracers.

Figure 1.1. The physics of positron emission tomography

A diagram summarising the detection of diverging photons that are created following the collision and annihiliation of a positron and a nearby electron. Applying the assumption that detected protons will have originated at some point along the line of coincidence, an image is derived over the period of scanning to provide a 3-dimensional topographic map of the emission of positrons, and hence the accumulation of radiotracer.

.

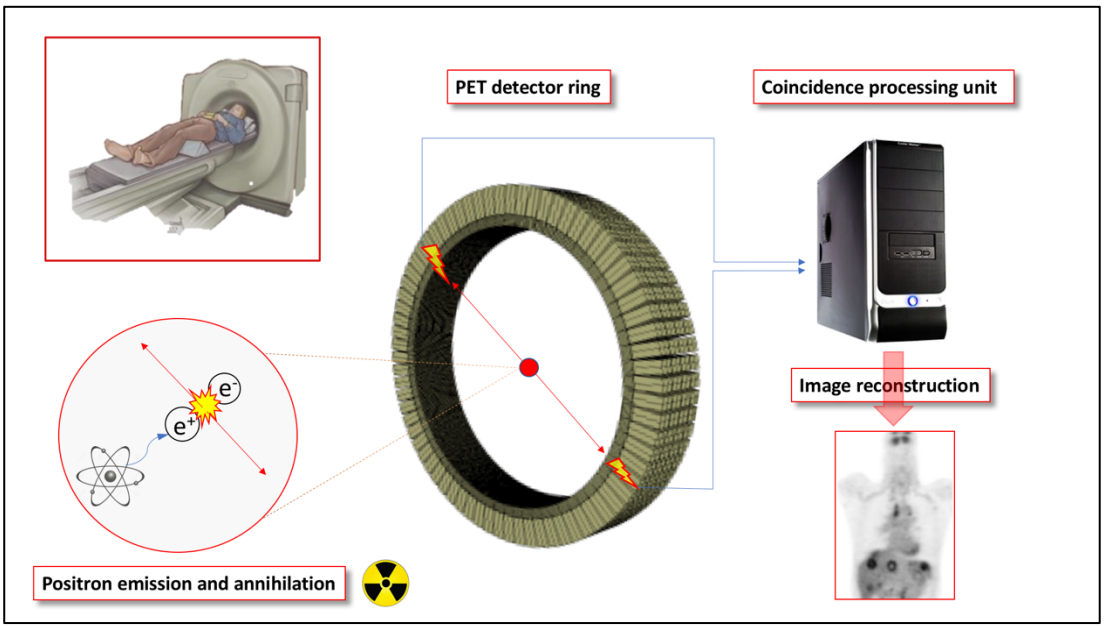

1.2.2. PET Image analysis

Quantification of PET activity is most commonly performed using the fused 3D image dataset by placing regions of interest around the anatomical structure in question and measuring the concentration of radiotracer that has accumulated within that tissue of interest using the calculated mean or maximum standardized uptake values (SUVs). The SUV is the decay-corrected tissue concentration of a tracer divided by the injected dose per body weight; each image voxel (a 3D pixel) represents an SUV value that is derived during image reconstruction.

These aggregate values may be further corrected for residual blood pool activity by expressing the activity as a ratio between activity within a vascular lumen (the superior vena cava, right atrium or left ventricle) and the tissue of interest: the tissue-to-background ratio (TBR). Cardiovascular PET imaging may be hampered by both cardiorespiratory motion and the significant proximity to the blood pool. These factors amount to potential sources of error when quantifying the radiotracer signal within a cardiovascular tissue of interest, making the use of TBR quantification preferential over SUV values alone.

Alternative methods for quantifying PET activity utilise a dynamic imaging approach. In this form, PET acquisition is started at the point of intravenous radiotracer administration and the PET data continuously acquired over a period of 30-90 minutes. The PET dataset may then be reconstructed to combine multiple 3D PET images of a shorter duration, forming a single dataset with sequential SUV values encompassing

the entire period of scanning. This allows the calculation of a time/activity curve (TAC) for each image voxel, enabling assessment of the tissue kinetics of the radiotracer; specifically, the *rate* of radiotracer uptake within each tissue, radiotracer half-life and rate of excretion, and the method by which the radiotracer interacts with the molecular process of interest. This may establish whether the radiotracer is reversibly or irreversibly incorporated into the tissue of interest, and therefore whether a quantification of cumulative SUV values are appropriate.(9-11)

PET/CT imaging of the heart presents some unique challenges, most notably those related to cardiac motion. Whilst the heart is more stationary in diastole, significant motion occurs during the course of the cardiac cycle, which if uncorrected can lead to imperfect signal localization. However, the PET signal can be configured to the electrocardiogram so that only counts arising from diastole, when the heart is relatively stationary, are used for image reconstruction. This 'gating' can greatly refine the resolution of a cardiac PET signal, and can be extended to account for motion that accompanies respiration, which can further improve the accuracy of signal localization.(12,13)

1.3. Pathophysiology of Aortic Stenosis: targets for molecular imaging

1.3.1. Prevalence and mechanisms of aortic stenosis

Calcific aortic stenosis represents a major cause of morbidity and mortality in the western world. A recent population-based survey noted the prevalence of valve disease to be 2.5% in the adult population: a figure that is set to increase with a progressively aging population.(14) Despite this underappreciated and mounting health burden, we lack medical therapies and accurate means of predicting disease progression. In part this reflects our relatively poor understanding of the pathological processes underlying these conditions, and increasingly investigators are turning to new imaging techniques, to improve this knowledge and to identify novel targets for pharmacological intervention.

Macroscopically, calcific aortic valve disease develops as early focal leaflet thickening and/or calcification without haemodynamic consequence. This 'aortic sclerosis' does not invoke a transvalvular pressure gradient. Over time valvular thickening and calcification causes reduction in the functional aortic valve area resulting in impedance to outflow and a significant transvalvular pressure gradient between the left ventricle and the aorta.(15) This may be quantified as mild, moderate and severe in severity depending on the degree of haemodynamic obstruction. The left ventricle initially adapts to this increase in pressure afterload with a cardiomyocyte hypertrophic

response. Ultimately however, the degree of haemodynamic obstruction will result in ventricular decompensation and reduction in cardiac output, characterized by the evolution of heart failure, myocardial ischaemia or arrhythmia.(16)

On a cellular level, there are four main active pathological processes that precipitate and propagate calcific thickening of the aortic valve; Inflammation, Calcification, Fibrosis and Angiogenesis.(17,18) Each will be discussed in due course.

1.3.2 Valvular Inflammation

The initial development and the progression of calcific aortic stenosis shares many similarities with the active atheroinflammatory processes seen in atherosclerosis. Histological evaluation of early valve lesions show subendothelial thickening on the aortic side of the leaflets with overlying disruption of the basement membrane and accumulation of lipid, protein, extracellular mineralization and cellular infiltration of macrophages, lipid-laden foam cells and T-lymphocytes.(19) This is in contrast to the standard presence of scattered macrophages and mast cells, but no T-lymphocytes, found in normal aortic valves.(20)

As with atherosclerosis, these early aortic valve lesions comprising of lipid-laden foam cells accumulate at sites of low shear stress and high mechanical stress (19,21). A combination of endothelial damage and lipoprotein accumulation likely triggers an inflammatory process within the valve. The low density lipoprotein (LDL) and lipoprotein(a) found within sclerotic valve leaflets are those also implicated in atherogenesis (22) and undergo oxidative modification. These oxidized lipoproteins are highly cytotoxic and proinflammatory, influencing the influx of macrophages and expression of adhesion molecules such as intercellular adhesion molecule-1 (ICAM-1) and vascular cell adhesion molecule-1 (VCAM-1), complement receptors C3a and C5a, transforming growth factor-β1 (TGF- β1) and interleukin-1β. (23)

Systemic increases of C-reactive protein concentrations in patients with aortic stenosis, (24) and an increase in temperature in stenotic aortic valve cusps (25)

reinforce the concept of a significant inflammatory component to CAVD pathophysiology. However as yet the benefit of anti-inflammatory lipid-lowering therapy in aortic stenosis remains unproven.(26,27)

1.3.3. Valvular Fibrosis

Stenotic aortic valve leaflets exhibit extensive remodeling of the extracellular matrix, manifested macroscopically as widespread leaflet thickening. Microscopically this fibrotic process is driven by fibroblast-like cells, or valve interstitial cells. These differentiate into myofibroblasts under the influence of the proinflammatory and profibrotic cytokines, integrin expression, TGF- β1 and angiotensin. These cells secrete α-smooth muscle actin (α –SMA) and type I collagen fibres, the production of which is increased in aortic stenosis leaflets.(28) They are also responsible for the imbalance of matrix metalloproteinases (MMP's) and tissue-inhibitors of metalloproteinases (TIMP's) that drives extracellular matrix remodeling.(29)

1.3.4. Valvular Angiogenesis

Upregulation of intraleaflet angiogenesis maintains the inflammatory environment within stenotic valve leaflets. While phenotypically normal valve tissue is avascular, thickened valves are characterised histologically by abundant T-lymphocytes and evolving microvasculature, found in the highest density around cell nodules and in calcifying areas.(30,31) The origin of these immature blood vessels is thought to be the valvular endothelial cells, proven capable of forming capillary-like sprouts and undergoing a partial transdifferentiation into vascular endothelium *ex vivo*.(32)

Expression of angiogenesis-promoting factors such as integrin receptor $\alpha_v\beta_3$, Vascular Endothelial Growth Factor (VEGF), its receptors Flk-1 and Flt-1, intercellular adhesion molecule-1 (ICAM-1) and vascular cell adhesion molecule-1 (VCAM-1) are increased in neovasculature in animal and human models,(30,33) stimulated by decreased oxygen tension and allowing inflammatory cell entry. This friable leafet neovasculature is prone to rupture and subsequent haemorrhage, itself a potentially pathological mechanism associated with increased macrophage infiltration and more rapid rates of disease progression.(34)

1.3.5. Valvular Calcification

The extent of aortic valvular calcification (AVC) burden on CT imaging is closely associated with the degree of haemodynamic severity,(35,36), and as a consequence may offer significant prognostic utility in the clinical assessment of aortic stenosis progression and outcome.(37-39) Progressive valvular calcification predominates the later stages of aortic stenosis and is largely responsible for its haemodynamic progression. In early sclerotic valve lesions microscopic areas of calcification exist as nodules containing hydroxyapatite, adherent to the extracellular matrix and co-localising to sites of lipid deposition and inflammatory cell infiltration. Indeed, it is likely that valvular calcification occurs as a dysfunctional healing response to endothelial injury and oxidative stress.(18) In approximately $1/6^{th}$ of patients with aortic sclerosis, progressive leaflet calcification propagates, and ultimately the valve mineralization shows increasing histological similarities to lamellar bone, with features of active bone remodeling (osteoblastic bone formation and osteoclastic bone resorption), microfractures and haematopoetic tissue.(40,41) The process is driven by osteoblasts, which differentiate from myofibroblasts and endothelial cells under the influence of the Runx2 pathway,(42) the osteoprotegerin (OPG)/Receptor Activator of Nuclear factor Kappa B (RANK)/RANK ligand (RANKL) pathway and increased levels of TNF-α.(43,44) Numerous studies have also demonstrated the presence of osteogenic markers and osteoblast-specific proteins in calcified aortic valves. These include osteocalcin, osteopontin, bone morphogenic protein 2 (BMP2) and bone sialoprotein.(41,45)

1.4 PET Imaging and Aortic Stenosis

1.4.1. Summary

The clinical management of aortic stenosis relies heavily on visualising and quantifying aortic valve function. Current guidelines advise regular clinical follow-up to track progression of haemodynamic obstruction and ultimately plan timely medical and / or surgical intervention. Echocardiography provides the most validated and established technique to evaluate aortic valve morphology, the degree of haemodynamic obstruction and the subsequent impacts on left ventricular structure and function. Cheap, portable and widely available, standardized echocardiographic measurements using Doppler analysis may clearly define the clinical severity of aortic stenosis allowing for serial comparisons over time. However, the technique is operator-dependent and vulnerable to variations in body-habitus, arrhythmia and cardiac output. More recently, alternative modalities have been evaluated including cardiac MRI with assessment of flow volumes, and the quantification of valvular calcification using computed tomography.(39,217) These techniques offer superior anatomical resolution, and in the latter case prognostic information, but are expensive, less widely available and involve the use of ionizing radiation.

The potential value that PET/CT offers over these aforementioned techniques is its ability not just to define clinical anatomy and the sequelae of a pathological process, but to define the activity of the pathological process itself. Whilst in principle PET can image any pathological process of interest, in practice clinical studies are limited by

the availability of tracers that have been approved for use in humans. As a result, with respect to the use of PET in aortic valve disease, the current literature has focused on two tracers, 18F-fluoride and 18F-fluorodeoxyglucose, which were originally developed for non-cardiac imaging but have recently provided key insights into different forms of cardiovascular disease (Figure 1.2).

Figure 1.2. PET in Aortic Stenosis

Fused PET/CT images of the heart. ***A)*** *An axial PET/CT image of the thorax taken 60 mins following the adminstration of 125MBq of 18F-fluoride. Intense tracer uptake (red,yellow) is observed within the skeleton but also in the aortic valve in the centre of image* ***B)*** *An ECG-gated, short-axis PET/CT image of a mildly calcified aortic valve showing 18F-fluoride tracer uptake (red, yellow) adjacent to an area of established calcium on CT (white).* ***C)*** *A cross-sectional PET/CT image using the radiotracer 18F-fluorodeoxyglucose (18F-FDG), displaying the intense myocardial uptake of radiotracer that is seen without a period of carbohydrate fasting prior to scanning* ***D)*** *A short-axis PET/CT image of the aortic valve following administration of 18F-FDG. Diffuse activity is observed within the calcified aortic valve.*

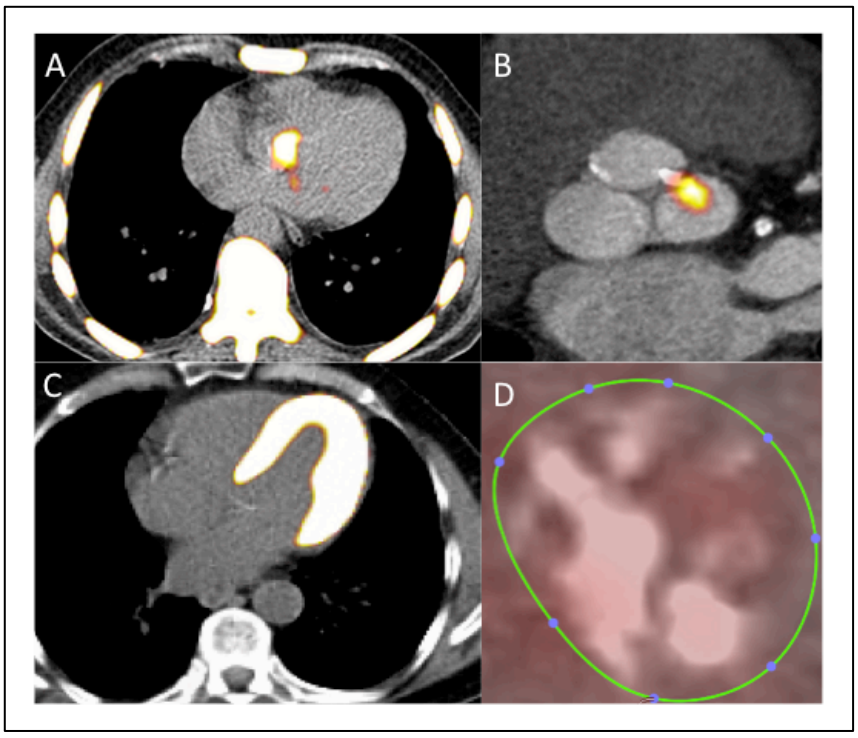

1.4.2. 18F-Fluorodeoxyglucose

18F-FDG is a glucose analogue that is irreversibly taken up into cells by glucose transporter proteins, where it enters the glycolytic metabolic pathway. It is phosphorylated to 18F-FDG-6-phosphate, which cannot be metabolized further and becomes trapped within the cell. 18F-FDG therefore accumulates within cells with high metabolic (glycolytic) requirements. 18F-FDG PET is widely used in oncology practice, due to the increased metabolic activity exhibited by most cancer cells. More recently however, it has been used as a marker of metabolic activity of atherosclerosis. The arterial 18-FDG signal correlates with plaque macrophage burden, symptom status and cardiovascular risk factors.(46-49) In addition, early data suggests that high arterial 18F-FGD uptake might be linked to future vascular events.(50-52) Imaging of the coronary arteries and other structures close to the heart is difficult, because glucose is the major energy source for the myocardium. Intense myocardial activity is therefore frequently observed, which may spill over, obscuring the structure of interest *(Figure 1.1C*).

The early stages of aortic stenosis share many similarities with atherosclerosis. Mechanical stress is believed to result in endothelial damage that permits lipid and inflammatory cell infiltration into the valve. These cells (predominantly macrophages) then secrete a series of inflammatory cytokines that drive the subsequent pro-fibrotic and pro-calcific processes responsible for progressive valve orifice narrowing.(17,18) There is therefore a clear rationale for using 18F-FDG to investigate the contribution of inflammation to aortic stenosis and this has been the focus of two recent studies.

Marincheva-Savcheva and colleagues retrospectively examined 18F-FDG activity in the aortic valves of 42 patients with aortic stenosis and 42 subjects with normal valves who underwent PET/CT as part of an oncological assessment.(53) They observed a diffuse increase in 18F-FDG activity within the valves of those patients with aortic stenosis compared to controls.

Our group followed this with a prospective study of 121 patients with a full spectrum of calcific aortic valve disease, including 20 control subjects with normal valves and 20 subjects with aortic sclerosis.(2) These participants did not have cancer and were recruited into the study from cardiology clinics. Once more there was an increase in the 18F-FDG signal amongst patients with aortic sclerosis and aortic stenosis compared to the control subjects (*Figure 1.1*), and the 18F-FDG signal steadily increased with progressive valve narrowing with no drop off amongst patients with severe stenosis (n=23).

To reduce myocardial 18F-FDG uptake we asked patients to avoid carbohydrates in the 24 hours prior to scanning in an attempt to switch the myocardium to a fat based metabolism, currently standard protocol in cardiac 18F-FDG imaging,(54), but this was only successful in two-thirds of subjects. However a combined approach where we also derived co-axial short axis images and restricted regions of interest to the center of the valve provided excellent measures of reproducibility without underestimating activity (presumably due to the diffuse nature of the 18F-FDG signal).

In combination, these studies demonstrate that the quantification of 18F-FDG activity in the aortic valve is both feasible and reproducible, and support an inflammatory basis for the pathophysiology of aortic stenosis. Further studies are required to provide histological validation of the 18F-FDG signal in the valve and to assess whether this technique might provide a useful marker of disease activity and progression.

1.4.3. 18F-Fluoride

18F-Fluoride has been used as PET bone tracer for 40 years. It is directly incorporated into hydroxyapatite, a key structural component of both bone and vascular calcification, via an exchange mechanism with hydroxyl groups. In the skeleton, 18F-fluoride uptake correlates with osteoblastic and osteoclastic activity, with uptake increased in conditions associated with high bone turnover and reduced in patients with osteoporosis (*Figure 1.1)*.(55-57) Furthermore 18F-fluoride is used clinically for the detection of primary bone tumours and bony metastases. Its mechanism of uptake in the vasculature is less well understood. Similar to bone it is believed to act as a marker of calcification activity, again binding to hydroxyapatite, which is laid down in the very earliest stages of new vascular calcium formation.

Calcification is a key contributor to the development and progression of aortic stenosis.(17) In the very early stages, microscopic areas of calcification exist as nodules containing hydroxyapatite that adhere to the extracellular matrix and can be observed co-localising to areas of lipid deposition and inflammatory cell infiltration. With time, fibroblasts within the valve differentiate first into myofibroblasts and then osteoblasts which subsequently co-ordinate calcification within the valve in a manner akin to skeletal bone formation.(42-44) Indeed, by the later stages of the disease, hydroxyapatite crystals coalesce and remodel to form bone-like structures within the valve.(40) The amount of established calcium present within the valve can be quantified using both CT and echocardiography, measures of which correlate closely with disease severity, progression and clinical outcomes in patients with aortic

stenosis.(35,36,38,39) However these techniques do not identify nor quantify the process of active calcification and remodeling, which is the rationale for 18F-fluoride PET scanning.

Hyafil *et al* performed a pilot study of 5 patients with aortic stenosis and 10 patients with normal aortic valves, using 18F-fluoride PET/CT. Unlike with 18F-FDG PET imaging of the heart, there is very little tracer uptake within the myocardium and dietary restrictions are unnecessary. 18F-Fluoride activity measured in the aortic valves of patients with known AS were about 50% higher compared to those in patients free of valvular calcification.(58)

Our group performed 18F-fluoride scanning on the same cohort of patients that had 18F-FDG PET imaging, described above.(2) In total 45% of patients with aortic sclerosis and 91% of those with aortic stenosis had increased 18F-fluoride uptake. Interestingly the pattern of 18F-fluoride activity in the valve was often poorly aligned with the presence of established calcium on CT (Figure 1.1B), indicating that these two techniques provide different yet complementary information. Similar to 18F-FDG, 18F-fluoride uptake rose progressively with increasing valvular stenosis, however the rate of rise for 18F-fluoride was much steeper so that particularly in those with moderate and severe aortic stenosis it considerably outweighed the 18-FDG signal. This suggests that calcification may predominate in the more advanced stages of the disease, supported by the increased CT calcium scores observed in the valves of these patients.

The pathological similarities between aortic stenosis and atherosclerosis led to the hypothesis that statin therapy might prove beneficial in the former. However this drug class has failed to impact on the progression of calcific aortic valve disease in three major randomised control trials: why was this?(26,27,59) Comparisons of 18F-fluoride and 18F-FDG activity in the valves of patients with aortic stenosis with their uptake in regions of coincident aortic atheroma were revealing. Calcification activity was greater in the valve compared to atheroma, based on their respective 18F-fluoride signals (18F-fluoride TBR: 2.66±0.84 vs.2.11±0.31, P = 0.001) but interestingly the reverse was true for 18-FDG with inflammatory activity being higher in regions of atherosclerosis (18F-FDG TBR: 1.56±0.21 vs. 1.81±0.24, respectively, P <0.001).(60) This observation suggests key differences in the pathophysiology of these two conditions, indicating that inflammation may have a lesser role in aortic stenosis than atherosclerosis and perhaps explaining the differential effects of statins.

The above studies underline the potential that PET/CT holds in assessing the pathological processes underlying aortic stenosis. It would appear that 18F-fluoride and 18F-FDG provide measures of calcification and inflammatory activity respectively, however several key questions still remain. First, there is a need to validate the PET signal histologically, particularly in the case of 18F-fluoride which has largely only been studied in bone. Secondly, it remains unclear whether this technique has the ability to predict disease progression in aortic stenosis. This remains clinically challenging, and a technique that might predict how quickly patients progress towards the need for intervention would be invaluable.

1.5. Pathophysiology of myocardial remodeling after myocardial infarction: targets for molecular imaging

1.5.1 Pathophysiology of myocardial remodeling

Over 1 million people suffer a myocardial infarction (MI) each year in the USA alone.(1) With improved treatment, more patients are surviving, resulting in an increased pool of candidates for maladaptive ventricular remodeling and heart failure after MI.(61) Importantly, as clinical presentation is changing with declining incidence of ST-elevation MI (STEMI) (62) and increasing age of the patients, the understanding of ventricular remodeling and approaches to risk stratification must also evolve.

Adverse left ventricular (LV) remodeling is comprised of both short- and long-term changes in the LV shape, size, function and both cellular type and configuration after MI.(63,64) On a histological basis it evolves as a combination of myocyte hypertrophy and apoptosis, myofibroblast proliferation and interstitial fibrosis, both in the region of myocardial infarct and in the remote myocardium.(65,66) Macroscopically this is manifested as ventricular hypertrophy, dilatation and the formation of replacement collagen scar. While these alterations are necessary to preserve and restore myocardial integrity, adverse remodeling, clinically defined as an increase in LV dimensions following MI by at least 20%,(67) may develop in up to 30% of patients with MI.(68) Although clinical definitions of adverse remodeling and reports of prevalence may

vary, it universally infers significant increase in risk of heart failure and death. (66,69-71)

Multiple pathophysiological factors govern the extent of remodeling and the risk of progression to heart failure. The foremost determinants are extent of the initial myocardial insult, and the sufficiency of the post-MI reparative process. (64,72) Improvements in the early identification of MI using high-sensitivity biomarkers and increasingly efficient and effective revascularization techniques continue to address the former.(62) However, understanding and successfully manipulating the latter proves more challenging and elusive, in part because of the difficulty in translating potential pathophysiological targets into successful therapeutic practices.

Myocardial healing following infarction can be divided into 3 sequential overlapping phases; an inflammatory phase, a proliferative phase (72hrs-7 days), and a maturation phase (7-14days).(73,74) During these stages, an interplay of angiogenesis, inflammation and fibrogenesis determines the subsequent extent of preservation and restoration of myocardial integrity.(63)

The inflammatory phase

Shortly after the onset of irreversible cardiomyocyte ischaemia, cell necrosis and apoptosis results in the release of intracellular contents and the initiation of an intense inflammatory response. Complement activation, oxidative stress and toll-like receptor-mediated pathways serve to activate the nuclear factor kappa-B system,

which in turn promotes the release of inflammatory cytokines, chemokines and cell adhesion molecules.(64,73,75) The subsequent margination and ingress of neutrophils, mast cells and monocytes into the infarcted region promotes ingestion of apoptotic debris and degradation of the extracellular matrix (ECM) through the release of matrix metalloproteinases to encourage formation of granulation tissue.(74,76) This inflammatory response is highly regulated however, and neutrophil levels peak early within myocardial infarct prior to apoptosis and clearance by activated monocytes/macrophages.(77) Indeed, exaggerated inflammation within the infarct may encourage degradation in ECM integrity, and elevated concentrations of circulating neutrophils and monocytes after MI have been associated with increased risk of adverse remodeling through LV dilatation and aneurysm formation. (74,78,79)

The proliferative phase

The progression into a proliferative phase of infarct healing is promoted by the inflammatory-cell-rich environment capable of repression of pro-inflammatory signals and regulating a process of angiogenesis, fibroblast proliferation and ECM metabolism.(80) This is stimulated firstly by the upregulation of cytokines and cellular adhesion molecules by macrophages and epithelial cells, including $\alpha_v\beta_3$ integrin, TGF-ß, Tissue necrosis factor (TNF)-α, VGEF, hypoxia-inducible factor (HIF)-1, interleukin (IL)-6 and IL-1ß.(81,82) Secondly, there is an upregulation of the sympathetic nervous system secondary to a fall in cardiac output, and the subsequent increase in naturetic peptides and activation of the renin- angiotensin-aldosterone system (RAAS), promoting angiotensin II and reactive oxygen species release.

At this stage the infarct may be infiltrated by vascular cells and fibroblasts.(80) The ensuing process of angiogenesis occurs as a means of restoring vascular integrity to infarcted tissue. This process is manifested in the formation of new blood vessels within the infarcted tissue (vasculogenesis), the proliferation of blood vessels in the ischaemic penumbra (angiogenesis) and re-epithelialisation of established vasculature perfusing the infarcted region.(82) Among other regulators, the $\alpha_v\beta_3$ integrin cell-surface receptor has been identified as a critical modulator of angiogenesis, and angiogenic vessels display increased expression of the $\alpha_v\beta_3$ integrin in response to angiogenic growth factors. These receptors are fundamental to endothelial cell migration, adhesion, proliferation and survival.(83)

The process of fibrogenesis may be further encouraged through the restoration of a capillary network. In this proliferative phase, enabled by migration and proliferation, activated fibroblasts become the dominant cell type within infarct tissue.(84) There are no reports of myofibroblasts in normal myocardial tissue.(85,86) Myofibroblasts express and incorporate a number of contractile proteins in the ECM, including α-smooth muscle actin (α-SMA), serving to limit the size of the infarct zone while also producing high amounts of type III interstitial collagen to increase the structural integrity of replacement fibrosis. Sharing similarities with activated vascular endothelial cells, myofibroblasts express high levels of $\alpha_v\beta_3$ integrin that are essential for the promotion of collagen genes and reducing the expression of genes encoding MMP's.(87-89)

The maturation phase

Maturation of infarct scar follows restoration of vascular and ECM integrity. Myofibroblasts and vascular cells undergo apoptosis through a number of regulatory signaling systems including Fas, TGF-ß1 and angiotensin II receptor pathways.(86,90-92) However, reduction in wall stress is a potent inducer of myofibroblast apoptosis *in vivo,*(93) and a failure to normalize mechanical wall stress alongside the myocardial upregulation of the RAAS system may encourage ongoing myofibroblast activity long after the proliferative phase. In some circumstances, maladaptive persistent processes may encourage remodeling and infarct expansion to extend into the myocardium long after the initial causative injury abates.(94) As a consequence of globally altered wall stress, myocardial interstitial modifications of the ECM post-MI is not limited to the site of infarction, and myofibroblast-driven fibrotic expansion may be seen in the remote myocardium, promoting LV dilatation, stiffness and myocardial recovery.(95) (96)

1.5.2 The $\alpha_v\beta_3$ integrin receptor and ventricular remodeling after MI

Cell–cell and cell–extracellular matrix interactions provide the structural, chemical, and mechanical substrate required for regulation of cellular phenotype in specific environments. Integrins are a group of molecules responsible for intercellular adhesion and signalling, providing the critical interface between the cell and the matrix and may serve as a candidate mechanotransducer during cardiac development or in response to injury during pathophysiological stress.(119) They comprise a superfamily of heterodimeric receptors that are composed of 18 different α and β subunits. In combination, they can generate 24 different receptor subtypes with a range of physiological and pathophysiological functions.(97) The $\alpha_v\beta_3$ integrin cell-surface receptor recognises the amino-acid arginine-glycine-aspartate (RGD) motif present on a number of ligands responsible for proliferation and migration, including fibrinogen, fibronectin, laminin, TGF-ß1, VEGF-R2, MMP2 and von Willebrand factor. It allows vital cell-cell and cell-ECM interactions, in turn promoting intracellular processes and gene upregulation accordingly.

The $\alpha_v\beta_3$ integrin is a unique receptor in that it is barely detectable on mature quiescent endothelial cells, monocytes and fibroblasts, but is markedly upregulated on activated vascular endothelial cells, macrophages and myofibroblasts to allow them to respond to extracellular ligands.(83,87,89,98,99) As such, $\alpha_v\beta_3$ integrin may be promoted as a prime candidate molecule for monitoring and manipulating the processes of angiogenesis, inflammation and fibrosis within the myocardium. Indeed, the receptor has been the focus of extensive oncological research as a potential target for diagnosis

and anti-angiogenic treatment. Numerous specialities have documented a reduction in pathological angiogenic activity through the modulation of $\alpha_v\beta_3$ integrin receptor activity. (100-106), and as a consequence it has become the focus of molecular imaging modalities that allow the real-time interrogation of angiogenic activity *in vivo*.(9,107,108)

1.5.3. The evolution of RGD nuclear imaging probes

A number of RGD-based imaging probes have been in development for over a decade. (109-113) Initially focused on oncological targets, they have shown utility in assessing the response to anti-angiogenic or cytotoxic therapy in both animal and human studies of malignancy.(9,109,114-117) Furthermore these tracers experience predominantly renal tracer elimination, resulting in low background activity in most regions of the body including lung and healthy myocardium.(10,110) High inter- and intra-individual variance in tracer accumulation between patients have been demonstrated, suggesting substantial heterogeneity of $\alpha_v\beta_3$ integrin expression.(110,112)

1.5.4 Integrin $\alpha_v\beta_3$ imaging and myocardial remodeling

It is recognised that expression of $\alpha_v\beta_3$ integrin by vascular endothelial cells facilitates angiogenesis in the peri-infarct zone, while also mediating the activated macrophage response to inflammatory signals and governing myofibroblast differentiation through the activation of latent TGF-β1.(118-120) As a result, there have been several pre-clinical studies assessing the utility of $\alpha_v\beta_3$ integrin following acute MI. In predominantly murine models of myocardial infarction, RGD-based radiotracers have been seen to accumulate in the peri-infarct site as early as 3 days post-MI, and peak between 1-3 weeks, representative of acute LV remodeling (Figure 1.3, panel A).(119,121-132) At later timepoints post-MI, the expression of $\alpha_v\beta_3$ integrin may persist and extend to myocardial regions remote to the infarct site.(119) Indeed, Higuchi et. al. reported persistent low-grade $\alpha_v\beta_3$ integrin expression within the myocardial scar up to 6 months after infarction, long after the initial inflammatory and angiogenic remodeling phase abates and during a delayed phase of LV remodeling that is predominantly myofibroblast-driven (Figure 1.3, panel A). (86,121) They present serial histological assessments identifying vascular endothelial cells as the principal origin of myocardial $\alpha_v\beta_3$ integrin expression early after infarction (day 3), whereas diffuse myofibroblasts were the predominant source of $\alpha_v\beta_3$ integrin expression 1-3 weeks and 6 months post-infarction.(121) A full summary of the preclinical findings are tabulated in Table 1.1.

Figure 1.3. The temporal and spacial distribution of $\alpha_v\beta_3$ integrin expression following myocardial infarction.

Panel A displays ^{18}F-Galacto-RGD uptake on autoradiography in the murine heart after ischaemia and reperfusion (adapted from Higuchi et. al. 2008); the left image displays the distribution of uptake in apex, middle, and basal segments at different time points. The right image plots the time course of myocardial ^{18}F-Galacto-RGD uptake along with sham-operated animals. Panel B displays co-localization of RGD-tracer uptake on SPECT 3 weeks after MI with CMR-verified evidence of fibrosis at 1 year (adapted from Verjans et. al. 2010). The first row demonstrates CMR images of anterior wall scar (white arrows) in short axis and 2-chamber views after 1 year. The second row shows equivalent views with 99mTc-RIP uptake 3 weeks after MI, corresponding to the subsequent scar formation on SPECT/MR fusion images on the third row.

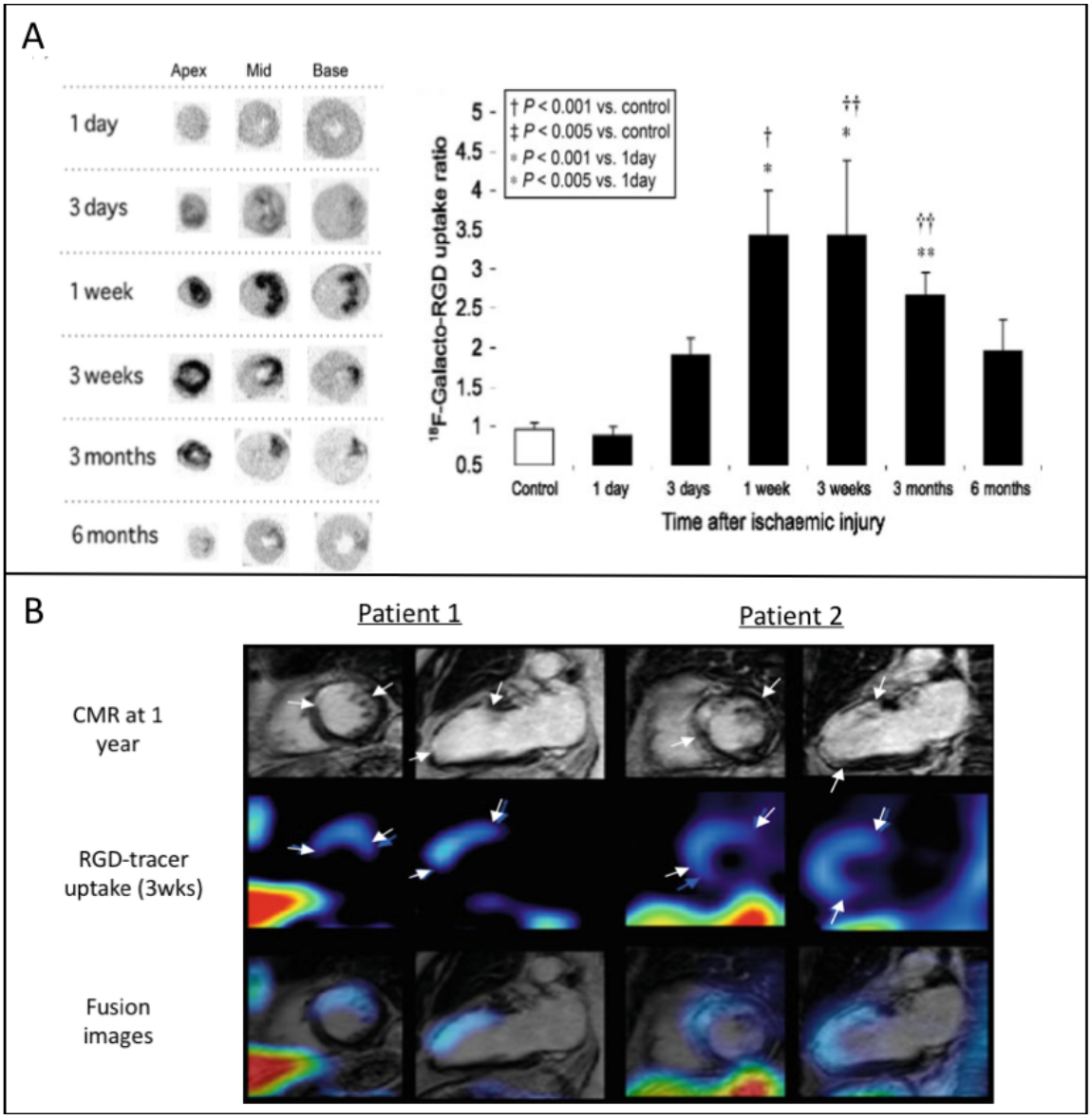
A
Apex
Mid
Base
1 day
3 days
1 week
3 weeks
3 months
6 months
† P < 0.001 vs. control
‡ P < 0.005 vs. control
* P < 0.001 vs. 1day
* P < 0.005 vs. 1day
18F-Galacto-RGD uptake ratio
5
4.5
4
3.5
3
2.5
2
1.5
1
0.5
Control
1 day
3 days
1 week
3 weeks
3 months
6 months
Time after ischaemic injury
B
Patient 1
Patient 2
CMR at 1 year
RGD-tracer uptake (3wks)
Fusion images

Table 1.1 Assessment of myocardial remodeling using RGD-imaging probes.

Author	Model	RGD Tracer	*n*	Imaging timepoints	RGD-tracer uptake	Histological $\alpha_v\beta_3$ integrin staining	Outcomes / therapeutics
Meoli et. al., 2004.(126)	*Rats*; LCA ligation. Canines; LAD catheter occlusion **SPECT imaging**	^{111}In-RP748	Rat; *n*=11 Canine; *n*=6	Rats; day 14. Canines; days 1,7 & 21.	Uptake in myocardial tissue corresponding to regions of reduced perfusion, uptake peaking between 1-3 weeks post-MI	$\alpha_v\beta_3$ integrin localized to peri-infarct and infarct capillaries and arterioles.	N/A
Higuchi et. al., 2008(121)	*Rats*, LCA ligation. **PET imaging**	^{18}F-Galacto-RGD	*n*=49, 5 sham-operated	Days 1, 3 & 7 Weeks 3,12 & 26. Sham rats; day 7.	No uptake in sham operated rats. Absent uptake at day 1, peaking between 1-3 weeks. Persistent low-grade uptake at 6 months. Uptake in infarct periphery at day 3, expanding into central infarct at day 7.	$\alpha_v\beta_3$ integrin staining localizing to peripheral angiogenic cells on day 3, and diffuse myofibroblast cells at 1-3 weeks and 6 months.	N/A
Johnson et. al., 2008.(130)	*Swine*, LCx constriction. *VGEF or saline intramyocardial injection day 21*. **SPECT imaging**	[^{123}I]Gluco-RGD	*n*=14	1 month (14 days after VGEF injection)	RGD-tracer uptake ratio 1.7 ± 0.1 of in infarct: remote myocardium in VGEF injected pigs. Ratio 1.0 ± 0.1 in sham-injected pigs.	None	Greater RGD-tracer infarct uptake in pigs following VGEF injection compared with saline-injected. P<0.001
van den Borne et. al., 2008(5)	*Rats*, LCA ligation, groups treated with captopril± losartan. **SPECT imaging**	[^{Tc99m}]-Cy5.5-RGD	*n*=46 11 sham-operated	Weeks 2,4 &12. Sham animals; week 4 Treatment animals; week 4	Peak infarct RGD-tracer uptake at 2-weeks, persistent but reduced uptake in weeks 4 and 12. Greater uptake in remote myocardium compared with sham operated.	Direct correlation of RGD-tracer uptake with myofibroblasts and thin collagen fibers. (r^2=0.45; p=0.001)	4-week RGD-tracer uptake reduced after captopril or captopril± losartan (both p<0.001) compared with untreated rats.

Gao et. al., 2012(122)	*Rats,* LCA ligation. **PET imaging**	^{18}F-AlF-NOTA-RAD	*n*=13, 5 sham-operated	3 days, weeks 1 and 3, 4 months.	RGD-tracer uptake in infarct from day 3 post-MI, peaking between 1 - 3 weeks. Uptake at 4 months remained greater than sham-operated animals.	infarct uptake peaking between 1- 3 weeks. $\alpha_v\beta_3$ Integrin localizing to angiogenic cells.	None.
Sherif et. al. 2012.(129)	*Rats.* LCA ligation. **PET imaging.**	18F-galacto-RGD	*n*=8, 9 sham-operated	1 week.	RGD-tracer uptake increased in infarct compared with remote myocardium and sham-operated rats (both p<0.001).	18F-RGD uptake strongly correlated with microvessel density (r=0.83) but inverse correlation with macrophage density (r=-20.8).	RGD-tracer showed inverse correlation with remodeling at 12-weeks (ΔEDV; r=-20.7, p<0.01, ΔEF; r=0.46, p=0.05).
Laitinen et. al. 2012.(123)	*Rats.* LCA ligation. **PET imaging.**	18F-galacto-RGD, 68Ga-NODAGA- & 68Ga-TRAP-RGD	*n*=31	1 week	RGD-tracer uptake increased in infarct, correlating with regions of hypoperfusion.	RGD infarct uptake correlated with β3 integrin (r=0.91)	None.
Menichetti et. al. 2013.(124)	*Rats.* LCA ligation. **PET imaging.**	^{68}Ga-NOTA-RGD	*n*=12, 4 sham-operated	4 weeks	RGD-tracer uptake increased in infarct and peri-infarct regions	RGD infarct uptake correlated with β3 integrin and angiogenic cells.	None
Lee et. al. 2016.(125)	*Rats.* MI/reperfusion. **SPECT imaging**	^{99m}Tc-IDAD-[c(RGDfK)]	*n*=4	Days 7, 14, and 28	Increased RGD-tracer uptake in hibernating myocardium, peaking at 7 days.	RGD infarct uptake correlated with β3 integrin expression	None
Rasmussen et. al. 2016.(127)	*Minipigs.* MI model not stated. **PET imaging.**	^{68}Ga-NODAGA-RGD	Not stated.	Days 7 and 28.	Increased RGD-tracer uptake in infarct on days 7 and 28.	None.	None.

Abbreviations: LAD, left anterior descending coronary artery; LCA, left coronary artery; LCx, left circumflex artery; MI, myocardial infarction; PET/CT, fused positron emission tomography / computed tomography; SPECT,single-photon emission computed tomography; VEGF,vascular endothelial growth factor.

Within these preclinical studies investigators addressed the potential for $\alpha_v\beta_3$ integrin imaging in the prediction of clinical outcome and to assess the response to therapeutic intervention. In a study by Johnson et. al. a VEGF-rich solution was injected directly into the myocardium of pigs 20 days after partial-thickness MI. Using single photon emission computed tomography (SPECT) 1 month after infarction, significantly greater RGD-radiotracer myocardial uptake was present in those animals receiving intra-myocardial VEGF compared with a similar injection of isotonic saline. Consistent with this observation, Sherif et. al. reported significant associations between increasing degrees of RGD-tracer infarct uptake on PET imaging performed 1 week after MI, and improvements in ejection fraction and end-diastolic volume.(129) Conflictingly however, Van den Borne documented an opposite response to therapy with captopril with or without losartan in rats; those treated with RAAS-inhibitors displayed significantly reduced levels RGD-radiotracer infarct uptake on SPECT imaging 4 weeks after MI when compared to non-treated animals.(128)

Despite encouraging preclinical findings however, there are limited translational studies reporting the use of RGD-radiotracers following MI in humans.(133-135) Sun et. al. report a series of 23 patients who underwent PET/CT with the RGD-tracer ^{68}Ga-PRGD2 between 3 days – 2 years after myocardial infarction. They observed myocardial uptake in 20 of these patients, although little additional clinical detail is provided. In the most thorough assessment to date in a cohort of 10 patients, Vergans et. al. report a close relationship between RGD-radiotracer myocardial uptake on SPECT imaging 3- and 8-weeks following acute myocardial infarction and residual myocardial fibrosis on cardiac MRI 6 months later.(134)

Non-invasive molecular imaging of the $\alpha_v\beta_3$ integrin receptor in acute MI therefore holds the potential offer a comprehensive and potentially modifiable quantification of myocardial remodeling activity. However, data from human studies remain sparse, with small numbers of patients studied, an absence of control groups, clinical follow-up, or histological validation. (119,121)

1.6. Atherosclerosis; pathophysiology and targets for molecular imaging

1.6.1. The role of nuclear imaging in atherosclerosis

Atherosclerotic cardiovascular disease is the commonest cause of death in the developed world. Elucidating the mechanisms underlying the propagation and rupture of the atherosclerotic plaque therefore remain a key public health goal.(1) Considered a systemic inflammatory disease, atherosclerosis develops over a period of decades as a continuum of early vascular endothelial dysfunction, circulating macrophage recruitment and intimal accumulation, plaque maturation into a necrotic core, atherosclerotic plaque destabilisation and ultimately cap erosion or rupture.(136,137) The majority of plaque disease remains sub-clinical (asymptomatic). Some lesions may become obstructive, inducing symptoms of flow-limitation (eg. angina, intermittent claudication or mesenteric ischaemia), while a small proportion may develop features of vulnerability with predisposition towards thrombosis.(138-140) The erosion or rupture of unstable atherosclerotic plaque within the coronary or carotid circulation represents the primary cause of myocardial infarction, and 1/3rd of cerebrovascular accidents.(141)

Over the last two decades' enormous progress has been made in the understanding of atherosclerosis pathophysiology. Despite this, on an individual basis the accurate prediction of clinical events remains elusive.(142) It is well known that the risks of

atherosclerotic plaque rupture are poorly correlated with the severity of stenosis; indeed for an assessment of future cardiovascular risk in the asymptomatic patient, an accurate quantification of luminal stenosis using coronary CT angiography may be equivalent to the simpler technique of coronary calcification quantification.(143) The majority of plaque erosion or rupture is subclinical in nature, and driven by a number of local and systemic factors which each individually may not dictate a clinical outcome.(144-146) There is therefore increasing demand for non-invasive imaging strategies that compliment luminal imaging and measure disease activity within the vasculature.(140) Furthermore, a broadening in focus from the identification and targeted treatment of a single vulnerable plaque to identifying effective global markers of atherosclerotic disease activity may provide incremental risk prediction to the quantification of disease burden alone.(147) Indeed, sub-clinical atherosclerotic disease frequently co-exists in several vascular beds, representing a multi-systemic marker of adverse cardiovascular prognosis.(148-152)

Fused PET/CT imaging holds great potential as a novel tool in the assessment of atherosclerotic disease, with an ability to non-invasively visualize active biological processes and thereby provide real-time quantification of multiple potentially modifiable processes driving atherosclerotic disease.(6,136,153) This technique is appealing to not only improve our understanding of plaque biology, but as a method to monitor overall disease activity and to assess response to anti-atherosclerotic therapy.

1.6.2. PET and the vulnerable plaque

Inflammation and Calcification in the atherosclerotic plaque

There are a number of pathophysiological processes of importance in atherosclerosis which hold the potential for visualisation using positron emission tomography. In particular, inflammation plays a critical role in plaque formation, progression and vulnerability. This chronic inflammatory state is initiated following the accumulation of low density lipoproteins (LDL) beneath sites of vascular endothelial disruption. In brief, these LDL particles undergo a process of oxidation and accumulation that results in an upregulation of pro-inflammatory molecules by the vascular endothelial cells, and the ingress of circulating monocytes and macrophages.(154,155) Regulated by $\alpha_v\beta_3$ integrin expression, monocyte-derived macrophages phagocytose oxidized LDL particles to create lipid-laden foam cells, forming a lipid pool. (156,157) This pathological intimal thickening is encapsulated through the formation of a 'fibrous cap', consisting of varying quantities of smooth muscle cells (SMC) within a collagenous-proteoglycan matrix.(138,155)

With time, cellular apoptosis and autophagy result in the development of a necrotic core, consisting of macrophages and cellular debris within the lipid pool. Macrophages drive expansion of the necrotic core, and secrete matrix metalloproteinases that weaken the fibrous cap, predisposing it to rupture. Macrophage density within plaque correlates closely with progression and the size of the necrotic core and therefore represent a feature of high risk plaque morphology.(155,158) Early deposits of

microcalcification may develop within this necrotic core, and are also associated with plaque vulnerability.(159) The exact link between calcification and inflammation is unclear, however they are thought to be exocytosed from the cell membranes of apoptotic macrophages and vascular smooth muscle cells and therefore are closely linked to the inflammatory process.(160)

Imaging of vascular inflammation using PET has been well documented. The glucose-analogue 18F-FDG has been visualized in the aorta and carotid and coronary arteries, representing predominantly macrophage activity within atheromatous deposits.(4,6,48,49,161) Extensively validated, it is now being utilized as an imaging end-point in anti-atherosclerotic pharmaceutical intervention.(162,163) More recently, Dweck *et al.* have established the radiotracer 18F-fluoride as a marker of active calcification within both unstable and stable coronary disease,(6,60,164) and prospective trials assessing its utility in the prediction of future cardiovascular events is ongoing.

Angiogenesis in the atherosclerotic plaque

With an expanding necrotic core, increasing macrophage metabolic requirements and increased oxidative stress, the growth of fibroatheromatous plaque results in both an increased oxygen demand and impaired endothelial oxygen diffusion. This hypoxic environment creates a powerful angiogenic stimulus, and as a consequence a potential target for molecular imaging.(165,166) In response to hypoxia and inflammation, pro-angiogenic growth factors including vascular endothelial growth factor A (VEGF-A),

platelet-derived growth factor (PDGF) and fibroblast growth factor (FGF) are released by macrophages, SMC's and endothelial cells. These factors serve to both further recruit circulating inflammatory cells and promote endothelial proliferation, migration, and the formation of the vascular tubes.(167,168) The migration and adherence of endothelial cells to the ECM is mediated and enabled by $\alpha_v\beta_3$ integrin upregulation and the formation of a $\alpha_v\beta_3$ integrin / VEGF-receptor complex.(167)

The histological characteristics of plaque angiogenesis reveal fragile microvessels sprouting from the adventitial *vasa vasorum* to perfuse the necrotic core. They are found in clusters within the shoulder regions, the intima-media border and in the fibrous cap – regions predisposed to fissuring and rupture.(167) While also providing a means of entry for inflammatory cells, these vessels often lack pericytes and smooth muscle cells and have poorly formed endothelial cell junctions, making them prone to leakage and rupture.(169) Microvessel rupture and intraplaque haemorrhage is a proinflammatory event and a key determinant of plaque destabilization. (166,167,170-173)

1.6.3. The imaging of integrin $\alpha_v\beta_3$ in atherosclerosis

The $\alpha_v\beta_3$ integrin plays a key role in atherosclerosis in humans, both in the mediation of angiogenesis and the regulation of macrophages within fibroatheromatous plaque. (174-177) Plaque inflammation and angiogenesis are two key pathological processes associated with disease progression, plaque rupture and clinical events. A non-invasive imaging technique that can inform about the activity of these two adverse pathological processes might therefore be useful in identifying patient with active high-risk atheroma.

Several preclinical studies have utilized the $\alpha_v\beta_3$ integrin receptor for *in vivo* imaging of atherosclerosis. First reports used $\alpha_v\beta_3$-targeted paramagnetic nanoparticles to identify atherosclerosis within the aortic wall of hypercholesterolaemic rabbits on MRI imaging.(178,179) Laitinen et. al. subsequently assessed the RGD-based radiotracer 18F-galacto-RGD alongside the 18F-FDG mimetic ^{3}H-deoxyglucose in the aorta of hypercholesterolaemic mice using PET/CT.(180) They demonstrated increased uptake in atherosclerotic plaque that was associated with macrophage density on histology and showed equivalence to ^{3}H-deoxyglucose uptake. Little angiogenesis was demonstrated within the atheroma, although further murine studies using SPECT and PET imaging have demonstrated aortic uptake of RGD-tracers within atherosclerotic plaque that correlated with histological markers of both inflammation and angiogenesis.(181-184) Importantly, serial PET/CT imaging by Saraste et. al. have shown that aortic 18F-galacto-RGD uptake may be modified using lipid-lowering diet intervention.(185)

Murine models of hypercholesterolaemic atherosclerosis are limited by the lack of chronicity, and subsequently a difference in plaque morphology when compared to human atheroma. Although Golestani et. al demonstrated an *ex vivo* association between RGD-tracer uptake and neovasculature by imaging carotid endarterectomy specimens using microPET,(186) the *in vivo* assessment of RGD-tracers in human atherosclerotic disease is limited to a single PET/CT study of symptomatic carotid atherosclerosis. Within a group of 10 patients, 18F-galacto-RGD accumulation was demonstrated in stenotic atherosclerotic carotid plaques. Following endarterectomy, the *in vivo* PET/CT uptake correlated with histological quantification of $\alpha_v\beta_3$ integrin expression but only weakly with macrophage and endothelial cell staining.(187)

The imaging of $\alpha_v\beta_3$ integrin expression in human atherosclerotic disease therefore remains in its infancy. Meanwhile, the oncological applications of RGD-tracer imaging have already demonstrated utility in the use of $\alpha_v\beta_3$ integrin imaging and assessment of response to antiangiogenic therapy.(188) Though early, the potential for $\alpha_v\beta_3$ integrin receptor blockade has been assessed both for the prevention of atherosclerosis and restenosis following arterial angioplasty,(175-177,189) furthering potential for the use of RGD-tracer imaging in the assessment of therapy response in humans. However, data from human studies remain sparse, and further studies are required.

1.7. 18F-Fluciclatide development and pharmacokinetics

The RGD tracer 18F-fluciclatide has been developed by GE Healthcare as a PET imaging probe for imaging human $\alpha_v\beta_3$ integrin expression. Pilot studies have confirmed that it is safe, metabolically stable and able to detect breast cancer lesions by PET in most anatomical sites.(9) 18F-Fluciclatide was either homogeneously distributed in the tumors or appeared within the tumor rim, consistent with general principles regarding the distribution of angiogenesis within the viable outer zones of breast tumors.(9) Biodistribution studies confirm that 18F-fluciclatide-$\alpha_v\beta_3$ integrin receptor binding is predominantly irreversible within the imaging timeframe (70min) and therefore can be assessed using a 2-compartmental kinetic model derived from 18F-FDG uptake analysis (the 'patlak' analysis). The biological half-life of 18F-fluciclatide in whole blood is 0.25 ± 0.07 h. The blood clearance is biexponential, meaning that there is a fast redistribution component through the tissue compartments and a slower renal clearance component. The reported half-life value is a composite of both, confirming suitability for an imaging timepoint beyond 20 minutes post-administration. However, while the faster component has a half-life of about 10 minutes, the slower component has a half-life of around 6 hours. Therefore beyond 1 hour post-administration it is this second term that predominates and imaging later is unlikely to improve a contrast to background ratio. Fortunately the mean (±SEM; 7 patients) percentage of parent radioligand in plasma at 60 min after injection of 18F-

fluciclatide was 74.48±3.18%, confirming minimal metabolism, with no evidence of active metabolites. (9,190,191)

1.8 Aims and hypotheses

The overall aims of these studies are to assess the role of novel PET/CT imaging techniques in cardiovascular disease. A multimodality approach for assessment of PET/CT markers of calcification, inflammation, angiogenesis and fibrosis was undertaken. Specifically, we extend the work of Dweck et. al. with a focus on the validation and prognostic utility of 18F-FDG and 18F-fluoride PET-CT as markers of inflammation and active calcification in aortic stenosis.(2) Additionally, we will conduct an in-depth assessment of the ability for the novel $\alpha_v\beta_3$ integrin radiotracer 18F-fluciclatide to provide complementary information to current imaging techniques in the assessment of atherosclerotic disease and remodeling following myocardial infarction.

In Chapter 3, we will develop the methodology for a validation of 18F-FDG and 18F-fluoride imaging of the aortic valve by combining a histological study of localising calcific and inflammatory processes with *in vivo* imaging findings and the confirmation of the specificity of radiotracer tissue uptake using autoradiography. We will then assess the ability of aortic valvular uptake of 18F-FDG and 18F-fluoride *in vivo* to predict the progression of aortic stenosis in a subgroup of patients using both echocardiographic and CT measures of disease severity.

In Chapter 4, we will evaluate the associations between 18F-FDG and 18F-fluoride aortic valvular uptake and both progression of aortic stenosis and clinical outcome in

a large cohort of patients over a prolonged follow-up period. Further comparisons will be made with current gold standard prognostic assessments of aortic stenosis severity.

In Chapter 5 we will perform a multimodality imaging and histological assessment of the heart following acute MI. Specifically, we will develop a methodology evaluating myocardial uptake of the novel radiotracer 18F-fluciclatide at multiple time points following MI using gated PET/CT, assessing its ability to assess myocardial remodeling activity *in vivo* and determining associations with temporal changes in myocardial structure and function on serial cardiac magnetic resonance imaging. Myocardial uptake of 18F-fluciclatide following MI will be compared to subjects with stable coronary disease and to healthy control patients.

In Chapter 6 we will perform a multimodality imaging assessment of atherosclerosis within the thoracic aorta using the novel $\alpha_v\beta_3$ integrin radiotracer 18F-fluciclatide. Specifically, we aim to evaluate the ability for 18F-fluciclatide to quantify the activity of inflammation and angiogenesis within a spectrum of atherosclerotic disease severity and stability, validating our findings with a histological and autoradiographical study of carotid plaque.

The following hypotheses will be addressed:

1. That 18F-FDG and 18F-fluoride PET/CT provide an *in vivo* quantification of valvular inflammation and calcification respectively in calcific aortic stenosis (Chapter 3)

2. That 18F-FDG and 18F-fluoride PET/CT aortic valvular uptake would correlate with subsequent disease progression and clinical outcome. (Chapter 3 and 4)

3. That the novel radiotracer 18F-Fluciclatide could identify the expression of the αvβ3 integrin receptor *in vivo* in man in 2 major cardiovascular disease areas; acute myocardial infarction and aortic atherosclerosis. Specifically, we hypothesized that 18F-Fluciclatide would
    a. Demonstrate selective uptake within the region of myocardial infarction in the early phase of recovery (1-3 weeks). (Chapter 5)
    b. Bind in both the infarct and remote regions of patients with substantial myocardial infarction in the later phases of recovery (6-12 weeks). (Chapter 5)
    c. Demonstrate associations with the temporal alterations in myocardial structure and function after myocardial infarction. (Chapter 5)
    d. Demonstrate atherosclerotic activity in aortic atherosclerotic plaque. (Chapter 6)

Chapter 2.

Methods

2.1 Overview.

The specific study designs and methodology for each of the cohorts are described in detail in the relevant chapters. The following sections will provide the overview of the patient populations and the novel imaging modalities utilised in these studies.

2.2 Study Populations

This thesis is based upon the study of 2 patient groups prospectively recruited from the Royal Infirmary of Edinburgh, Edinburgh, UK. One group of patients with a spectrum of calcific aortic valve disease had undergone PET imaging with 18F-FDG and 18F-fluoride as part of a pre-existing research study ('The Ring of Fire Study', NCT01358513). In the second group a population of patients with either ischaemic heart disease or calcific aortic valve disease underwent PET imaging with 18F-fluciclatide. All PET-CT and CMR studies were performed by speciality radiographers under the supervision of study investigators at the Clinical Research Imaging Centre (CRIC) in the University of Edinburgh. Validation of the *in vivo* imaging findings was obtained through histological and autoradiographical analysis of human tissue samples obtained from the study population and carried out in the Queens Medical Research Institute of the University of Edinburgh. The studies were performed with the written informed consent of all participants.

2.2.1. 18F-Fluoride and 18F-FDG in Aortic Stenosis

Patients aged >50 years with aortic sclerosis and mild, moderate or severe aortic stenosis attending the outpatient department of the Royal Infirmary of Edinburgh were considered for participation in this prospective cohort study, alongside age- and sex-matched control subjects, as described previously.(2,164) Exclusion criteria were insulin-dependent diabetes mellitus, blood glucose >200 mg/dL, end-stage renal failure (estimated glomerular filtration rate <15 ml/min), life expectancy of <2 years, metastatic malignancy, and inability to undergo PET/CT scanning. In the prospective cohort, an additional exclusion condition included planned aortic valve surgery (and therefore symptoms attributed by their physician to their valve disease). In addition, for the purposes of a histological validation of PET findings patients with severe symptomatic aortic stenosis under evaluation for surgical aortic valve replacement were considered for PET/CT imaging pre-operatively. Intra-operatively the resected aortic valve tissue was retained for histological examination and autoradiography. Patients were not approached if they fulfilled any of the exclusion criteria or if their clinician felt participation was not appropriate. Control subjects were selected on an age- and sex-matched basis with a structurally normal aortic valve and similar degree of co-morbidity.

2.2.2. 18F-Fluciclatide in Myocardial Infarction and Aortic Atherosclerosis

PET/CT scanning with 18F-fluciclatide and CMR were performed in participants recruited from Royal Infirmary of Edinburgh. Exclusion criteria were age <40 years, women of childbearing potential not taking contraception, severe renal failure (serum creatinine >2.8 mg/dL) or hepatic failure (Childs-Pugh grade B or C), atrial fibrillation, contrast allergy, inability to undergo scanning and inability to provide informed consent. Patients were not approached if they fulfilled any of the exclusion criteria, showed evidence of clinical instability or if the designated clinical team felt participation was not appropriate. The following 4 groups of participants were considered:

- *Acute MI group.* Patients with recent acute ST-segment elevation MI and peak high-sensitivity cardiac troponin I (hs-cTnI) >10,000 ng/L treated at the Royal Infirmary of Edinburgh.
- *Chronic Total Occlusion (CTO) group.* Patients with an angiographically-documented complete occlusion of a major epicardial artery and stable cardiac symptoms for >6 months.
- *Control group.* Healthy volunteers with normal left ventricular systolic function, no structural heart disease, and no symptoms of heart failure or MI underwent a single PET/CT with 18F-fluciclatide and CMR.

- *Aortic Stenosis group.* Patients with aortic sclerosis and mild, moderate and severe aortic stenosis attending the outpatient department of the Royal Infirmary of Edinburgh.

2.2.3. 18F-Fluciclatide histological validation studies

For *ex vivo* histological validation studies, two groups of patients were considered. These patients did not undergo 18F-fluciclatide PET/CT imaging:

- *Myocardial biopsy group*. Patients with large ST-elevation MI (<14 days, hs-cTnI >10,000 ng/L) scheduled to undergo coronary artery bypass grafting at the Royal Infirmary of Edinburgh were considered for intra-operative myocardial biopsy.
- *Carotid endarterectomy group.* Patients with a recent TIA or minor ischemic stroke and a high grade internal carotid artery stenosis (≥50% by NASCET (North American Symptomatic Carotid Endarterectomy Trial) criteria for men, ≥70% for women) scheduled to undergo carotid endarterectomy (CEA) were considered for retention of endarterectomy samples.(192)

2.3. Ethical considerations

All studies gained ethical approval from the South East Scotland Research Ethics Committee and were conducted in accordance with the Declaration of Helsinki of the World Medical Association. Administration of the radiopharmaceutical was approved by the Administration of Radioactive Substance Advisory Committee, United Kingdom. The studies were registered on www.clinicaltrials.gov (reference numbers NCT01358513, NCT01813045 and NCT01837160). Written informed consent was obtained for all patients.

2.4 Positron Emission Tomography and Computed Tomography

For each patient enrolled in to the PET/CT studies, combined PET/CT scans of the thorax were performed using a hybrid scanner (Biograph mCT, Siemens Medical Systems, Erlangen, Germany). On arrival in the CRIC all following study procedures were reviewed and opportunities for study withdrawal at any stage were clearly emphasised. Patient height and weight were measured on a consistent set of scales, calibrated to the PET scanner. An intravenous cannula was inserted and 30 mls of blood drawn. Clinical assessment was performed including clinical examination, measurement of blood pressure and pulse rate and 12-lead electrocardiography. Bloods were sent for measurement of full blood count, urea and electrolytes, serum calcium, phosphate and alkaline phosphatase. Serum C-reactive protein concentration was measured using the MULTIGENT CRP Vario assay on the ARCHITECT system (Abbott Laboratories, Abbott Park, IL, USA). The remainder was centrifuged at room temperature (10 minutes, 3000rpm) and serum was aliquoted and stored in event of future use at -70 degrees Celsius. Patients were then transferred to the lead lined uptake room where video surveillance was performed throughout. Patients rested on phlebotomy couches for the duration of radiotracer uptake. Toileting facilities with restricted access to the general public and other staff members were in close proximity and patients were encouraged to bring reading material with them. A proportion of patients underwent dynamic PET acquisition from the moment of IV radiotracer administration. Following PET/CT scanning, patients were allowed to leave the department under instruction to avoid close physical contact with babies or pregnant

females for the remainder of the day. Standardised pre-scan procedures and image acquisition varied for each radiotracer studied and are described below. Although additional 18F-fluoride and 18F-FDG PET/CT scans were performed for the purposes of the histological validation study, the imaging protocols for the 'Ring of Fire' study are well validated, have been described previously (2,60,164) and will be discussed in brief.

2.4.1. 18F-Fluoride PET/CT

18F-Fluoride tracer was synthesized in the Clinical Research Imaging Centre by radiopharmaceutical staff and administered intravenously to the patient in the uptake room. A target dose of 125 MBq was delivered with precautions taken to minimize radiation exposure to the operator. Patients rested in the quiet environment of the uptake room for 60-minutes before being transferred to the PET scanner. Patients lay supine with their hands above their head and 3-lead ECG monitoring was attached to permit ECG-gating. An attenuation correction CT scan (non-enhanced low-dose 120 kV and 50 mAs, pitch 0.8, field of view 780mm, 5mm slice thickness, 3mm increment, B19f LowDose kernel, standard filtered back projection reconstruction algorithm) was performed followed by PET imaging covering two bed positions centered over the heart in 3-dimensional mode for 10 min. Immediately after PET acquisition an ECG-gated breath-hold cardiac CT scan (non enhanced, 40 mAs/rot [CareDose], 100 kV, Pitch 0.24, field of view 210mm, 3mm slice thickness, 1.5mm increment, B35f kernel, standard filtered back projection reconstruction algorithm) was performed for calculation of the aortic valve calcium scores. Under standardized acquisition protocols the mean radiation dose for each 18F-fluoride PET scan was 2.9±0.1mSv (range 2.8-3.1mSv). The mean attenuation correction CT acquisition radiation dose was 1.0 ± 0.4mSv (range 0.5-1.8mSv) and CT calcium scoring scan dose 1.3±0.5 mSv.

2.4.2. 18F-FDG PET/CT

The 18F-FDG tracer was synthesized in the Clinical Research Imaging Centre by radiopharmaceutical staff and administered intravenously to the patient in the uptake room. A target dose of 200 MBq 18F-FDG was injected and patients rested in the uptake room for 90 min. Patients were then transferred to the PET scanner in a similar manner but without ECG gating. Combined PET/CT imaging was then performed as described for the 18F-fluoride scan but over an acquisition period of only 15min. The duration of radiotracer uptake for 18F-fluoride and 18F-FDG was based on previous cardiovascular PET studies and aimed to allow for optimal contrast between the aortic valve and blood pool.(49,193,194)

Due to the high metabolic requirements of cardiomyocytes, 18F-FDG is naturally sequestered within the left ventricle in cardiomyocyte uptake, leading to significant spillover of PET signal into adjacent structures. While certain diagnostic applications of 18F-FDG PET may utilize this, aortic valve imaging requires suppression of this uptake. All patients undergoing 18F-FDG imaging were asked to observe a carbohydrate-free diet for 24 hours prior to their 18F-FDG scan to switch cardiomyocytes from a glucose to free-fatty acid metabolism.(54,195) Patients were provided with a list of food and drink to avoid. Adequate myocardial tracer uptake was then assessed during image analysis by measuring the maximum standardised uptake value (SUV, *kBq/mL*) in the LV septum. The SUV is a semiquantitative unit of radiotracer activity within the tissue of interest that is corrected for both isotope decay and the injected dose per body weight. It is a widely used and validated measure of

tissue radiotracer uptake.(196) Low myocardial 18F-FDG uptake was derived as an SUV value <5.0 kBq/mL uptake, indicating successful myocardial suppression. Inadequately suppressed myocardial uptake was defined by measurements ≥5.0 kBq/mL.(197) Under standardized acquisition protocols the mean radiation dose for each 18F-FDG PET/CT scan was 4.9±0.5 mSv.

2.4.3. 18F-Fluciclatide PET/CT

18F-Fluciclatide was manufactured at the Clinical Research Imaging Centre on an automated module (FASTlab synthesiser; GE Healthcare) by coupling an amino-oxy-functionalized peptide precursor (AH111695) with 4-18F-fluorobenzaldehyde at pH 3.5 to form 18F-fluciclatide. A full description of this synthesis has been published previously. (117,190,198) Subjects were administered a target dose of 230 MBq. To assess 18F-fluciclatide cardiovascular pharmacodynamics and the optimum timing of PET scanning following radiotracer administration, dynamic PET imaging of the thorax was performed in the first 20 subjects in 3-dimensional mode with a single bed position for 70 min. These patients received radiotracer administration within the scanner simultaneous to initiating PET acquisition. The remainder of study subjects underwent static imaging performed at the optimal time point (40 min post-injection) using a single 30-min bed position in list mode. An attenuation-correction CT scan (non-enhanced 120 kV and 50 mA, 3-mm slices) was performed prior to PET acquisition, and electrocardiographic (ECG) gating was performed throughout. Under standardized acquisition protocols the mean radiation dose for each 18F-fluciclatide

PET scan was 5.9 mSv (range 5.2-6.4 mSv). The mean attenuation correction CT acquisition radiation dose was 1.4 mSv (range 0.8-1.9 mSv).

To enable an accurate definition of cardiac anatomy cardiac CT angiography was performed on the hybrid scanner immediately after the PET acquisition. If necessary and clinically appropriate, 5 mg intravenous metoprolol was administered in patients with a heart rate of greater than 60 beats/min. For the acquisition, the following settings were used: 330 ms rotation time, 100 (body mass index <25 kg/m^2) or 120 (body mass index >25 kg/m^2) kV tube voltage, 160-245 mAs tube current, 3.8 mm/rotation table feed, prospective (heart rate regular and <60 /min), or retrospective (heart rate >60 /min) electrocardiogram-gated. Depending on the body mass index, a bolus of 80-100 mL contrast (400 mgI/mL; Iomeron, Bracco, Milan, Italy) was injected intravenously at 5 mL/s, after determining the appropriate trigger delay with a test bolus of 20 mL contrast material. Cardiac CT contrast angiography dosing was 6.7mSv (range 2.1-11.7 mSv); the wide dose range accounted for the potential presence of atrial fibrillation that prevents prospective ECG gating.

2.5 Image Reconstruction and Analysis

2.5.1. Image reconstruction

The PET data were reconstructed using the Siemens Ultra-HD (time of flight +True X) reconstruction algorithm. Corrections were applied for attenuation, dead time, scatter and random coincidences. All image analysis was performed on fused PET/CT data sets. For 18F-FDG and 18F-fluoride scans, the field of view was 780mm and a 512 matrix size was used for reconstructions so the voxel size was 1.5 × 1.5 × 3.0mm.

For the static gated 18F-fluciclatide imaging datasets, ECG-gated PET images were reconstructed in diastole (40-70 min post-injection, 50–75% of the R-R interval) using the Ultra-HD algorithm in 2 iterations, 24 subsets with zoom of x2 and 200 pixels. For the kinetic analysis of 18F-fluciclatide scans, the dynamic PET data were reconstructed with the Ultra-HD algorithm, in 2 iterations, 21 subsets, 256 pixels and 1.6-mm pixel size. Using a dynamic protocol without ECG gating, following time frames were applied; 60s x 5, 120s x 5, 180s x 5, 300s x 8.

2.5.2. Image Analysis

Anonymised PET image datasets were analysed by experienced observers blinded to the clinical details using an OsiriX workstation (OsiriX version 6.0 64-bit; OsiriX Imaging Software, Geneva, Switzerland). The PET images were fused with CT or contrast CT datasets and regions of interest (ROI's) were drawn within the tissues of interest. (2,6,48,60,161,164) The mean and maximum SUV measurements from each ROI were collated in each tissue of interest to derive a mean measure of radiotracer accumulation corrected for residual blood pool activity within the superior vena cava (SVC). Specifically, quantification of aortic valve PET uptake was performed on modified co-axial views of the non-contrast fused PET/CT datasets (Figure 2.1), while myocardial 18F-fluciclatide uptake was quantified on modified co-axial views of the left ventricle using contrast-enhanced CT/PET, both by delineating regions of myocardial infarct confirmed on cardiac MRI, and additionally by segmenting the myocardium into a standardised 16-segment model (Figure 2.2). Aortic 18F-fluciclatide uptake was quantified using non-contrast CT/PET images in the axial views (Figure 2.3).

Kinetic analysis was undertaken on the dynamic PET data to examine the mechanisms of uptake of 18F-fluciclatide within the myocardium and vasculature. ROI's drawn in the tissue of interest were used to derive time-activity curves after decay correction. An input function calculation based on the PET image–derived activity curve from the aorta blood pool (199) and the myocardial time-activity curve were used to estimate the tissue influx rate K_i (the slope of the linear regression) and the volume of

distribution (the *y*-axis intercept) using a 2-tissue irreversible Patlak model.(9,10) Thoracic 18F-fluciclatide dynamic activity was then normalized for the blood-pool input function on a voxel-by-voxel basis, and after 3D Gaussian filtering (5-mm FWHM) a parametric 3-dimensional image of 18F-fluciclatide uptake was generated (PMod version 3.409, Pmod technologies limited, Switzerland). Using this image, regions of 18F-fluciclatide binding were identified and manually delineated for subsequent *K*i analysis.

Figure 2.1. Quantifying radiotracer uptake within the aortic valve

*18F-Fluoride and 18F-FDG valvular uptake was quantified by re-orientating the sagittal **(A)** and coronal **(B)** views to create a modified co-axial view of the aortic valve **(C)**. The PET dataset was then re-registered into this plane **(D)** and fused with the CT **(E)**. Regions of interest around the aortic valve were drawn **(F)** to calculate standardized uptake values.*

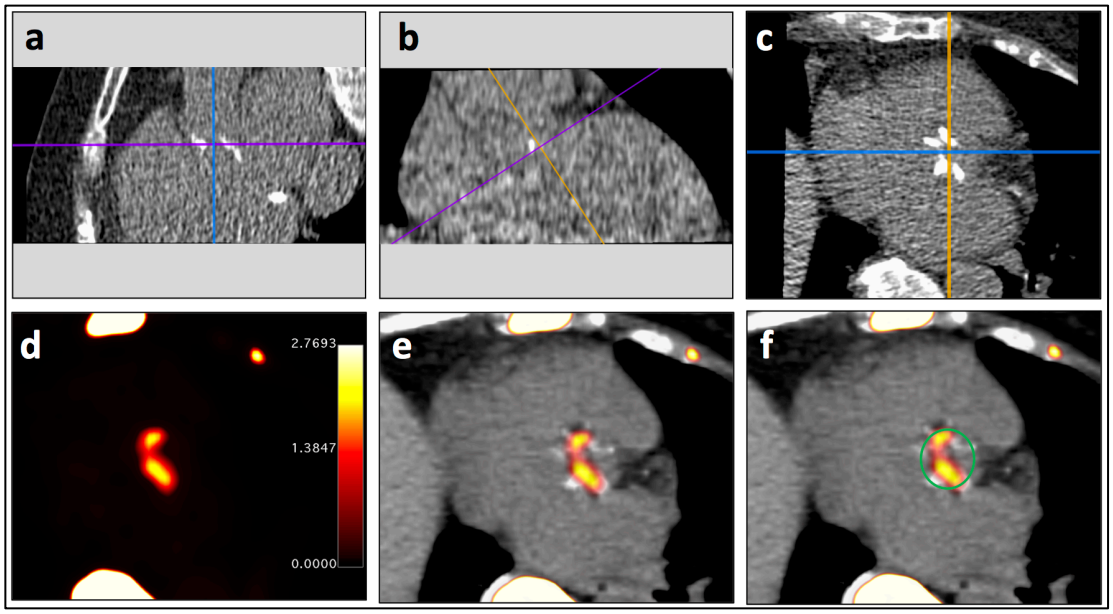

Figure 2.2. Assessment of myocardial 18F-fluciclatide uptake.

For quantification of myocardial 18F-fluciclatide uptake, the sagittal and axial planes of the CT coronary angiogram (CTCA) ***(A)*** *were reorientated to provide a short axis view of the left ventricle (****B****) that corresponds to the views obtained from late gadolinium enhancement (LGE) imaging during cardiac MRI (****C****). 18F-Fluciclatide PET datasets were re-registered to the short axis CTCA images (****D****) and fused to create a PET/CTCA image* ***(E).*** *Assisted by the location of myocardial infarct on LGE imaging (****i****), we can delineate the regions of myocardial infarct (****ii****; anterior, anteroseptal and inferoseptal segments) and remote myocardium (****iii****; basal lateral and inferolateral segments) (****F****) to calculate standardized uptake values.*

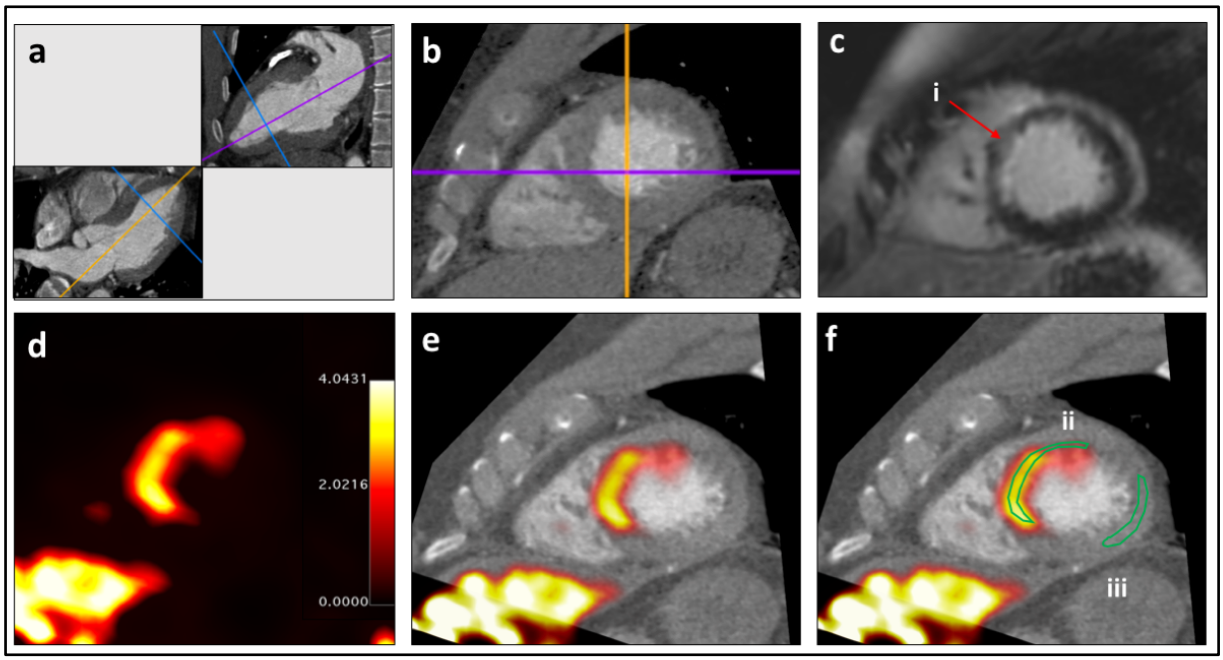

Figure 2.3. Assessment of aortic 18F-Fluciclatide uptake

*In this illustration, we can identify regions of calcified and non-calcified atheroma within the descending aorta on the axial CTCA images (**A**). By manually drawing regions of interest along the adventitial border of the aorta on the attenuation CT (**B**), we both calculated CT calcium scores (**C**) and applied them to the PET image to derive the standardised uptake values (**D**).*

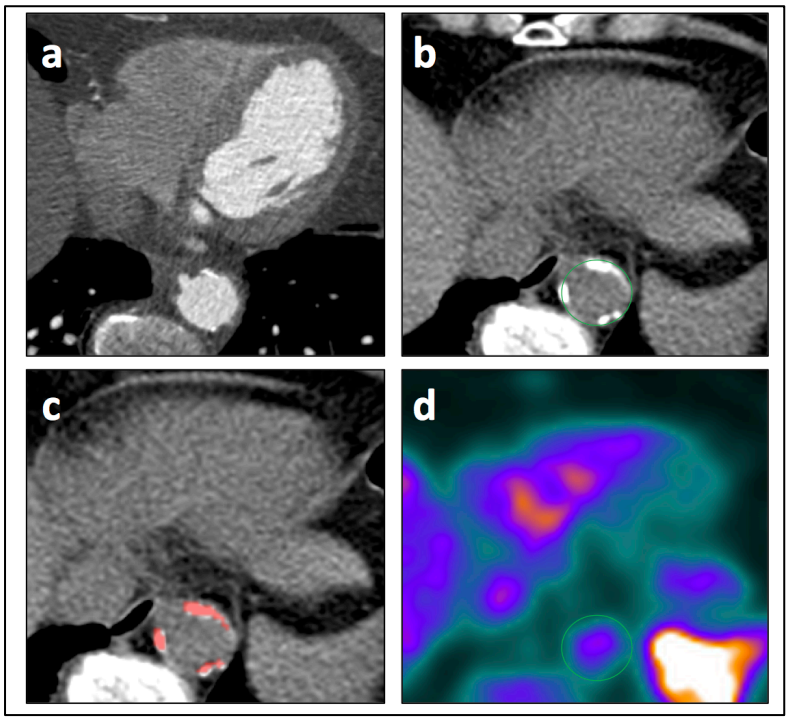

2.6. PET Repeatability Studies

The reproducibility of the quantification of aortic valvular 18F-FDG and 18F-fluoride uptake has been previously reported.(2) Each analysis favoured a method re-orientating the PET/CT images into a modified-coaxial plane, providing a short-axis view of the aortic valve, left ventricular outflow tract (LVOT) and ascending aorta. Briefly, quantification of 18F-fluoride valvular uptake (TBR_{mean}) displayed excellent reproducibility. There were no fixed or proportional biases, and the majority of data fell within narrow limits of agreement (±0.20). Intraclass coefficients for interobserver and intraobserver repeatability were all >0.95.

The reproducibility of 18F-FDG valvular uptake quantification was impacted by potential spillover of PET signal from adjacent myocardium, necessitating the use of smaller regions of interest limited to the central portion of the valve. This was termed the 'center-valve technique', and demonstrated no fixed or proportional biases in the differences between interobserver and intraobserver measurements with narrow limits of agreement (<±0.20). Intraclass coefficients were all >0.90, indicating excellent agreement.(2)

All repeatability studies in this thesis were performed with the observers blinded to identifying data within the PET datasets using cloaking programs within the image analysis software, with the assistance of study investigators. Similarly, in histological repeatability studies the assessor was blinded to any identifiable information by a separate study investigator.

The intraobserver and interobserver reproducibility of myocardial 18F-fluciclatide uptake quantification was assessed by two experienced observers (Dr. William Jenkins, Dr. Catriona Moles) in both the blood pool and the myocardium in 10 subjects selected at random. Residual blood pool radiotracer activity was quantified within both the SVC and right atrium.

For the assessment of aortic 18F-fluciclatide uptake, datasets from 10 randomly selected subjects were assessed independently by two experienced observers (Dr. William Jenkins and Dr. Anna Vickers) and the inter-observer reproducibility of 18F-fluciclatide SUV and TBR measurements assessed.

2.7. Histological Validation Studies

2.7.1. Overview

In order to determine the validity of the imaging observations made during these studies we applied a number of histological techniques in valvular, myocardial and vascular tissue. The histological analyses were performed by study investigators (Dr William Jenkins, Dr Marc Dweck and Dr Alexander Vesey) under the guidance and tuition of the Queens Medical Research Institute histopathology director (Dr Mike Miller) with support of Consultant Pathologists Dr William Wallace and Professor Donald Salter. Specifically we assessed for *ex vivo* evidence of calcification (tissue-specific alkaline phosphatase [TNAP], osteocalcin, von kossa stain), inflammation (CD68), fibrogenesis (smooth muscle actin [SMA]), angiogenesis (CD31) and the presence of integrin $\alpha_v\beta_3$ antibody.

Calcification is the key propagator of calcific aortic valve disease, and was studied histologically using measures of calcification activity (TNAP, osteocalcin) and established calcification (von Kossa staining). The enzyme TNAP is a key regulator of the availability of extracellular pyrophosphate, and its expression leads to a reduction in the inhibition of biomineralisation.(200) Osteocalcin is a small protein secreted by osteoblasts and is an active modulator of VSMC cell signaling and osteochondrogenic differentiation. (201,202) The histological assessment of TNAP and osteocalcin has been associated with 18F-fluoride uptake in the vasculature. (6)

Von Kossa stain allows the identification of elemental phosphate (i.e. calcium orthophosphate) through a precipitation-reaction.

Inflammation is a key component of calcific aortic valve disease, atherosclerosis and myocardial remodeling.(17,203,204) The glycoprotein CD-68 is a expressed on activated macrophages, and its cellular staining has previously closely correlated with carotid uptake of 18F-FDG.(49)

The tissue detection of active fibrogenesis may be visualized histologically using staining for alpha-SMA (aSMA). Activated myofibroblasts that express the protein complex aSMA are key to the proliferative phase of scar formation within the myocardium(75,80) and as such, histological examination for aSMA-positive myofibroblasts provides a well validated measure of fibrogenesis. (205) Similarly, the CD31, or platelet endothelial cell adhesion molecule-1 (PECAM-1), is found in large quantities on the surface of activated vascular endothelial cells, and plays a major role in a number of cellular interactions during angiogenesis.(206)It is a well validated marker of angiogenesis activity and has been utilized both in the assessment of atherosclerosis and the healing response post-MI. (207,208)

2.7.2. Aortic Valve Histological Assessment

In the patients undergoing aortic valve replacement, the aortic valve was removed at the time of operation with care taken to preserve the integrity of the valve architecture. Samples were then fixed in 4% paraformaldehyde for 24 hours. Plaques were decalcified in ethylenediaminetetraacetatic acid for 10 days, embedded in paraffin and 5-μm sections prepared. Immunohistochemical staining for osteocalcin (anti-human mouse mAb ab13418, Abcam), CD68 (anti-human mouse clone PG-M1 m0876, DAKO) and tissue non-specific alkaline phosphatase (TNAP; anti-human rabbit pAb CAT#LF PA50004, Abfrontier) was then undertaken following heat-induced epitope retrieval (HIER) using a Citrate Buffer pH 6 (Novocastra Leica microsystems) in a decloaking chamber. Osteocalcin staining required no HIER. Sections were stained using a Leica Vision Biosystems Bond x immunostaining robot. After blocking in peroxide for 10 min, sections were incubated with the specific anti-human antibodies for 2 hours at room temperature at the following dilutions: osteocalcin 1:200, tissue non-specific alkaline phosphatase 1:100 and CD-68 1:100. All incubation steps were followed by washing in TBS/Tween. Sections for osteocalcin and CD68 were incubated for 15 min with pre-polymer/post primary followed by 15 min with polymer (HRP) for all antibodies prior to DAB (3,3'diaminobenzidine) visualization and haematoxylin counterstain. Sections were dehydrated in graded ethanol, cleared in xylene before cover slipping in Pertex.

Images were taken on a Zeiss Axioskop2 fitted with an Axiocam MRc digital camera using Axiovision software. Tissue cross-sectional area on each section was manually

delineated using Image Pro Plus 5 (Rockville, MD, USA). Immunohistochemical staining for osteocalcin and TNAP was identified by visual assessment and quantified using automated color-based segmentation by a trained observer blinded to the PET data. Staining was expressed as a percentage of the total valve area. Macrophage infiltration using CD68 was assessed using a similar approach but with an object size set threshold applied at 20 x 10 pixels, to limit counting to cell-sized objects. The density of cell staining in the valve tissue was expressed as cells per mm^2. This technique was also utilized to identify cellular staining for TNAP and osteocalcin.

Interobserver reproducibility of the immunohistochemical data was also investigated. Tissue staining with alkaline phosphatase, CD68 and osteocalcin was quantified in 5 valves independently by two trained observers (Dr William Jenkins, Dr Alex Vesey).

2.7.3. Aortic Valve Autoradiography

Clinical PET systems have limited resolution. In order to gain further information about the precise localization of the 18F-fluoride signal in aortic valve tissue, we undertook autoradiography. Non-decalcified valvular tissue was rapidly cooled in dry ice and then sectioned at 7-µm thickness using a cryostat (CM1520 Wetzlar, Germany). Sections for autoradiography were mounted on Superfrost slides (Gerhard Menzel, Braunschweig, Germany) before treatment with spray fixative. Sections were bathed in a solution of 18F-fluoride at a concentration close to *in vivo* imaging concentrations (1 kBq/mL) for 60 min and then rinsed with PBS. A freshly blanked phosphor screen was then placed over the slides and an overnight exposure undertaken. The screen was then read using a FujiFilm FLA-5100 Fluorescent Image Analyser (Raytek Scientific Limited, Sheffield, UK). Sections adjacent to those used for autoradiography were stained for elemental phosphate (i.e. calcium orthophosphate) using Von Kossa's stain, and following surface decalcification in situ with Von Ebner's solution, for TNAP and osteocalcin. Sections were then manually registered and examined for co-localization with 18F-fluoride signal.

2.7.4. Myocardial biopsy histological assessment

Myocardial biopsy samples were obtained from patients undergoing coronary artery bypass grafting following myocardial infarction. A core cardiac biopsy was taken intra-operatively under direct visualisation by an experienced surgeon from the peri-infarct zone. Samples were fresh frozen and mounted in cryosection medium. The tissue samples were then cut in sequential, longitudinal 4-µm sections at -20 °C and thaw-mounted onto microscope slides. They were dried for 15 min and spray-fixed with neutral buffered formalin. After rinsing in distilled water, sections were stained with hematoxylin-eosin (HE) and van-Gieson (VG) for conventional histopathological examination. In order to optimize immunohistochemistry, an antigen-unmasking step was performed by microwave treatment for 30 s. Endogenous peroxidase was blocked by incubation with hydrogen peroxide for 5 min. Sections were subsequently incubated with the primary antibodies; smooth muscle actin, CD31, CD68 (clone PG-M1), and integrin $\alpha_v\beta_3$ antibody, clone LM609 (Millipore) for 30 min at room temperature. After washing the sections were incubated with Envision Flex (DAKO, K5007) for 30 min at room temperature, followed by incubation with diaminobenzamine (Sigma) for 10 min. The slides were finally counterstained with hematoxylin and digitally imaged (Axioscan.Z1, Zeiss, UK) before assessment.

2.7.5. Carotid atheroma histological assessment

After obtaining informed consent, four human carotid intimal samples were obtained from patients undergoing carotid endarterectomy for symptomatic carotid artery atherosclerotic disease. Segments of dissected carotid atheroma were frozen in mounting medium. The tissue samples were then cut in sequential, longitudinal 4 μm and 20 μm slices sections at -20°C and thaw-mounted onto microscope slides. Effort was made to align segments of ruptured plaque alongside non-atheromatous segments within the same slide. The slides were then dried for 15 min and spray-fixed with neutral buffered formalin. After rinsing in distilled water the 4 μm sections were stained with hematoxylin-eosin (HE) and van-Gieson (VG) for conventional histopathological examination. In order to optimize immunohistochemistry, an antigen-unmasking step was performed by microwave treatment for 30 s. Endogenous peroxidase was blocked by incubation with hydrogen peroxide for 5 min. Sections were subsequently incubated with the primary antibodies; smooth muscle actin, CD31, CD68 (clone PG-M1), and integrin $\alpha_V\beta_3$ antibody, clone LM609 (Millipore) for 30 min at room temperature. After washing, the sections were incubated with Envision Flex (DAKO, K5007) for 30 min at room temperature, followed by incubation with diaminobenzamine (Sigma) for 10 min. The slides were finally counterstained with hematoxylin and digitally imaged (Axioscan.Z1, Zeiss, UK).

2.7.6. Carotid atheroma autoradiography

To gain more detailed information about the precise localization of 18F-fluciclatide binding in atherosclerotic tissue, we undertook autoradiography. The 20 μm frozen sections adjacent to those used for immunohistochemical analysis were warmed to room-temperature and bathed in a solution of 18F-fluciclatide at a concentration close to in vivo imaging concentrations (1 kBq/mL) for 60 minutes and then rinsed with phosphate buffer solution. An unlabeled highly concentrated solution of fluciclatide was added to selected slides in order to competitively bind to $\alpha_v\beta_3$ to assess for non-specific tracer uptake. A freshly blanked phosphor screen was then placed over the slides and an overnight exposure undertaken. The screen was read using a FujiFilm FLA-5100 Fluorescent Image Analyser (Raytek Scientific Limited, Sheffield, UK). Sections were then manually registered and examined for co-localization with histological markers of atherosclerotic disease activity.

2.8. Cardiac MRI

Cardiac MRI was performed at 3 T (MAGNETOM Verio, Siemens AG, Healthcare Sector, Erlangen, Germany), within the Clinical Research Imaging Centre, University of Edinburgh. For the sake of patient convenience, great effort was made to ensure patients received MRI scanning on the day of PET/CT imaging. For the assessment of left ventricular function, short-axis cine images from the mitral valve annulus to the apex were obtained using a balanced steady-state free-precession sequence (8-mm parallel slices with 2-mm spacing). Quantification of left ventricular function and volumes indexed to body surface area was assessed with dedicated software (Siemens AG Healthcare Sector, Erlangen, Germany). Regional systolic function assessments were performed from the basal, mid, and apical short-axis slices by calculating the end-diastolic and end-systolic wall thicknesses and expressed as the wall motion score index (WMSI; 0, normal; 1, mild or moderate hypokinesia; 2, severe hypokinesia; 3, akinesia; 4, dyskinesia).(95) The assessment of focal replacement myocardial fibrosis was performed with late gadolinium enhancement (LGE) imaging, 15 min after administration of 0.1 mmol/kg gadobutrol (Gadovist/Gadavist, Bayer Pharma AG, Berlin, Germany). An inversion recovery fast gradient-echo sequence was applied to the left ventricular short-axis stack with the inversion time optimized to achieve satisfactory nulling of the myocardium. The amount of LGE was quantified with QMASS software (Medis Medical Imaging Systems, Leiden, the Netherlands) using a signal intensity threshold greater than twice the standard deviation above the mean value in a normal region of myocardium sampled on the same short-axis image. The transmural extent of infarction within each segment was classified using a

transmurality score (transmurality index; 0, no LGE; 1, 1-50%; 2, 51-75% or 3, 76-100%) and recorded as either subendocardial (1-2) or transmural (3).(209) Areas thought to represent inversion artefact or blood pool contamination were manually excluded. Myocardial extracellular volume fraction (ECV) has been demonstrated to act as a measure of myocardial fibrosis in a variety of cardiac conditions.(210,211) Recently, our group has described a highly reproducible standardized approach to analyze myocardial ECV.(212) Briefly, myocardial T1 mapping was performed in the mechanism cohort using the modified look-locker inversion recovery sequence: flip angle, 35°; minimum TI, 100 ms; TI increment, 80 ms; and time delay, 150 ms with a heartbeat acquisition scheme of 3-3-5.(213) Regions of interest were drawn around the myocardium on the short-axis, pre-contrast, motion-corrected myocardial T1 maps and copied onto corresponding 20-min post-contrast maps, with minor adjustments made to avoid partial volume effects and artifact (OsiriX version 4.1.1, Geneva, Switzerland). ECV was calculated according to the following formula:

$$ECV=(\Delta R1_{myocardium}/\Delta R1_{blood\text{-}pool}) \times(1-hematocrit)$$

where:

$$\Delta R1=(1/postcontrast\ T1-1/precontrast\ T1).$$

Hematocrit was sampled at the time of MRI.(214)

2.9. Statistical Analysis

Specific statistical analysis has been described in each chapter. Statistical analysis was performed with Graph Pad Prism version 6 (GraphPad Software Inc., California USA), JMP version 10.0 (SAS Software, North Carolina, USA) or SPSS 19.0 (SPSS Inc., Chicago, Illinois) where appropriate. Continuous data were assessed for normality visually and using the D'Agostino-Pearson omnibus test. Parametric variables were expressed as mean ± standard deviation and compared using Student's t-tests or repeat measure one-way ANOVA. Non-parametric data were presented as median [interquartile range] and compared with Mann-Whitney test or Wilcox matched-pairs signed rank where appropriate. Reproducibility was estimated using the Bland Altman method and presented as mean bias ± 2 standard deviation and intra-class correlation coefficients.(215) A two-sided $P<0.05$ was taken as statistically significant.

Chapter 3.

18F-Fluoride uptake is a marker of active calcification and disease progression in patients with aortic stenosis

Published by Jenkins WS*, Dweck MR*, Vesey AT, Pringle MA, Chin CW, Malley TS, Cowie WJ, Tsampasian V, Richardson H, Fletcher A, Wallace WA, Pessotto R, van Beek EJ, Boon NA, Rudd JH, Newby DE. 18F-NaF uptake is a marker of active calcification and disease progression in patients with aortic stenosis. Circulation; Cardiovascular Imaging. 2014 Mar;7(2):371-8.

*Denotes equal contribution

3.1 Overview

18F-Fluoride and 18F-fluorodeoxyglucose (18F-FDG) are promising novel biomarkers of disease activity in aortic stenosis. We compared 18F-fluoride and 18F-FDG uptake with histological characterization of the aortic valve and assessed whether they were associated with disease progression.

Thirty patients with aortic stenosis underwent combined positron emission and computed tomography (PET/CT) using 18F-fluoride and 18F-FDG radiotracers. In 12 patients undergoing aortic valve replacement surgery (10 for each tracer), radiotracer uptake (mean TBR) was compared to CD68 (inflammation), alkaline phosphatase and osteocalcin (calcification) immunohistochemistry of the excised valve. In 18 patients (6 aortic sclerosis; 5 mild, 7 moderate), aortic valve CT calcium scoring was performed at baseline and after 1 year.

Aortic valve 18F-fluoride uptake correlated with both alkaline phosphatase ($r=0.65$, $P=0.04$) and osteocalcin ($r=0.68$, $P=0.03$) immunohistochemistry. There was no significant correlation between 18F-FDG uptake and CD68 staining ($r=-0.43$, $P=0.22$). After 1 year, aortic valve calcification increased from 314 (193-540) to 365 (207-934) Agatston units ($P<0.01$). Baseline 18F-fluoride uptake correlated closely with the change in calcium score ($r=0.66$, $P<0.01$) and this improved further ($r= 0.75$, $P<0.01$) when 18F-fluoride uptake overlying CT-defined macrocalcification was excluded. No significant correlation was noted between valvular 18F-FDG uptake and change in calcium score ($r=-0.11$, $P=0.66$).

In conclusion, valvular 18F-fluoride uptake identifies active tissue calcification and is associated with disease progression in patients with calcific aortic stenosis.

3.2 Introduction

The mechanisms underlying aortic stenosis remain incompletely understood and the accurate prediction of disease progression remains a challenge.(14) Calcification and inflammation are believed to play key pathophysiological roles. Indeed, the amount of established calcium in the valve correlates with disease severity and predicts future adverse cardiovascular events.(38,39,216) Whilst computed tomography and echocardiography can provide measures of established valvular calcification, they cannot directly assess ongoing calcification activity, which is considered to be the main driver of disease progression.

Recent reports have investigated two positron emission tomography (PET) radiotracers, 18F-fluoride (18F-NaF) and 18F-fluorodeoxyglucose (18F-FDG), as measures of calcification activity and inflammation respectively in the aortic valve,(2) coronary arteries(6,164) and major vessels.(49,193) 18F-FDG PET has become a widely used tool for the assessment of inflammation in the aorta and carotid arteries with uptake correlating with macrophage burden.(47) Several studies have investigated its uptake in aortic stenosis although histological validation is lacking.(2,53) 18F-Fluoride has been used as a bone tracer for over 40 years, displaying increased activity in conditions associated with increased bone metabolism such as Paget's disease. In bone, it is believed to bind and then incorporate into exposed hydroxyapatite crystals, via an exchange mechanism with hydroxyl groups to form fluoroapatite. Given that hydroxyapatite is also a key structural component of calcification in the aortic valve and vascular atheroma, it is presumed that similar

mechanisms explain its accumulation in these tissues. However, this remains hypothetical. The principal aims of the present study were therefore to validate the use of 18F-fluoride and 18F-FDG in aortic stenosis by comparing *in vivo* radiotracer uptake with immunohistochemistry of calcification and inflammation in excised valvular tissue, and to investigate whether either of these agents may be associated with disease progression over 1 year.

3.3 Methods

3.3.1 Patient Populations

Two cohorts of patients with aortic stenosis were recruited into this study: (i) 12 patients undergoing valve replacement surgery, and (ii) 18 patients with asymptomatic disease under surveillance at the Edinburgh Heart Centre. The latter cohort were randomly selected for repeat scanning from a larger, previously described population who underwent baseline PET imaging.(2,60,164)

All patients were aged >50 years and exclusion criteria included a normal aortic valve, insulin-dependent diabetes mellitus, end-stage renal failure, life expectancy of <2 years, and metastatic malignancy. Patients with severe AS were excluded from the cohort of patients under surveillance because of the potential for disease progression and symptom development before the follow up 1-year scan. The study was performed in accordance with the Declaration of Helsinki and after local research ethics committee approval. All patients provided written informed consent before participating. This study was registered with the clinical trials unique identifier NCT01358513.

3.3.2 Baseline Assessment

All patients underwent full clinical assessment at baseline and aortic stenosis severity was assessed using Doppler and two-dimensional echocardiography by means of the peak transvalvular velocity, mean gradient and aortic valve area according to American Heart Association/American College of Cardiology guidelines.(217) Aortic sclerosis was defined as thickening of the aortic valve cusps in the absence of accelerated flow (<2 m/s) through the valve. Combined positron emission and computed tomography (PET/CT) scans of the aortic valve were performed using a hybrid scanner (Biograph mCT, Siemens Medical Systems, Erlangen, Germany) 60 min after administration of 125 MBq of 18F-fluoride. Subsequently a second PET/CT scan was performed using the same hybrid scanner 90 min following administration of 200 MBq of 18F-FDG. The total effective radiation dose from study participation was 9.73±1.19mSv: 18F-Fluoride (3.8±0.3 mSv) and 18F-FDG (4.9±0.5 mSv) PET-CT, and calcium score (1.3±0.5 mSv). Glucose is a major energy source of the myocardium, so that intense 18F-FDG uptake frequently occurs, spilling over and contaminating the signal in the valve. We attempted to reduce myocardial uptake by asking patients to avoid carbohydrates for 24 hours prior to their 18F-FDG scan, thereby switching the myocardium from glucose to free fatty-acid metabolism. Myocardial 18F-FDG uptake was assessed within regions of interest placed in the basal septum of the left ventricle and classified as being adequately suppressed if mean SUV values were <5.0.(2) An ECG-gated breath-hold CT scan (non-contrast enhanced, 40 mA/rot [CareDose], 100 kV) was performed for calculation of the aortic valve calcium score using dedicated analysis software (VScore, Vital Images,

Minnetonka, USA) on axial scans.(35) Particular care was taken to differentiate valvular calcium from that in the aortic root and mitral valve annulus. At one-year follow up, patients in the surveillance cohort underwent repeat clinical assessment and CT calcium scoring using the same protocol.

3.3.3 Quantification of Aortic Valve PET activity

18F-Fluoride and 18F-FDG uptake in the aortic valve was quantified using an Osirix workstation (OsiriX version 3.5.1 64-bit; OsiriX Imaging Software, Geneva, Switzerland) as reported previously.(2,6) Briefly, fused PET-CT images were re-orientated into the plane of the valve and circular regions of interest (ROIs) drawn on adjacent 3-mm slices until the entire valve had been examined. For 18F-fluoride, ROIs were placed around the perimeter of the valve whilst excluding the aortic root (whole-valve technique). In order to reduce the potential for myocardial 18F-FDG activity contaminating the aortic valve signal, ROIs for this tracer were drawn in the center of the valve as previously described (center-valve technique).(2,53) Within these ROIs, mean standard uptake values (SUV) were calculated for each slice, averaged and corrected for blood pool activity to provide mean tissue-to-background ratios (TBRs). Mean TBRs were selected prospectively for subsequent comparisons with histology and disease progression as this measure was felt to best represent tracer uptake across the valve as a whole.

Distribution of 18F-fluoride in the aortic valve relative to calcium scoring

We undertook a voxel-by-voxel analysis comparing the distribution of calcium on CT with 18F-fluoride uptake. Regions of interest were drawn around the valve, and each voxel was assessed for the presence of calcium (>130 HU) and increased 18F-fluoride uptake (TBR max >1.97, based upon the highest uptake in the control cohort of our previous study (2)) using dedicated software MATLAB® (Mathworks inc.,

Massachusetts USA). We hypothesized that regions of completely novel calcium development might have an even more important impact upon disease progression and we therefore calculated the percentage of the valve with increased radiotracer uptake in the absence of underlying calcium on CT (% of PET positive but CT negative pixels).

3.3.4 Histological Assessment

In the patients undergoing aortic valve replacement, the aortic valve was removed at the time of operation with care taken to preserve the integrity of the valve architecture. Samples were then fixed in 4% paraformaldehyde for 24 hours. Plaques were decalcified in ethylenediaminetetraacetatic acid for 10 days, embedded in paraffin and 5-μm sections prepared. Immunohistochemical staining for osteocalcin (anti-human mouse mAb ab13418, Abcam), CD68 (anti-human mouse clone PG-M1 m0876, DAKO) and tissue non-specific alkaline phosphatase (TNAP; anti-human rabbit pAb CAT#LF PA50004, Abfrontier) was then undertaken following heat-induced epitope retrieval (HIER) using a Citrate Buffer pH 6 (Novocastra Leica microsystems) in a decloaking chamber. Osteocalcin staining required no HIER. Sections were stained using a Leica Vision Biosystems Bond x immunostaining robot. After blocking in peroxide for 10 min, sections were incubated with the specific anti-human antibodies for 2 hours at room temperature at the following dilutions: osteocalcin 1:200, tissue non-specific alkaline phosphatase 1:100 and CD-68 1:100. All incubation steps were followed by washing in TBS/Tween. Sections for osteocalcin and CD68 were incubated for 15 min with pre-polymer/post primary followed by 15 min with polymer (HRP) for all antibodies prior to DAB (3,3'-diaminobenzidine) visualization and haematoxylin counterstain. Sections were dehydrated in graded ethanol, cleared in xylene before cover slipping in Pertex.

Images were taken on a Zeiss Axioskop2 fitted with an Axiocam MRc digital camera using Axiovision software. Tissue cross-sectional area on each section was manually delineated using Image Pro Plus 5 (Rockville, MD, USA). Immunohistochemical

staining for osteocalcin and TNAP was identified by visual assessment and quantified using automated color-based segmentation by a trained observer blinded to the PET data. Staining was expressed as a percentage of the total valve area. Macrophage infiltration using CD68 was assessed using a similar approach but with an object size set threshold applied at 20 x 10 pixels, to limit counting to cell-sized objects. The density of cell staining in the valve tissue was expressed as cells per mm^2. This technique was also utilized to identify cellular staining for TNAP and osteocalcin.

Reproducibility Studies

Interobserver reproducibility of the immunohistochemical data was investigated. Tissue staining with alkaline phosphatase, CD68 and osteocalcin was quantified in 5 valves independently by two trained observers (Dr William Jenkins, Dr Alex Vesey).

3.3.5 Autoradiography

Clinical PET systems have limited resolution. In order to gain further information about the precise localization of the 18F-fluoride signal in aortic valve tissue, we undertook autoradiography. Non-decalcified valvular tissue was rapidly cooled in dry ice and then sectioned at 7-µm thickness using a cryostat (CM1520 Wetzlar, Germany). Sections for autoradiography were mounted on Superfrost slides (Gerhard Menzel, Braunschweig, Germany) before treatment with spray fixative. Sections were bathed in a solution of 18F-fluoride at a concentration close to *in vivo* imaging concentrations (1 kBq/mL) for 60 min and then rinsed with PBS. A freshly blanked phosphor screen was then placed over the slides and an overnight exposure undertaken. The screen was then read using a FujiFilm FLA-5100 Fluorescent Image Analyser (Raytek Scientific Limited, Sheffield, UK). Sections adjacent to those used for autoradiography were stained for elemental phosphate (i.e. calcium orthophosphate) using Von Kossa's stain, and following surface decalcification in situ with Von Ebner's solution, for TNAP and osteocalcin. Sections were then manually registered and examined for co-localization with 18F-fluoride signal.

3.3.6 Statistical methods

Continuous variables were assessed for normality both visually and using the D'Agostino-Pearson test. Variables were expressed as either mean ± standard deviation or median with interquartile ranges subject to whether they approximated a normal distribution. Categorical data were presented as n (%). The 95% normal range for differences between sets of immunohistochemical measurements (the limits of agreement) were estimated using Bland-Altman analysis by multiplying the standard deviation of the mean difference by 1.96.(215) Intra-class correlation coefficients with 95% confidence intervals were calculated for inter-observer variation. Baseline and follow-up calcium scores approximated a normal distribution, and were compared using a paired *t*-test. However, despite attempts at data transformation, the changes in calcium scores were not normally distributed and correlations with CT progression data were assessed using Spearman's correlation and linear regression analysis. We acknowledge the limitations in using linear regression in the context of a non-normal distribution. A two-sided $P<0.05$ was regarded as statistically significant. Statistical analysis was performed with the use of Graph Pad Prism version 6.0 (GraphPad Software Inc, California USA).

3.4 Results

3.4.1 Histology Cohort

Twelve patients with symptomatic aortic stenosis were recruited into the histology cohort (8 male, age 76±6, peak aortic valve velocity 4.6±0.9 m/s). Patients underwent PET scanning a median of 92 days prior to surgical aortic valve replacement. Eight patients received both 18F-fluoride and 18F-FDG PET scans. Additionally, two had a single 18F-fluoride scan whilst two more had a single 18F-FDG scan. Thus 10 valves were available for the histological validation of each tracer. No patient suffered a significant peri-operative complication (Table 3.1). Effective myocardial suppression of 18F-FDG activity was achieved in 40% (median myocardial SUV 5.4, IQR 1.9-10.4).

Table 3.1. Baseline characteristics of histology cohort

Baseline Characteristics	
Number	12
Age (years)	76±6
Male	9 (75)
Hypertension	8 (66)
Hyperlipidaemia	5 (42)
Ischaemic Heart Disease	4 (33)
Cigarette Smoking	1 (8)
Diabetes	0 (0)
Serum Creatinine (μmol/L)	87±26
Peak aortic valve velocity (m/s)	4.6±0.9
Aortic Valve area (cm^2)	0.70 (0.53-0.97)
Mean Gradient (mmHg)	48 (44-65)
Aortic Valve Calcium Score (AU)	5343 (3114-6292)
Aortic sclerosis	0 (0%)
Mild aortic stenosis	0 (0%)
Moderate aortic stenosis	3 (25%)
Severe aortic stenosis	9 (75%)
Time between 18F-NaF scan & AVR (days)	92 (24-345)
Time between 18F-FDG scan & AVR (days)	96 (23 – 331)
18F-FDG dose injected (MBq)	200 (193-209)
18F-NaF dose injected (MBq)	129 (119-132)
In vivo aortic valve PET Data	
18F-NaF Uptake (mean TBR)	2.15 (1.98-2.48)
18F-FDG Uptake (mean TBR)	1.40 (1.31–1.76)

Histology			
	Osteocalcin	**TNAP**	**CD-68**
Number	10	10	10
Mean valve area analysed (mm^2)	234±152	253±116	190±86
% staining of the valve	17±7	17±5	n/a
Positive cellular staining (cells/mm^2)	130 (85-274)	225 (143-328)	172 (73-271)
Inter-observer Reproducibility			
Mean Difference	-2.1%	-1.5%	0.8%
Limits of Agreement	-13.4-9.3%	-8.0-5.0%	-7.9-9.6%
ICC	0.88 (0.60-0.97)	0.90 (0.35-0.99)	0.99(0.99-1.00)

Categorical data is displayed as n (%). Normally distributed data displayed as mean±SD. Non-normally distributed data as median (inter quartile range). Inter-class correlation coefficients (ICC) as value (95% confidence interval). Abbreviations: AVR – aortic valve replacement, 18F-NaF – 18F- fluoride, 18F-FDG – 18F-fluorodeoxyglucose.

Immunohistochemistry and Autoradiography

All valve samples displayed positive cellular staining for TNAP (225 cells/mm^2 valve tissue; IQR 143-328), osteocalcin (130 cells/mm^2 valve tissue, IQR 85-274) and CD68 (172 cells/mm^2 valve tissue; IQR 73-271) (Figure 3.1). Extensive TNAP and osteocalcin staining was also observed in the extracellular matrix, occupying approximately a sixth of the valve area sampled (17±5% and 17±7% respectively).

On autoradiography, 18F-fluoride uptake was observed to co-localise closely with staining for structural calcium phosphate, TNAP and osteocalcin (Figure 3.1). However signal was also clearly apparent in areas free of macroscopically visible calcium thus highlighting the sensitivity of 18F-fluoride in the detection of newly evolving calcification.

Figure 3.1. Histology and 18F-fluoride autoradiography of excised aortic valve tissue from patients with aortic stenosis.

A-F; *Fixed, decalcified and paraffin embedded aortic valve tissue after exposure to tissue non-specific alkaline phosphatase (TNAP), osteocalcin and CD68 antibodies. Images* ***A-C*** *display widespread positive staining for TNAP, osteocalcin and CD68 (x4 magnification) in the extracellular matrix (ECM), which is also observed on an individual cellular level (****D-F,*** *x20 magnification) respectively.*

G-I; *Three adjacent and consecutive aortic valve leaflet sections displaying positive immunohistochemical staining for osteocalcin (****I,*** *x4 magnification****)*** *that co-localizes to areas of maximal 18F-fluoride uptake on autoradiography (****H****). These likely represent areas of ongoing calcification activity, which extend beyond the areas of established calcium identified in black by Von Kossa's stain (****G****, x4 magnification).*

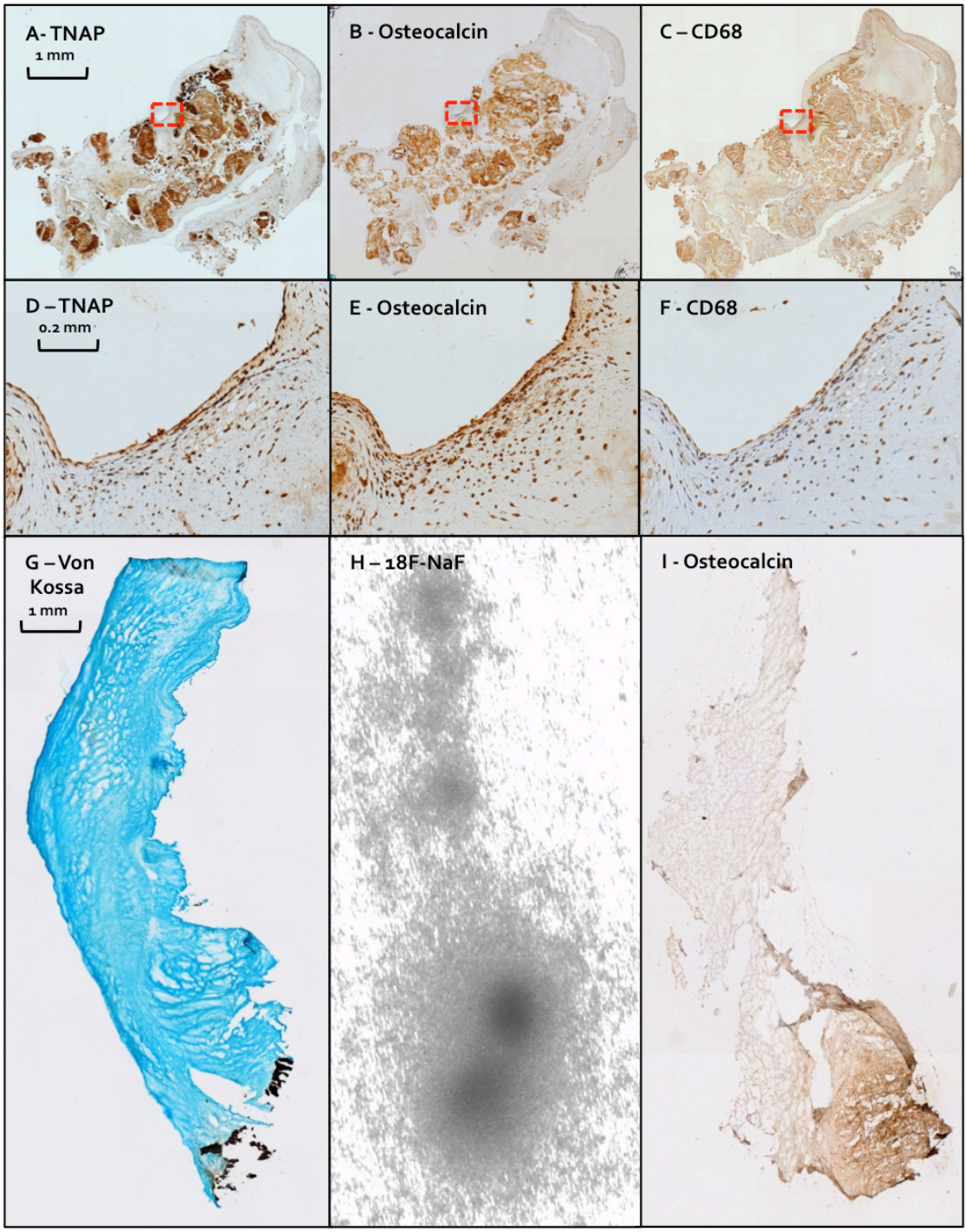
A- TNAP
1 mm
B - Osteocalcin
C – CD68
D – TNAP
0.2 mm
E - Osteocalcin
F - CD68
G – Von Kossa
1 mm
H – 18F-NaF
I - Osteocalcin

Reproducibility of Immunohistochemistry

Interobserver reproducibility was good for the quantification of osteocalcin and TNAP staining as well as CD68 cell counting. All observations were characterised by an absence of fixed or proportional biases, narrow limits of agreement (-13.4-9.3%, -8.0-5.0% and -7.9-9.6% respectively) and ICC values of 0.90 (0.35-0.99), 0.88 (0.60-0.97) and 0.99 (0.99-1.00) respectively (Table 3.1).

Correlation with radiotracer uptake

There was a good correlation between *in vivo* valvular 18F-fluoride uptake and both alkaline phosphatase (r=0.65 (95% confidence interval: 0.03-0.90), P=0.04) and osteocalcin (r=0.68 (0.10-0.91), P=0.03; Figure 3.2) staining of the excised tissue. By comparison there was no association between 18F-FDG uptake and CD68 staining in the valve (r=-0.43 P=0.22).

Figure 3.2. Correlations between *in vivo* aortic valve PET activity and histological markers of calcification and inflammation.

Panel A displays the close association between the percentage aortic valve tissue staining for tissue non-specific alkaline phosphatase (TNAP) and valvular 18F-fluoride activity (mean tissue to background ratio, TBR); r=0.65, P=0.04. A similar association can be seen in panel B between the percentage surface area of the valve stained with osteocalcin and the aortic valve 18F-fluoride PET activity (mean TBR); r=0.68, P=0.03. In panel C we observe a poor association between CD68 staining on immunohistochemistry and 18F-FDG PET activity in the aortic valve (mean TBR); r=-0.43, P=0.22.

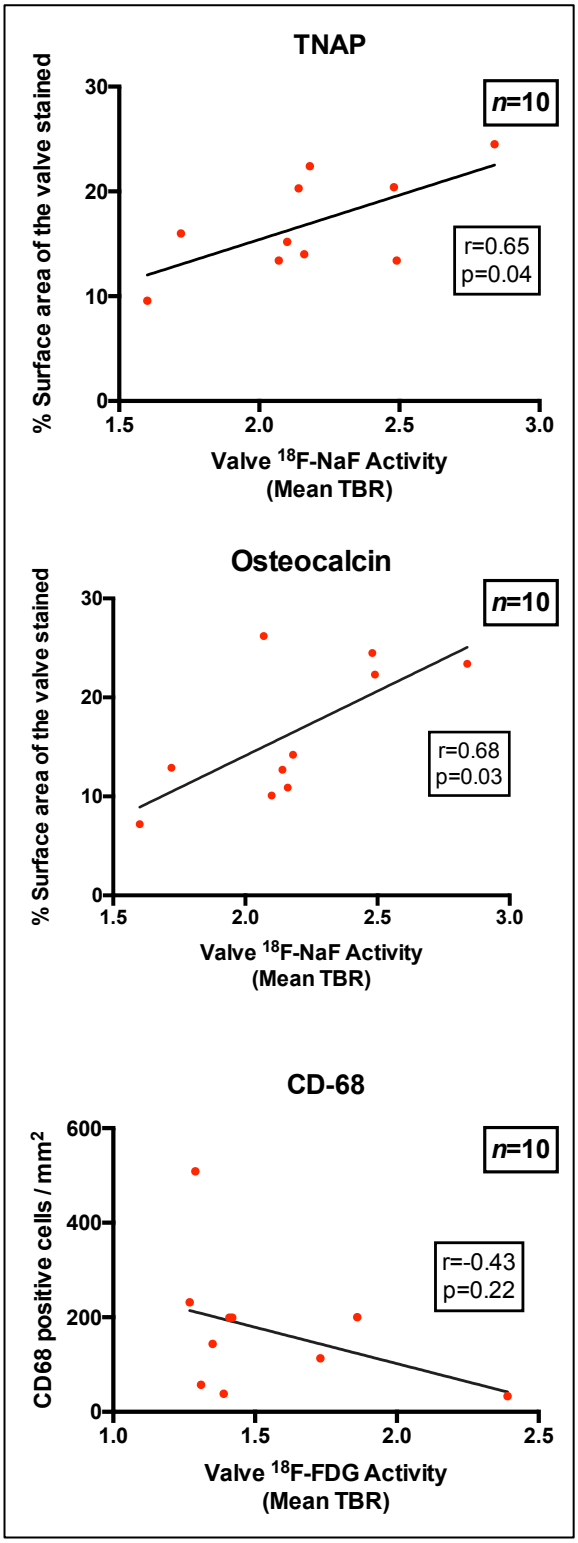
TNAP
% Surface area of the valve stained
n=10
r=0.65
p=0.04
Valve 18F-NaF Activity
(Mean TBR)
Osteocalcin
% Surface area of the valve stained
n=10
r=0.68
p=0.03
Valve 18F-NaF Activity
(Mean TBR)
CD-68
CD68 positive cells / mm2
n=10
r=-0.43
p=0.22
Valve 18F-FDG Activity
(Mean TBR)

3.4.2 Disease Progression

Of the 18 patients (age 75±6 years, 17 male, peak aortic-jet velocity 2.6±0.9 m/s) reassessed at a median interval of 386 days (Table 3.2), 6 had aortic sclerosis, and 7 had mild and 5 moderate aortic stenosis. Effective myocardial suppression of 18F-FDG uptake was achieved in 66% (median myocardial SUV 3.6, IQR 2.0 – 5.4).

A correlation was observed between baseline aortic valve calcium scores on CT and 18F-fluoride activity on PET (r=0.74 (0.42-0.90), P≤0.001). However, as described previously the pattern of 18F-fluoride uptake was distinct from the distribution of established calcium.(2,60,193) Indeed 18F-fluoride uptake in the absence of underlying calcium occupied a median of 8.3% (IQR 1.6-23.4) of the total valve area, emphasizing that 18F-fluoride provides distinct and complementary information to CT calcium scoring (Figure 3.3).

At one year, aortic valve calcium scores increased from 314 (193-540) to 365 (207-934) AU (P<0.01). Interestingly these regions of novel calcium developed in much the same distribution as the observed baseline 18F-fluoride uptake (Figure 3.3A-B). Indeed we observed an excellent correlation between baseline valvular 18F-fluoride PET uptake and the change in calcium score after 1 year (r=0.66 (0.27-0.86), P=0.003; Figure 3.3C). This was similar to that observed for the current gold-standard method of prediction: the baseline calcium score (r=0.58 (0.15-0.82), P=0.01; Figure 3.3D) and improved further when only increased 18F-fluoride uptake in the absence of underlying CT macrocalcification was considered (r= 0.75 (0.42-0.90), P=0.01). No

statistically significant correlation was observed between 18F-FDG uptake and the subsequent change in CT calcium score (r=-0.11 (-0.56-0.39), P=0.66; Figure 3.3E).

Table 3.2. Baseline Characteristics of Progression Cohort

	Total	Aortic Sclerosis	Mild Aortic Stenosis	Moderate Aortic Stenosis
Number	18	6 (33)	7 (39)	5 (28)
Age (years)	75 (71-79)	74 (70-78)	74 (69-80)	79 (70-83)
Male	15 (83)	4 (66)	7 (100)	4 (80)
Hypertension	13 (72)	3 (50)	5 (71)	5 (100)
Hyperlipidaemia	12 (67)	4 (66)	5 (71)	3 (60)
Diabetes	5 (28)	1 (16)	4 (57)	0 (0)
Ischaemic Heart Disease	13 (72)	4 (66)	6 (86)	3 (60)
Serum Creatinine (μmol/L)	92±29	85 (72-92)	91 (67-125)	84 (69-133)
Cigarette Smoking	0 (0)	0 (0)	0 (0)	0 (0)
Peak aortic valve velocity (m/s)	2.6 (1.8-3.1)	1.7 (1.6-1.8)	2.4 (2.1-2.6)	3.4 (3.2-3.6)
Aortic Valve area (cm^2)	1.68 (1.26-2.28)	1.92 (1.8-2.1)	1.63 (1.42-1.87)	1.03 (0.78-1.18)
Mean Gradient (mmHg)	10.8 (7.0-16.5)	6.2 (4.8-7.0)	11.0 (9.3-14.0)	22.0 (18.8-27.2)
Aortic Valve Calcium Score (AU)	314 (193-540)	106 (13-204)	355 (211-536)	1167 (436-1472)
Time between CT Scans (days)	386 (377-409)	390 (375-408)	394 (376-426)	183 (360-399)
18F-FDG dose injected (MBq)	193 (188-196)	193 (185-205)	191 (185-194)	194 (190-206)
18F-NaF dose injected (MBq)	123 (120-126)	124 (117-127)	123 (117-128)	123 (120-126)

Categorical data is displayed as total number (percentage). Median data (inter quartile range). Abbreviations: CT - Computed tomography, 18F-NaF – 18F-fluoride, 18F-FDG – 18F-fluorodeoxyglucose

Figure 3.3. Change in aortic valve CT calcium score and 18F-fluoride PET activity after 1 year

A-B; *Co-axial short axis views of the aortic valve from 2 patients with mild aortic stenosis (top and bottom rows). On baseline CT scans (left) established regions of macro calcification appear white. Baseline fused 18F-fluoride PET and CT scans (middle) show intense 18F-fluoride uptake (red, yellow regions) both overlying and adjacent to existing calcium deposits on the CT. 1 year follow up CT scans (right) demonstrate increased calcium accumulation in much the same distribution as the baseline PET activity.*

C-E; *Predictors of progression in aortic valve calcium score. An excellent correlation was observed between baseline 18F-fluoride activity in the aortic valve and the subsequent change in calcium score at 1 year r=0.66, P<0.01* ***(A).*** *This matched the current gold standard predictor of disease progression the baseline calcium score r=0.58 P=0.01* ***(B)****. By contrast there was a poor correlation with 18F-FDG activity in the valve r=-0.11 P=0.66* ***(C)****.*

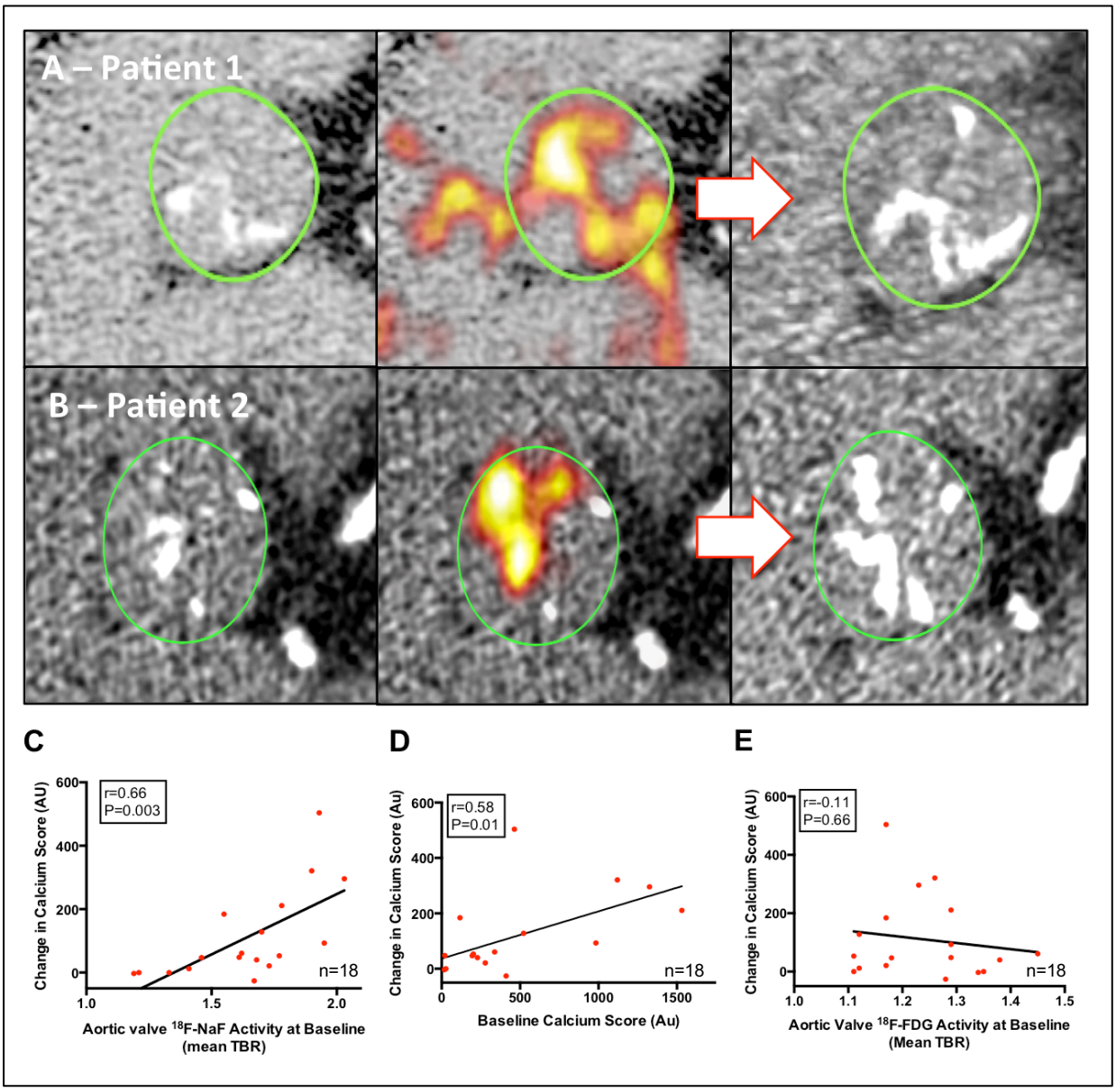
A – Patient 1
B – Patient 2
C
r=0.66
P=0.003
n=18
Change in Calcium Score (AU)
Aortic valve 18F-NaF Activity at Baseline (mean TBR)
D
r=0.58
P=0.01
n=18
Change in Calcium Score (Au)
Baseline Calcium Score (Au)
E
r=-0.11
P=0.66
n=18
Change in Calcium Score (AU)
Aortic Valve 18F-FDG Activity at Baseline (Mean TBR)

3.5. Discussion

We provide the first preliminary evidence that valvular 18F-fluoride uptake acts as a marker of calcification activity in patients with aortic stenosis. Not only did uptake values demonstrate a correlation with histological markers of active calcification (TNAP and osteocalcin) but they were also closely associated with the subsequent progression in aortic valve CT calcium scores at 1 year. In contrast, 18F-FDG uptake did not correlate with CD68 staining on histology nor the progression in calcium scores. Our data indicate that 18F-fluoride holds promise as a biomarker of disease activity in patients with aortic stenosis.

The pathophysiology of aortic stenosis is incompletely understood, delaying the development of biomarkers and effective medical therapies. Calcification and inflammation are thought to play a key pathological role,(17,18) so that non-invasive markers of their activity are of interest in better understanding the etiology of this condition as well as in predicting disease progression.

Recent studies have investigated 18F-fluoride PET as a marker of vascular calcification in aortic stenosis (2) and atherosclerosis affecting the aorta,(218) and coronary (6,164) and carotid arteries.(219) However this is the first study to provide histological validation of 18F-fluoride uptake in vascular tissue. In bone, 18F-fluoride is believed to incorporate onto the surface of hydroxyapatite crystal.(193) Given that hydroxyapatite is also a key component of vascular calcification, it too has been the presumed radiotracer target in aortic stenosis and atherosclerosis. This hypothesis is

supported by our autoradiography and immunohistochemical data, demonstrating a good correlation between 18F-fluoride activity and osteocalcin staining: a well-recognized osteogenic protein that itself binds to hydroxyapatite.

Given that 18F-fluoride binds to a structural component of vascular calcification, why then does it not simply label all regions of macrocalcification identified by CT? Indeed it is common for regions of dense calcium on CT to show no 18F-fluoride uptake. This phenomenon is likely related to the available surface area of exposed hydroxyapatite crystal to which the 18F-fluoride ion can adsorb and the inactivity of established areas of calcification. 18F-Fluoride uptake is much greater at sites of evolving powdery microcalcification than established regions of field calcification in which the core of hydroxyapatite is internalized and therefore hidden from the 18F-fluoride tracer. Thus 18F-fluoride binds more readily to regions of developing calcium and acts as a marker of calcification activity providing distinct information to calcium scoring. In contrast, the latter quantifies regions of established macroscopic calcium in the valve but cannot inform whether the process of calcification is quiescent or active. Again this hypothesis is supported by our data. We have demonstrated a strong correlation between *in vivo* 18F-fluoride uptake and staining for one of the key enzymes regulating mineralization: tissue non-specific alkaline phosphatase. This enzyme is expressed in the early stages of new calcium formation and is known to work by breaking down pyrophosphate: a potent inhibitor of mineralization.(220) Furthermore, as one would expect from a measure of activity, baseline 18F-fluoride uptake closely correlated with the subsequent change in calcium score at 1 year. Indeed 18F-fluoride uptake performed as well as the current gold standard method of prediction, the degree of

established calcium in the valve at baseline.(216,221) However, larger studies are now required to compare these two techniques and whilst calcium scoring may be easier to obtain, changes in the 18F-fluoride PET signal are likely to occur more quickly, making it a more attractive technique with which to assess the early and more immediate effects of novel treatment strategies.

Interestingly the pattern of 18F-fluoride uptake may be important, with 18F-fluoride uptake remote from established macrocalcification on CT offering the closest association with calcium score progression in our cohort. The spatial resolution of PET/CT is ~4 mm, and we acknowledge that the voxel-by-voxel analysis used to establish this observation is at the limit of resolution for PET imaging. Nevertheless the strong correlation with progression is of interest and indicates that further investigation of the spatial distribution of 18F-fluoride uptake is warranted.

The results for valvular 18F-FDG imaging were somewhat disappointing and surprising given previous data suggesting an important role for inflammation in aortic stenosis.(25) Whilst correlations between 18F-FDG uptake and macrophage burden have previously been demonstrated in regions of aortic and carotid atheroma,(47) we were unable to replicate this with respect to the valve. There are several explanations for this discrepancy. The first is the close proximity of the valve to the myocardium. As discussed, avid uptake of 18F-FDG by the left ventricular myocardium can spill over into the aortic valve contaminating its signal. Unfortunately even despite the stringent dietary restrictions and center-valve analysis technique, it remains possible that myocardial contamination occurred, confounding the correlation with CD68

immunohistochemistry. Indeed poor myocardial suppression was achieved in the histology group perhaps reflecting their advanced disease and symptomatic status. Alternative methods have been utilized to reduce further this myocardial uptake, including administration of heparin and a high-fat drink prior to scanning.(195,222) However these make the practicalities of scanning more difficult and are yet to show a clear advantage over dietary restrictions. An alternative explanation for the poor correlation with histology is that the aortic valve 18F-FDG signal relates to uptake by non-macrophage cell types within the valve, such as osteoblasts, or is governed by external factors such as hypoxia.(223) In this scenario, one might still expect 18F-FDG to predict disease progression but once again this was not evident in our cohort. It would therefore appear that 18F-FDG holds less potential as a predictor of disease progression than 18F-fluoride, although it remains possible that longer periods of follow-up are required to detect such an association. Indeed on occasion we also observed 18F-fluoride activity that did not translate into a detectable change in calcium score at 1 year. Aortic stenosis is a slowly developing condition, so that it is likely to take time for relatively low levels of 18F-fluoride or 18F-FDG uptake to translate into new areas of macrocalcification detectable on CT imaging. Larger studies with longer follow up are therefore required to address this issue, to confirm our preliminary data and to assess whether 18F-fluoride PET can predict disease progression with respect to echocardiographic parameters of valvular stenosis.

In conclusion, we provide the first preliminary data to support 18F-fluoride as a marker of valve calcification activity in aortic stenosis and as a potential method for predicting disease progression.

Chapter 4.

Valvular 18F-fluoride and 18F-fluorodeoxyglucose uptake are associated with disease progression and clinical outcome in patients with aortic stenosis

Published by Jenkins WS, Vesey AT, Shah AS, Pawade TA, Chin CW, White AC, Fletcher A, Cartlidge TR, Mitchell AJ, Pringle MA, Brown OS, Pessotto R, McKillop G, Van Beek EJ, Boon NA, Rudd JH, Newby DE, Dweck MR. Valvular 18F-fluoride and 18F-FDG uptake predict disease progression and clinical outcome in patients with aortic stenosis. Journal of the American College of Cardiology. 2015 Sep 8;66(10):1200-1.

4.1 Overview

18F-Fluoride and 18F-fluorodeoxyglucose (18F-FDG) are positron emission tomography (PET) radiotracers of calcification and inflammation activity respectively. We sought to assess their ability to predict disease progression and clinical outcome in patients with aortic stenosis.

PET and computed tomography (CT) were performed in 121 volunteers (72±8 years, 68% men) with and without aortic valve disease (20 controls; 20 aortic sclerosis; 25 mild, 33 moderate, and 23 severe aortic stenosis) using 18F-fluoride (125 MBq) and 18F-FDG (200 MBq). Disease progression was assessed at 1 and 2 years using CT aortic valve calcium score and echocardiography. Primary clinical outcome endpoint was a composite of cardiovascular death and aortic valve replacement (AVR).

Aortic valve calcium score increased by 61 (5–226) AU/year and aortic valve mean gradient increased by 0.7 (-0.2–2.9) mmHg/year. After a median of 1,526 (IQR 1475-1615) days, 29 patients had undergone AVR whilst 7 had a cardiovascular death.

Baseline valvular 18F-fluoride uptake correlated strongly with the rate of progression in aortic valve calcium score ($r=0.80$, $p<0.001$) and moderately with echocardiographic measures of progression (mean aortic valve gradient $r=0.32$, $p=0.001$). It emerged as independantly associated with clinical outcome after age and sex-adjustment (HR 1.55 [1.33-1.81], $p<0.001$).

18F-FDG demonstrated moderate correlations with disease progression as assessed by CT ($r=0.43$, $p=0.001$) and echocardiography (18F-FDG $r=0.30$, $p=0.001$) and also was associated with clinical outcomes independent of age and sex (HR 1.35 [1.16-1.58], $p<0.001$).

In conclusion, valvular 18F-fluoride and 18F-FDG PET uptake are closely associated with disease progression and clinical outcome in calcific aortic valve disease.

4.2 Introduction

Aortic stenosis is the commonest form of valvular heart disease in the developed world and a major cause of morbidity and mortality, affecting 0.5% of the adult population and rising to 12% of those aged over 75 years. This translates to 2.7 million elderly patients in North America and 4.9 million patients in Europe alone.(224) Furthermore, with a progressively increasing life-expectancy, the health burden attributable to this condition is only set to increase.(14) However, despite its prevalence, we lack biomarkers of disease activity, accurate clinical methods of predicting disease progression, and medical therapies capable of halting the disease process.

Our understanding of the pathogenesis of aortic stenosis has evolved over recent years. What was considered a passive and degenerative process is now appreciated to be a complex and highly regulated response to injurious stimuli with inflammation and calcification playing key roles.(17,18) In particular, calcification appears to be of central importance in driving disease progression and valve narrowing, with its accumulation in the valve resulting in progressive leaflet thickening and stiffness.(18,225)

Our group and others have investigated combined positron emission tomography (PET) and computed tomography (CT) as a means of measuring inflammation and calcification activity in aortic stenosis and other cardiovascular diseases.(2,53,58,226) 18F-Fluorodeoxyglucose (18F-FDG) is a PET radiotracer and glucose analogue taken up by metabolically active cells. In the vasculature, its uptake localizes to sites of

macrophage infiltration and activity. On this basis, 18F-FDG has become widely used as a marker of vascular inflammation, and for testing the safety and efficacy of novel therapies.(47,162) 18F-Fluoride is an alternative radiotracer that binds hydroxyapatite, the key structural component of cardiovascular calcification. Recent data have shown that 18F-fluoride preferentially binds to regions of newly developing microcalcification in the vasculature (beyond the resolution of CT) and correlates with histological markers of calcification activity in aortic stenosis.(226,227) Given the central role played by calcification, 18F-fluoride therefore holds promise as a biomarker of disease activity in aortic stenosis. Indeed in our recent pilot study of 18 patients, valvular 18F-fluoride PET uptake correlated closely with the progression of aortic valve CT calcium scores after 1 year.(226)

The aim of the current study was to assess the ability of these two tracers to predict longer-term disease progression and adverse clinical outcomes in a larger prospective cohort of patients with calcific aortic valve disease.

4.3 Methods

4.3.1 Patient Population

Patients aged >50 years with aortic sclerosis and mild, moderate or severe aortic stenosis attending the outpatient department of the Edinburgh Heart Centre were approached for recruitment in this prospective cohort study alongside age- and sex-matched control subjects, as described previously.(2,60,164,226) Exclusion criteria were insulin-dependent diabetes mellitus, end-stage renal failure, life expectancy of <2 years, and metastatic malignancy. The study was performed with the written informed consent of all participants, with research ethics committee approval, and in accordance with the Declaration of Helsinki. This study was registered with the clinical trials unique identifier NCT01358513.

4.3.2 Baseline Assessment

All participants underwent full clinical assessment at baseline and aortic stenosis severity was assessed using Doppler and two-dimensional echocardiography by means of the peak transvalvular velocity, mean gradient, peak gradient and aortic valve area (calculated using the continuity equation) according to American Heart Association/ American College of Cardiology guidelines.(228) Multiple acoustic windows with the S51 and D2cwc probes (Philips Medical Systems, the Netherlands) were assessed. Aortic sclerosis was defined as thickening of the aortic valve cusps in the absence of accelerated flow (<2 m/s) through the valve.(228) We also assigned the valve a semi-quantitative echocardiographic calcium score (ECS) as described by Rosenhek and colleagues.(38) Finally, aortic stenosis disease severity was assessed using an ECG-gated breath-hold CT scan (non-contrast enhanced, 40 mA/rot [CareDose], 100 kV) that was used to measure the aortic valve CT calcium score.(36)

PET/CT scans of the aortic valve were performed as described previously using a hybrid scanner (Biograph mCT, Siemens Medical Systems, Erlangen, Germany) 60 min after administration of 125 MBq of 18F-fluoride.(2) On a separate occasion, a second PET/CT scan was performed using the same hybrid scanner 90 min following administration of 200 MBq of 18F-FDG. (2) In an attempt to minimise cardiomyocyte uptake of 18F-FDG, patients were asked to avoid carbohydrate for 24 h prior to their 18F-FDG scan.(195)

4.3.3 Image Analysis

Calcium score analysis was performed on axial scans by an experienced investigator (WJ) blinded to clinical data using dedicated analysis software (Vitrea Advanced, Vital Images, Minnetonka, USA). Care was taken to differentiate valvular calcium from that in the aortic root and mitral valve annulus.

Valvular 18F-fluoride and 18F-FDG uptake was quantified using an OsiriX workstation (OsiriX version 3.5.1 64-bit; OsiriX Imaging Software, Geneva, Switzerland) as reported previously.(2) Briefly, fused PET/CT images were re-orientated to the short-axis plane of the aortic valve and circular regions of interest (ROIs) drawn on adjacent 3-mm slices until the entire valve apparatus had been examined. For 18F-fluoride, ROIs were placed around the perimeter of the valve (whole-valve technique). For 18F-FDG, ROIs were drawn in the center of the valve to reduce the impact of myocardial spillover, as described previously (center-valve technique).(2,53) From these regions, standard uptake values (SUV) were used to calculate tissue-to-background ratios (TBR) in the valve, after correcting for blood pool activity measured within the lumen of the superior vena cava. We have previously noted difficulty in defining the limits of the valve in the z-axis. As well as introducing potential for bias and variability, this problem frequently results in signal dilution if more slices than necessary are assessed. In keeping with an image analysis technique established in the aorta,(163) we therefore also calculated a modified "most diseased segment" SUV (SUV_{MDS}) in the aortic valve. This was based upon the average of the SUV_{mean} values derived from the 2 adjacent slices within the valve that had the highest

signal. This value was then used to calculate the most diseased segment TBR after blood-pool correction (TBR_{MDS}).

In order to assess the reproducibility of our methods for measuring the CT-calcium score, the echocardiographic calcium score and the valvular PET uptake, the scans from 25 study subjects with a range of aortic valve disease were selected at random and analysed independently by two trained observers (WSAJ, TP).

4.3.4 Assessment of Disease Progression

Subjects who had survived and had not undergone AVR were invited to return for repeat clinical assessment and echocardiography at both 1 and 2 years after enrolment. A single experienced research echocardiographer performed each echocardiogram under standardised conditions (AW). Annualized rates of echocardiographic progression for aortic stenosis were calculated over three time-points: baseline, 1 year and 2 years.

A subgroup of patients underwent repeat CT-calcium scoring after 1 year.(226) To limit their exposure to ionizing radiation, these subjects did not undergo further calcium scoring. In the remaining eligible patients, repeat CT scoring of the valve was performed after 2 years. The annualized change in CT calcium score was calculated for all subjects. For both echocardiography and CT, the same scanner and imaging protocol was used for all the baseline and follow up scans.

4.3.5 Follow-up for Clinical Events

The primary outcome measure was a composite of cardiovascular mortality or aortic valve replacement (AVR).(229) All deaths were captured from the General Register of Scotland. Cardiovascular death was defined as death due to myocardial infarction, sudden cardiac death, heart failure, stroke, death related to cardiovascular procedures, and death due to other cardiovascular causes. Each death was classified as cardiac or non-cardiac by two independent investigators blinded to the imaging data, with any discrepancy resolved by consensus. All events, including AVR (either surgical or transcutaneous), were confirmed by independent review of each patient's healthcare record. All patients were managed in our tertiary cardiac center, and reviewed at a multi-disciplinary meeting prior to undergoing aortic valve replacement. Only patients with established indications according to contemporary guidelines were referred for AVR.(230)

4.3.6 Statistical Methods

Continuous variables were expressed as either mean ± standard deviation for normally distributed data and median (interquartile range; IQR) for skewed distributions. Non-parametric datasets were log-transformed in an attempt to achieve normality. Parametric (unpaired Student's *t*-test) and non-parametric (Mann-Whitney U) tests were used for normally distributed and skewed data respectively. Categorical data were presented as n (%) and compared when appropriate using a contingency table and Fisher's or Chi-squared tests. Correlation was undertaken with either Pearson's r or Spearman's Rho subject to the normality of the variables tested.

To assess inter and intra-observer repeatability of the two PET analysis techniques and the aortic valve CT-calcium scoring, the intra-class correlation coefficient (ICC) was calculated and Bland-Altman analysis undertaken. Due to its categorical nature, repeatability studies of the echocardiographic calcium score were assessed using Cohen's kappa coefficient.

Adjusted and unadjusted Cox regression models were used to assess whether 18F-fluoride and 18F-FDG were associated with aortic valve replacement or cardiovascular mortality. Statistical analyses were performed with the use of Graph Pad Prism version 6.0 (GraphPad Software Inc, California, USA), SPSS version 18 (SPSS Inc, Chicago, IL) and RStudio version 0.98.501 (2013). Statistical significance was taken as two-sided $P<0.05$.

4.4. Results

4.4.1. Study Population

A total of 121 patients were recruited (aged 72±8 years; 69% male) and underwent both 18F-fluoride (66±7 min after 124±10 MBq) and 18F-FDG (94±7 min after 197±14 MBq) PET/CT imaging of their aortic valve. The study cohort comprised 20 control subjects, 20 patients with aortic sclerosis, and 25 patients with mild, 33 with moderate, and 23 with severe aortic stenosis as described previously.(2) Subjects were well matched for age, sex, and comorbidity (Figure 1, Table 1). The total effective radiation dose from study participation was 11.03±1.26mSv: 18F-Fluoride (3.8±0.3 mSv) and 18F-FDG (4.9±0.5 mSv) PET-CT, and repeated calcium scoring (1.3±0.5 mSv per scan). In those patients who received a single CT calcium score, the total effective radiation dose was 9.73±1.19 mSv. Dietary restrictions effectively suppressed 18F-FDG myocardial uptake (SUV <5) in 67% of patients.(2)

Figure 4.1. Study model and clinical outcomes.

A flow chart describing patient assessment and follow-up. The number of patients undergoing each assessment are included in parentheses.

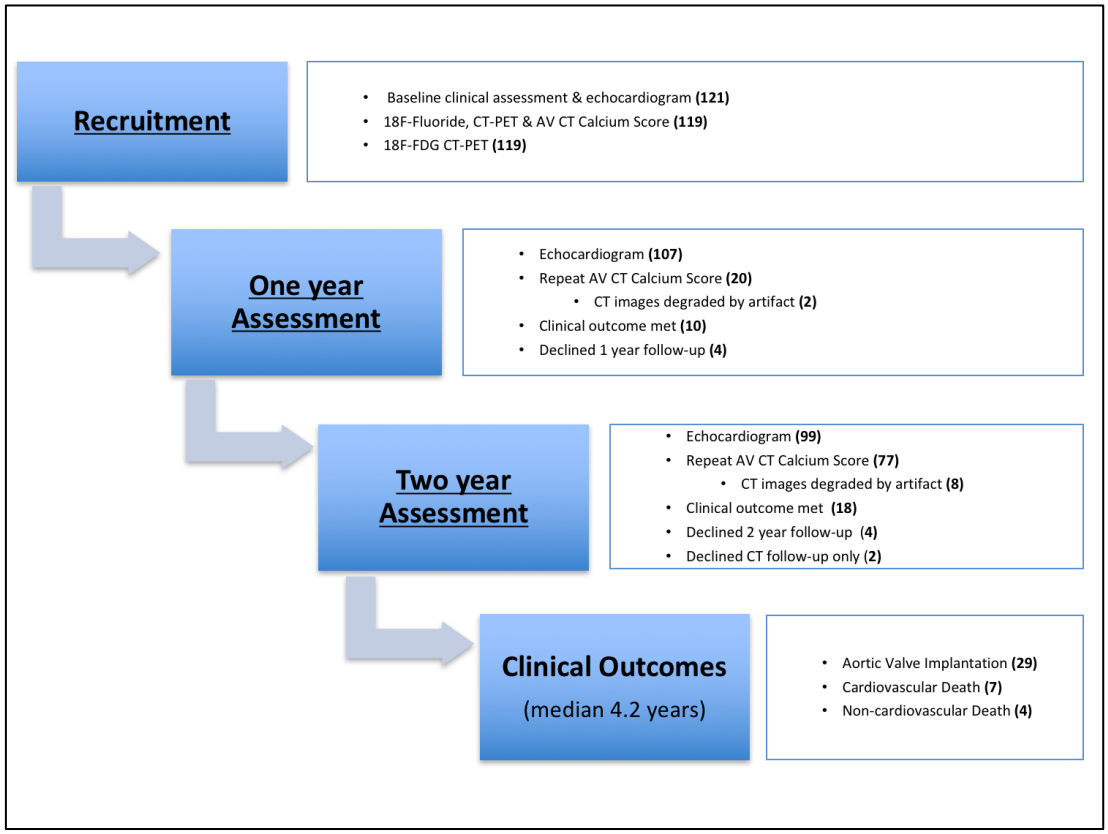

Abbreviations: AV: aortic valve; CT: computed tomography; FDG: fluorodeoxyglucose

Table 4.1. Baseline Clinical Characteristics

	All Patients	Echo Follow-up Cohort	Calcium Score Follow-up Cohort	Patients with Clinical Outcome (AVR / CV Death)
Number	121	99	87	36
Age (years)	72±8	72±8.5	72±8	71±9
Male	83 (69)	66 (65)	45 (51)	26 (72)
Body Mass Index (kg/m^2)	27±4	28±4	28±6	29±5
Systolic Blood Pressure (mmHg)	142±18	143±19	144±19	139±21
Co-morbidity				
Diabetes Mellitus	18 (15)	13 (13)	12 (14)	6 (17)
Hypertension	73 (60)	59 (60)	53 (61)	23 (64)
Documented CAD	43 (35)	36 (36)	38 (44)	12 (33)
Current smoker	14 (12)	11 (11)	7 (8)	8 (22)
Serum Creatinine (mg/dL)	1.01±0.29	1.02±0.32	1.00±0.28	0.98±0.29
Medications				
ACE inhibitors	47 (39)	36 (36)	36 (41)	16 (44)
AIIRB	13 (11)	11 (11)	10 (11)	3 (8)
Beta Blockers	48 (40)	41 (41)	40 (46)	15 (42)
Statins	65 (54)	54 (54)	54 (62)	23 (64)
Echocardiographic Assessment				
AV jet velocity (m/s)	2.8 [1.7-3.7]	2.6 [1.7-3.6]	2.6 [1.7-3.6]	4.0 (3.3-4.6)
AV peak gradient (mmHg)	31 [11-53]	28 [11-51]	28 [12-51]	61 [42-82]
AV mean gradient (mmHg)	16 [6-29]	14 [6-27]	14 [6-27]	34 [24-46]
AV area (cm^2)	1.34 [0.98-2.09]	1.37 [1.06-2.12]	1.33 [1.06-1.99]	0.91 [0.70-1.16]
Calcium Score	1.6±0.9	1.5±0.9	1.5±0.9	2.0±0.9
ECG Findings				
LVH	28 (23)	19 (19)	17 (20)	11 (31)
LV Strain	13 (11)	9 (9)	8 (9)	7 (19)

CT/PET Assessment				
Total radiation dose (mSv)	11.03±1.26	-	-	-
AV Calcium Score (AU)	554 [19-1762]	530 [13-1515]	585 [46-1487]	3218 [1371-4171]
Log_{10} AV Calcium Score	2.74 [1.27-3.25]	2.72 [1.11-3.18]	2.77 [1.66-3.17]	3.51 [3.14-3.62]
18F-FDG Dose (MBq)	196.6±13.9	197.0±13.8	197.0±12.0	199.2±11.9
18F-fluoride Dose (MBq)	123.8±9.5	123.6±9.0	124.0±7.8	126.6±12.4
18F-FDG Valve uptake (TBR_{MDS})	1.38±0.19	1.35±0.15	1.46±0.21	1.47±0.18
18F-FDG valve uptake (mean TBR_{CV})	1.34±0.17	1.32±0.14	1.33±0.18	1.42±0.15
18F-fluoride Valve uptake (TBR_{MDS})	1.80±0.47	1.73±0.45	1.64±0.45	2.18±0.39
18F-fluoride Valve uptake (mean TBR_{WV})	1.75±0.42	1.69±0.41	1.66±0.41	2.08±0.38
Time in study (days)	742±38	743±38	739±32	443 (325-796)

Parametric data are presented as mean±SD. Non-parametric data are presented as median [IQR]. Categorical data are presented as number (percentage). Abbreviations: ACE, angiotensin converting enzyme; AIIRB, angiotensin 2 receptor antagonists; AS, aortic stenosis; AV, aortic valve; CAD, coronary artery disease; CV, centre valve; FDG, Fluorodeoxyglucose; TBR, tissue to background ratio; AU, arbitrary unit; LV, left ventricle; LVH, left ventricular hypertrophy. WV, whole valve.

4.4.2 Image Analysis Reproducibility Studies

The novel TBR_{MDS} method demonstrated superior interobserver reproducibility compared to the established TBR_{mean} approach for the quantification of valvular 18F-FDG uptake. The two techniques performed equally well with respect to 18F-fluoride (Table 4.2, Figure 4.2).

Baseline uptake of the two radiotracers across the cohort using the TBR_{mean} technique have been reported previously.(2) The TBR_{MDS} technique resulted in no major differences compared to the original observations and no fixed or proportional bias (Table 4.2, Figure 4.2). Indeed valvular radiotracer uptake and therefore calcification activity increased steadily with more advanced aortic stenosis severity and in line with the extent of existing calcium observed on CT calcium scoring ($r=0.84$ $p<0.001$, Figure 2A-B). Moreover, the choice of uptake analysis technique had no impact on the strength of the correlations observed between baseline PET uptake and disease progression (Table 4.3). Given the improved interobserver reliability for 18F-FDG, TBR_{MDS} was used for all subsequent analyses.

The intra and inter-observer repeatability of aortic valve CT calcium scoring in the axial plane using the Agatston technique was excellent (Table 4.4, Figure 4.4) with the echocardiographic calcium score performing more modestly (Table 4.4).

Table 4.2. Reproducibility Studies – PET Radiotracer uptake

	TBR_{mean}		TBR_{MDS}	
	Mean absolute difference[a]	Intra-class coefficient[b]	Mean absolute difference[a]	Intra-class coefficient[b]
Number	25	25	25	25
18F-Fluoride	0.07 (-0.13-0.27)	0.98 (0.96-0.99)	-0.08 (-0.31-0.15)	0.99 (0.97-0.99)
18F-FDG	0.06 (-0.22-0.34)	0.76 (0.52-0.89)	<0.001 (-0.11-0.11)	0.97 (0.94-0.99)

[a] Mean difference between TBR measurements (95% limits of agreement), and [b] ICC values (95% confidence intervals) for 18F-fluoride and 18F-FDG valvular uptake, assessing the use of mean whole/centre valve quantification technique versus the MDS technique. Abbreviations: FDG: fluorodeoxyglucose; ICC: intraclass correlation coefficient; MDS: most diseased segment; TBR: tissue to background ratio

Figure 4.2. Valvular PET Radiotracer assessment: Bland-Altman plots

The figure below displays Bland-Altman plots with the percentage difference plotted against the tissue to background values for 'mean' and 'most disease segment' methodologies, assessing interobserver agreement in both 18F-fluoride (upper) and 18F-FDG (lower) aortic valve uptake.

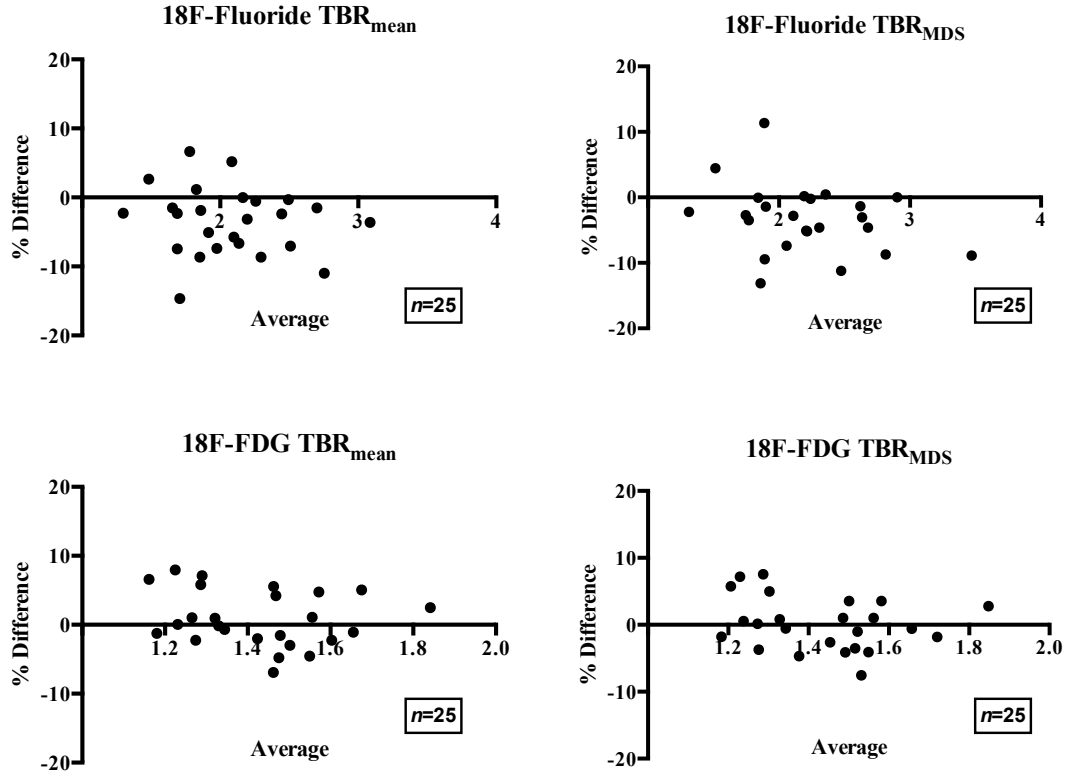

Abbreviations: FDG: fluorodeoxyglucose; MDS: most diseased segment; TBR: tissue to background ratio

Figure 4.3. Positron Emission Tomography, Aortic Valve Calcification and the Progression in Disease Severity.

A & B. *Disease progression as measured by CT calcium scoring and echocardiography increased steadily as disease severity increased. The changes in CT calcium score were however larger and more consistent than those observed for echocardiography.*

C & D *A close association was observed between the baseline CT calcium score and valvular 18F-fluoride (18F-NaF) activity ($r=0.84$, $p<0.001$). Patients with higher than expected 18F-fluoride uptake for a given CT calcium score (dots in the red section above the regression line) demonstrated disease progression rates that were 3-fold greater than those with lower than expected 18F-fluoride uptake (dots in the blue section below the regression line (B).*

E & F*. Whilst an association between 18F-FDG activity and the baseline CT calcium score was again observed ($r=0.45$, $p<0.001$), those with higher than expected 18F-fluorodeoxyglucose (18F-FDG) activity did not appear to progress faster than patients with lower than expected PET uptake.*

Patient numbers are included in italics above each datapoint.

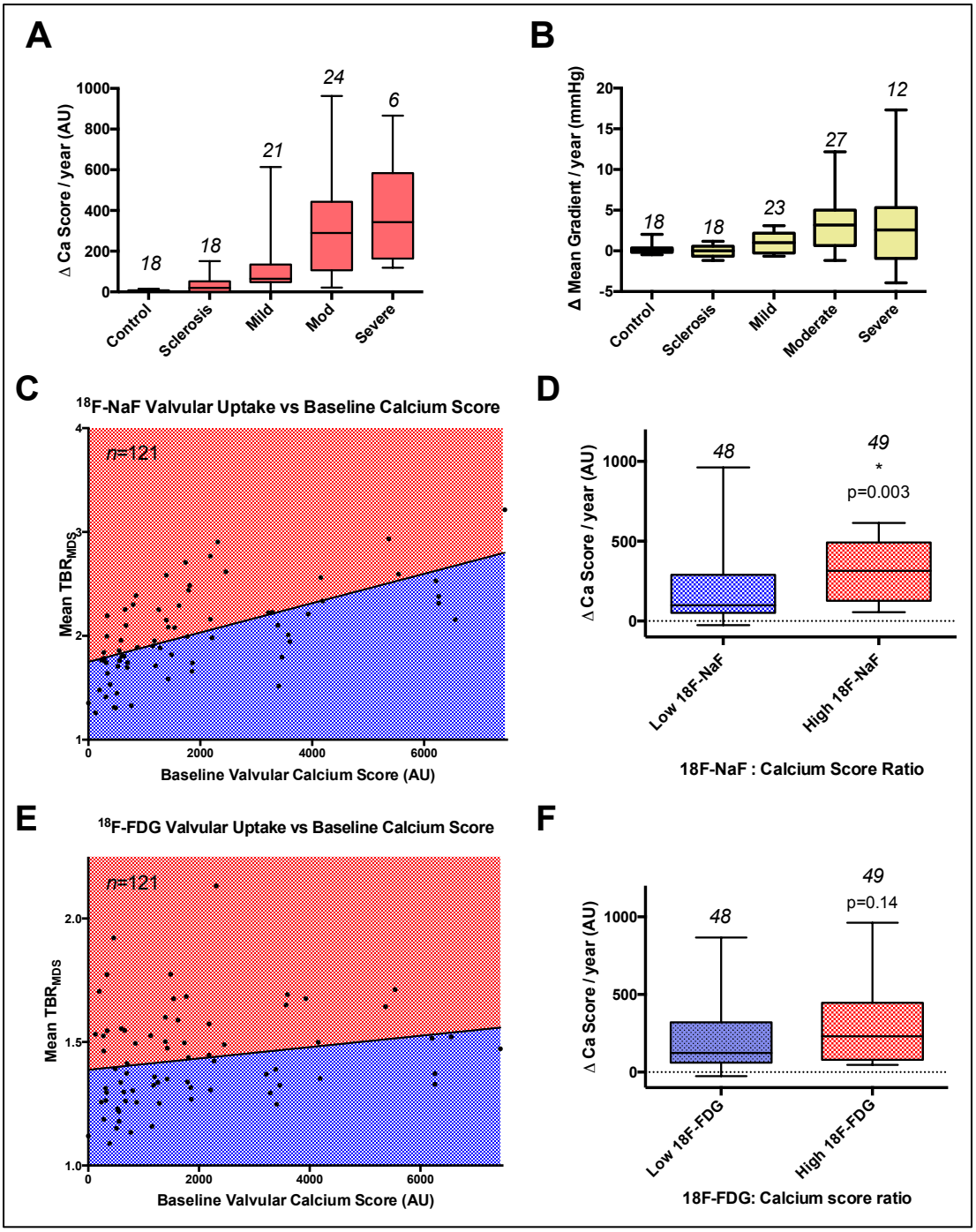
A
Δ Ca Score / year (AU)
1000
800
600
400
200
0
18
18
21
24
6
Control
Sclerosis
Mild
Mod
Severe
B
Δ Mean Gradient / year (mmHg)
20
15
10
5
0
-5
18
18
23
27
12
Control
Sclerosis
Mild
Moderate
Severe
C
18F-NaF Valvular Uptake vs Baseline Calcium Score
n=121
Mean TBR MDS
4
3
2
1
0
2000
4000
6000
Baseline Valvular Calcium Score (AU)
D
Δ Ca Score / year (AU)
1000
500
0
48
49
*
p=0.003
Low 18F-NaF
High 18F-NaF
18F-NaF : Calcium Score Ratio
E
18F-FDG Valvular Uptake vs Baseline Calcium Score
n=121
Mean TBR MDS
2.0
1.5
1.0
0
2000
4000
6000
Baseline Valvular Calcium Score (AU)
F
Δ Ca Score / year (AU)
1000
500
0
48
49
p=0.14
Low 18F-FDG
High 18F-FDG
18F-FDG: Calcium score ratio

Table 4.3. Baseline radiotracer uptake – correlation with disease progression

Baseline Imaging Assessment	Δ AV Calcium Score (AU/year)	Δ aortic jet velocity (m/sec/yr)	Δ mean gradient (mmHg/yr)	Δ peak gradient (mmHg/yr)	Δ Aortic Valve Area (cm^2/yr)
Number	87	99	99	99	99
^{18}F-fluoride mean TBR_{WV}	r=0.79 (0.69-0.86) P<0.001	r=0.20 (0.00-0.39) P=0.04	r=0.29 (0.10-0.47) P=0.003	r=0.29 (0.09-0.47) P=0.004	r=0.13 (-0.08-0.33) P=0.20
^{18}F-fluoride mean TBR_{MDS}	r=0.80 (0.60-0.86) P<0.001	r=0.23 (0.03-0.41) P=0.001	r=0.32 (0.13-0.50) P=0.001	r=0.32 (0.12-0.49) P=0.001	r=0.11 (-0.10-0.31) P=0.29
^{18}F-FDG mean TBR_{CV}	r=0.47 (0.28-0.62) P<0.001	r=0.23 (0.03-0.42) P=0.02	r=0.26 (0.06-0.44) P=0.01	r=0.33 (0.14-0.50) P<0.001	r=-0.12 (-0.32-0.08) P=0.23
^{18}F-FDG mean TBR_{MDS}	r=0.43 (0.23-0.59) P<0.001	r=0.28 (0.08-0.46) P=0.005	r=0.30 (0.10-0.47) P=0.002	r=0.36 (0.17-0.53) P<0.001	r=-0.14 (-0.33-0.07) P=0.18
^{18}F-fluoride mean SUV_{WV}	r=0.64 (0.49-0.75) P<0.001	r=0.28 (0.08-0.46) P=0.006	r=0.36 (0.16-0.52) P<0.001	r=0.34 (0.14-0.51) P<0.001	r=0.10 (-0.12-0.29) P=0.34
^{18}F-fluoride mean SUV_{MDS}	r=0.67 (0.53-0.77) P<0.001	r=0.23 (0.03-0.41) P=0.02	r=0.32 (0.13-0.49) P=0.001	r=0.34 (0.15-0.51) P<0.001	r=0.15 (-0.06-0.34) P=0.02
^{18}F-FDG mean SUV_{CV}	r=0.41 (0.21-0.57) P<0.001	r=0.26 (0.07-0.45) P=0.004	r=0.25 (0.05-0.44) P=0.01	r=0.29 (0.09-0.47) P=0.004	r=0.01 (-0.20-0.20) P=0.98
^{18}F-FDG mean SUV_{MDS}	r=0.42 (0.23-0.59)) P<0.001	r=0.29 (0.09-0.46) P=0.004	r=0.31 (0.11-0.48) P=0.002	r=0.31 (0.11-0.48) P=0.002	r=0.27 (0.08-0.45) P=0.008

AV CT Calcium Score (AU)	r=0.88 (0.82-0.92) P<0.001	r=0.36 (0.16-0.53) P<0.001	r=0.40 (0.21-0.56) P<0.001	r=0.46 (0.27-0.61) P<0.001	r=0.060 (-0.15-0.27) P=0.54
Aortic Jet Velocity (m/sec)	r=0.79 (0.70-0.86) P<0.001	r=0.28 (0.08-0.45) P=0.006	r=0.40 (0.22-0.56) P<0.001	r=0.39 (0.21-0.55) P<0.001	r=0.08 (-0.13-0.27) P=0.45

Abbreviations: AV: aortic valve; AU: arbitrary units; CT: computed tomography; CV: centre valve; FDG: fluorodeoxyglucose; MDS: Most Diseased Segment; TBR: tissue to background ratio; WV: whole valve

Table 4.4. CT calcium scoring – reproducibility studies

	Interobserver		**Intraobserver**	
	Bias (95% limits of agreement)[a]	*ICC (95% CI)*[b]	*Bias (95% limits of agreement)*[a]	*ICC (95% CI)*[b]
Number	25	25	25	25
CT Calcium Score (AU)	22 (-35 to 79)	1 (1.0 to 1.0)	10 (-67 to 88)	1 (1.0 to 1.0)

	Interobserver Kappa (SE)[c]	**Intraobserver Kappa (SE)**[c]
Echocardiographic Calcium Score	0.447 (0.138)	0.501 (0.132)

[a] *mean difference;* [b] *Intraclass correlation co-efficient. 2-way mixed effects for absolute agreement;* [c] *Kappa statistic. Abbreviations: AU: arbitrary units; CT: computed tomography; ICC: intraclass correlation coefficient; SE: standard error*

Figure 4.4. CT calcium scoring: Bland-Altman plots

The figure below displays Bland-Altman plots with the difference plotted against the average CT calcium score for intraobserver (A) and interobserver (B) agreement.

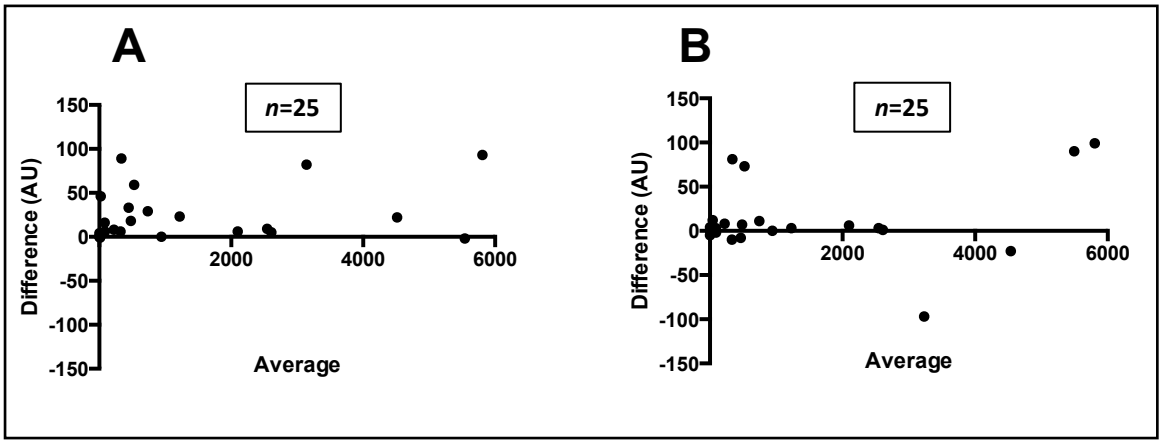

Abbreviations: AU: arbitrary units; CT: computed tomography

4.4.3. Patient follow-up

One year after enrollment, 107 subjects returned for clinical follow-up and echocardiography. As part of a pilot study, 20 subjects had received a repeat ECG-gated cardiac CT at one year and did not undergo further CT at two years.(226)

Ninety-nine subjects (81%) returned for repeat clinical assessment and echocardiography at the 2-year time point (median 736 [722–760] days from enrollment). Repeat CT calcium was performed in 77 of these subjects. Including the patients scanned at 1 year, a total of 97 (78%) subjects underwent a repeat ECG-gated cardiac CT during the 2-year follow up period. CT scans were not interpretable in 10 subjects (including 2 at the 1-year time point) due to motion artifact and were excluded from subsequent analysis. In the remaining patients (n=87), the annualized change in the aortic valve CT calcium score was calculated and used for subsequent analysis (Figure 4.1).

Across all disease cohorts, modest progression of each echocardiographic measure of aortic stenosis severity was observed (Table 4.5). Peak aortic jet velocity increased by 0.08 (-0.02–0.18) m/s/year, the mean transvalvular gradient by 0.7 (-0.2–2.9) mmHg/year and the peak gradient by 1.3 (-0.3–4.0) mmHg/year. The aortic valve area fell by -0.06 (-0.14–0.02) cm^2/year. In contrast, relatively large annualized changes in the CT valvular calcium scores were observed (61 [5–226] AU/year [$p<0.001$]), especially amongst patients with moderate and severe disease (Table 4.5 and Figure 4.3). Indeed for all the variables assessed, more rapid disease progression was

observed in patients with more advanced aortic stenosis (median change in calcium score: mild AS, 65 [48-134]; moderate AS, 289 [106-443], and severe AS, 343 [164-583] AU/year). Finally, the change in the valve CT calcium score correlated moderately with the different haemodynamic measures of aortic stenosis progression (change in mean gradient, r=0.45 [0.26-0.61], p<0.001; and change in peak gradient, r=0.41 [0.22-0.58], p<0.001).

Clinical outcomes were assessed at a median of 1,526 (1,475-1,1615) days after enrollment. At this point, 29 (24%) patients had undergone either aortic valve replacement (AVR; n=25) or transcatheter aortic valve implantation (n=4). There were 7 (6%) cardiovascular deaths (with 4 further deaths due to a non-cardiovascular cause). Overall, 36/121 (30%) subjects were adjudicated to have reached the primary end-point (Table 4.5).

Table 4.5. Disease progression and clinical outcomes

	All patients	Control Subjects	Aortic Sclerosis	Mild Aortic Stenosis	Moderate Aortic Stenosis	Severe Aortic Stenosis
Echocardiography ***Baseline Assessment***						
No. of patients	121	20	20	25	33	23
Aortic-jet velocity (m/s)	2.8±1.2	1.3±0.2	1.7±0.2	2.5±0.2	3.4±0.3	4.6 ±0.6
Mean gradient (mm Hg)	16.2 [5.9-29.2]	3.6±1.0	5.9±1.4	13.2±2.7	25.2±4.1	48.6±15.4
Peak gradient (mm Hg)	31.1 [11.0-53.0]	7.1±2.1	11.1±2.6	25.8±5.0	46.5±7.5	84.2±24.8
Aortic-valve area (cm^2)	1.34 [0.98-2.09]	2.54±0.49	2.27±0.41	1.42±0.30	1.13±0.27	0.76±0.21
Echocardiography ***Progression***						
No. of patients	99	20	17	24	26	12
Δ aortic jet velocity (m/s/year)	0.08 [-0.02-0.18] P<0.001	0.05 [-0.03-0.09]	0.03 [-0.08-0.08]	0.08 [-0.01-0.18]	0.17 [0.07-0.30]	0.10 [-0.11-0.19]
Δ mean gradient (mmHg/year)	0.7 [-0.2-2.9] P<0.001	0.1 [-0.5-0.3]	0.0 [-0.7-0.6]	1.0 [-0.3-2.2]	3.2 [0.7-5.0]	2.6 [-0.1-5.3]
Δ peak gradient (mmHg/year)	1.3 [-0.3-4.0] P<0.001	0.4 [-0.3-0.7]	0.3 [-0.9-1.1]	1.4 [-0.2-3.1]	4.1 [1.6-9.0]	3.2 [-3.7-6.8]
Δ aortic-valve area (cm^2/year)	-0.05 [-0.14-0.02) P<0.001	-0.10 [-0.25--0.01]	-0.04 [-0.12-0.07]	-0.09 [-0.16--0.02]	-0.05 [-0.13--0.03]	-0.04 [-0.08--0.02]

Computed Tomography						
Baseline assessment						
No. of patients	112	20	20	23	30	19
AVC (AU)	554	0	46	489	1427	3386
	[19-1762]	[0-3]	[2-224]	[281-693]	[777-2215]	[1770-6211]
Log_{10} AVC	1.79	0.30	1.28	1.81	2.46	2.53
	[0.70-2.35]	[0.0-0.91]	[0.0-1.71]	[1.68-2.13]	[2.02-2.65]	[2.21-2.75]
Computed Tomography						
Progression						
No. of patients	87	18	18	21	24	6
Δ AVC (AU /	61	2	19	64	289	342
year)	[5-226]	[0-8]	[0-52]	[48-134]	[106-443]	[163-583]
Δ Log_{10} AVC	0.96	0.30	1.2	1.81	2.46	2.53
(Log_{10} AU/ year)	[0.69-2.35]	[0.0-0.91]	[0.0-1.71]	[1.68-2.13]	[2.02-2.65]	[2.21-2.75]
Clinical Outcome						
Event-free days	1526	1492	1522	1538	1461	727
	[1475-1615]	[1421-1520]	[1456-1615]	[1477-1587]	[810-1617]	[335-1471]
All cause mortality	11	1	1	1	2	6
Cardiovascular Mortality	7	0	1	1	0	5
Aortic-valve replacement	29	0	0	0	13	16
Composite outcome	34	0	1	1	13	19

Parametric data are presented as mean±SD. Non-parametric data are presented as median [IQR]. Abbreviations: AV, aortic valve; AVC, aortic valve calcification score; AU, arbitrary unit

4.4.4. Prediction of disease progression

A strong correlation was observed between baseline 18F-fluoride uptake in the valve and the subsequent rate of progression in the aortic valve calcium score (r=0.80 [0.69–0.87], p<0.001; Table 4.6 and Figure 4.5). Moderate correlations were observed between valvular 18F-fluoride uptake and echocardiographic indices of disease progression, i.e. the rate of change in mean gradient (r=0.32 [0.13–0.50], p=0.001), peak aortic jet velocity (r=0.23 [0.03–0.41], p=0.001), and peak gradient (r=0.32 [0.12–0.49], p=0.002).

Moderate correlations were also observed between baseline 18F-FDG valvular uptake and the rate of progression of the CT calcium score (r=0.43 [0.23–0.59], p<0.001), the mean gradient (r=0.30 [0.10–0.47], p=0.002), the peak velocity (r=0.28 [0.08–0.46], p=0.005), and peak gradient (r=0.36 [0.17–0.53], p<0.001).

There were strong associations between the baseline CT valvular calcium score and rate of change in calcium score (r=0.88 [0.82-0.92], p<0.001), similar to those observed for 18F-fluoride. Moderate associations were also observed between the baseline calcium score and the progression in echocardiographic measures of disease severity (change in mean gradient, r=0.40 [0.21–0.56], p<0.001; change in peak velocity, r=0.36 [0.16–0.53], p<0.001; and change in peak gradient, r=0.46 [0.27–0.61], p<0.001).

Given the degree of co-linearity that exists between CT calcium scoring and 18F-fluoride uptake in the valve, it is difficult to assess whether 18F-fluoride uptake provides incremental prognostic information to CT. Using the regression line between the CT calcium score and 18F-fluoride uptake as a cut off, patients with aortic stenosis and higher than expected 18F-fluoride uptake for a given CT calcium score demonstrated progression rates that were 3-fold greater than subjects with lower than expected uptake (median change in calcium score: 315 [127-492] vs 99 [51-290] AU/year respectively; p=0.003). When a similar analysis was performed for 18F-FDG, there was no significant difference (median change in calcium score: 231 [79-446] vs 124 [61-321] AU/year, p=0.14; Figure 4.3).

Figure 4.5. 18F-Fluoride Positron Emission Tomography and the Progression in Aortic Valve Calcification

Co-axial short-axis views of the aortic valve in 3 separate study subjects and disease severity categories.

A *Baseline CT calcium score scans with relatively little in the way of established calcium in the valve (white)*

B *Fused PET/CT images with increased 18F-fluoride valvular uptake (red and yellow regions) that does not well align with the established calcium on the CT. Also note the increased uptake in the proximal left anterior descending coronary artery*

C *Repeat CT calcium score at 2 years, demonstrating an increase in the amount of established macroscopic calcium in much the same distribution as the baseline PET uptake.*

D-E *Scatterplots demonstrating the close relationship between progression in the aortic valve computed tomography calcium score and baseline valvular 18F-fluoride (**D**) and 18F-FDG (**E**) uptake. To better demonstrate the lower calcium score data a log_{10} scale has been used on the y-axis.*

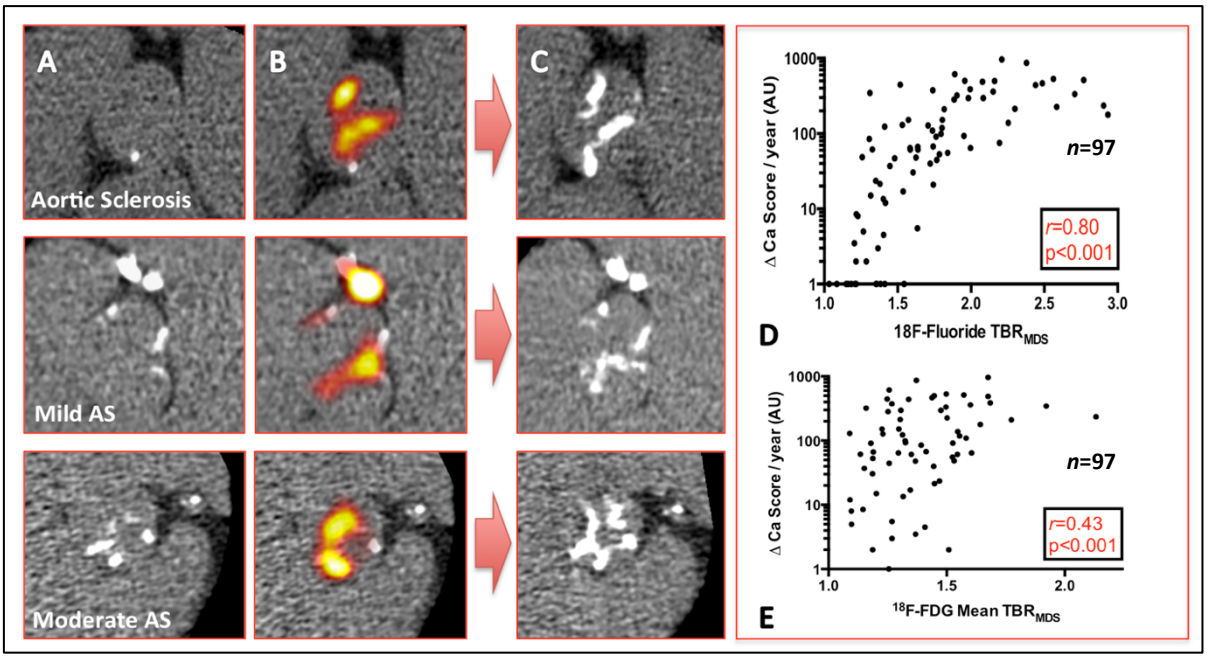

Table 4.6. Baseline imaging and associations with disease progression

Baseline Imaging Assessment	Rate of change in AV Calcium Score (AU/yr)	Rate of change in aortic jet velocity (m/s/yr)	Rate of change in mean gradient (mmHg/yr)	Rate of change in peak gradient (mmHg/yr)	Rate of change in Aortic Valve Area (cm^2/yr)
PET Valvular Radiotracer Uptake					
18F-fluoride mean TBR_{MDS}	*r*=0.80 (0.69-0.87) P<0.001	*r*=0.23 (0.03-0.41) P=0.001	*r*=0.32 (0.13-0.50) P=0.001	*r*=0.32 (0.12-0.49) P=0.001	*r*=0.11 (-0.10-0.31) P=0.29
18F-FDG mean TBR_{MDS}	*r*=0.43 (0.23-0.59) P<0.001	*r*=0.28 (0.08-0.46) P=0.005	*r*=0.30 (0.10-0.47) P=0.002	*r*=0.36 (0.17-0.53) P<0.001	*r*=-0.14 (-0.33-0.07) P=0.18
CT Assessment					
AV Calcium Score (AU)	*r*=0.88 (0.82-0.92) P<0.001	*r*=0.36 (0.16-0.53) P<0.001	*r*=0.40 (0.21-0.56) P<0.001	*r*=0.46 (0.27-0.61) P<0.001	*r*=0.06 (-0.15-0.27) P=0.54
Echocardiographic Assessment					
Aortic Jet Velocity (m/s)	*r*=0.79 (0.70-0.86) P<0.001	*r*=0.28 (0.08-0.45) P=0.006	*r*=0.40 (0.22-0.56) P<0.001	*r*=0.39 (0.21-0.55) P<0.001	*r*=0.08 (-0.13-0.27) P=0.45

Abbreviations: AV: aortic valve; AU: arbitrary unit; CT: computed tomography; FDG: fluorodeoxyglucose; MDS: most diseased segment; PET: positron emission tomography; TBR: tissue to background ratio

4.4.5. Associations with clinical outcome

Using Cox regression analysis, valvular 18F-fluoride uptake was significantly associated with clinical outcome (cardiovascular mortality and AVR) independent of age and sex (HR (hazard ratio): 1.55, 95% CI (confidence interval): 1.33 to 1.81; $p<0.0001$). The same was true of baseline 18F-FDG activity (HR: 1.35, 95% CI 1.16 to 1.58; $p<0.001$). To facilitate comparison, the HRs are expressed per decile of the full range of TBR_{MDS} values for each tracer. The baseline aortic valve CT calcium score also emerged as independently associated with clinical outcomes (HR per 10^{th} of the range change in calcium score: 4.31 95% CI: 2.60 to 7.14; $p<0.0001$ after adjustment for age and sex). Finally we assessed the echocardiographic calcium score. However this performed poorly, with only a maximum score of 4 holding any prognostic value (Table 4.7 and Figure 4.6).

Figure 4.6. Prediction of clinical outcome

A *18F-Fluoride (HR are per 10th of range of mean TBR_{MDS} values).*

B *18F-Fluorodeoxyglucose (HR are per 10th of range of mean TBR_{MDS} values).*

C *Echocardiographic calcium score (with ECS score of 0 as reference).*

D *CT Calcium Score (HR are per 10th of range of AU values).*

Red bars are 95% confidence intervals.

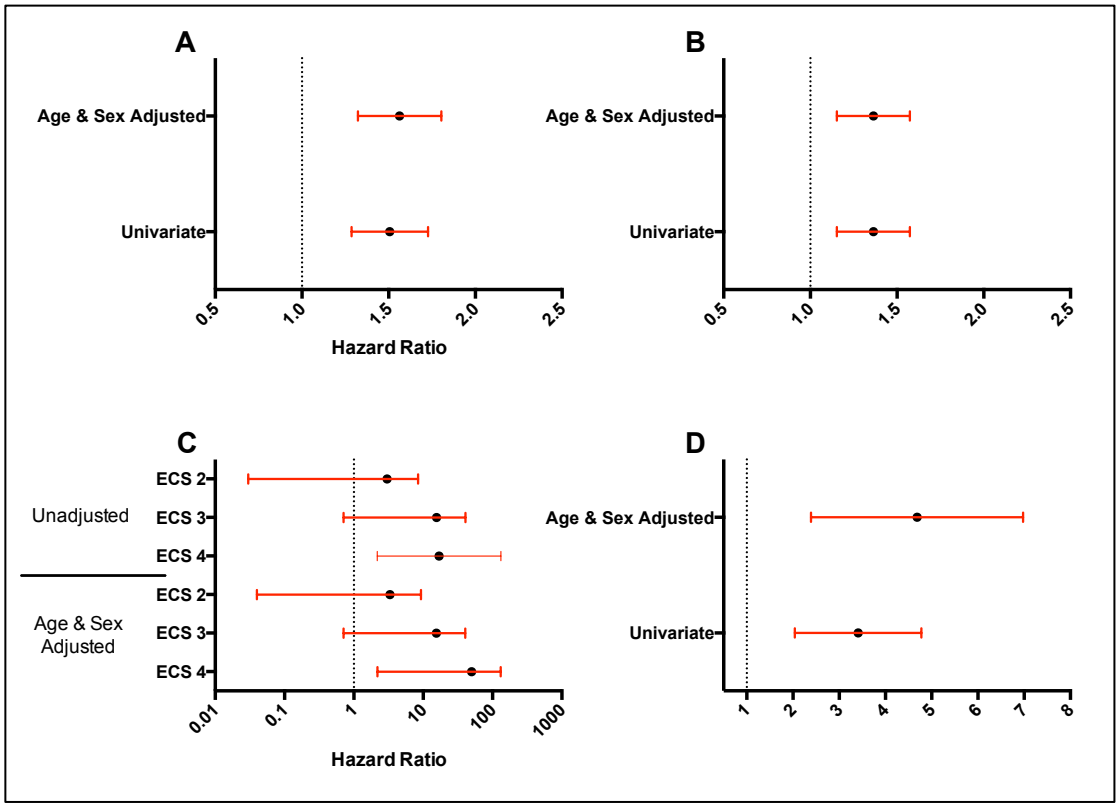

Abbreviations: ECS: echocardiographic calcium score; HR: hazard ratio

Table 4.7. Imaging and the prediction of clinical outcome

	Unadjusted HR (95% CI)	P Value	Age and Sex Adjusted HR (95% CI)	P Value
^{18}F-fluoride Valvular Uptake TBR_{MDS} (per 10th of range)	1.50 (1.29 - 1.73)	<0.001	1.55 (1.33 – 1.81)	<0.001
^{18}F-FDG Valvular Uptake TBR_{MDS} (per 10th of range)	1.35 (1.16 – 1.58)	<0.001	1.35 (1.16 – 1.58)	<0.001
CT AV Calcium Score (per 10th of range)	3.23 (2.14 – 4.86)	<0.001	4.31 (2.60 – 7.14)	<0.001

		Unadjusted HR (95% CI)	P Value	Age and Sex Adjusted (95% CI)	P Value
Echocardiographic AV Calcium Score (ECS)	**ECS**				
	1	Reference	-	Reference	-
	2	0.58 (0.04 - 9.31)	0.702	0.53 (0.03 - 8.458)	0.650
	3	5.35 (0.71 - 40.41)	0.104	5.36 (0.71 - 40.68)	0.104
	4	16.9 (2.19 - 130.86)	0.007	17.0 (2.18 - 132.4)	0.007

Abbreviations: AV: aortic valve; AU: Arbitrary Unit; CI, confidence interval; CT: computed tomography; ECS: echocardiographic calcium score; FDG: fluorodeoxyglucose; HR, hazard ratio; MDS: Most Diseased Segment; TBR: tissue to background ratio

4.5 Discussion

We here report the first prospective longitudinal study to investigate the utility of 18F-fluoride and 18F-FDG PET/CT imaging in patients with aortic stenosis. We have demonstrated that both tracers are associated with disease progression and adverse clinical outcomes. In particular 18F-fluoride proved closely associated with the change in CT calcium score over a 2-year period, appearing to offer incremental information to baseline CT imaging. Moreover, in an exploratory analysis, it emerged independently associated with cardiovascular death and AVR after adjustment for both age and sex. This would support PET/CT imaging as a novel method for measuring disease activity in aortic stenosis with implications on risk stratification.

The main advantage that PET holds over other mainstream imaging modalities, such as CT, is that it goes beyond anatomy and is able to resolve valvular biology and pathophysiology. PET can provide immediate non-invasive quantification of on-going and potentially modifiable pathological processes within the body. This includes vascular calcification activity. Indeed recent interest has surrounded 18F-fluoride as a marker of newly developing microcalcification in the coronary arteries that can be used to identify culprit and high-risk atheromatous plaque.(6) This tracer has also been investigated in aortic stenosis, with studies confirming that 18F-fluoride uptake correlates closely with histological markers of valvular calcification activity.(226) In a small interim analysis, we have previously reported that 18F-fluoride is associated with the change in the aortic valve calcium score after 1 year.(226) We here extend these observations to a larger, broader population with longer follow up.

Valvular 18F-fluoride PET uptake, as a marker of calcification activity, increases steadily with more advanced stages of aortic stenosis.(2) In this study, we have confirmed that this observation translates into a similar step-wise increase in disease progression across patients with mild, moderate and severe aortic stenosis (Figure 4.3). 18F-Fluoride demonstrated excellent associations with disease progression as assessed by CT (r=0.80, p<0.001) and standard echocardiographic haemodynamic markers . Whilst CT calcium scoring also predicted disease progression, our data would suggest that PET can provide incremental information, with patients demonstrating higher than expected valvular 18F-fluoride uptake progressing three times fast than subjects with lower than expected activity. Moreover, whilst only a small number of clinical events occurred in this study, 18F-fluoride uptake was independently associated with cardiovascular death and AVR after adjustment for age and sex. In combination with the existing literature, these observations would indicate that 18F-fluoride PET is a non-invasive measure of disease activity in aortic stenosis, with the ability to predict its natural history.

Might 18F-fluoride PET be of use in the clinical setting as a tool for predicting disease progression and risk stratifying patients? Whilst our initial data suggests that PET might provide some incremental prognostic information over and above CT, we have also demonstrated that CT calcium scoring on its own provides excellent prediction of disease progression (231). Although CT is unable to measure calcification activity in the valve directly, it is able to reliably and accurately quantify the progressive accumulation of macroscopic areas of established calcium within the valve. Indeed our

data would suggest that tracking disease progression with CT is perhaps easier than with traditional hemodynamic echocardiography measures given the relatively larger increases in the CT calcium score with time and its excellent reproducibility. Furthermore, because calcification activity increases proportionally with disease severity (thereby explaining the more rapid disease progression observed in those with more advanced disease, Figure 4.3), baseline CT calcium scoring also provides a good surrogate marker of disease activity. This would explain the excellent associations demonstrated between disease progression and clinical outcomes, and CT calcification in this and other recent studies.(39,221) Therefore we believe that this simple and widely available technique is likely to assume a greater clinical role in the future, supported by its superior reproducibility to echocardiographic calcium scoring and incremental prognostic utility over and above the more traditional hemodynamic severity assessments.(232,233)

What then is the future role of 18F-fluoride PET? As discussed it is possible that 18F-fluoride will be able to complement the ability of CT to identify high risk phenotypes for disease progression. In addition we believe that it is likely to prove an excellent means of testing the efficacy of novel therapeutic agents in aortic stenosis.(234) We have previously hypothesized that calcification is the predominant driver of disease progression in aortic stenosis, and that anti-calcific interventions may slow or halt disease progression.(17) In this context the instantaneous readout of valvular calcification activity provided by 18F-fluoride PET has the potential to rapidly detect beneficial treatment effects without the need for protracted follow up. This contrasts favorably with more established imaging modalities such as CT calcium scoring and

echocardiography that take many years to identify the anatomic and hemodynamic consequences of such alterations in disease activity. Ultimately 18F-fluoride PET therefore has the potential to reduce the duration of clinical studies investigating the efficacy of novel treatments, and thereby to expedite their development. Indeed this hypothesis will be tested in future randomised control trials using valvular 18F-fluoride uptake as a pre-defined end-point (clinicaltrials.gov NCT02132026).

In this study, we applied a novel method of assessing valvular radiotracer uptake: the *Most Diseased Segment* (MDS). This approach is simpler than previous methods and was highly reproducible, demonstrating a clear advantage to standard techniques with respect to 18F-FDG imaging. Cardiac 18F-FDG imaging has been hampered by myocardial uptake, making assessment of adjacent structures such as the aortic valve and coronary arteries challenging. In this study, we observed a moderate association between baseline 18F-FDG uptake in the valve and disease progression at 2 years. This result should, however, be interpreted with a degree of caution as the exact mechanisms underlying 18F-FDG activity in the valve remain unclear. Previous studies have established a correlation between macrophage burden and 18F-FDG uptake in carotid atheroma. We have previously failed to demonstrate any such association in the aortic valve.(226) This may be because we only examined severely stenotic valves where inflammation may be of less importance. However questions remain whether 18F-FDG is acting exclusively as a marker of macrophage infiltration in aortic stenosis, or perhaps reflect the metabolic requirements of a wide range of cells.(223) Further work is required to resolve this key issue and to better understand the information that 18F-FDG is providing in aortic stenosis.

There are a number of limitations that we should acknowledge. The strong co-linearity between 18F-fluoride PET activity and the CT calcium score means that much larger studies are required to assess definitively whether 18F-fluoride provides incremental predictive information to CT. The same is true with respect to 18F-FDG. We should also acknowledge the relatively small number of clinical events observed in this study. However given that this was the first study to prospectively investigate 18F-fluoride PET imaging in aortic stenosis, it is possible we can improve the information provided by this technique by incorporating contrast CT angiography and PET motion correction, as we have recently employed in the coronary arteries (20).

We also need to establish whether modification of 18F-fluoride PET uptake can be achieved by potential therapeutic interventions, such as anti-calcific therapies, and whether any such reduction translates in to improved clinical outcomes. These are key priorities that should be addressed in prospective studies using gated PET acquisitions.

In conclusion, the valvular uptake of 18F-fluoride and 18F-FDG on positron emission tomography is associated with disease progression and clinical outcomes in patients with aortic stenosis. These observations support PET/CT imaging as a novel method for measuring disease activity in aortic stenosis with the ability to predict its natural history. This may be of particular use in rapidly assessing the treatment effects of novel medical therapies for this important condition.

Chapter 5.

Cardiac Alpha-V Beta-3 Integrin Expression Following Acute Myocardial Infarction in Humans.

Published by Jenkins WS, Vesey AT, Stirrat C, Connell M, Lucatelli C, Neale A, Moles C, Vickers A, Fletcher A, Pawade T, Wilson I, Rudd JH, van Beek EJ, Mirsadraee S, Dweck MR, Newby DE. Cardiac Alpha-V Beta-3 Integrin Expression Following Acute Myocardial Infarction in Humans. Heart. 2017;103(8):607-615.

5.1. Overview

Maladaptive repair contributes towards the development of heart failure following myocardial infarction (MI). The $\alpha_v\beta_3$ integrin receptor is a key mediator and determinant of cardiac repair. We aimed to establish whether $\alpha_v\beta_3$ integrin expression determines myocardial recovery following MI.

18F-Fluciclatide (a novel $\alpha_v\beta_3$-selective radiotracer) positron emission tomography (PET) and computed tomography (CT) imaging, and gadolinium-enhanced magnetic resonance imaging (CMR) were performed in 21 patients 2 weeks after ST-segment elevation MI (anterior, n=16; lateral, n=4; inferior, n=1). Cardiac CMR was repeated 9 months after MI. Seven stable patients with chronic total occlusion (CTO) of a major coronary vessel, and 9 healthy volunteers underwent a single PET/CT and CMR.

18F-Fluciclatide uptake was increased at sites of acute infarction compared to remote myocardium (tissue-to-background ratio (TBR_{mean}) 1.34±0.22 vs 0.85±0.17; $p<0.001$) and myocardium of healthy volunteers (TBR_{mean} 1.34±0.22 vs 0.70±0.03; $p<0.001$). There was no 18F-fluciclatide uptake at sites of established prior infarction in CTO patients, with activity similar to the myocardium of healthy volunteers (TBR_{mean} 0.71±0.06 vs. 0.70±0.03, p=0.83). 18F-Fluciclatide uptake occurred at sites of regional wall hypokinesia (wall motion index ≥1 vs 0; TBR_{mean} 0.93±0.31 vs 0.80±0.26 respectively, $p<0.001$) and subendocardial infarction. Importantly, although there was no correlation with infarct size (r=0.03, p=0.90) or inflammation (C-reactive protein,

r=-0.20, p=0.38), 18F-fluciclatide uptake was increased in segments displaying functional recovery (TBR_{mean} 0.95±0.33 vs 0.81±0.27, p=0.002) and associated with increase in probability of regional recovery.

In conclusion, 18F-Fluciclatide uptake is increased at sites of recent MI acting as a biomarker of cardiac repair and predicting regions of recovery.

5.2. Introduction

Ischemic heart disease remains the leading cause of death globally, with over 1 million people suffering acute myocardial infarction (MI) per year in the USA alone. As the acute management of MI improves, the number of patients surviving acute myocardial injury is higher than ever before. In this population, adverse cardiac remodeling and the syndrome of delayed heart failure represents a major cause of morbidity.(70) Understanding reparative mechanisms following infarction is becoming increasingly important.

Repair following MI is triggered by a complex interaction of neurohormonal activation and up-regulation of angiogenic and pro-fibrotic transcription factors that initiate the restoration of a capillary network through angiogenesis and re-endothelialization, as well as extracellular matrix (ECM) remodeling through macrophage accumulation and fibroblast activation. This interplay of angiogenesis, inflammation and fibrosis determines the extent of preservation and restoration of myocardial integrity.(235) In some circumstances, maladaptive persistent processes may encourage remodeling and scarring to extend into the myocardium long after the initial causative injury. This may lead to progressive ventricular dilatation, ventricular dysfunction and heart failure.

The $\alpha_v\beta_3$ integrin is a trans-membrane cell surface receptor that facilitates migration, proliferation and interaction with the ECM, thereby allowing cells to respond to, and in turn modify, their extracellular environment. Expressed at low levels by quiescent endothelial cells, $\alpha_v\beta_3$ integrin is markedly up regulated in states of angiogenesis

within the myocardium after infarction.(121,126) In addition, pre-clinical and clinical studies document $\alpha_v\beta_3$ integrin expression by both activated cardiac myofibroblasts and macrophages during margination and chemotaxis. Thus, $\alpha_v\beta_3$ integrin expression appears central to the co-ordination of repair following MI.

In this study, we investigated the expression of $\alpha_v\beta_3$ integrin following MI using the novel $\alpha_v\beta_3$ integrin-selective radiotracer, 18F-fluciclatide, combined with cardiac positron emission tomography (PET), computed tomography (CT) and cardiovascular magnetic resonance (CMR). The study aims were to describe and characterize the uptake of this radiotracer, and to correlate it with clinical markers of disease severity and functional recovery in patients with recent MI.

5.3. Methods

PET/CT scanning with 18F-fluciclatide and CMR were performed in 3 groups of participants recruited from Royal Infirmary of Edinburgh between July, 2013, and February, 2015. Exclusion criteria were age <40 years, women of childbearing potential not taking contraception, severe renal failure (serum creatinine >2.8 mg/dL) or hepatic failure (Childs-Pugh grade B or C), atrial fibrillation, contrast allergy, inability to undergo scanning and inability to provide informed consent. Studies were performed with approval of the local research ethics committee, in accordance with the Declaration of Helsinki, and with the written informed consent of each participant.

5.3.1. Study participants

Acute MI group.

Patients with recent acute ST-segment elevation MI and peak high-sensitivity cardiac troponin I (hs-cTnI) >10,000 ng/L were invited to attend for PET/CT with 18F-fluciclatide 14±7 days after their initial presentation. CMR was performed within 7 days of PET/CT scanning. Patients were then invited to return for a second PET/CT with 18F-fluciclatide 10 weeks after MI and for a follow-up CMR at 9 months.

Chronic Total Occlusion (CTO) group.

Patients with an angiographically-documented complete occlusion of a major epicardial artery and stable cardiac symptoms for >6 months were invited to attend for a single PET/CT with 18F-fluciclatide and CMR.

Control group.

Volunteers with normal left ventricular systolic function, no structural heart disease, and no symptoms of heart failure or MI underwent a single PET/CT with 18F-fluciclatide and CMR.

Histology Cohort

For histological analysis, myocardial biopsy samples were obtained from patients undergoing coronary artery bypass grafting following recent MI. Patients with large ST-elevation MI (<14 days, hs-cTnI >10,000 ng/L) were considered for inclusion forming a separate cohort from the acute MI group.

5.3.2. Imaging procedures

Radiosynthesis of 18F-Fluciclatide

The radiotracer was manufactured at the Clinical Research Imaging Centre, University of Edinburgh on an automated module (FASTlab synthesizer; GE Healthcare) by coupling an amino-oxy-functionalized peptide precursor (AH111695) with 4-18F-fluorobenzaldehyde at pH 3.5 to form 18F-fluciclatide. Full description of this synthesis has been published.(9,10,190)

Imaging assessments

All patients underwent PET-CT imaging of the thorax with a hybrid scanner (Biograph mCT, Siemens Medical Systems, Erlangen, Germany) at the Clinical Research Imaging Centre, University of Edinburgh. No dietary restrictions were required prior to radiotracer administration. Subjects were administered a target dose of 230 MBq 18F-fluciclatide. An attenuation-correction CT scan (non-enhanced 120 kV and 50 mA, 3-mm slices) was performed, followed by the PET acquisition with electrocardiographic (ECG) gating. To assess tracer pharmacodynamics and the optimum timing of scanning, dynamic PET imaging of the thorax was initially performed in 10 subjects in 3-dimensional mode with a single bed position for 70 min. The remainder of study subjects underwent static imaging performed at the optimal

time point as determined from the dynamic studies (40-min post-injection) using a single 30-min bed position in list mode.

To enable an accurate definition of cardiac anatomy cardiac CT angiography was performed on the hybrid scanner immediately after the PET acquisition: 330 ms rotation time, 100 (body mass index <25 kg/m^2) or 120 (body mass index >25 kg/m^2) kV tube voltage, 160-245 mAs tube current, 3.8 mm/rotation table feed, prospective (heart rate regular and <60 /min), or retrospective (heart rate >60 /min) electrocardiogram-gated. Depending on the body mass index, a bolus of 80-100 mL contrast (400 mgI/mL; Iomeron, Bracco, Milan, Italy) was injected intravenously at 5 mL/s, after determining the appropriate trigger delay with a test bolus of 20 mL contrast material.

5.3.3. PET Reconstruction and Analysis

Kinetic PET analysis

Kinetic analysis of the dynamic scans was undertaken to investigate the uptake of 18F-fluciclatide within the myocardium. The dynamic PET data were reconstructed (Ultra-HD, 2 iterations, 21 subsets, 256 pixels, 1.6-mm pixel size) using a dynamic protocol without ECG gating in following time frames; 60s x 5, 120s x 5, 180s x 5, 300s x 8. Regions of interest (ROI's) were drawn in the descending aorta blood pool and myocardium, and used to derive time activity curves after decay correction. An input function calculation based on the PET image–derived activity curve from the aorta blood pool (199) and the myocardial time-activity curve were used to estimate the tissue influx rate *K*i (the slope of the linear regression) and the volume of distribution (the *y*-axis intercept) using a 2-tissue irreversible Patlak model.(9,10) Thoracic 18F-fluciclatide dynamic activity was then normalized for the blood-pool input function on a voxel-by-voxel basis, and after 3D Gaussian filtering (5-mm FWHM) a parametric 3-dimensional image of 18F-fluciclatide uptake was generated (PMod version 3.409, Pmod technologies limited, Switzerland). Using this image, regions of 18F-fluciclatide binding in the myocardium were identified and manually delineated for subsequent *K*i analysis.

Static PET analysis

For all patients, static ECG-gated PET images were reconstructed in diastole (40-70 min post-injection, 50–75% of the R-R interval, Ultra-HD, 2 iterations, 24 subsets,

zoom x2, 200 pixels). Myocardial 18F-fluciclatide uptake was assessed by an experienced observer (WJ) using an OsiriX workstation (OsiriX version 6.0 64-bit; OsiriX Imaging Software, Geneva, Switzerland). PET images were fused and aligned with CT angiography datasets in diastole. Myocardial radiotracer uptake was quantified using two methods.

First, using a standardized approach PET/CT datasets were re-orientated into traditional short-axis, 2-chamber, 3-chamber and 4-chamber views with a slice thickness of 3 mm in order to fully visualize myocardial radiotracer uptake and allow comparison with CMR imaging. Regions of interest (ROIs) were drawn at sites that corresponded to the areas of acute infarction seen on CMR late gadolinium enhancement imaging. To define referent 'remote' myocardial regions, ROI's were drawn within proximal regions of the myocardial territory that displayed no CMR evidence of infarction. Care was taken to avoid blood-pool contamination. ROIs were copied onto the PET dataset and mean radiotracer activity measured using standard uptake values (SUV; the decay corrected tissue concentration of the tracer divided by the injected dose per body weight).

Second, the CT angiography dataset was re-orientated into the left ventricular short axis (slice thickness 8 mm). Basal, mid-cavity, and apical regions were manually delineated into segmental ROI's according to the standard 17-segment model recommended by the American College of Cardiology/American Heart Association.(236) We excluded the true apex as it was not possible to avoid partial

volume effects. ROI's were then copied onto the re-orientated PET image dataset and segmental SUV and TBR data extracted using the technique above.

PET data were corrected for residual blood pool activity (standard uptake value, SUV) in the superior vena cava and expressed as a mean tissue-to-background ratio (TBR_{mean}). SUV_{max} and TBR_{max} values were also calculated alongside the corrected SUV (SUV_C) values, where blood pool activity was subtracted from myocardial uptake.(2,226)

In a substudy of 10 randomly selected subjects, interobserver reproducibility was assessed by two experienced observers (WJ,CM).

5.3.4. CMR Imaging

Cardiac MRI was performed at 3 T (MAGNETOM Verio, Siemens AG, Healthcare Sector, Erlangen, Germany). For the assessment of left ventricular function, short-axis cine images from the mitral valve annulus to the apex were obtained using a balanced steady-state free-precession sequence (8-mm parallel slices with 2-mm spacing). Quantification of left ventricular function and volumes indexed to body surface area was assessed using standard methods with dedicated software (Siemens AG Healthcare Sector, Erlangen, Germany).(270) Using this software papillary muscle delineation was not included in the analysis. Regional systolic function assessments were performed from the basal, mid, and apical short-axis slices by calculating the end-diastolic and end-systolic wall thicknesses and expressed as the wall motion score index (WMSI; 0, normal; 1, mild or moderate hypokinesia; 2, severe hypokinesia; 3, akinesia; 4, dyskinesia).(95)

The assessment of focal replacement myocardial fibrosis was performed with late gadolinium enhancement (LGE) imaging, 15 min after administration of 0.1 mmol/kg gadobutrol (Gadovist/Gadavist, Bayer Pharma AG, Berlin, Germany). LGE imaging was performed between 8 and 15 min using two approaches: an inversion-recovery fast gradient-echo sequence and a phase-sensitive inversion recovery sequence, performed in two phase encoding directions to differentiate true enhancement from artefact. The inversion time was optimized for each slice to achieve satisfactory nulling of the myocardium.(212) The amount of LGE was quantified with QMASS software (Medis Medical Imaging Systems, Leiden, the Netherlands) using a signal

intensity threshold greater than twice the standard deviation above the mean value in a normal region of myocardium sampled on the same short-axis image. The transmural extent of infarction within each segment was classified using a transmurality score (transmurality index; 0, no LGE; 1, 1-50%; 2, 51-75% or 3, 76-100%) and recorded as either subendocardial (1-2) or transmural (3).(209) Areas thought to represent inversion artefact or blood pool contamination were manually excluded.

Myocardial extracellular volume fraction (ECV) has been demonstrated to act as a measure of myocardial fibrosis in a variety of cardiac conditions.(210,211) Recently, our group has described a highly reproducible standardized approach to analyse myocardial ECV. (212) To achieve this, T1 mapping was performed using the MOdified Look-Locker Inversion recovery (MOLLI; flip angle 358; minimum TI 100 ms; TI increment of 80 ms; time delay of 150 ms with a heart beat acquisition scheme of 3-3-5) with built-in motion correction.(213) A gradient echo field map and associated shim were performed to minimize off-frequency artefact. Short-axis T1 maps of the mid-cavity slice were acquired in diastole before and at 2, 5, 10, 15, 20, and 30 min following the administration of 0.1 mmol/kg of gadobutrol (Gadovist/Gadavist, Bayer Pharma AG, Germany). The basal slice was defined as the first complete ring of myocardium below the aortic outflow tract, and the mid-cavity slice as the most basal slice to include both papillary muscles. The apical slice was selected between the apex and the mid-cavity on the image least affected by trabeculations and partial volume averaging.(212) Regions of interest were drawn around the myocardium on the short-axis, pre-contrast, motion-corrected myocardial T1 maps and copied onto corresponding 20-min post-contrast maps, with minor

adjustments made to avoid partial volume effects and artefact (OsiriX version 4.1.1, Geneva, Switzerland). ECV was calculated according to the following formula:

$$ECV=(\Delta R1_{myocardium}/\Delta R1_{blood\text{-}pool}) \times(1-hematocrit)$$

where:

$$\Delta R1=(1/postcontrast\ T1-1/precontrast\ T1).$$

Hematocrit was sampled at the time of MRI.(214)

5.3.5. Histology

For histological analysis, myocardial biopsy samples were obtained from patients undergoing coronary artery bypass grafting following myocardial infarction. Patients with recent large ST-elevation myocardial infarction (<14 days, hs-cTnI >10,000 ng/L) were considered for inclusion. A core cardiac biopsy was taken intra-operatively under direct visualisation by an experienced surgeon from the peri-infarct zone. Samples were fresh frozen and mounted in cryosection medium. Histological processing was performed by trained staff in the Histopathology department at the Queens Medical Research Institute. The tissue samples were then cut in sequential, longitudinal 4-µm sections at -20 °C and thaw-mounted onto microscope slides. They were dried for 15 min and spray-fixed with neutral buffered formalin. After rinsing in distilled water, sections were stained with hematoxylin-eosin (HE) and van-Gieson (VG) for conventional histopathological examination. In order to optimize immunohistochemistry, an antigen-unmasking step was performed by microwave treatment for 30 s. Endogenous peroxidase was blocked by incubation with hydrogen peroxide for 5 min. Sections were subsequently incubated with the primary antibodies; smooth muscle actin, CD31, CD68 (clone PG-M1), and integrin $\alpha_v\beta_3$ antibody, clone LM609 (Millipore) for 30 min at room temperature. After washing the sections were incubated with Envision Flex (DAKO, K5007) for 30 min at room temperature, followed by incubation with diaminobenzamine (Sigma) for 10 min. The slides were finally counterstained with hematoxylin and digitally imaged (Axioscan.Z1, Zeiss, UK) before visual assessment by Dr William Jenkins under the supervision of Consultant Pathologist Professor Donald Salter to ascertain the distribution and

characterisation of integrin $\alpha_v\beta_3$ staining in relation to myocardial structure and cell type.

5.3.7. Statistical Analysis

We explored myocardial radiotracer uptake in 3 groups of patients, comparing them to CMR and clinical indices of cardiac function. Continuous data were tested for normality with the D'Agostino and Pearson Omnibus test. Continuous normal variables were expressed as mean±standard deviation and compared using Students t-testing or analysis of variance (ANOVA) testing when comparing more than 2 groups. Continuous non-normal variables were presented as median [interquartile range] and compared using the Mann-Whitney or Kruskal-Wallis test when evaluating two/more than two groups. Interobserver reproducibility was calculated by Bland-Altman method and presented as mean bias ±2 standard deviations, and intraclass correlation coefficients (ICC) with 95% confidence intervals (CI). The chi-squared test was used for analysis of categorical variables. Univariable and multivariable logistic regression models were used to determine factors associated with an improvement in segmental myocardial function. Statistical analysis was performed with GraphPad Prism version 6 (GraphPad Software Inc., USA) and JMP version 10.0 (SAS Software, North Carolina, USA) where appropriate. A two-sided P-value<0.05 was considered statistically significant.

5.4. Results

5.4.1. Baseline clinical characteristics

Thirty-seven subjects underwent PET/CT after injection of 229±12 MBq 18F-fluciclatide: 21 patients with acute MI, 7 patients in the CTO group and 9 healthy volunteers (Table 5.1). The groups were generally well balanced for age, sex and body-mass index. Healthy subjects had a lower prevalence of cardiovascular risk factors (Table 5.1). The mean radiation dose for each 18F-fluciclatide PET scan was 5.9 mSv (range 5.2-6.4 mSv). The mean attenuation correction CT acquisition radiation dose was 1.4 mSv (range 0.8-1.9 mSv). Cardiac CT contrast angiography dosing was 6.7mSv (range 2.1-11.7 mSv); the wide dose range accounted for the potential presence of atrial fibrillation that prevents prospective ECG gating. The mean radiation dose per participant for those who received a single PET/CT imaging assessment was 15.1 (range 7.8-18.9) mSv, and 21.9 (range 16.5-28.7) mSv in those who underwent repeat PET scanning.

Table 5.1. Baseline participant characteristics

	All (n=37)	Acute Myocardial Infarction Group (n=21)	Chronic Total Occlusion Group (n=7)	Control Group (n=9)	*p* value*
Patient Characteristics					
Age (years)	64±10	62±12	69±7	66±7	0.06
Male Sex	27(73)	16(76)	5(71)	6(67)	0.46
BMI (kg/m^2)	28±4	28±5	31±3	27±4	0.74
18F-Fluciclatide Dose (mBq)	229±12	227±13	227±14	232±9	0.86
Current Smoker	9(24)	8(38)	1(14)	0(0)	0.01
Diabetes Mellitus	4(11)	3(14)	1(14)	0(0)	0.06
Hypertension	16(43)	7(33)	5(71)	4(44)	0.04
Hypercholesterolemia	22(60)	14(66)	6(86)	2(22)	<0.001
Cardiovascular History					
Prior myocardial infarction	7(19)	1(5)	6(86)	0(0)	<0.001
Angiographically documented CAD	28(76)	21(100)	7(100)	0(0)	<0.001
Previous PCI	4(11)	1(5)	3(42)	0(0)	<0.001
CCS Class					
0	28(76)	17(81)	2(29)	9(100)	0.02
I or II	7(19)	4(19)	3(42)	0(0)	0.03
III or IV	2(6)	0(0)	2(29)	0(0)	0.51
NYHA Class					
I	29(78)	15(71)	3(42)	9(100)	0.32
II	7(19)	5(24)	2(29)	0(0)	0.39
III or IV	2(6)	1(5)	1(14)	0(0)	0.25
Medications					
Aspirin	27(73)	21(100)	6 (86)	0(0)	<0.001
Clopidogrel	22(59)	19(90)	3(42)	0(0)	<0.001
Statin	29(78)	21(100)	7(100)	1(11)	0.004
β-Blocker	26(70)	20(95)	6(86)	0(0)	<0.001
ACEi / ARB	27(73)	20(95)	5(71)	2(22)	0.02
Clinical Features					

Systolic BP (mm Hg)	137±22	128±18	140±24	155±21	0.06
Heart rate (bpm)	64±12	62±13	61±11	68±10	0.42
Creatinine (μmol/L)	79±15	82±19	77±14	73±12	0.54
hs-CRP (mg/L)	3.5[1.3-9.8]	5.6[2.0-11.7]	2.2[1.0-9.1]	1.5[1.2-3.3]	0.008

*Mean±SD, median [IQR] or number (percentage). *Analysis of variance, Students t-test (continuous data) or Chi squared test (categorical data). Abbreviations: BMI, body-mass index; CAD, coronary artery disease; PCI, percutaneous coronary intervention; CCS, Canadian Cardiovascular Society; NYHA, New York Heart Association; ACEi, angiotensin-converting enzyme inhibitor, ARB, angiotensin receptor blocker; BP, blood pressure; hs-CRP, high-sensitivity c-reactive protein*

5.4.2. CMR characterisation of myocardial infarction & remodeling

There were no areas of infarction in control subjects. All patients within the acute MI cohort (n=21) had visible infarction on CMR 13±5 days after MI. These infarcts were large (infarct size 12±7 g/m^2, peak cardiac troponin I 50,000 [26,753-50,000] ng/L) and featured the anterior (n=16) and lateral (n=4) territories predominantly, while 1 patient had an inferior MI. All subjects received emergency coronary angiography with successful revascularization 197 [148-342] min from the onset of symptoms (Table 5.2).

Old infarcts were present in 6 of 7 patients in the CTO group. Although there was no difference in infarct size [g/m^2] between MI and CTO groups ($p=0.34$), the left ventricular ejection fraction (LVEF) was reduced with a larger WMI score in those with recent MI ($p<0.01$ compared to either the CTO or control group, Table 5.3).

Seventeen patients from the acute MI group received follow-up CMR imaging 287±37 days after MI. During this timeframe, there were improvements in LVEF ($p<0.01$) and regional wall motion (WMI; $p<0.005$). In total, 43 of 272 myocardial segments (16%) showed an improvement in regional wall motion, while 226 segments remained unchanged and 3 segments displayed functional deterioration. Infarct size and LV mass also improved ($p=0.03$ and $p<0.01$ respectively, Table 5.4).

Table 5.2. Characteristics of patients with acute myocardial infarction

Clinical Data	**Acute MI Group (n=21)**
Peak cardiac troponin I (ng/L)	50,000 [26,753-50,000]
Percutaneous coronary intervention	20 (95)
Symptom onset to reperfusion (min)	197 [148-342]
Single vessel disease	10 (48)
Myocardial Infarction Territory	
Anterior	16 (76)
Lateral	4 (19)
Inferior	1 (5)
Adverse Outcome	
TIMI Flow post-PCI <3	1 (5)
Cardiogenic Shock	3 (14)
IABP	2 (10)
Aborted cardiac arrest	2 (10)

Median [interquartile range] and number (%). Abbreviations; TIMI, trials in myocardial infarction; PCI, percutaneous coronary intervention; IABO, intra-aortic balloon pulsation

Table 5.3. Baseline Imaging Assessment

	All	Acute Myocardial Infarction Group	Chronic Total Occlusion Group	Control Group	p value*
	(n=37)	*(n=21)*	*(n=7)*	*(n=9)*	
CMR Imaging					
LVEF (%)	58±10	52±9	62±8	65±5	<0.001
LV Mass (g/m^2)	79±20	85±20	66±17	75±16	0.07
LVEDV (mL/m^2)	77±18	80±18	69±13	76±17	0.35
LVESV (mL/m^2)	34±13	39±14	30±10	27±9	0.046
WMI	0.25±0.13	0.40±0.20	0.09±0.05	0.0±0.0	<0.001
ECV (%)	31±5	34±4	28±3	28±2	<0.001
Presence of LGE	27(73)	21(100)	6(86)	0(0)	<0.001
Infarct size (g/m^2)	8±8	12±7	8±8	0±0	<0.001
PET Imaging					
SUV_{mean} (kBq/mL)					
SVC	2.73±0.51	2.85±0.51	2.57±0.39	2.58±0.57	0.27
Total LV uptake	2.24±0.51	2.33±0.48	1.96±0.53	1.77±0.27	<0.001
Myocardial Infarct Uptake	3.23±1.03	3.72±0.63	1.76±0.26	-	<0.001
Remote Myocardial Uptake	2.21±0.60	2.41±0.57	1.62±0.14	-	0.001
TBR_{mean}					
Total LV Uptake	0.77±0.16	0.82±0.18	0.71±0.06	0.70±0.03	0.08
Myocardial Infarct Uptake	1.05±0.37	1.34±0.22	0.70±0.14	-	<0.001
Remote Myocardial Uptake	0.80±0.18	0.85±0.17	0.64±0.12	-	0.009
SUV_{max} (kBq/mL)					
Total LV uptake	2.71±0.58	2.86±0.56	2.24±0.40	2.07±0.31	<0.001
Myocardial Infarct Uptake	3.53±1.00	3.98±0.68	2.18±0.35	-	<0.001
Remote Myocardial Uptake	2.59±0.64	2.75±0.65	2.18±0.35	-	0.02
TBR_{max}					
Total LV uptake	0.98±0.19	1.02±0.19	0.89±0.20	0.81±0.09	0.01
Myocardial Infarct Uptake	1.28±0.34	1.42±0.25	0.86±0.16	-	<0.001
Remote Myocardial Uptake	0.94±0.19	0.97±0.20	0.84±0.13	-	0.11

SUV$_C$ (kBq/mL)					
Total LV uptake	-0.55±0.57	-0.52±0.55	-0.61±0.67	0.81±0.42	0.85
Myocardial Infarct Uptake	0.75±0.91	1.13±0.67	-0.40±0.46	-	<0.001
Remote Myocardial Uptake	-0.19±0.52	-0.11±0.54	-0.45±0.37	-	0.12

*Mean±SD or number (percentage). *Analysis of variance, Students t-test (continuous data) or Chi squared test (categorical data). Abbreviations: CMR,cardiac magnetic resonance; LVEF,left ventricular ejection fraction; LVEDV,left ventricular end diastolic volume; LVESV,left ventricular end systolic volume; WMI,wall motion index; ECV,extracellular volume; LGE,late gadolinium enhancement; SVC; superior vena cava; SUV,standardized uptake value; TBR,tissue-to-background ratio, SUV_C, corrected SUV*

Table 5.4. Acute myocardial infarction assessments

CMR Imaging			**p-value**
	Initial CMR	**Follow-up CMR**	
	(n=21)	***(n=17)***	
MI to CMR (days)	13±5	287±37	<0.01
LVEF (%)	52±9	55±8	<0.01
Indexed LV Mass (g/m^2)	85±20	74±13	<0.01
LVEDV (mL/m^2)	80±18	82±16	0.88
LVESV (mL/m^2)	39±14	38±12	0.36
Wall Motion Index	0.40±0.20	0.22±0.15	<0.01
ECV (%)	34±4	33±2	0.58
Infarct size (g/m^2)	13 [7-17]	6 [3-14]	0.03
PET Imaging			
	Initial PET/CT	**Repeat PET/CT**	
	(n=21)	***(n=17)***	
MI to PET (days)	12±4	76±19	<0.01
Total LV Uptake (TBR_{mean})	0.82±0.18	0.85±0.18	0.96
Myocardial Infarct Uptake (TBR_{mean})	1.34±0.22	1.20±0.21	0.02
Remote Myocardial Uptake (TBR_{mean})	0.85±0.17	0.82±0.15	0.38
Segmental uptake (TBR_{mean}) & Regional Wall Motion (WMI)			
Normal function (0)	0.80±0.26	0.83±0.23	0.14
Mild-mod hypokinesia (1)	0.89±0.33	0.97±0.29	0.33
Severe hypokinesia (2)	0.97±0.28	0.91±0.34	0.47
Akinesia (3)	0.77±0.21	0.73±0.24	0.66
Dyskinesia (4)	-	-	-
Segmental uptake & Transmurality of MI (TBR_{mean})			
No infarct	0.75±0.23	0.81±0.23	NA
Subendocardial infarct (1-75%)	0.95±0.29	1.08±0.28	NA
Transmural infarct (76-100%)	0.89±0.29	0.88±0.27	NA

Mean±SD or median [IQR]. Abbreviations: MI, myocardial infarction; LV, left ventricle; TBR_{mean}, mean tissue-to-background ratio; CMR, magnetic resonance imaging; LVEF, left-ventricular ejection fraction; LVEDV, left-ventricular end diastolic volume; LVESV, left ventricular end systolic volume; WMI, wall motion index; ECV, mean extracellular volume.

5.4.3. Histology & Dynamic Myocardial 18F-Fluciclatide PET

In an exploratory analysis, 2 patients scheduled for coronary artery bypass surgery within 14 days of infarction underwent myocardial biopsies from the peri-infarct zone (Figure 5.1). This showed predominantly viable myocardium with widespread positive staining for $\alpha_v\beta_3$ integrin, largely in regions that co-localized to CD31-positive vascular endothelial cells. Interestingly, these sites represented mainly angiogenic microvasculature, although there was scattered co-localisation with dual smooth muscle actin- and CD31-positive arterioles. There were lesser numbers of CD68-positive inflammatory cells and smooth muscle actin-positive myofibroblasts, but where present, they also co-registered with $\alpha_v\beta_3$ integrin expression (Figure 5.1).

Figure 5.1. $\alpha_v\beta_3$ Integrin expression in patient with recent myocardial infarction

The figure below displays images from adjacent fresh frozen and cryosectioned biopsies from the peri-infarct area of a patient with recent anterior MI. Immunohistochemical staining for ***(A)*** *$\alpha_v\beta_3$ integrin displayed multiple regions of positive staining that co-localize to regions of staining for vascular endothelial cells (CD31,* ***B****) visible at x4 magnification. At x20 magnification, these regions of $\alpha_v\beta_3$ staining* ***(C)*** *correspond predominantly to arterioles and the microvasculature* ***(D)****, and also to regions of staining for smooth muscle actin* ***(E)****, representative of both arterioles (co-staining with CD31) and myofibroblasts. There were relatively few macrophages* ***(F)****.*

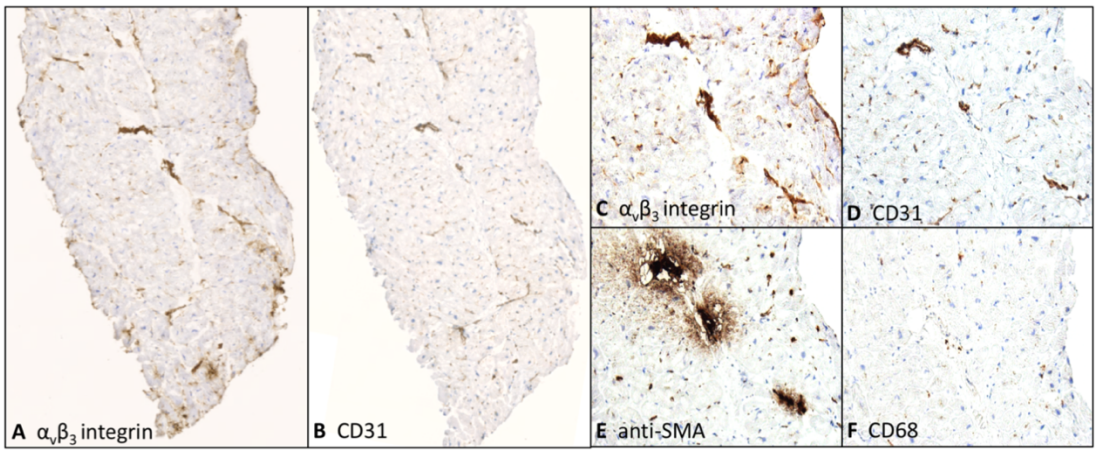

Dynamic PET studies were performed in a subgroup of 10 patients. 18F-Fluciclatide activity within the region of myocardial infarction increased gradually and reached a plateau at around 30-40 min (Figure 5.2). The injected activity was cleared from the blood pool with a half-life of about 10 min, so that it remained relatively high during the period of PET acquisition (superior vena cava SUV_{mean} 2.73±0.51 at 40-70 min post-injection). The optimum contrast between 18F-fluciclatide uptake in the site of infarction compared to the blood pool was observed at 40 min (Figure 5.2B). This time point was therefore used for subsequent static imaging.

Using a 2-compartment Patlak model,(9) 18F-fluciclatide uptake displayed a distinct linear phase and a steep *K*i slope, in keeping with irreversible binding of 18F-fluciclatide to $\alpha_v\beta_3$ integrin during the 70-min period of evaluation (Figure 5.2D). The three-dimensional parametric images generated from Patlak analysis (Figure 5.2E, Figure 5.3F) confirmed regions of increased 18F-fluciclatide binding in sites of acute infarction, supporting an up-regulation of $\alpha_v\beta_3$ integrin within the infarct zone.

Figure 5.2. Dynamic Analysis of 18F-Fluciclatide Uptake

*Axial and sagittal CT angiography of the thorax in a patient with recent anterior MI (**A**). The time-activity curves generated from the descending aorta and the apical interventricular septum (blue crosshairs) show increased uptake in the infarct relative to blood pool. Optimal contrast between 18F-fluciclatide tissue and blood pool activity was observed after 40 min (dotted line, **B**). The PET image in the axial and sagittal plane shows increased uptake within the apical septum, although there is some background activity (**C**). Patlak analysis of ROI's placed in the interventricular septum confirms integrin binding, as evidenced by the gradient of the slope and the y-intercept (**D**), and using a Ki-generated image we can better identify and delineate focal uptake within myocardium (**E**). A region of remote myocardium within the same patient generates a Patlak curve with significantly lower gradient and intercept in comparison (**F**).*

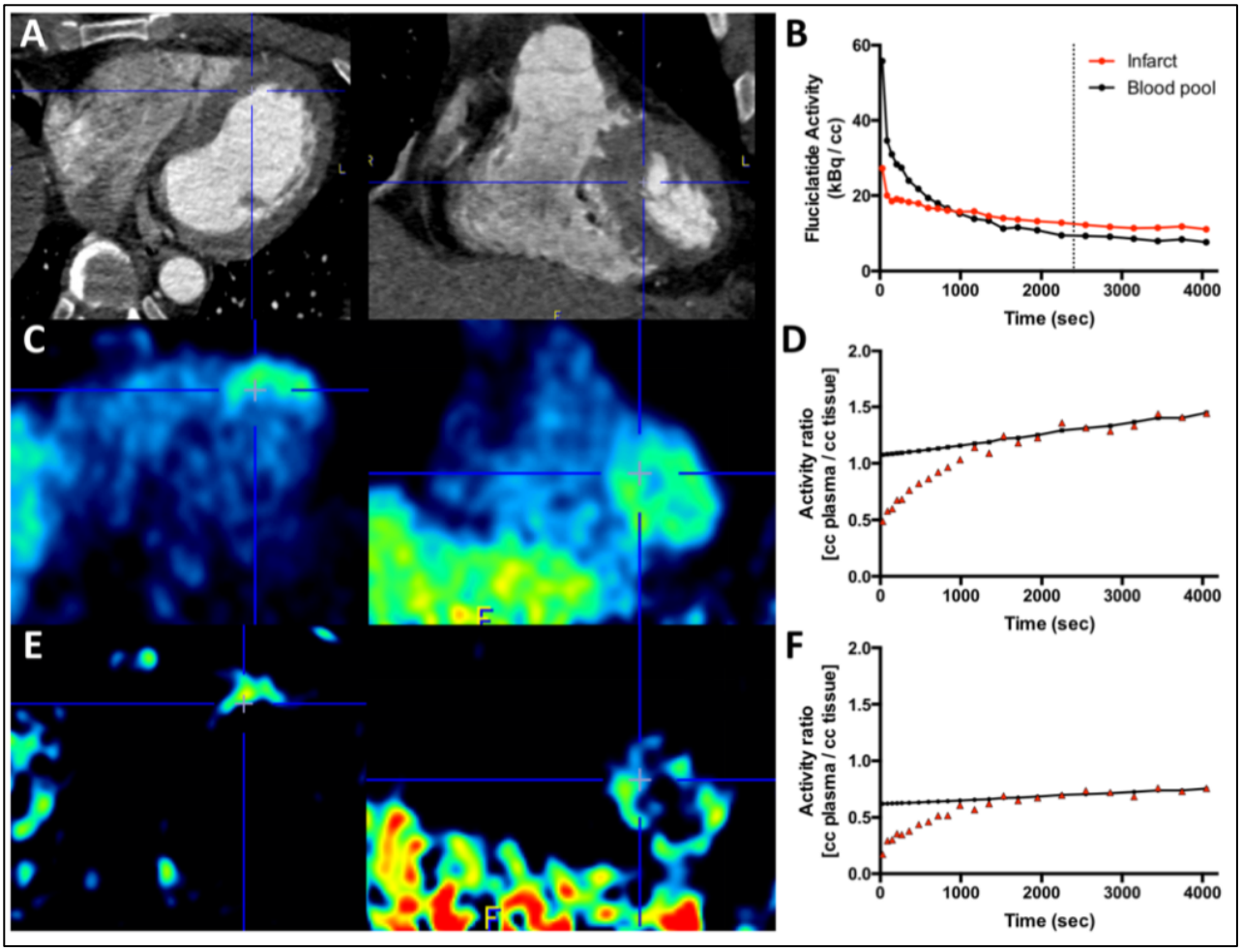
A
B
Infarct
Blood pool
Fluciclatide Activity (kBq / cc)
Time (sec)
C
D
Activity ratio [cc plasma / cc tissue]
Time (sec)
E
F
Activity ratio [cc plasma / cc tissue]
Time (sec)

5.4.4. Static 18F-Fluciclatide PET in Myocardial Infarction

PET Repeatability Studies

The reproducibility of 18F-fluciclatide uptake quantification was assessed in both the blood pool and the myocardium in 10 subjects selected at random. Residual blood pool radiotracer activity was quantified within both the SVC and right atrium. While both methods displayed no fixed or proportional biases with narrow limits of agreement and high ICC values of >0.94, the SVC-approach appeared to hold a slight advantage (ICC 0.97 [95% CI; 0.93-0.99]) and this therefore was applied throughout the study to quantify latent radiotracer blood activity (Table 5.5).

Quantification of radiotracer uptake within the region of myocardial infarction was assessed using the mean Standard Uptake Value (SUV_{mean}), the mean tissue to background ratio (TBR_{mean}) and a novel method subtracting the target tissue mean SUV from the blood pool mean SUV ($SUV_{target - blood\ pool}$).(134) The SUV_{mean} and TBR_{mean} both proved highly reproducible, displaying no fixed or proportional biases (mean % difference [95% limits of agreement]; 3.0 [-27.2 - 33.3], and 3.0 [-24.0-29.9] respectively) and a high ICC value (0.93 [0.82-0.97] and 0.94 [0.83-0.98] respectively). Selecting repeatable regions of remote myocardium proved less reliable, with wider limits of agreement (-18.9-66.2) and a moderate intra-class coefficient value of 0.60. Quantification of the regional 18F-fluciclatide TBR_{mean} in individual myocardial segments also proved reproducible with no fixed or proportional biases (mean % difference -8.97 [95% CI -31.6 to 13.6]) and a high ICC value (0.90 [95%

CI 0.590-0.975]). The TBR_{mean} method was therefore preferentially used for subsequent analysis to compensate for potential contamination from residual blood pool activity.

Table 5.5. 18F-Fluciclatide Reproducibility

	Reproducibility Analysis	
	Mean % difference[a]	**Intra-class coefficient[b]**
Blood pool assessment (SUV)		
SVC	3.1 (-9.5–15.6)	0.971 (0.928-0.989)
Right Atrium	-0.46 (-11.7-10.7)	0.943 (0.868-0.975)
Infarct assessment		
TBR_{mean}		
Whole Ventricle	-8.97 (-31.6-13.6)	0.898 (0.590-0.975)
Infarct	3.0 (-24.0-29.9)	0.940 (0.833-0.978)
Remote myocardium	23.7 (-18.9-66.2)	0.604 (-0.280-0.847)
SUV_{mean}		
Whole ventricle technique	-6.7 (-25.3–11.9)	0.957 (0.830-0.989)
Infarct	3.0 (-27.2-33.3)	0.930 (0.819-0.973)
Remote myocardium	21.2 (-11.1-53.7)	0.787 (0.448-0.918)
Infarct:remote myocardium ratio	-18.2 (-60.6-24.1)	0.687 (0.187-0.879)
$SUV_{target\ tissue\ -\ blood\ pool}$		
Whole Ventricle	24.1 (-19.2–67.3)	0.410 (-0.372-0.698)
Infarct	77.7 (-464.6–620.1)	0.933 (0.814-0.976)
Remote Myocardium	-43.8 (-120.4-32.7)	0.574 (-0.106-0.836)

[a] Mean % difference between standard uptake value (SUV; kBq/mL) measurements (95% limits of agreement), and [b] ICC (intraclass correlation coefficient) values (95% confidence intervals) for 18F-fluciclatide myocardial uptake and residual blood pool activity. Abbreviations: SVC, superior vena cava; TBR_{mean}, mean tissue to background ratio.

Static PET Studies

All patients in the acute MI cohort had increased focal myocardial uptake of 18F-fluciclatide on baseline PET/CT scanning (12±4 days after MI), which co-localized to regions of infarction on CMR (Figures 5.2 & 5.3, Tables 5.2 & 5.3). Hepatic uptake of 18F-fluciclatide was common. However, in the patient with inferior MI, basal inferior and infero-septal myocardial uptake of 18F-fluciclatide was quantifiable. 18F-Fluciclatide uptake was greater in the acute myocardial infarct when compared to regions of old infarction in the CTO cohort and healthy myocardium in the control group, regardless of the measure of PET uptake used (for example, TBR_{mean} 1.34±0.22 vs. 0.70±0.14 vs. 0.70±0.10, $p<0.001$ respectively). Indeed, no focal increase in 18F-fluciclatide uptake was observed in regions of chronic infarction, with similar PET uptake measurements compared to control subjects (e.g. TBR_{mean}, $p=0.83$). In regions of myocardium remote to the site of acute infarction, 18F-fluciclatide activity was modestly but uniformly increased when compared to comparative regions in CTO patients (TBR_{mean} 0.85±0.17 vs 0.64±0.12, $p=0.009$). Across our population there were no age-related (TBR_{mean}, r=-0.19 [-0.53-0.19], $p=0.31$) or sex-related (TBR_{mean} 1.14±0.07 vs. 1.25±0.17, $p=0.46$) differences in 18F-fluciclatide uptake.

Seventeen subjects agreed to return for a second 18F-fluciclatide PET/CT 76±19 days post-MI, with similar results noted. All these patients were clinically stable between the scans. 18F-Fluciclatide uptake remained elevated at the site of infarction (MI vs. CTO group, TBR_{mean} 1.20±0.21 vs. 0.70±0.15 respectively, $p<0.001$), although the intensity was reduced compared to earlier imaging ($p=0.01$; Figure 5.3). Increased 18F-fluciclatide uptake also persisted in regions of remote myocardium when

compared to uptake in CTO patients (TBR_{mean} 0.82±0.15 vs 0.64±0.12 respectively, p=0.01) and interestingly remained equivalent in terms of intensity compared to the initial PET scan (TBR_{mean} 0.85±0.17 vs 0.82±0.15 respectively, p=0.38).

Figure 5.3. 18F-Fluciclatide uptake in acute myocardial infarction

18F-Fluciclatide uptake in 3 patients with recent subendocardial myocardial infarction (MI). Patient 1, 13 days after anterior MI, displaying a short-axis PET image of the left ventricle with crescentric 18F-fluciclatide uptake ***(A)*** *that correlates with the interventricular septum and anterior wall on CT angiography* ***(B)****. The fused PET/CT-angiography image* ***(C)*** *shows this uptake corresponds exactly to the region of late gadolinium enhancement (LGE) on CMR* ***(D)****. Further delineation of myocardial uptake on PET/CT is clearer in the 2-chamber view* ***(E)*** *and on a fused CT/3D-Patlak image, which shows this uptake to follow a watershed-pattern emerging from the coronary stents present in the left anterior descending coronary artery* ***(F)****. Panels* ***G & H:*** *patient 2, 8 days following anterior MI, displaying focal uptake of 18F-fluciclatide in the anterior wall and apex in the 3-chamber view on PET/CT* ***(G)*** *which corresponds to the region of infarction on LGE CMR imaging* ***(H).*** *Panels* ***I & J****: patient 3, showing focal uptake of 18F-fluciclatide in the inferior wall 19 days following MI on PET/CT* ***(I)*** *that again corresponds to the infarction on CMR LGE imaging* ***(J)****.*

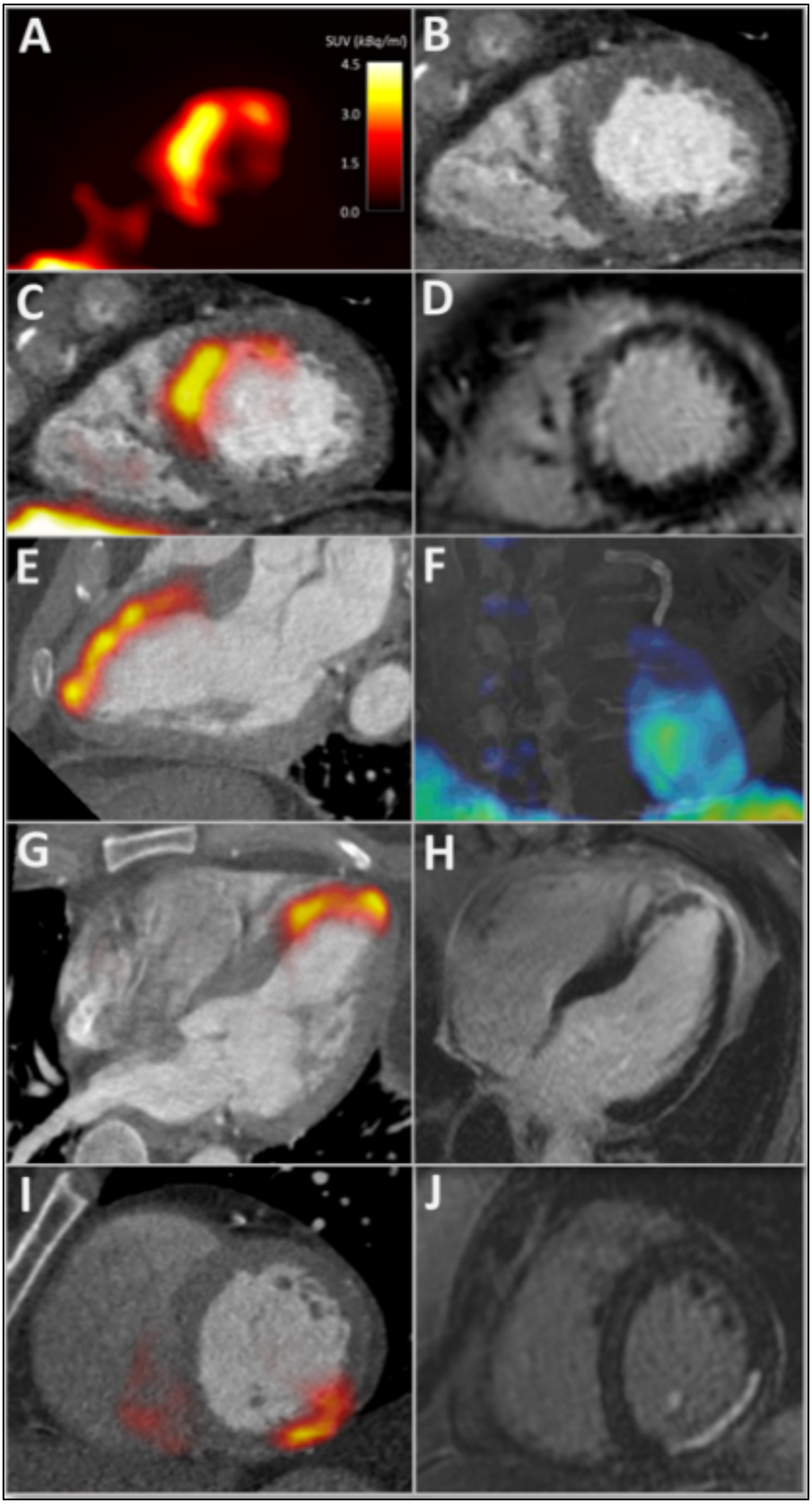
A
SUV (kBq/ml)
4.5
3.0
1.5
0.0
B
C
D
E
F
G
H
I
J

5.4.5. Myocardial 18F-Fluciclatide Uptake and Cardiac Function

The extent of 18F-fluciclatide uptake following MI was compared with clinical and imaging measures of MI severity and subsequent repair (Table 5.6). Although segmental 18F-fluciclatide uptake displayed a moderate correlation with the degree of extracellular volume on CMR T1 mapping (r =0.37, p<0.001), it did not correlate with many of the standard measures of infarct severity, in particular there were no associations with infarct size on CMR (r=0.03, p=0.90), LVEF (r=-0.08, p=0.72), hs-TnI (r=0.13, p=0.36) or C-reactive protein (r=-0.20, p=0.38) (Table 5.6). This may be explained by the absence of increased uptake in the largest akinetic infarcts (normal wall motion vs. akinetic segments; TBR_{mean} 0.80±0.26 vs. 0.77±0.21, p=0.77). Rather 18F-fluciclatide activity was highest in segments with hypokinesis (WMI 1&2 vs. 0; TBR_{mean} 0.92±0.03 vs 0.80±0.26, p<0.001; Figure 5.4) and segments associated with a subendocardial pattern of LGE (subendocardial LGE vs no LGE; TBR_{mean} 0.95±0.06 vs. 0.75±0.03 respectively, p<0.001; Figure 5.4).

18F-Fluciclatide uptake was higher in hypokinetic regions that subsequently demonstrated functional recovery compared to regions with no change or a worsening in contractile function (TBR_{mean} 0.95±0.33 vs 0.81±0.02 respectively, p=0.002; Figure 5.4). Using logistic regression analysis, 18F-fluciclatide TBR_{mean} was significantly associated with recovery in segmental cardiac function on univariable analysis (OR 1.27 [95% CI 1.08-1.50] per 10% increase in TBR_{mean}, p=0.003), which persisted after adjustment for age and sex (OR 1.27 [95% CI 1.07-1.51] per 10% increase in TBR_{mean}, p=0.005). This effect was however attenuated following additional adjustment for the

transmurality of LGE (OR 1.03 [95% CI 0.83-1.26] per 10% increase in TBR_{mean}, p=0.80) and ECV (OR 1.02 [0.91-1.32] per 10% increase in TBR_{mean}, p=0.35).

Table 5.6. Comparison of 18F-fluciclatide uptake and indices of infarction

	18F-Fluciclatide Infarct uptake (TBR_{mean})	Δ18F-Fluciclatide Infarct uptake (1^{st}-2^{nd} scan, TBR_{mean})	Mean ECV (%)	Infarct Size (g/m^2)
Clinical Characteristics				
Peak hs-cTnI (ng/l)	*r*=0.13 (-0.31-0.54) p=0.56	*r*=-0.27 (-0.66-0.24) p=0.30	*r*=0.61 (0.23-0.82) p=0.003	*r*=0.59 (0.22-0.81) p=0.004
hs-CRP (mg/L)	*r*=-0.20 (-0.58-0.25) p=0.38	*r*=-0.04 (-0.54-0.48) p=0.90	*r*=-0.02 (-0.45-0.41) p=0.92	*r*=0.55 (0.16-0.80) p=0.009
Baseline CMR Assessment				
LVEF (%)	*r*=-0.08 (-0.49-0.36) p=0.72	*r*=0.03 (-0.46-0.50) p=0.91	*r*=-0.12 (0.53-0.32) p=0.59	*r*=-0.44(-0.73--0.01) p=0.05
LV mass (g/m^2)	*r*=-0.19 (0.57-0.26) p=0.03	*r*=0.28 (-0.23-0.67) p=0.26	*r*=0.18 (-0.27-0.57) p=0.43	*r*=0.52 (0.12-0.78) p=0.01
Infarct size (g/m^2)	*r*=0.03 (-0.41-0.45) p=0.90	*r*=0.07 (-0.43-0.52) p=0.82	*r*=0.47 (0.06-0.75) p=0.03	-
ECV / segment (%)[Ψ]	*r*=0.37 (0.28-0.45) p<0.001	r=0.22 (0.09–0.34) p=0.003	-	-
Follow-up CMR Assessment (9 months)				
Δ LVEF (%)	*r* =-0.23 (-0.65-0.30) p=0.39	*r*=-0.37 (-0.75-0.19) p=0.13	*r*=-0.24 (-0.66-0.28) p=0.36	*r*=0.12 (-0.40-0.58) p=0.66
Δ LV mass (g/m^2)	*r*=0.14 (-0.38-0.60) p=0.60	*r*=0.16 (-0.39-0.64) p=0.57	*r*=-0.60(-0.85--0.16) p=0.01	*r*=-0.35 (-0.72-0.17) p=0.17
Δ LVEDV (mL/m^2)	*r*=0.34 (-0.19-0.71) p=0.20	*r*=-0.47 (-0.80-0.08) p=0.09	*r*=-0.22 (-0.64-0.31) p=0.41	*r*=-0.06 (-0.54-0.45) p=0.83
Δ Infarct size (g/m^2)	*r*=0.25 (-0.28-0.66) p=0.35	*r*=-0.14 (-0.62-0.41) p=0.62	*r*=-0.61 (-0.85-0.16) p=0.01	*r*=-0.42 (-0.76-0.08) p=0.10
Δ ECV / segment (%)	*r*=-0.11 (-0.22-0.01) p=0.07	*r*=-0.33 (-0.70-0.16) p=0.18	-	-

[Ψ] *ECV and PET association assessed per segment. Abbreviations: hs-cTnI, high sensitivity cardiac troponin I; hs-CRP, high sensitivity c-reactive protein; LVEF, left ventricular ejection fraction; LV, left ventricular; LVEDV, left ventricular end diastolic volume; ECV, mean extracellular volume*

Figure 5.4. 18F-Fluciclatide uptake in myocardial infarction

*Uptake of 18F-fluciclatide in **(A)** patients with acute myocardial infarction at 2 and 10 weeks, patients with chronic total occlusion and healthy control subjects. Uptake was greatest at 2 weeks after myocardial infarction **(B).** 18F-Fluciclatide uptake in the acute MI group was greater in regions of hypokinesis when compared to sites of normal function or akinesis (**C**). This translated to a higher 18F-fluciclatide uptake in those regions which subsequently improved in function on follow-up CMR (**D**). Data bars represent the mean and standard deviation.*

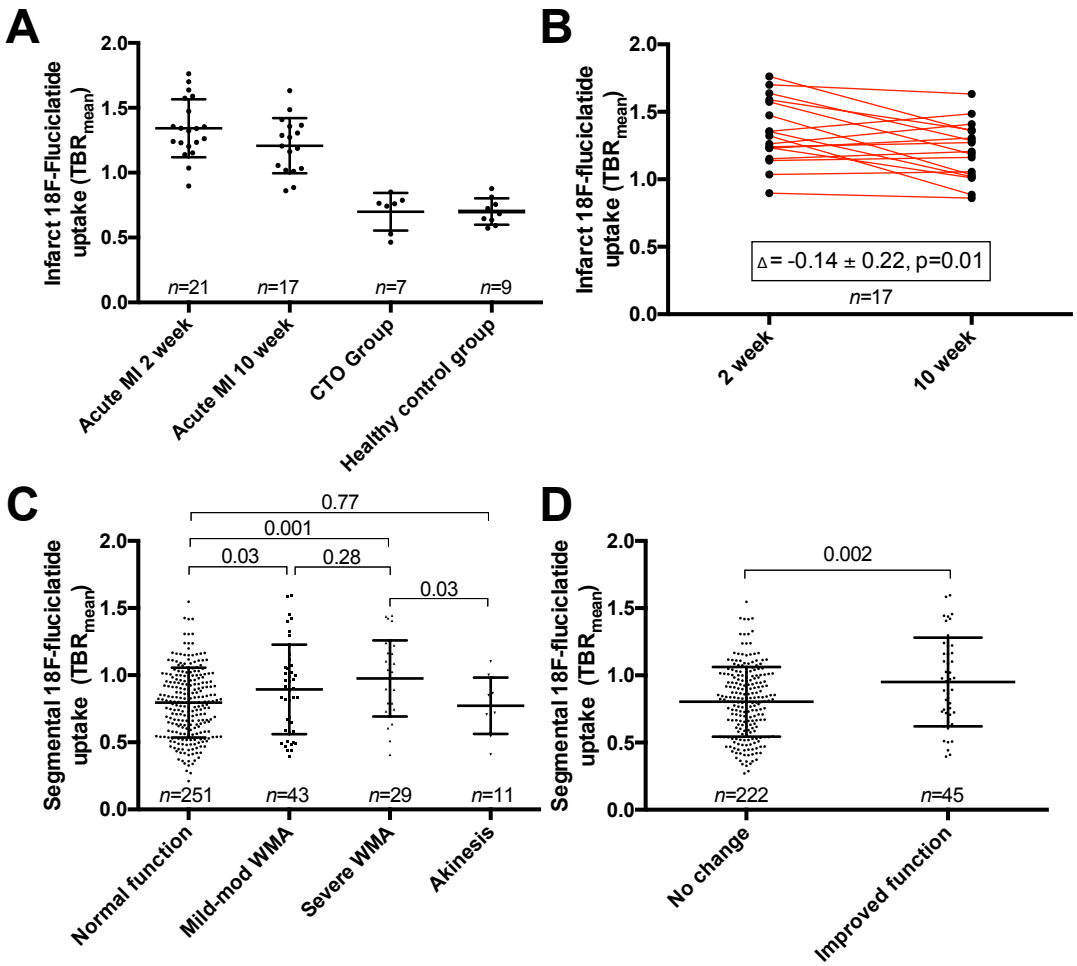

5.5. Discussion

Using the novel radiotracer 18F-fluciclatide, we have for the first time described the temporal expression of myocardial $\alpha_v\beta_3$ integrin receptor in patients with recent acute MI. We demonstrate intense early uptake attributable to regions of recent infarction, in particular subendocardial, hypokinetic infarcts that appeared to demonstrate subsequent functional recovery. Our data suggest that $\alpha_v\beta_3$ integrin receptor expression can be readily quantified in the infarct zone, and that 18F-fluciclatide PET may hold promise as a clinical biomarker of healing activity with application to novel pharmacological or cell-based therapies aimed at improving outcome after MI.

Expression of $\alpha_v\beta_3$ integrin by vascular endothelial cells facilitates myocardial salvage through angiogenesis in the peri-infarct zone, while also mediating the activated macrophage response to inflammatory signals and governing myofibroblast differentiation through the activation of latent TGF-β1.(118-120) The $\alpha_v\beta_3$ integrin contains a binding site for an RGD-peptide subunit (the arginine-glycine-aspartate motif) and this is the target for a number of molecular imaging probes. In murine and human studies of acute MI, RGD-based radiotracers accumulate at the site of infarction as early as 3 days, peaking at 1-3 weeks post-MI (121,135) and correlating with adverse remodeling and infarct scar formation at 12 months.(129,237) For the first time, we have here confirmed and extended these findings using the highly selective and sensitive PET RGD-radiotracer, 18F-fluciclatide. Moreover, given the study sample size and comprehensive imaging assessment, we have been able to make

several significant observations as well as incorporate a number of important controls and comparisons.

We have compared 18F-fluciclatide uptake in patients with recent acute MI with healthy control subjects and patients with established infarction. We have demonstrated that 18F-fluciclatide uptake is specific for acute infarction and does not bind to old established infarcts. Perhaps more importantly, we did not see a correlation with acute infarct size, quantified as the mass of LGE on CMR. Indeed binding of 18F-fluciclatide in akinetic infarcts was relatively low, and was instead highest in sub-endocardial infarcts associated with hypokinesia. This would suggest that 18F-fluciclatide uptake is not a surrogate of infarction itself but relates more to the tissue healing response to injury, although without additional CMR sequencing we were unable to distinguish between 18F-fluciclatide uptake in regions of infarction versus regions of viable 'stunned' myocardium with LGE patterns that represented myocardial oedema.

There are a number of potential explanations for the preferential binding of 18F-fluciclatide to subendocardial infarcts. It is possible that microvascular obstruction in larger infarcts prevented tissue penetration by 18F-fluciclatide or that the presence of tissue necrosis resulted in loss of tissue architecture and altered 18F-fluciclatide kinetics. However a number of our observations suggest that 18F-fluciclatide uptake reflects novel $\alpha_v\beta_3$ integrin expression due to re-endothelialisation and angiogenesis in the peri-infarct zone. First, *ex vivo* histological examination 2 weeks following MI demonstrated that $\alpha_v\beta_3$ integrin expression predominantly co-localizes within

endothelial cells of the microvasculature, aligning with prior reports of a relative reduction in inflammatory cell activity in the infarct and peri-infarct tissue at this timepoint.(63) Second, increased ^{18}F-fluciclatide uptake was associated with functional recovery of hypokinetic infarcts. Third, we did not observe 18F-fluciclatide uptake in patients with CTO who have chronic and well established collateral vasculature. Fourth we did not observe large regions of microvascular obstruction on CMR imaging. This suggests that, within our imaging timeframe, predominantly newly forming vessels or repopulation of vessels with endothelial cells will result in $\alpha_v\beta_3$ integrin expression and ^{18}F-fluciclatide uptake. This is consistent with similar observations in other diseased states such as angiogenesis associated with malignancy.(9,10) In our patients with MI, intense binding was observed in the peri-infarct regions of sub-endocardial MIs with only poorly-defined uptake in the central necrotic area. Given these associations and the likelihood that 18F-fluciclatide identifies areas of re-endothelialisation and angiogenesis, it is perhaps not surprising that 18F-fluciclatide uptake, while visible to a certain degree throughout the region of myocardial infarction, appeared to intensely localise to segments that demonstrated subsequent functional recovery. Taken together our data suggest that assessing $\alpha_v\beta_3$ integrin expression in the acute phase of repair might be of use in investigating the healing processes that occur following acute MI. Larger studies are required to confirm these initial findings and assess whether 18F-fluciclatide PET provides incremental benefit to CMR (our study was not sufficiently powered). However as a marker of activity 18F-fluciclatide may be of particular use in assessing the effects of novel therapies aimed at accelerating repair post-MI.

At 10 weeks following MI, 18F-fluciclatide uptake persisted in the region of infarction but was reduced compared to the 2-week assessment. This delayed phase of repair is characterized pathologically by a reduction in inflammation and angiogenesis, and a more moderated reorganization of the ECM through myofibroblast-driven type I and III collagen production.(238) From our study, we are unable to determine whether this reduction in 18F-fluciclatide uptake reflects the waning of re-endothelialisation and angiogenesis, or represents a switching to myofibroblast cell types indicative of an enhanced fibrotic response. There was some heterogeneity in the time course of 18F-fluciclatide uptake since uptake increased at 10 weeks in 6 subjects. However, we detected no adverse effects of this increase in uptake and there was no corresponding increase in LGE or ECV on T1 mapping.

Modification of the extracellular matrix following MI is not only limited to the site of infarction. Indeed, the myofibroblast-driven fibrotic expansion seen in the remote myocardium influences global myocardial recovery.(96) Expression of $\alpha_v\beta_3$ integrin in remote myocardial regions has been reported up to 6 months following MI.(86,119) In keeping with this, 18F-fluciclatide activity was consistently increased in the remote myocardium at both 2 and 10 weeks when compared to comparative myocardial regions in patients with CTO, and healthy controls.

There are some limitations of our study that we should acknowledge. First, despite accounting for systolic motion using electrocardiographic gating, cardiac PET is also limited by respiratory motion and this may affect sensitivity in particular due to the high activity in the closely adjacent blood pool and hepatic tissue. This is likely to be

a particular problem for inferior infarcts (present in only one of our study subjects), although these less commonly lead to adverse remodelling and heart failure. Novel motion tracking may in the future help to negate some of these issues and enable even greater definition of regional $\alpha_v\beta_3$ integrin expression.(239) Second, limited cardiac tissue was available for histological assessment, preventing complete stoichiometric and temporal assessment of $\alpha_v\beta_3$ integrin expression in man post-MI. Fortunately inference can be drawn from extensive animal models of infarction. However prior to the validation of 18F-fluciclatide as an imaging biomarker for a specified pathological process, a more extensive and specific histological characterization is required, given the variation in pathology within an acutely healing myocardial infarct. Third, our study was not powered to address the incremental value of 18F-fluciclatide PET over established predictors markers of cardiac recovery such as CMR. This will require larger patient populations. Instead this study provides the first description of increased 18F-fluciclatide in the myocardium following MI, indicating that it provides important information about the LV remodeling response. Further studies will be required to establish the clinical utility of this approach.

In conclusion, we report the largest and most comprehensive analysis of an $\alpha_v\beta_3$ integrin radiotracer in the assessment of myocardial repair following acute MI. We have demonstrated that increased 18F-fluciclatide uptake occurs at sites of acute myocardial infarction, in particular regions of sub-endocardial infarction and hypokinesia associated with subsequent functional recovery. Our data suggest myocardial $\alpha_v\beta_3$ integrin expression represents a marker of ongoing cardiac repair, and

that 18F-fluciclatide is a potentially useful imaging biomarker for investigating this healing response post-MI.

Chapter 6.

In Vivo Alpha-V Beta-3 Integrin Expression in Human Aortic Atherosclerosis

Presented by Jenkins WS, Vesey AT, Vickers A, Neale A, Moles C, Connell M, Joshi NV, Lucatelli C, Fletcher AM, Spratt JC, Mirsadraee S, van Beek EJR, Rudd JHF, Newby DE, Dweck MR. *In Vivo Alpha-V Beta-3 Integrin Expression in Human Aortic Atherosclerosis.* **Manuscript under review.**

6.1. Overview

Intra-plaque angiogenesis and inflammation are key promoters of atherosclerosis and are mediated by the $\alpha_v\beta_3$ integrin receptor pathway. We investigated the applicability of the novel $\alpha_v\beta_3$-integrin receptor-selective positron emission tomography (PET) radiotracer 18F-fluciclatide in assessing human aortic atherosclerosis.

Vascular 18F-fluciclatide binding was evaluated using *ex vivo* analysis of carotid endarterectomy samples with autoradiography and immunohistochemistry, and *in vivo* kinetic modeling following radiotracer administration. Forty-six subjects with a spectrum of atherosclerotic disease categorized as stable (n=27) or unstable (n=19; recent myocardial infarction) underwent PET and computed tomography (CT) imaging of the thorax after administration of 226±13 MBq 18F-fluciclatide. Thoracic aortic 18F-fluciclatide uptake was quantified on fused PET-CT images and corrected for blood-pool activity using the maximum tissue-to-background ratio (TBR_{max}). Aortic atherosclerotic burden was quantified by CT plaque thickness, plaque volume and calcium scoring.

18F-Fluciclatide uptake co-localised with regions of increased $\alpha_v\beta_3$ integrin expression, and markers of inflammation and angiogenesis. 18F-fluciclatide vascular uptake was confirmed *in vivo* using kinetic modeling, and on static imaging correlated with each measure of aortic atherosclerotic burden: plaque thickness (r=0.57,p=0.001), total plaque volume (r=0.56,p=0.001) and aortic CT calcium score (r=0.37,p=0.01).

Patients with recent myocardial infarction had greater aortic 18F-fluciclatide uptake than those with stable disease (TBR_{max} 1.33 vs 1.21, p=0.01).

In conclusion, In vivo expression of $\alpha_v\beta_3$ integrin in human aortic atheroma is associated with plaque burden and is increased in patients with recent myocardial infarction. Quantification of $\alpha_v\beta_3$ integrin expression with 18F-fluciclatide PET has potential to assess plaque vulnerability and disease activity in atherosclerosis.

6.2. Introduction

Atherosclerotic cardiovascular disease is the commonest cause of death worldwide, and elucidating the mechanisms underlying the propagation and rupture of atherosclerotic plaques remains a key public health goal.(1) Although progress has been made in our understanding of the pathogenesis underlying atherosclerosis over the last two decades, the accurate prediction of clinical events remains elusive. There is therefore considerable interest in non-invasive imaging techniques that go beyond the detection of luminal stenoses and instead focus on measuring disease activity within the vasculature.(240,241)

Combined positron emission tomography (PET) and computed tomography (CT) is a non-invasive hybrid imaging technique that integrates targeted functional molecular imaging with high-detail anatomical definition. This technique has been used to quantify vascular inflammation and calcification activity with success in both carotid and coronary atherosclerosis.(6,48,164,242) Recently, intraplaque angiogenesis and neovascularization has emerged as a key factor in the development, progression, and instability of atherosclerotic plaques.(243) The integrin $\alpha_v\beta_3$ cell surface receptor is up regulated on endothelial cells in states of angiogenesis and is also observed on macrophages at sites of increased vascular inflammation, another key contributor to plaque instability. This receptor helps coordinate interaction between cellular components and the extra-cellular matrix and contains a distinctive RGD-amino acid sequence in the cell-ligand interaction site. On this basis, several PET tracers targeting the RGD sequence have been developed for monitoring angiogenesis in malignant

tumours.(9,199) These tracers have also shown promise in monitoring atherosclerotic activity in pre-clinical models (181,182,243-245) and in a recent small study of patients with carotid atheroma.(242)

18F-Fluciclatide is a novel RGD-based PET radiotracer with high affinity for the $\alpha_v\beta_3$ integrin receptor.(9,10,190) We hypothesized that 18F-fluciclatide may act as an imaging marker of atherosclerotic disease activity *in vivo*, informing about both inflammation and angiogenesis. In this study we sought to characterize the cellular and imaging characteristics of 18F-fluciclatide uptake in human atherosclerosis using a clinical cohort of patients with both stable and unstable clinical disease.

6.3. Methods

6.3.1. Study populations

In total we studied 50 patients. Four patients were recruited who had sustained a recent stroke and were undergoing carotid endarterectomy. In these patients, excised carotid plaques were examined using histology and 18F-fluciclatide autoradiography. For *in vivo* imaging, 46 patients were recruited from the Royal Infirmary of Edinburgh between July 2013 and December 2014. This cohort comprised 19 *unstable* patients with a recent acute ST-segment elevation myocardial infarction,(246) and 27 *stable* patients with either stable angina (n=6) or asymptomatic atherosclerotic disease (n=21; 12 had calcific aortic valve disease). Exclusion criteria were age <40 years, women of childbearing potential, severe renal failure (estimated glomerular filtration rate <30 mL/min/1.73 cm^2) or hepatic failure (Childs-Pugh grade B or C), atrial fibrillation, known contrast allergy, inability to undergo scanning and inability to provide informed consent. All 46 subjects underwent 18F-fluciclatide PET imaging alongside clinical assessment that included evaluation of cardiovascular risk and high sensitivity C-reactive protein (hs-CRP) measurement (Biocheck inc.; Foster City, California).

Studies were approved by the local research ethics committee, and conducted in accordance with the Declaration of Helsinki and with the written informed consent of each participant.

6.3.2. Radiosynthesis of 18F-Fluciclatide

18F-Fluciclatide was manufactured at the Clinical Research Imaging Centre on an automated module (FASTlab synthesiser; GE Healthcare) by coupling an amino-oxy-functionalized peptide precursor (AH111695) with 4-18F-fluorobenzaldehyde at pH 3.5 to form 18F-fluciclatide.(247) A full description of this synthesis has been published previously.(190)

6.3.3. Histological validation

After obtaining informed consent, four human carotid intimal samples were obtained from patients undergoing carotid endarterectomy for symptomatic carotid artery atherosclerotic disease.(192) Both atheromatous and non-atheromatous segments of dissected carotid atheroma were frozen in mounting medium. The tissue samples were then cut in sequential, longitudinal 4 μm and 20 μm slices sections at -20°C and thaw-mounted onto microscope slides. Effort was made to align segments of ruptured plaque alongside non-atheromatous segments within the same slide. The slides were then dried for 15 min and spray-fixed with neutral buffered formalin. After rinsing in distilled water the 4 μm sections were stained with hematoxylin-eosin (HE) and van-Gieson (VG) for conventional histopathological examination. In order to optimize immunohistochemistry, an antigen-unmasking step was performed by microwave treatment for 30 s. Endogenous peroxidase was blocked by incubation with hydrogen peroxide for 5 min. Sections were subsequently incubated with the primary antibodies; smooth muscle actin, CD31, CD68 (clone PG-M1), and integrin $\alpha_V\beta_3$ antibody, clone LM609 (Millipore) for 30 min at room temperature. After washing, the sections were incubated with Envision Flex (DAKO, K5007) for 30 min at room temperature, followed by incubation with diaminobenzamine (Sigma) for 10 min. The slides were finally counterstained with hematoxylin and digitally imaged (Axioscan.Z1, Zeiss, UK). Image analysis was performed on ImageJ32 software (NIH, Bethesda, Maryland). Staining was expressed as a percentage of the total plaque area and with an object size set threshold applied at 20 x 10 pixels, to limit counting to cell-sized

objects. The density of cell staining in the endarterectomy tissue was expressed as cells per mm^2.(226)

Clinical PET systems have limited resolution. To gain more detailed information about the precise localization of 18F-fluciclatide binding in atherosclerotic tissue, we undertook autoradiography. The 20 μm frozen sections adjacent to those used for immunohistochemical analysis were warmed to room-temperature and bathed in a solution of 18F-fluciclatide at a concentration close to in vivo imaging concentrations (1 kBq/mL) for 60 minutes and then rinsed with phosphate buffer solution. An unlabeled highly concentrated solution of fluciclatide was added to selected slides in order to competitively bind to $\alpha_v\beta_3$ to assess for non-specific tracer uptake. A freshly blanked phosphor screen was then placed over the slides and an overnight exposure undertaken. The screen was read using a FujiFilm FLA-5100 Fluorescent Image Analyser (Raytek Scientific Limited, Sheffield, UK). Sections were then manually registered and examined for co-localization with histological markers of atherosclerotic disease activity by Dr. William Jenkins and Dr. Alexander Vesey under the supervision of the histopathology director Dr. Mike Millar in the Queens Medical Research Institute.

6.3.4. Clinical 18F-fluciclatide PET imaging

All patients in the imaging cohort underwent PET-CT imaging of the thorax with a hybrid scanner (Biograph mCT, Siemens Medical Systems, Erlangen, Germany) at the Clinical Research Imaging Centre, University of Edinburgh. Subjects were administered a target dose of 230 MBq 18F-fluciclatide. An attenuation correction CT scan (non-enhanced 120 kV and 50 mA, 3-mm slices) was performed prior to PET acquisition. To define tracer pharmacodynamics and the optimum timing of scanning, dynamic PET imaging of the thorax was performed in the initial 20 patients in 3-dimensional mode using a single bed position for 70 min. For the remainder of the study subjects, static imaging was performed at the optimal time point (found to be 40 min post-injection) using a single 30-min bed position in list mode with electrocardiographic gating.

Immediately after PET acquisition, thoracic CT angiography was performed: 330 ms rotation time, 100 (body mass index <25 kg/m^2) or 120 (body mass index >25 kg/m^2) kV tube voltage, 160-245 mAs tube current, 3.8 mm/rotation table feed, prospective (heart rate regular and <60 /min), or retrospective (heart rate >60 /min) electrocardiogram-gated. Depending on body mass index, a bolus of 80-100 mL contrast (400 mgI/mL; Iomeron, Bracco, Milan, Italy) was injected intravenously at 5 mL/s, after determining the appropriate trigger delay with a test bolus of 20 mL contrast material.

6.3.5. PET image reconstruction and analysis

Kinetic analysis was performed on the dynamic PET studies to investigate the pharmacodynamics of 18F-fluciclatide uptake within atheroma. PET data were reconstructed (Ultra-HD, 2 iterations, 21 subsets, 256 pixels, 1.6-mm pixel size) in a dynamic profile using the following time frames; 60s x 5, 120s x 5, 180s x 5, 300s x 8. Regions of interest (ROI's) were drawn both in the blood pool and sites of aortic atheroma visible on CT and used to derive time activity curves after decay correction. These were used to define a timeframe for static imaging based upon the point at which optimum contrast between blood pool and tissue activity was observed. To define 18F-fluciclatide uptake in aortic atheroma, a kinetic modeling input function calculation was based on the PET image-derived activity curve from the aortic blood pool (PMod version 4.3.1, Pmod technologies limited, Switzerland).(9) This input function was applied to a tissue activity curve generated from ROI's placed in the myocardial interventricular septum, to estimate the tissue influx rate *K*i (the slope of the linear regression) and the volume of distribution (the intercept with the *y* axis) using a 2-tissue irreversible Patlak model, with t* set to 20 min, as described previously.(9,10) Thoracic 18F-fluciclatide dynamic activity was then normalized for the blood-pool input function on a voxel-by-voxel basis, and after 3D Gaussian filtering (5-mm FWHM), a parametric 3-dimensional image of 18F-fluciclatide uptake was generated accordingly. Using this image, regions of 18F-fluciclatide binding in the vasculature were identified and manually delineated for subsequent *K*i analysis.

In all patients, static electrocardiogram-gated PET images were reconstructed in diastole (40-70 min post-injection, 50–75% of the R-R interval, Ultra-HD, 2 iterations, 21 subsets, zoom x2, 200 pixels). Images were analyzed by experienced observers blinded to the demographic data (WJ, AV) using an OsiriX workstation (OsiriX version 6.0 64-bit; OsiriX Imaging Software, Geneva, Switzerland). PET images were fused with the attenuation correction CT, and regions of interest (ROIs) drawn around the thoracic aorta on serial axial slices just beyond the discernible adventitial border. Aortic uptake was assessed in three regions: the ascending thoracic aorta (from the level of mid-right pulmonary artery (RPA) up to the last slice where the aorta maintained its circular cross-sectional appearance), the descending thoracic aorta (the region extending from the tip of the diaphragm up to the last circular slice) and the aortic arch (the region of the aorta connecting the ascending and descending aortae). Within these regions, mean and maximum tracer activities were measured using standard uptake values (SUV; the decay corrected tissue concentration of the tracer divided by the injected dose per body weight, kBq/mL) and corrected for mean radiotracer blood pool activity to provide a mean of the maximum tissue-to-background ratios (mean TBR_{max}), as described previously. (2,6,161,248) The blood pool radiotracer activity was quantified in the superior vena cava (SVC), measured in the axial plane on 4-5 sequential 5-mm axial slices above the level of the junction of the left innominate vein. In a sub-study of 10 randomly selected subjects, images were assessed independently by two experienced observers (Dr. William Jenkins, Dr. Anna Vickers) and the inter-observer reproducibility of 18F-fluciclatide SUV and TBR measurements assessed.

6.3.6. CT image reconstruction and analysis

The aortic CT calcium score was calculated for the aorta as a whole and for its different regions using axial slices on the attenuation correction CT dataset (OsiriX version 6.0 64-bit; OsiriX Imaging Software, Geneva, Switzerland) and expressed in arbitrary units (AU).(60) Further measures of the aortic atherosclerotic plaque burden were made using CT angiography datasets on dedicated plaque analysis software (Vital Images, Minnetonka, Minnesota, USA). Using the sagittal plane, the entire portion of the descending thoracic aorta within the field of contrast CT acquisition was delineated and the luminal blood pool removed using semi-automated thresholding. The mean aortic wall thickness was recorded and corrected for the vessel diameter providing the indexed wall thickness. Additionally the aortic wall volume was recorded and corrected for total vessel volume to provide an indexed plaque volume.

6.3.7. Statistical analysis

Continuous data were tested for normality visually and with the D'Agostino and Pearson Omnibus test. Continuous parametric variables were expressed as mean±standard deviation and compared using Pearson correlation. Non-parametric data were presented as median [interquartile range] and compared using Spearman correlation or Wilcoxon signed-rank test as appropriate. Aortic calcium score and hs-CRP were log-transformed to base 10 to achieve normality prior to statistical analysis. Interobserver reproducibility was calculated by Bland Altman method and presented as mean bias ± 2 standard deviations, and intraclass correlation coefficients (ICC).(215) Student's *t*-test or Mann-Whitney U test was used for analysis of categorical variables. Statistical analysis was performed with Graph Pad Prism version 6 (GraphPad Software Inc., California USA). A two-sided $P<0.05$ was taken as statistically significant.

6.4. Results

6.4.1. Plaque autoradiography and histology

Autoradiography of carotid plaque demonstrated focal 18F-fluciclatide binding in regions of advanced atherosclerosis that was blocked by un-labeled fluciclatide (Figure 6.1 A and B). Regions of *ex vivo* 18F-fluciclatide uptake co-localised with intense cellular staining of $\alpha_v\beta_3$ integrin (45.2 [29.1-66.9] cells/mm^2, % area 4.2 [3.2-5.7]), microvascular endothelial cells at sites of angiogenesis and positive remodeling (CD31+; 23.0 [6.5-63.0] cells/mm^2, % area 2.5 [2.2-4.9]), and inflammatory macrophages deeper adjacent to the necrotic core (CD68+; 32.0 [21.0-49.8] cells/mm^2, % area 3.7 [2.4-5.6], Figure 6.1 C-H). By comparison control regions of the carotid endarterectomy specimens without visible atheroma did not demonstrate 18F-fluciclatide uptake, and had much lower levels of $\alpha_v\beta_3$ integrin receptor expression (4.5 [4.3-5.2] cells/mm^2, % area 0.6 [0.5-2.0], both p=0.05 compared to areas with increased 18F-fluciclatide expression), as well as staining for both angiogenic endothelial cells (CD31+; 2.1 [1.8-2.4] cells/mm^2, % area 0.9 [0.6-1.2], both p=0.05) and inflammatory macrophages (CD68+; 4.3 [2.8-4.4] cells/mm^2, % area 0.6 [0.5-1.2], both p=0.03) .

Figure 6.1. 18F-Fluciclatide Uptake in Carotid Atheroma

*(**A**) Autoradiography image of segments of ruptured carotid plaque (left) and proximal healthy segments (right). Greater 18F-fluciclatide uptake is visible within plaque rupture segments. Uptake within the tissue segments (demarcated) was successfully blocked by the addition of a more concentrated un-labelled solution of fluciclatide (**B**). Adjacent tissue sections displayed intense cellular staining of $\alpha_v\beta_3$ integrin (**C** [x4 magnification] and **D**, [x20 magnification]) that co-localised to the regions of ex vivo 18F-fluciclatide uptake (**A**) and also featured dense cellular staining for vascular endothelial cells (CD31, **E** and **F**) and inflammatory cells (CD68, **G** and **H**).*

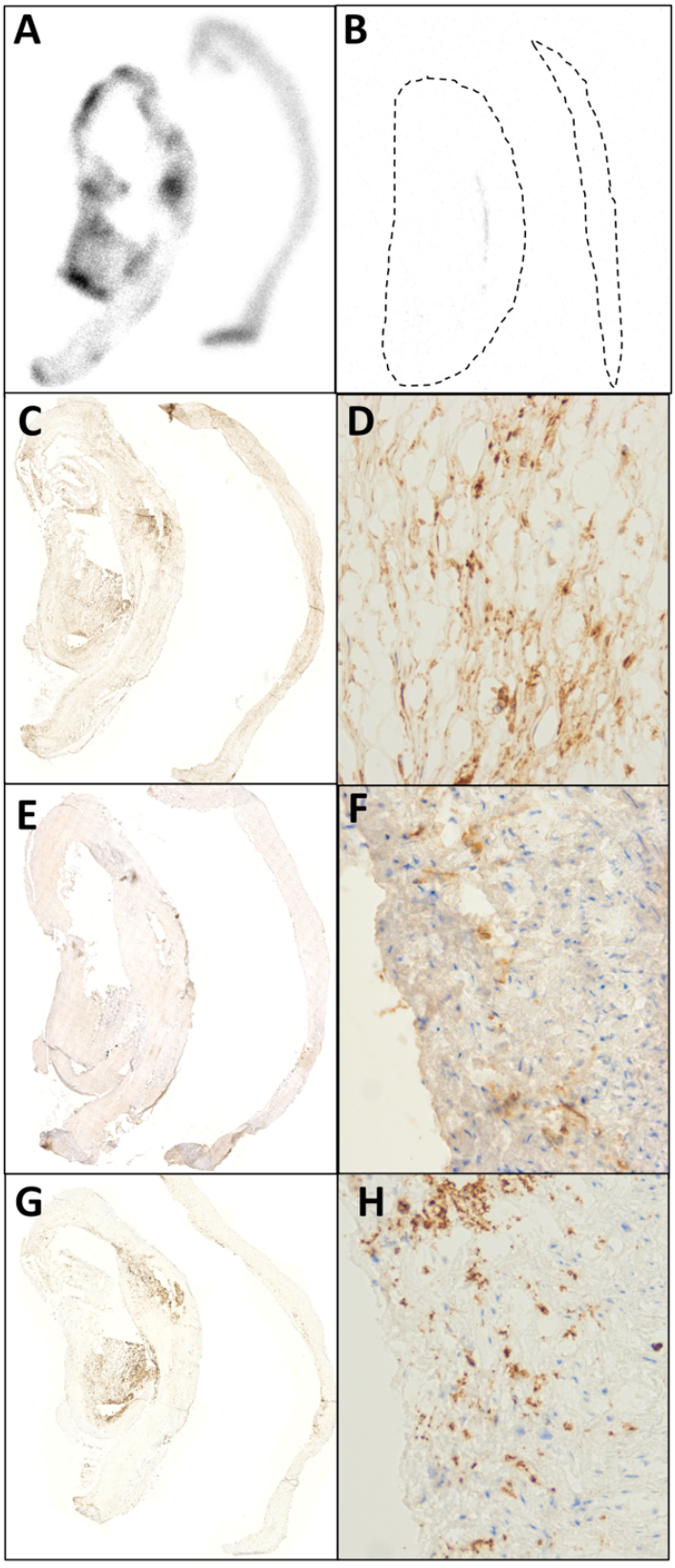
A
B
C
D
E
F
G
H

6.4.2. In Vivo Imaging Cohort

A total of 46 subjects underwent PET imaging with CT angiography (age 66±10 years, 74% male; Table 6.1) following injection of 226±13 mBq 18F-fluciclatide. Of the 46 subjects recruited, 19 had suffered a recent myocardial infarction (*unstable cohort*), and 27 had imaging evidence of aortic atherosclerosis on CT but no recent cardiovascular events (*stable cohort*: 6 with stable angina and 21 with sub-clinical disease who were asymptomatic with no prior cardiovascular events). Those in the stable cohort had greater aortic calcification than patients in the unstable group (AU [IQR]; 326 [11-1114] vs 19 [0-483], $p<0.01$), reflecting their greater age (years; 70±8 vs 61±12, $p<0.01$). The groups were well matched for gender ($p=0.97$) and body-mass index ($p=0.25$), and were both characterized by a high prevalence of atherosclerotic risk factors, with more smokers in the unstable group ($p=0.02$) and more patients with hypertension in the stable group ($p=0.001$). No adverse events were reported following administration of 18F-fluciclatide. The mean radiation dose for each 18F-fluciclatide PET scan was 5.9 mSv (range 5.2-6.4 mSv). The mean attenuation correction CT acquisition radiation dose was 1.4 mSv (range 0.8-1.9 mSv). Cardiac CT contrast angiography dosing was 6.7mSv (range 2.1-11.7 mSv); the wide dose range accounted for the potential presence of atrial fibrillation that prevents prospective ECG gating. The average total radiation dose per participant was 15.1 mSv.

Table 6.1. Study participant baseline characteristics

	All ***(n=46)***	**Stable Atherosclerosis** ***(n=27)***	**Unstable Atherosclerosis** ***(n=19)***	***P* value**
Age (years)	66±10	70±8	61±12	0.006
Male Sex	34 (74)	20 (74)	14 (74)	0.97
BMI (kg/m^2)	28±4	28±4	29±5	0.25
Systolic BP (mmHg)	140±22	149±19	127±19	<0.001
18F-Fluciclatide dose (MBq)	226±13	225±13	228±14	0.62
Cardiovascular History				
Angiographically documented CAD	26 (57)	7 (26)	19 (100)	<0.001
Prev MI	24 (52)	5 (19)	19 (100)	<0.001
Prev PCI	20 (43)	2 (7)	18 (95)	<0.001
Prev CVD	4 (11)	4 (14)	0 (0)	0.08
Risk Factors				
Current smoker	9 (20)	1 (4)	8 (42)	0.001
Diabetes Mellitus	6 (13)	4 (14)	2 (10)	0.58
Prior hypertension	23 (50)	18 (67)	6 (32)	0.02
Prior Hypercholester-olemia	25 (54)	12 (44)	12 (63)	0.21
hs-CRP (mg/l)	3.5 [1.4-7.8]	2.7 [1.4-5.8]	5.6 [2.0-11.7]	<0.001
Log_{10} hs-CRP (mg/l)	0.51±0.51	0.41±0.44	0.65±0.56	<0.001
Medications				
Aspirin	28 (61)	10 (37)	19 (100)	<0.001
Clopidogrel	19 (41)	4 (14)	19 (100)	<0.001
Statin	31 (67)	13 (48)	19 (100)	<0.001
β-Blocker	27 (59)	8 (30)	19 (100)	<0.001
ACEi/ARB	31 (67)	10 (37)	18 (95)	<0.001
Calcium Channel Blocker	7 (15)	6 (22)	1 (5)	0.11

Categorical data are displayed as n (%). Normally distributed data displayed as mean±SD. Non-normally distributed data displayed as median [interquartile range]. Abbreviations: IHD - ischemic heart disease; AS - aortic stenosis; CAD - coronary artery disease; MI - myocardial

infarction; CVD – cerebrovascular disease; PCI - percutaneous coronary intervention; hs-CRP - high sensitivity c-reactive protein; ACEi - ACE-inhibitor; ARB - Angiotensin Receptor Blocker.

6.4.3. Dynamic analysis of aortic 18F-fluciclatide aptake

On kinetic analysis, activity within aortic atheroma increased gradually, reaching a plateau at 40–70 min. Injected 18F-fluciclatide activity has a biexponential blood pool clearance with a half-life of about 10 min consisting of a fast redistribution component with a slower clearance component, causing relatively high residual blood pool activity during PET acquisition (40-70 min post-injection, SVC SUV_{mean} 2.74±0.49; Figure 6.2). Consequently, whilst 18F-fluciclatide uptake in aortic atheroma was measurable above background, tissue-to-background ratios were relatively low (TBR_{max} range 1.08-1.68; Table 6.2, Figures 6.2, 6.3). In the 3-D Patlak slope (Ki) parametric images, 6 datasets (30%) were uninterpretable due to patient movement. In the remaining studies, increased aortic 18F-fluciclatide uptake was observed in half of subjects. Patlak modelling demonstrated a discernible linear phase suggesting irreversible ligand-receptor binding over the selected acquisition time and a greater *K*i slope in these subjects compared to patients with no aortic uptake (Figure 6.2). Subjects with uptake present on Patlak analysis also appeared to have higher 18F-fluciclatide uptake on standard analysis (TBR_{max} 1.32±0.05 vs 1.19±0.03, p=0.08) and greater aortic calcification (aortic calcium score 704 [28-1788] vs 0 [0-119] AU, p=0.06) than those without visible uptake, although this did not reach statistical significance.

Figure 6.2. Kinetic analysis of aortic 18F-fluciclatide uptake

*Sagittal views of the thorax following kinetic analysis in two participants with (patient 1: **A-E**) and without (patient 2; **F-H**) aortic arch 18F-fluciclatide uptake. Computed tomography (CT) images confirm presence (**A**) or absence (**F**) of aortic arch calcification as a marker of established atheroma. Patlak slope (Ki) parametric images (**B** and **G**) identify focal uptake within the aortic arch in the region of atheroma (red arrow) localising to the vessel wall on the fused Patlak and CT images (**C** and **H**). Patlak modelling (**D**) confirms irreversible integrin binding within the region of aortic arch calcification (red arrow). Time activity curves (TAC) within the same region (**E**) show a persistently high blood pool fraction, but uptake within atheroma that exceeds the blood pool fraction beyond 40 min (dash*

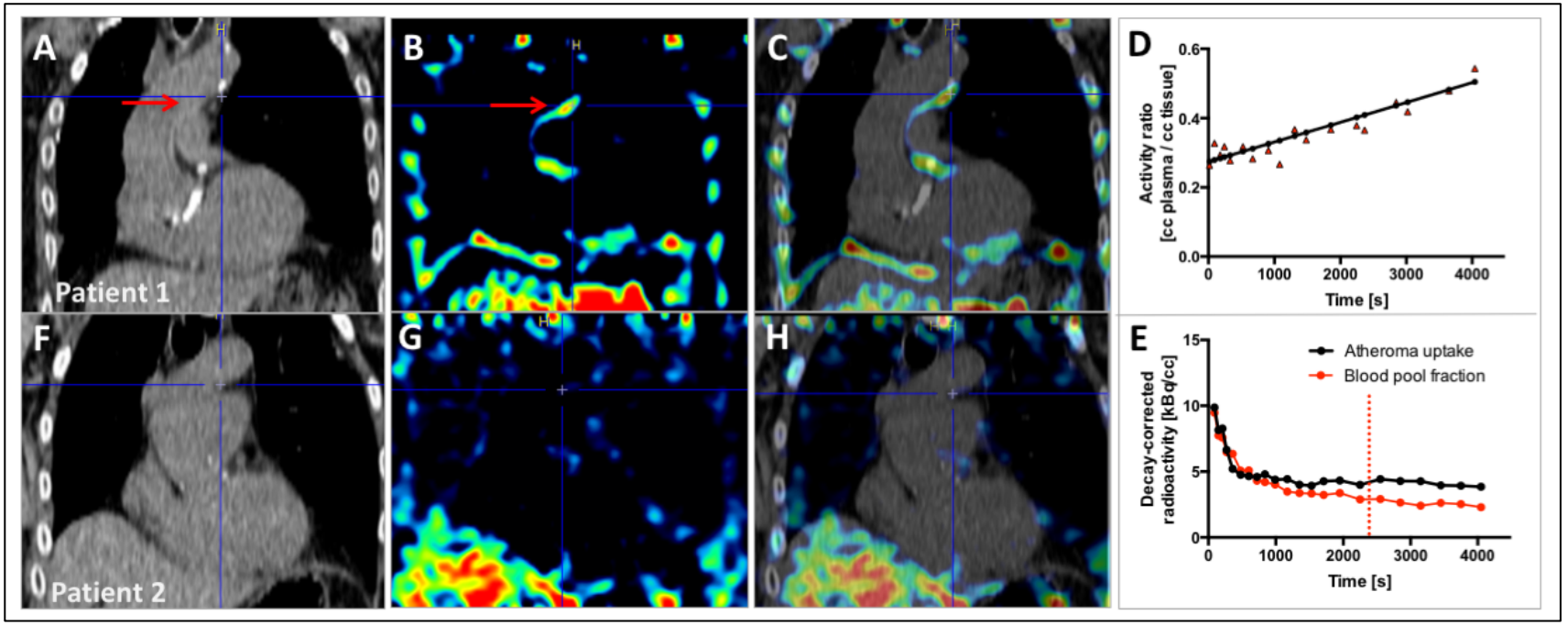

Figure 6.3. 18F-Fluciclatide aortic uptake

Patient 3: *Modified coronal view of the aortic arch showing radiotracer uptake at the inner curvature of the aortic arch closely related to a region of aortic calcification. This activity is demonstrated on axial sections of the aorta (i and ii). Red lines indicate the adventitial borders of the aortic arch used for quantification of PET uptake.* ***Patient 4:*** *Sagittal view of the thorax displaying focal 18F-fluciclatide uptake within a region of vascular calcification in the aortic arch.*

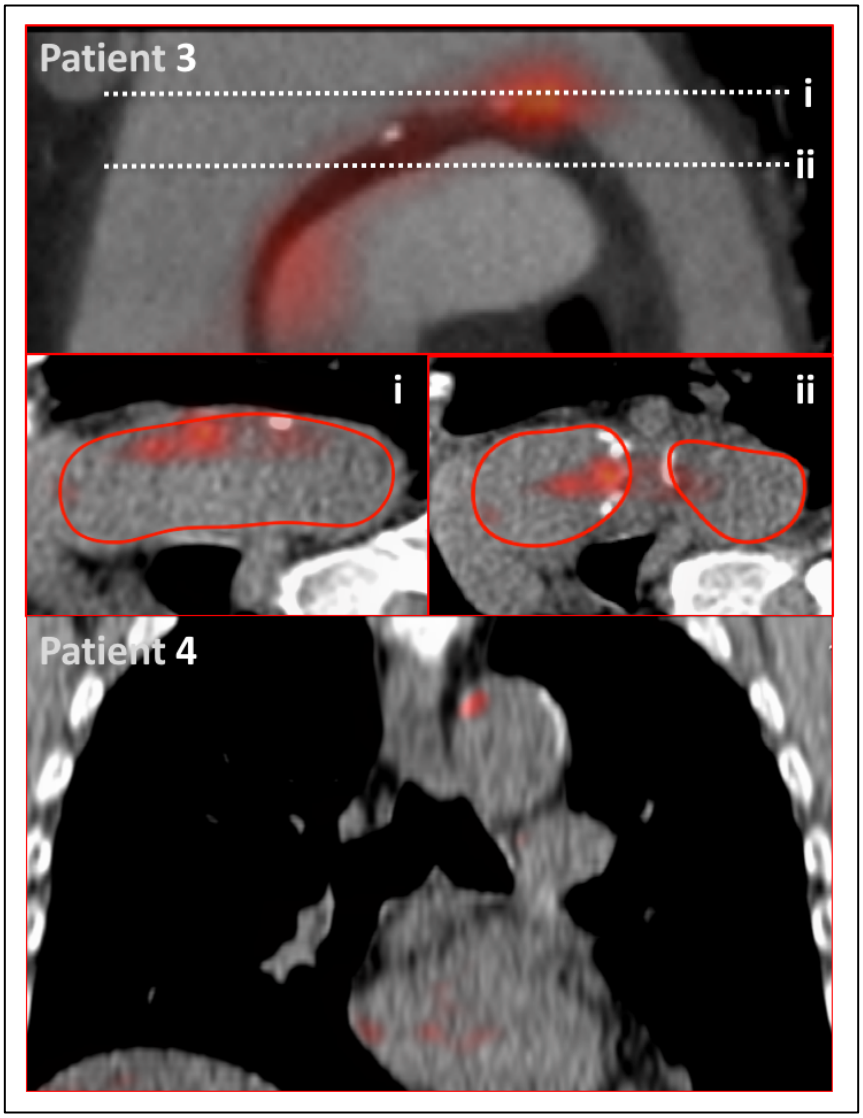

Table 6.2. Imaging results

	All ***(n=46)***	**Stable Atherosclerosis** ***(n=27)***	**Matched Stable Atherosclerosis** ***(n=19)***	**Unstable Atherosclerosis** ***(n=19)***	***P*** **value***
18F-Fluciclatide PET uptake					
SVC, SUV_{mean}	2.74±0.49	2.62±0.46	2.54±0.40	2.9±0.48	0.02
Whole aorta, SUV_{max}	3.59±0.62	3.40±0.62	3.19±0.65	3.84±0.55	0.001
Ascending aorta, SUV_{max}	3.60±0.66	3.42±0.70	3.16±0.56	3.87±0.51	<0.001
Aortic Arch, SUV_{max}	3.51±0.62	3.29±0.61	3.05±0.52	3.84±0.48	<0.001
Descending aorta, SUV_{max}	3.61±0.68	3.46±0.65	3.28±0.65	3.83±0.66	0.01
Whole aorta, TBR_{max}	1.32±0.14	1.30±0.12	1.26±0.09	1.33±0.18	0.14
Ascending aorta, TBR_{max}	1.32±0.16	1.31±0.17	1.25±0.10	1.34±0.17	0.05
Aortic Arch, TBR_{max}	1.30±0.14	1.26±0.14	1.21±0.1	1.33±0.15	0.008
Descending aorta, TBR_{max}	1.32±0.17	1.32±0.13	1.29±0.11	1.33±0.21	0.56
CT Calcium Score (AU)					
Whole aorta	95 [0-852]	326 (11-1114)	36 (0-469)	19 [0-483)	0.85
Ascending aorta	0 [0-11]	0 (0-46)	0 (0-0)	0 [0-0}	0.15
Aortic arch	29 [0-352]	102 (0-586)	13 (0-469)	0 [0-263]	0.76
Descending aorta	7.5 [0-78]	0 (0-123)	0 (0-123)	8 [0-71]	0.43
CTA Plaque analysis (descending aorta)					
Mean wall thickness (% vessel diameter)	10.3±4.9	8.4±2.8	8.4±3.1	14.0±6.3	0.003
Plaque burden (% total volume)	9.1±3.9	7.7±2.3	7.7±2.5	12.0±4.7	0.004

*$^{\Psi}$ Stable group subjects paired to equivalent calcium score in unstable group. * P-values are quoted for comparisons between matched stable and unstable groups. SUV - standard uptake value; TBR - tissue-to-background ratio*

6.4.4. Aortic 18F-fluciclatide uptake reproducibility studies

Using static PET images, the quantification of 18F-fluciclatide activity in the SVC blood pool demonstrated excellent interobserver reproducibility, with no fixed or proportional biases (SUV_{mean} mean difference; -0.11 [-0.36 – 0.15]) and an excellent intraclass correlation co-efficient (0.95, Table 6.3). The quantification of 18F-fluciclatide uptake in the aorta using the established mean TBR_{max} approach (2,6) also displayed no fixed or proportional bias (mean difference; 0.08 [-0.01–0.16]) with an excellent intra-class correlation (0.92) (Table 6.3).

Table 6.3. Vascular 18F-fluciclatide uptake reproducibility analysis

18F-Fluciclatide activity	Mean absolute difference[a]	Intra-class coefficient[b]
Superior Vena Cava		
Mean SUV (SUV [kBq/cc])	-0.11 (-0.36 – 0.15)	0.947
Aorta		
Mean SUV (SUV [kBq/cc])	-0.005 (-0.14 – 0.13)	0.986
Mean SUV_{MDS} (SUV [kBq/cc])	0.01 (-0.17 – 0.15)	0.980
Max SUV (SUV [kBq/cc])	0.07 (-0.13 – 0.27)	0.971
Max SUV_{MDS} (SUV [kBq/cc])	0.06 (-0.22 – 0.34)	0.957
Mean TBR	0.04 (-0.02 – 0.10)	0.954
Mean TBR_{MDS}	0.04 (-0.04 – 0.10)	0.940
Max TBR	0.08 (-0.01 – 0.16)	0.912
Max TBR_{MDS}	0.07 (-0.03 – 0.17)	0.919
$SUV_{Target-background}$	0.19 (-0.05 – 0.43)	0.612

[a] Mean difference between TBR_{max} measurements (95% limits of agreement), and [b] ICC values for 18F-Fluciclatide throughout the thoracic aorta and SVC. Abbreviations: ICC: intraclass correlation coefficient; MDS: most diseased segment; TBR: tissue to background ratio; SVC: Superior Vena Cava

6.4.5. Aortic 18F-fluciclatide uptake and atheroma burden

Our study cohort comprised patients with a wide spectrum in aortic atherosclerotic disease burden (aortic calcium score range 0-6857 AU). Using static images, aortic 18F-fluciclatide uptake demonstrated a close relationship with disease burden in the aorta regardless of whether it was measured using CT calcium scoring (r=0.37 [0.08-0.60], p=0.01) or the indexed plaque volume (r=0.56 [0.26-0.75]; p<0.001) (Table 6.4, Figure 6.4). Interestingly a good correlation was also observed with the relative vessel wall thickness (expressed as a percentage of vessel diameter, r=0.57 [0.28-0.76]; p<0.001). There was no correlation between aortic 18F-fluciclatide uptake and the systemic inflammatory marker C-reactive protein (log_{10} hs-CRP r=0.18, p=0.28).

Table 6.4. PET uptake and baseline characteristics

	Total Aortic 18F-Fluciclatide Uptake (TBR_{max})		
	All patients	**Stable Cohort**	**Unstable Cohort**
Continuous variables			
CT calcium score ($Log^{10}AU$)	*r*=0.37 (0.08-0.60) p=0.01	*r*=0.62 (0.43-0.81) p<0.001	*r*=0.20 (-0.28-0.60) p=0.41
Mean wall thickness (% vessel diameter) $^{\Psi}$	*r*=0.57 (0.28-0.76) p<0.001	*r*=0.18 (-0.26-0.56) p=0.43	*r*=0.69 (0.15-0.91) p=0.02
Plaque volume (% total volume) $^{\Psi}$	*r*=0.56 (0.26-0.75) p<0.001	*r*=0.16 (-0.28-0.55) p=0.47	*r*=0.68 (0.13-0.90) p=0.02
Log_{10} hs-CRP (mg/l)	r=0.18 (-0.14-0.46) p=0.28	r=0.32 (-0.07-0.62) p=0.10	*r*=-0.24 (-0.63-0.24) p=0.06
Categorical variables			
Hypertension	1.31±0.05 vs 1.32±0.04 p=0.66	1.31±0.05 vs 1.32±0.04 p=0.66	1.34±0.06 vs 1.30±0.04 p=0.66
Established IHD	1.34±0.06 vs 1.28±0.06 p=0.15	1.37±0.04 vs 1.28±0.03 p=0.08	-
Hypercholesterolemia	1.34±0.06 vs 1.28±0.06 p=0.16	1.37±0.04 vs 1.24±0.06 p=0.007	1.32±0.05 vs 1.36±0.07 p=0.04
Diabetes mellitus	1.40±0.10 vs 1.30±0.05 p=0.15	1.41±0.08 vs 1.28 ±0.02 p=0.06	1.37±0.03 vs 1.33±0.05 p=0.77
Current Smokers	1.36±0.10 vs 1.30±0.04 p=0.30	N too small	1.36±0.06 vs 1.31±0.05 p=0.51

$^{\Psi}$18F-Fluciclatide uptake assessed in the descending aorta only, to correspond with CT analysis.

CT – computed tomography; hs-CRP - high sensitivity C-reactive protein; IHD – ischaemic heart disease

Figure 6.4. 18F-Fluciclatide uptake, atheroma burden and clinical stability

Graphs displaying the relationship between aortic 18F-fluciclatide uptake and aortic plaque burden, assessed using both the plaque volume when available ***(A)*** *and calcium score* ***(B)****. Moreover 18F-Fluciclatide uptake was greater in patients with unstable (recent myocardial infarction) versus stable (no recent cardiovascular events) atherosclerotic disease* ***(C)****. Data bars represent the mean and standard deviation.*

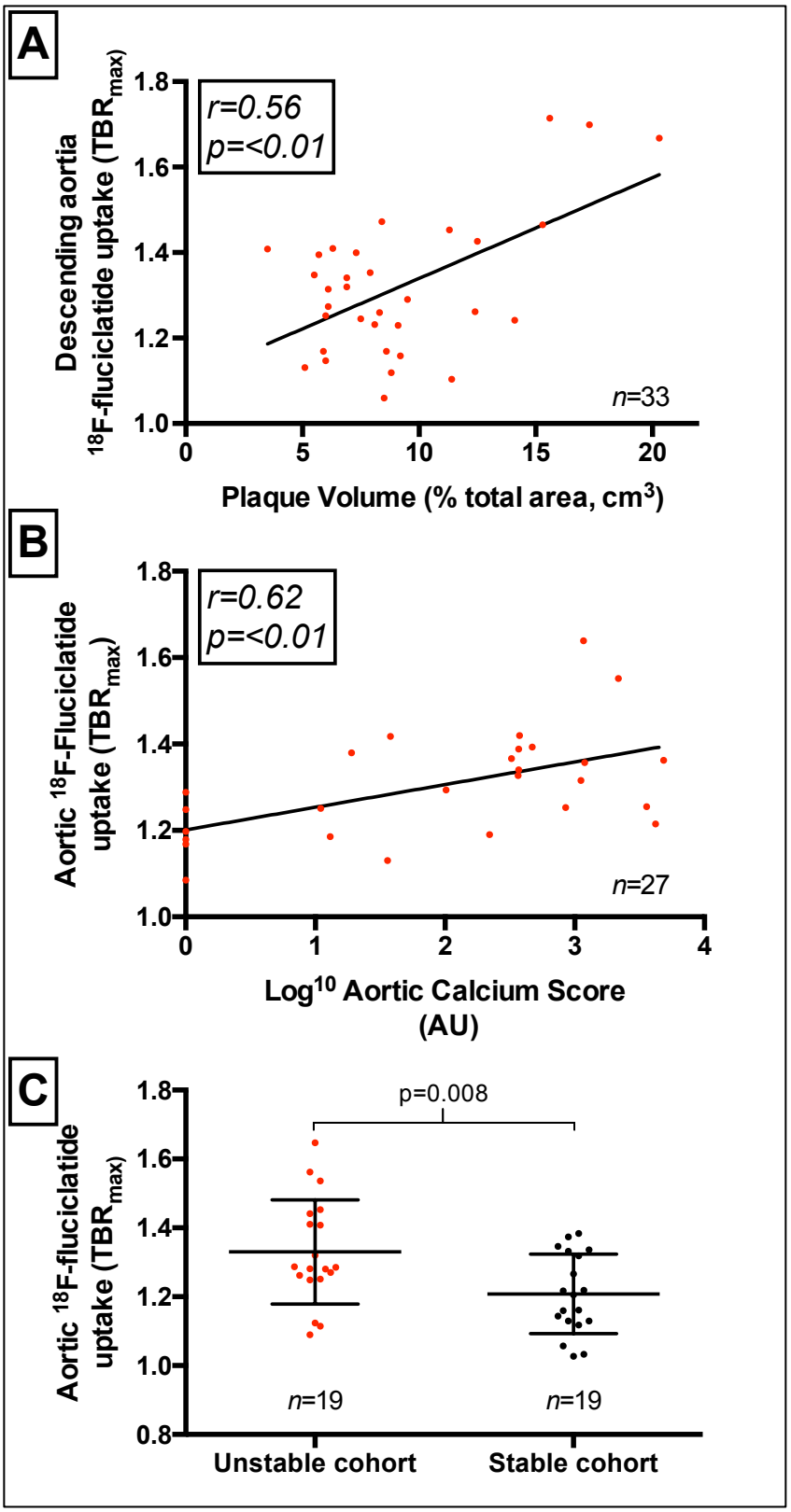
A
Descending aortia
18F-fluciclatide uptake (TBRmax)
r=0.56
p=<0.01
n=33
Plaque Volume (% total area, cm3)
B
Aortic 18F-Fluciclatide
uptake (TBRmax)
r=0.62
p=<0.01
n=27
Log10 Aortic Calcium Score
(AU)
C
Aortic 18F-fluciclatide
uptake (TBRmax)
p=0.008
n=19
n=19
Unstable cohort
Stable cohort

6.4.6. Aortic 18F-fluciclatide uptake in stable and unstable patients

To establish whether 18F-fluciclatide uptake may be a marker of unstable atherosclerotic activity, we compared uptake in patients who had sustained a recent myocardial infarction to those with stable atheroma. Given the strong relationship between 18F-fluciclatide activity and plaque burden, we matched patients in the two groups according to CT calcium score. We demonstrated increased 18F-fluciclatide aortic uptake in the patients with recent myocardial infarction compared to those in the stable cohort (TBR_{max}; 1.33±0.15vs 1.21±0.1, p=0.008) despite equivalent aortic calcium scores (Table 6.2, Figure 6.4). Moreover, in patients with recent myocardial infarction, a stronger correlation was observed between aortic plaque burden and 18F-fluciclatide uptake than in the patient population as a whole (aortic wall thickness r=0.68, p=0.02). When aortic SUV measurement were assessed these were consistently increased in the unstable groups compared to the stable groups across all regions of the aorta even before attempts were made to match these groups by calcium score ($p<0.05$ for all aortic regions, Table 6.2).

6.4.7. Aortic 18F-fluciclatide and cardiovascular risk factors

Amongst patients in the stable cohort aortic 18F-fluciclatide uptake correlated with a number of risk factors (Table 6.4). 18F-fluciclatide activity was higher in patients with hypercholesterolemia compared to those without (1.37±0.04 vs 1.24±0.06, p=0.007). Apparent observed trends were also seen in patients with diabetes (1.41±0.08 vs 1.28±0.02, p=0.06) and those with an established diagnosis of coronary heart disease (1.37±0.04 vs 1.28±0.03, p=0.08). Again a strong correlation was observed between 18F-fluciclatide uptake and the CT calcium score (r=0.62, p<0.001) in this subgroup.

6.5. Discussion

We present the largest multimodality imaging study to date evaluating the application of an RGD-based $\alpha_v\beta_3$ integrin receptor radiotracer in the assessment of human atheroma. We have demonstrated that *ex vivo* 18F-fluciclatide binding co-localises to sites of $\alpha_v\beta_3$ integrin receptor expression in excised carotid plaques, and this was associated with regions of both angiogenesis and inflammation. We have further demonstrated *in vivo* that 18F-fluciclatide uptake increased with progressive atherosclerotic plaque burden and is higher in patients with unstable versus stable clinical disease. These data would suggest that 18F-fluciclatide holds promise as a non-invasive marker of disease activity in atherosclerosis, informing us about two key characteristics of high risk atheroma: inflammation and angiogenesis. This tracer may therefore aid our pathophysiological understanding of this important condition and help identify patients at increased risk of adverse cardiovascular events.

Plaque inflammation and angiogenesis are two key pathological processes associated with atheroma progression, plaque rupture and clinical events. Macrophages drive expansion of the necrotic core and secrete matrix metalloproteinases that weaken the fibrous cap, predisposing it to rupture. Angiogenesis is believed to occur in response to hypoxic conditions within the necrotic core and is associated with high-risk plaque characteristics.(167) In addition these new vessels are prone to leakage and rupture resulting in plaque hemorrhage that itself results in an intense inflammatory response, plaque destabilization and clinical events. A non-invasive imaging technique that can inform about the activity of these two adverse pathological processes might therefore

be useful in identifying patients with active high-risk atheroma. Indeed it is hoped that non-invasive markers of atherosclerotic disease activity may identify the vulnerable patient and provide incremental risk prediction to an assessment of radiographic disease burden alone.(147,240) We have here demonstrated that 18F-fluciclatide PET-CT is an emerging and promising approach to achieve these aims.

Our autoradiographic data showed focal 18F-fluciclatide binding within carotid atheroma that localised to $\alpha_v\beta_3$ integrin expression with no evidence of non-specific binding. Regions of 18F-fluciclatide uptake on autoradiography also corresponded to sites of immunohistochemical cellular staining for vascular endothelial cells and macrophages. This is in keeping with previous RGD-radiotracer studies and supports its role as a selective marker for angiogenic and inflammatory components of atherosclerotic activity.(135,186) Due to the close relationship between intraplaque inflammation and angiogenesis, it was challenging to ascertain whether 18F-fluciclatide was binding preferentially to one or the other of these processes. However high sensitivity c-reactive protein concentrations did not correlate with aortic 18F-fluciclatide uptake, perhaps suggesting that uptake of this tracer relates more closely to plaque angiogenesis and local cellular inflammation rather than systemic inflammation. This issue warrants further study in larger histological cohorts.

Dynamic *in vivo* imaging studies in 20 subjects confirmed irreversible 18F-fluciclatide binding over the selected acquisition time to regions of aortic atherosclerosis and demonstrated that the optimum time for 18F-fluciclatide imaging in the aorta is between 40 and 70 min. This timeframe was used for subsequent static PET imaging

across the cohort as a whole. Static *in vivo* imaging demonstrated reproducible quantification of 18F-fluciclatide in aortic atheroma of all 46 patients, and this was closely correlated with the severity of aortic atherosclerotic burden. Indeed associations were observed with the aortic calcium score, aortic plaque thickness and overall plaque volume.(249,250) In patients with clinically stable disease, aortic uptake of 18F-fluciclatide was increased in subjects with hypercholesterolemia with strong trends towards higher uptake in patients with diabetes mellitus and those with ischemic heart disease. Perhaps most importantly, 18F-fluciclatide uptake in aortic atheroma was increased in patients with unstable clinical disease (recent myocardial infarction) irrespective of plaque burden. Interestingly, using 18F-fluorodeoxyglucose, we have previously demonstrated a similar pattern of increased metabolic activity in aortic atheroma amongst patients with recent myocardial infarction.(161) These data therefore lend support to the hypothesis that acute myocardial infarction causes inflammation and instability in systemic atherosclerosis, as has been suggested in preclinical murine models.(251) It also provides further validity to the concept that 18F-fluciclatide uptake can identify higher risk plaques. However whether this increased disease activity truly represents a response to the infarct or rather the underlying trigger remains to be determined.

We acknowledge that there are some limitations of our study that include potential partial volume artefacts, a limited histological cohort and the use of surrogate measures for aortic histology. The dynamic imaging approach proved sensitive to patient movement during the prolonged period of acquisition, limiting its overall utility, but in the future this may be readdressed by novel motion tracking systems that

allow for correction of both cardiac and respiratory motion to enable even greater definition of regional $\alpha_v\beta_3$ integrin expression.(239) Nonetheless, we believe that the totality of our comprehensive evidence using multiple approaches and imaging modalities provides a robust and cogent argument to support our findings.

In conclusion, this is the largest study to date assessing $\alpha_v\beta_3$ integrin expression in human atherosclerotic disease. We have demonstrated that 18F-fluciclatide uptake localises to regions of inflammation and angiogenesis, correlates with the plaque burden and is increased in patients with clinically unstable disease. Although further study is required, our data indicate that 18F-fluciclatide shows major promise as a non-invasive marker of disease activity and instability in atherosclerosis.

Chapter 7.

Conclusions and Future Directions

7.1 Summary of Findings

Despite advances seen over recent decades, cardiovascular disease remains the most common cause of death worldwide.(1) Although the clinical manifestation of a cardiovascular event is commonly unanticipated, the preceding pathophysiological processes are chronic, asymptomatic and may be difficult to detect on both an individual or population perspective.(147) When developing and delivering medical therapy for a chronic disease process, and particularly aortic stenosis, ventricular remodeling and atherosclerotic disease, ascertaining short- and long-term efficacy poses a significant challenge, both within an individual and a population. We counter this chronicity through meta-analyses or large multicenter trials, thus increasing the expense of novel drug development due a prerequisite for large numbers of participants and prolonged follow-up, which often may identify only marginal treatment responses.(252)

Combined PET/CT now provides a method of combining high resolution anatomical imaging with the real-time quantification of adverse biological processes *in vivo,* and as a consequence has generated significant interest as a novel imaging tool in cardiovascular disease.(5,240,253) This technology should encourage the practice of individualized medicine through targeting therapy based upon real-time disease activity, providing new biological insights, risk stratifying patients, and providing a non-invasive measure of early therapeutic response that may otherwise not be clinically manifested for several years.

The purpose of this thesis was to study the utility of PET to identify fundamental pathophysiological processes driving 3 forms of cardiovascular disease: aortic stenosis, myocardial infarction, and atherosclerosis. Our comprehensive multimodality approach featured both novel and established cardiovascular imaging techniques including PET, CT, MRI and echocardiography, and findings were supported with *ex vivo* and *in vivo* methods of validation. From the series of studies presented in this thesis, we can conclude that the use of 18F-fluoride PET, and to a lesser extent 18F-FDG PET, holds major promise as a marker of disease activity (chapter 3), with important prognostic implications (chapter 4). Furthermore, the αvβ3 integrin radiotracer 18F-fluciclatide holds great potential as a marker of acute ventricular remodeling and functional recovery following myocardial infarction (chapter 5), and aortic atherosclerotic disease activity (chapter 6).

7.1.1. Aortic Valvular 18F-Fluoride uptake is associated with both valvular calcification activity and clinical disease progression in aortic stenosis.

Progressive valvular calcification and inflammation are key pathophysiological processes driving aortic stenosis. 18F-Fluoride is a PET radiotracer that preferentially binds to regions of newly forming vascular micro-calcification beyond the resolution of computed tomography(227), while 18F-FDG has been widely used to measure vascular inflammation.(48) Recent studies have suggested that these tracers can measure the activity of these processes in aortic stenosis, although validation of this technique has previously been lacking.(2,58)

In this study, we sought to provide such validation, comparing aortic valve 18F-fluoride and 18F-FDG uptake with both histological measures of calcification and inflammatory activity, and the progression of aortic valve calcification on CT. Valvular 18F-fluoride uptake on PET imaging performed prior to aortic valve replacement demonstrated a strong correlation with histological markers of calcification activity on the excised aortic valve tissue. No such association with histological markers was seen with 18F-FDG. We extended our findings to a small cohort of patients with aortic stenosis who underwent 18F-fluoride and 18F-FDG PET and CT-calcium scoring of the aortic valve both at baseline and after 1 year. In this cohort, a good correlation was observed between baseline 18F-fluoride uptake and progression in valve calcification. There was no such association seen with 18F-FDG.

Our results therefore provided the first validation of 18F-fluoride as a marker of calcification activity in the aortic valve. To determine the utility of 18F-fluoride PET further, we extended our period of follow-up to a larger cohort of patients with a range of calcific aortic valve disease, and examined the role of PET imaging as a means of predicting haemodynamic progression and clinical outcome in aortic stenosis (chapter 4).

7.1.2. Valvular 18F-Fluoride and 18F-FDG uptake on PET are associated with disease progression and clinical outcome in Aortic Stenosis.

Within this chapter, we expanded on the validation of 18F-fluoride in Chapter 3 to report the first prospective longitudinal study to investigate whether 18F-fluoride and 18F-FDG may be associated with disease progression and clinical outcome in aortic stenosis.

In total, 121 volunteers with and without aortic valve disease previously imaged with 18F-fluoride and 18F-FDG PET/CT (2) underwent clinical follow-up including assessment of disease progression using CT aortic valve calcium scoring and echocardiography at 1 and 2 years. Volunteers were followed for a primary clinical outcome endpoint of cardiovascular death or aortic valve replacement (AVR).

After 2 years, new valvular calcium on CT was visible in a similar distribution as the 18F-fluoride activity on baseline PET imaging. Baseline 18F-fluoride uptake correlated strongly with the subsequent rate of progression in aortic valve calcium score and with echocardiographic measures of haemodynamic progression. 18F-FDG demonstrated moderate correlations with disease progression. Both 18F-fluoride and 18F-FDG emerged independently associated with of adverse clinical outcome after multivariate adjustment.

There were strong associations between the baseline CT valvular calcium score and rate of change in calcium score. Indeed, on baseline imaging assessment the aortic valve calcification score was more closely associated with disease progression and clinical outcome than established gold-standard echocardiographic assessments of valve disease severity. Given the degree of co-linearity between CT calcium scoring and 18F-fluoride uptake in the valve, assessing whether 18F-fluoride uptake provides incremental information to CT was challenging. However, in a retrospective analysis using the regression line between the CT calcium score and 18F-fluoride uptake as a cut off, patients with aortic stenosis and higher than expected 18F-fluoride uptake for a given CT calcium score progressed three times faster than subjects with lower than expected uptake. When a similar analysis was performed for 18F-FDG, no significant difference was observed.

In conclusion, we demonstrated that both 18F-fluoride and 18F-FDG may predict disease progression and adverse clinical outcome in aortic stenosis. In particular, 18F-fluoride demonstrated close correlations with the change in CT calcium score, appearing to be of incremental value to baseline CT imaging. Larger studies are required to confirm the incremental predictive value of PET compared to CT. However our data would support PET/CT as a novel method for measuring disease activity in aortic stenosis, with the ability to prognosticate natural history. This may be of particular value in studies investigating novel therapies, where beneficial treatment effects are likely to be detected rapidly without the need for protracted follow-up.

7.1.3. 18F-Fluciclatide uptake is increased at sites of recent MI acting as a biomarker of cardiac repair.

The incidence of heart failure in survivors of myocardial infarction (MI) remains high and infers poor clinical outcome. Indeed, most deaths after MI occur in patients who develop heart failure, with the greatest risk experienced in patients with late- versus early-onset heart failure.(254) These changes call for new approaches to understand the mechanisms of adverse remodeling following MI, to both guide the short-term allocation of therapy and resources, and predict long-term clinical outcome.

In this chapter, we evaluated the utility of the novel $\alpha_v\beta_3$-selective PET radiotracer 18F-fluciclatide as a marker of myocardial remodeling after MI. The cell surface receptor integrin $\alpha_v\beta_3$ is markedly upregulated on activated vascular endothelial cells, macrophages and myofibroblasts and as such plays a multifaceted role in regulating the inflammatory, angiogenic and fibrotic processes that restore myocardial integrity following MI, potentially contributing to maladaptive ventricular remodeling and the progression to heart failure.

In a study of 37 volunteers using PET imaging with kinetic analysis, computed tomography (CT) contrast angiography and cardiac magnetic resonance imaging we have demonstrated 18F-fluciclatide binding with αvβ3 integrin receptors in regions of acute myocardial infarction and in the remote myocardium, both early and late after MI. In patients with established myocardial scar and stable ischaemic heart disease, myocardial uptake approximated that seen in healthy control patients.

18F-fluciclatide uptake correlated with functional impairment and may be associated with myocardial recovery.

Our study fulfils a key step validating αvβ3 integrin receptor imaging in humans following MI. This novel characterisation of myocardial remodeling may hold potential as a biological end-point in the study of novel therapies following MI.

7.1.4. Quantification of $\alpha_v\beta_3$ integrin expression in human aortic atheroma using 18F-fluciclatide is associated with plaque burden and is increased following myocardial infarction.

Atherosclerotic cardiovascular disease is the commonest cause of death worldwide. However, despite recent advances in diagnostic techniques an accurate prediction of clinical events remains elusive, and there is considerable interest in non-invasive imaging techniques that go beyond the detection of luminal stenoses and instead focus on measuring disease activity within the vasculature.

Intra-plaque angiogenesis and inflammation are key promoters of atherosclerosis and are mediated by the $\alpha_v\beta_3$ integrin receptor pathway. In chapter 6 we investigated the applicability of the novel $\alpha_v\beta_3$-integrin receptor-selective PET radiotracer 18F-fluciclatide in assessing human aortic atherosclerosis. We undertook CT and PET imaging of the thorax with 18F-fluciclatide in 46 volunteers with a spectrum of stable and unstable coronary disease. 18F-Fluciclatide binding with $\alpha_v\beta_3$ integrin expressed on inflammatory and angiogenic cells within atheroma was confirmed using *ex-vivo* histological assessment and *in-vivo* kinetic modeling. Aortic 18F-fluciclatide uptake correlated with vascular calcification and atheroma burden. In keeping with recent findings demonstrating an upregulation of atherogenesis following myocardial infarction,(251) we demonstrated an increase in aortic 18F-fluciclatide atheroma uptake following acute myocardial infarction when compared to patients with stable atheroma.

In conclusion, in the largest study to date assessing $\alpha_v\beta_3$ integrin expression in atherosclerosis we demonstrated that 18F-fluciclatide uptake localises to regions of inflammation and angiogenesis, and correlates with disease burden and activity. Although further study is required, our data indicate that 18F-fluciclatide shows promise as a non-invasive marker of disease activity in atherosclerosis.

7.2. Future Directions

Several opportunities arise from the conclusions of this thesis, with potential to expand and strengthen the role of novel imaging techniques in the assessment of cardiovascular pathology, disease activity and prognosis. Several projects are ongoing that aim to exploit the data and expertise gained during the formulation of this thesis.

Specifically, work is ongoing evaluating;

a) 18F-fluoride PET as an imaging biomarker in the assessment of novel therapies for aortic stenosis.
b) the assessment of valvular calcification in aortic stenosis using CT.
c) 18F-fluciclatide as a marker of $\alpha_v\beta_3$ integrin-related myocardial fibrosis in aortic stenosis.
d) pulmonary 18F-fluciclatide uptake as a marker of $\alpha_v\beta_3$ integrin-related pulmonary fibrogenesis in interstitial lung disease.

7.2.1. 18F-fluoride PET as an imaging biomarker in the assessment of novel therapies for aortic stenosis.

In Chapters 3 and 4, we have demonstrated that calcification activity is the major driver to disease progression in aortic stenosis and that this can be measured using 18F-fluoride PET. Further assessment is now required to define a role for 18F-fluoride PET imaging in the clinical setting. The standard management of patients with asymptomatic aortic stenosis relies upon repeated evaluations of cardiac physiology using clinical history, examination and multimodality imaging. At present, an individualisation of disease trajectory and prognosis at the time of diagnosis is challenging, particularly in the setting of mild calcific disease or prosthetic aortic valve. 18F-Fluoride PET may therefore hold a role at the point of clinical diagnosis in stratifying indolent compared to accelerated states of valvular calcification, thereby identifying high-risk patients appropriate for closer clinical observation or future drug therapies. However, larger longitudinal studies are required to define thresholds of valvular 18F-fluoride activity that hold clinical relevance.

Funding has now been awarded and recruitment has commenced for a double-blind, randomised, placebo-control trial in patients with calcific aortic stenosis, using 18F-fluoride as a biomarker of calcification activity and as an end-point measuring the efficacy of novel pharmacotherapy in aortic stenosis. (NCT02132026; Study Investigating the Effect of Drugs Used to Treat Osteoporosis on the Progression of Calcific Aortic Stenosis. [SALTIRE II])

In total, 150 subjects with aortic stenosis of moderate haemodynamic severity will be randomized to taking either taking a weekly dose of a matched placebo, the bisphosphonate 'alendronate' or the human monoclonal antibody to RANKL 'denosumab', which is a potent inhibitor of osteoclast differentiation and bone resorption. The study intends to demonstrate that, in patients with aortic stenosis, therapies targeted at calcium metabolism, such as bisphosphonates and denosumab, will reduce valvular calcification activity *in vivo* using 18F-fluoride PET imaging, and halt or delay disease progression.

Aortic stenosis severity will be assessed at baseline and at 1 and 2 years by CT calcium scoring and echocardiography. 18F-Fluoride PET uptake will be measured at baseline, 3 months and 1 year to assess the early (3 months) and sustained (1 year) impact of the intervention on valvular calcification activity. Recruitment is ongoing, and since commencing the study 20 patients have undergone repeat PET/CT imaging within 2 weeks of their baseline scan to investigate scan-rescan reproducibility, demonstrating excellent repeatability with minimal variation in valve signal between imaging assessments.(255)

A modification of disease-pathways not directly influencing valvular calcification may also be effective, particularly in the early stages of valvular remodeling that precede gross macroscopic calcification. Indeed, an effective drug therapy for aortic stenosis should target valve-specific signaling pathways while achieving optimal biomechanical function, by restoring or at least preserving valve function and tissue integrity.(256) The failure of statin therapy to attenuate aortic stenosis is well

documented; however, alternative forms of lipid modulation will likely be assessed in the near-future, in particular lipoprotein(a)-lowering therapies.(257) Serum lipoprotein(a) concentrations are not impacted by statin therapy, and in a recent study of almost 7000 participants, serum lipoprotein(a) concentrations are closely associated with the development of calcific aortic stenosis.(256,258) Other therapeutic strategies include modulators of the renin-angiotensin system (RAS), given the apparent contribution of RAS to the initiation and propagation of leaflet thickening, and a recent trial of ACE-inhibition using CMR and echocardiographic end-points has shown promising results.(259). However, given the complexity and chronicity of aortic stenosis pathophysiology, a multifaceted approach to disease-modification is likely required, with 18F-fluoride PET providing an effective imaging-based biomarker of disease activity.

7.2.2. The assessment of valvular calcification in aortic stenosis using computed tomography.

Calcification of the aortic valve is the prevailing pathological mechanism driving aortic stenosis.(18) Recently, aortic valve calcification (AVC) quantification using CT has been closely associated with disease severity and clinical outcome,(39,216) and in a small study, has been shown to correlate with aortic stenosis progression.(221) In our study we have demonstrated that AVC quantification outperforms echocardiographic assessments of aortic stenosis in both associations with haemodynamic progression and clinical outcome.

Prior to the adoption of CT AVC quantification as a clinical method of evaluating AS severity, further assessments must be made to establish clinically appropriate thresholds for AS severity. This is of particular relevance given the significant disparity between genders in the quantity of valvular calcification required to generate haemodynamically severe aortic stenosis, even after correcting for differences in body size and LVOT diameter.(260) Therefore our group is heading an international multicenter collaboration to form a cohort of 918 patients with moderate to severe aortic stenosis who have received aortic valve CT calcium scoring. The group's aim is to validate previously proposed thresholds that identify severe calcific aortic valve disease (232) and clarify the prognostic utility of AVC quantification using a multinational dataset. We acknowledge that while unlikely to replace echocardiography in the diagnosis and surveillance of aortic stenosis, CT AVC quantification should hold value in cases of unclear severity, where discordant

echocardiographic findings (such as low-gradient aortic stenosis with low aortic valve area), low haemodynamic flow states or unclear symptomatology may cloud clinical judgement. These cases account for up to a third of patients presenting with significant haemodynamic obstruction,(232) and the presence of severe aortic valve calcification on CT holds significant prognostic implications that may guide clinical decision making and ultimately influence patient outcome.(39)

7.2.3. 18F-Fluciclatide as a marker of $\alpha_v\beta_3$ integrin-related myocardial fibrosis in aortic stenosis

Fibrosis plays a key role in aortic stenosis, both in progressive leaflet thickening and within the myocardium, where fibrogenesis occurs as the hypertrophic response of the left ventricle decompensates. Indeed progressive myocardial fibrosis is believed to be a key driver in the progression from hypertrophy to heart failure.(261) Established myocardial replacement fibrosis in aortic stenosis can be identified using CMR with LGE, where a mid-wall pattern of fibrosis is associated with advanced hypertrophy and an 8-fold increase in mortality.(16)

As demonstrated in Chapter 5, the integrin $\alpha_v\beta_3$ is upregulated by activated cardiac myofibroblasts and vascular endothelial cells in states of angiogenesis and fibrosis, and may be visualized *in-viv*o using the PET radiotracer 18F-fluciclatide. An imaging tool capable of detecting fibrogenesis in the early stages of ventricular decompensation secondary to haemodynamically severe aortic stenosis, prior to the establishment of replacement fibrosis, would therefore be of great value, affording the prediction of left ventricular decompensation.

Patients with a spectrum of calcific aortic stenosis severity were recruited for imaging with 18F-fluciclatide PET/CT and CMR with assessment of LGE (NCT01837160, 'Angiogenesis and Fibrosis in Aortic Stenosis'). In total, 12 patients with aortic stenosis underwent imaging assessment; this cohort was included in our assessment of 18F-fluciclatide in atherosclerotic disease (Chapter 6). Early results suggest that the

sub-acute nature of myocardial fibrogenesis in such pressure-overload models of myocardial remodeling may be insufficient to generate an identifiable myocardial uptake due to the low signal-to-noise ratio. However, further advances may be anticipated with the evolution of both dual cardiac/respiratory gating, which may minimalise myocardial PET signal loss from respiratory movement,(262) and hybrid PET/MRI technology.

Similar to PET/CT, MRI and PET scanners are loaded on to the same gantry, facilitating co-registration of the scans and attenuation correction. PET/MRI therefore harnesses the cardiac imaging strengths of MRI which principally relate to cine imaging of the right and left ventricles and myocardial tissue characterization.(263) In particular this may be of value for fibrosis radiotracers, where myocardial PET activity may be compared to the distribution of late gadolinium enhancement or other CMR markers of myocardial fibrosis in order to define ongoing remodeling activity.

Ultimately however, a potential future drawback of integrin $\alpha_v\beta_3$ receptor imaging may be the lack of specificity the integrin $\alpha_v\beta_3$ receptors hold to a single pathophysiological process. While 18F-fluciclatide PET/CT may prove a sensitive marker of remodeling activity after myocardial infarction, a lack of specificity in its myocardial signal may reduce its utility as an investigative tool in trials of focused anti-angiogenic or anti-fibrotic therapy. Development of such specific fibrogenic or angiogenic radiotracers is ongoing. Collagen-specific radiotracer probes, in particular, appear to provide a direct means of quantifying fibrotic activity *in vivo*. A collagen-targeted peptidomimetic of the platelet collagen receptor Glycoprotein VI has proven effective

in identifying focal myocardial fibrotic activity in mouse models of myocardial infarction,(264) while more recently the amino acid, *proline*, a major constituent of collagen and widely used as a marker of collagen synthesis, has been incorporated into radiotracers for the assessment of type III collagen production in pulmonary and musculoskeletal systems.(265,266) The translation of these tracers beyond murine models of ischaemia is in progress, while alternative tracers targeting the renin/angiotensin/aldosterone axis, which is believed to drive fibrosis both in the valve and myocardium, may also prove of use. Recently, ^{11}C-KR31173 has been used to investigate cardiac angiotensin II type 1 receptor (AT1R) expression in the left ventricle of humans and in a pig model of myocardial infarction, demonstrating no adverse effects and a detectable cardiac signal.(267)

Aside from the integrin $\alpha_v\beta_3$ receptor, targets for clinical imaging of myocardial angiogenesis are limited to the vascular endothelial growth factor (VEGF) receptor. Receptors for this potent angiogenesis-stimulating factor have been extensively imaged in the context of tumour angiogenesis, and radiotracer accumulation the murine myocardium has been demonstrated early after experimental myocardial infarction.(132,268) However, as per a number of other pre-clinical angiogenic imaging targets described, including the α7 nicotinic acetylcholine receptor,(269) reports of successful VEGF-receptor imaging in human hearts is awaited, highlighting the difficulty and expense of translating these advanced technologies into a clinically useful imaging tool.

7.2.4. Pulmonary 18F-fluciclatide uptake as a marker of $\alpha_v\beta_3$ integrin-related pulmonary fibrogenesis in interstitial lung disease.

Idiopathic pulmonary fibrosis (IPF) is a disease of unknown cause characterised by progressive injury, inflammation, and fibrosis of the lung parenchyma. Systemic sclerosis is a complex connective tissue disorder featuring pulmonary hypertension and pulmonary fibrosis predominantly. The pathogenesis of pulmonary fibrosis is incompletely understood, but TGF-ß activation mediated by integrins including $\alpha_v\beta_3$ is an accepted common pathway.(87)

From our study cohort of patients with calcific aortic stenosis (NCT01837160), concomitant fibrotic lung disease was present on CT imaging in one patient. We demonstrated a significant focal increase in 18F-fluciclatide uptake within the region of fibrotic changes when compared to the contralateral lung region. On this basis funding was granted for a pilot study of 20 patients with either IPF or systemic sclerosis to undergo PET/CT with 18F-fluciclatide to determine the utility of 18F-fluciclatide PET in assessing fibrogenesis in fibrotic lung disease. Tracer uptake will be correlated with volumetric CT and CT pulmonary perfusion as imaging markers of pulmonary fibrosis and microvascular changes. If validated, this technique may be employed to assess drug efficacy and disease progression. Indeed as a secondary objective serial lung function tests will be performed over 12 months to determine any association between 18F-fluciclatide uptake and rates of disease progression.

7.3. Perspective

The novel imaging techniques described in this thesis have illuminated the potential that molecular imaging holds to fundamentally alter our approach to the assessment and the quantification of cardiovascular disease processes *in vivo*. By applying these technologies, we may continue to evolve the practice of individualized medicine within cardiovascular science, while developing a scaffold by which to trial the real-time effects of emergent treatments, including stem cell therapies. Particularly in this thesis we have developed robust methodologies to potentially study large numbers of patients using molecular imaging in a spectrum of cardiovascular disease. Further work is now required to ensure that these techniques ultimately translate to an improvement in the clinical care of patients.

Bibliography

1. Mozaffarian D, Benjamin EJ, Go AS, Arnett DK, Blaha MJ, Cushman M, et al. Heart Disease and Stroke Statistics-2015 Update: A Report From the American Heart Association. Circulation. 2015 Jan 27;131(4):e29-322

2. Dweck MR, Jones C, Joshi NV, Fletcher AM, Richardson H, White A, et al. Assessment of Valvular Calcification and Inflammation by Positron Emission Tomography in Patients With Aortic Stenosis. Circulation. 2012 Jan 3;125(1):76–86.

3. Millar BC, Prendergast BD, Alavi A, Moore JE. 18FDG-positron emission tomography (PET) has a role to play in the diagnosis and therapy of infective endocarditis and cardiac device infection. International Journal of Cardiology. 2013 Sep 1;167(5):1724-36.

4. Chen W, Dilsizian V. PET Assessment of Vascular Inflammation and Atherosclerotic Plaques: SUV or TBR? Journal of Nuclear Medicine. 2015 Apr 1;56(4):503–4.

5. van den Borne SWM, Isobe S, Verjans JW, Petrov A, Lovhaug D, Li P, et al. Molecular Imaging of Interstitial Alterations in Remodeling Myocardium After Myocardial Infarction. Journal of the American College of Cardiology. 2008 Dec;52(24):2017–28.

6. Joshi NV, Vesey AT, Williams MC, Shah ASV, Calvert PA, Craighead FHM, et al. (18)F-fluoride positron emission tomography for identification of ruptured and high-risk coronary atherosclerotic plaques: a prospective clinical trial. Lancet. 2014 Feb 22;383(9918):705-13

7. Gaemperli O, Kaufmann PA. PET and PET/CT in cardiovascular disease. Annals of the New York Academy of Sciences. 2011 Jun 30;1228(1):109–36.

8. Pichler BJ, Wehrl HF, Judenhofer MS. Latest advances in molecular imaging instrumentation. Journal of Nuclear Medicine. 2008 Jun;49 Suppl 2:5S–23S.

9. Kenny LM, Coombes RC, Oulie I, Contractor KB, Miller M, Spinks TJ, et al. Phase I trial of the positron-emitting Arg-Gly-Asp (RGD) peptide radioligand 18F-AH111585 in breast cancer patients. Journal of Nuclear Medicine. Society of Nuclear Medicine; 2008 Jun;49(6):879–86.

10. Tomasi G, Kenny L, Mauri F, Turkheimer F, Aboagye EO. Quantification of receptor-ligand binding with [18F]fluciclatide in metastatic breast cancer patients. Eur J Nucl Med Mol Imaging. 2011 Sep 3;38(12):2186–97.

11. Zhao L, Ashek A, Wang L, Fang W, Dabral S, Dubois O, et al. Heterogeneity in lung (18)FDG uptake in pulmonary arterial hypertension: potential of dynamic (18)FDG positron emission tomography with kinetic analysis as a bridging biomarker for pulmonary vascular remodeling targeted treatments. Circulation. 2013 Sep 10;128(11):1214–24.

12. Berman DS, Germano G, Slomka PJ. Improvement in PET myocardial perfusion image quality and quantification with flurpiridaz F 18. J Nucl Cardiol. 2012 Feb;19 Suppl 1:S38–45.

13. Woo J, Tamarappoo B, Dey D, Nakazato R, Le Meunier L, Ramesh A, et al. Automatic 3D registration of dynamic stress and rest 82Rb and flurpiridaz F 18 myocardial perfusion PET data for patient motion detection and correction. Med Phys. 2011;38(11):6313.

14. Nkomo VT, Gardin JM, Skelton TN, Gottdiener JS, Scott CG, Enriquez-Sarano M. Burden of valvular heart diseases: a population-based study. Lancet. 2006 Sep 15;368(9540):1005–11.

15. Rajamannan NM, Evans FJ, Aikawa E, Grande-Allen KJ, Demer LL, Heistad DD, et al. Calcific Aortic Valve Disease: Not Simply a Degenerative Process. Circulation. 2011. Oct 18; 124(16):1783-1791

16. Dweck MR, Joshi S, Murigu T, Alpendurada F, Jabbour A, Melina G, et al. Midwall Fibrosis Is an Independent Predictor of Mortality in Patients With Aortic Stenosis. Journal of the American College of Cardiology. ; 2011 Sep 13;58(12):1271–9.

17. Dweck MR, Boon NA, Newby DE. Calcific Aortic Stenosis. Journal of the American College of Cardiology; 2012 Nov 6;60(19):1854–63.

18. Pawade TA, Newby DE, Dweck MR. Calcification in Aortic Stenosis: The Skeleton Key. Journal of the American College of Cardiology. 2015 Aug 4;66(5):561–77.

19. Otto CM, Kuusisto J, Reichenbach DD, Gown AM, O'Brien KD. Characterization of the early lesion of "degenerative" valvular aortic stenosis. Histological and immunohistochemical studies. Circulation. 1994 Aug 1;90(2):844–53.

20. Kaden JJ, Dempfle C-E, Grobholz R, Fischer CS, Vocke DC, Kiliç R, et al. Inflammatory regulation of extracellular matrix remodeling in calcific aortic valve stenosis. Cardiovasc Pathol. 2005 Mar;14(2):80–7.

21. Thubrikar MJ, Aouad J, Nolan SP. Patterns of calcific deposits in operatively excised stenotic or purely regurgitant aortic valves and their relation to mechanical stress. The American Journal of Cardiology. 1986 Aug 1;58(3):304–8.

22. O'Brien KD, Reichenbach DD, Marcovina SM, Kuusisto J, Alpers CE, Otto CM. Apolipoproteins B, (a), and E accumulate in the morphologically early lesion of "degenerative" valvular aortic stenosis. Arteriosclerosis, Thrombosis, and Vascular Biology. 1996 Apr;16(4):523–32.

23. Parolari A, Loardi C, Mussoni L, Cavallotti L, Camera M, Biglioli P, et al. Nonrheumatic calcific aortic stenosis: an overview from basic science to pharmacological prevention☆. European Journal of Cardio-Thoracic Surgery. 2009 Mar;35(3):493–504.

24. Galante A, Pietroiusti A, Vellini M, Piccolo P, Possati G, De Bonis M, et al. C-reactive protein is increased in patients with degenerative aortic valvular stenosis. Journal of the American College of Cardiology. 2001 Oct;38(4):1078–82.

25. Toutouzas K, Drakopoulou M, Synetos A, Tsiamis E, Agrogiannis G, Kavantzas N, et al. In Vivo Aortic Valve Thermal Heterogeneity in Patients With Nonrheumatic Aortic Valve Stenosis. Journal of the American College of Cardiology. 2008 Aug;52(9):758–63.

26. Carabello BA. The SEAS Trial. Curr Cardiol Rep. 2010 Mar;12(2):122–4.

27. Cowell SJ, Newby DE, Prescott RJ, Bloomfield P, Reid J, Northridge DB, et al. A randomized trial of intensive lipid-lowering therapy in calcific aortic stenosis. N Engl J Med. Massachusetts Medical Society; 2005 Jun 9;352(23):2389–97.

28. Eriksen HA, Satta J, Risteli J, Veijola M, Väre P, Soini Y. Type I and type III collagen synthesis and composition in the valve matrix in aortic valve stenosis. Atherosclerosis. 2006 Nov;189(1):91–8.

29. Fondard O. Extracellular matrix remodelling in human aortic valve disease: the role of matrix metalloproteinases and their tissue inhibitors. European Heart Journal. 2005 Feb 25;26(13):1333–41.

30. Mazzone A, Epistolato MC, De Caterina R, Storti S, Vittorini S, Sbrana S, et al. Neoangiogenesis, T-lymphocyte infiltration, and heat shock protein-60 are biological hallmarks of an immunomediated inflammatory process in end-stage calcified aortic valve stenosis. Journal of the American College of Cardiology. 2004 May 5;43(9):1670–6.

31. Soini Y, Salo T, Satta J. Angiogenesis is involved in the pathogenesis of nonrheumatic aortic valve stenosis. Hum Pathol. 2003 Aug;34(8):756–63.

32. Chalajour F, Treede H, Ebrahimnejad A, Lauke H, Reichenspurner H, Ergun S. Angiogenic activation of valvular endothelial cells in aortic valve stenosis. Experimental Cell Research. 2004 Aug 15;298(2):455–64.

33. Waters EA, Chen J, Allen JS, Zhang H, Lanza GM, Wickline SA. Detection and quantification of angiogenesis in experimental valve disease with integrin-targeted nanoparticles and 19-fluorine MRI/MRS. J Cardiovasc Magn Reson. 2008;10(1):43.

34. Akahori H, Tsujino T, Naito Y, Matsumoto M, Lee-Kawabata M, Ohyanagi M, et al. Intraleaflet haemorrhage is associated with rapid progression of degenerative aortic valve stenosis. European Heart Journal. 2011 Apr;32(7):888–96.

35. Cowell, Newby, Burton, White, Northridge, Boon, et al. Aortic Valve Calcification on Computed Tomography Predicts the Severity of Aortic Stenosis. Clin Radiol. 2003 Aug 31;58(9):5–5.

36. Messika-Zeitoun D, Aubry M-C, Detaint D, Bielak LF, Peyser PA, Sheedy PF, et al. Evaluation and clinical implications of aortic valve calcification measured by electron-beam computed tomography. Circulation. American Heart Association Journals; 2004 Jul 20;110(3):356–62.

37. Davies SWS, Gershlick AHA, Balcon RR. Progression of valvar aortic stenosis: a long-term retrospective study. European Heart Journal. 1991 Jan 1;12(1):10–4.

38. Rosenhek RR, Binder TT, Porenta GG, Lang II, Christ GG, Schemper MM, et al. Predictors of outcome in severe, asymptomatic aortic stenosis. N Engl J Med. 2000 Aug 30;343(9):611–7.

39. Clavel M-A, Pibarot P, Messika-Zeitoun D, Capoulade R, Malouf J, Aggarval S, et al. Impact of aortic valve calcification, as measured by MDCT, on survival in patients with aortic stenosis: results of an international registry study. Journal of the American College of Cardiology. 2014 Sep 23;64(12):1202–13.

40. Steiner I, Kasparová P, Kohout A, Dominik J. Bone formation in cardiac valves: a histopathological study of 128 cases. Virchows Arch. 2007 Jun;450(6):653–7.

41. Mohler ER, Gannon F, Reynolds C, Zimmerman R, Keane MG, Kaplan FS. Bone formation and inflammation in cardiac valves. Circulation. 2001 Mar 20;103(11):1522–8.

42. Steitz SA, Speer MY, Curinga G, Yang HY, Haynes P, Aebersold R, et al. Smooth muscle cell phenotypic transition associated with calcification: upregulation of Cbfa1 and downregulation of smooth muscle lineage markers. Circulation Research. 2001 Dec 7;89(12):1147–54.

43. Kaden JJ, Bickelhaupt S, Grobholz R, Haase KK, Sarikoç A, Kiliç R, et al. Receptor

activator of nuclear factor kappaB ligand and osteoprotegerin regulate aortic valve calcification. J Mol Cell Cardiol. 2004 Jan;36(1):57–66.

44. Kaden JJ, Kiliç R, Sarikoç A, Hagl S, Lang S, Hoffmann U, et al. Tumor necrosis factor alpha promotes an osteoblast-like phenotype in human aortic valve myofibroblasts: a potential regulatory mechanism of valvular calcification. Int J Mol Med. 2005 Nov;16(5):869–72.

45. Rajamannan NM, Subramaniam M, Rickard D, Stock SR, Donovan J, Springett M, et al. Human aortic valve calcification is associated with an osteoblast phenotype. Circulation. 2003 May 6;107(17):2181–4.

46. Kaneko K, Kawasaki T, Masunari S, Yoshida T, Omagari J. Determinants of Extraaortic Arterial 18F-FDG Accumulation in Asymptomatic Cohorts: Sex Differences in the Association with Cardiovascular Risk Factors and Coronary Artery Stenosis. Journal of Nuclear Medicine. 2013 Mar 7.

47. Tawakol A, Migrino RQ, Bashian GG, Bedri S, Vermylen D, Cury RC, et al. In Vivo 18F-Fluorodeoxyglucose Positron Emission Tomography Imaging Provides a Noninvasive Measure of Carotid Plaque Inflammation in Patients. Journal of the American College of Cardiology. 2006 Nov;48(9):1818–24.

48. Rudd JHF, Myers KS, Bansilal S, Machac J, Rafique A, Farkouh M, et al. 18Fluorodeoxyglucose Positron Emission Tomography Imaging of Atherosclerotic Plaque Inflammation Is Highly Reproducible. Journal of the American College of Cardiology. 2007 Aug;50(9):892–6.

49. Rudd JHF, Warburton EA, Fryer TD, Jones HA, Clark JC, Antoun N, et al. Imaging atherosclerotic plaque inflammation with [18F]-fluorodeoxyglucose positron emission tomography. Circulation. 2002 Jun 11;105(23):2708–11.

50. Saam T, Rominger A, Wolpers S, Nikolaou K, Rist C, Greif M, et al. Association of inflammation of the left anterior descending coronary artery with cardiovascular risk factors, plaque burden and pericardial fat volume: a PET/CT study. Eur J Nucl Med Mol Imaging. 2010 Jun;37(6):1203–12.

51. Paulmier B, Duet M, Khayat R, Pierquet-Ghazzar N, Laissy J-P, Maunoury C, et al. Arterial wall uptake of fluorodeoxyglucose on PET imaging in stable cancer disease patients indicates higher risk for cardiovascular events. J Nucl Cardiol. 2008 Mar;15(2):209–17.

52. Marnane M, Merwick A, Sheehan OC, Hannon N, Foran P, Grant T, et al. Carotid plaque inflammation on 18F-fluorodeoxyglucose positron emission tomography predicts early stroke recurrence. Ann Neurol. 2012 May;71(5):709–18.

53. Marincheva-Savcheva G, Subramanian S, Qadir S, Figueroa A, Truong Q, Vijayakumar J, et al. Imaging of the Aortic Valve Using Fluorodeoxyglucose Positron Emission Tomography. Journal of the American College of Cardiology; 2011 Jun 21;57(25):2507–15.

54. Williams G, Kolodny GM. Suppression of myocardial 18F-FDG uptake by preparing patients with a high-fat, low-carbohydrate diet. AJR Am J Roentgenol. 2008 Feb;190(2):W151–6.

55. Grant FD, Fahey FH, Packard AB, Davis RT, Alavi A, Treves ST. Skeletal PET with 18F-fluoride: applying new technology to an old tracer. Journal of Nuclear Medicine. 2008 Jan;49(1):68–78.

56. Cook GJR, Blake GM, Marsden PK, Cronin B, Fogelman I. Quantification of Skeletal

Kinetic Indices in Paget's Disease Using Dynamic18F-Fluoride Positron Emission Tomography. J Bone Miner Res. 2002 May 1;17(5):854–9.

57. Frost ML, Fogelman I, Blake GM, Marsden PK, Cook G. Dissociation between global markers of bone formation and direct measurement of spinal bone formation in osteoporosis. J Bone Miner Res. 2004 Nov;19(11):1797–804.

58. Hyafil F, Messika-Zeitoun D, Burg S, Rouzet F, Benali K, Iung B, et al. Detection of 18fluoride sodium accumulation by positron emission tomography in calcified stenotic aortic valves. The American Journal of Cardiology. 2012 Apr 15;109(8):1194–6.

59. Chan KL, Teo K, Dumesnil JG, Ni A, Tam J, ASTRONOMER Investigators. Effect of Lipid lowering with rosuvastatin on progression of aortic stenosis: results of the aortic stenosis progression observation: measuring effects of rosuvastatin (ASTRONOMER) trial. Circulation. 2010 Jan 19;121(2):306–14.

60. Dweck MR, Khaw HJ, Sng GKZ, Luo ELC, Baird A, Williams MC, et al. Aortic stenosis, atherosclerosis, and skeletal bone: is there a common link with calcification and inflammation? European Heart Journal. 2013 Jun;34(21):1567-74.

61. Velagaleti RS, Pencina MJ, Murabito JM, Wang TJ, Parikh NI, D'Agostino RB, et al. Long-term trends in the incidence of heart failure after myocardial infarction. Circulation. American Heart Association. 2008 Nov 11;118(20):2057–62.

62. Roger VL, Weston SA, Gerber Y, Killian JM, Dunlay SM, Jaffe AS, et al. Trends in incidence, severity, and outcome of hospitalized myocardial infarction. Circulation. American Heart Association. 2010 Feb 23;121(7):863–9.

63. Sutton MGSJ, Sharpe N. Left Ventricular Remodeling After Myocardial Infarction. Circulation. 2000 June. 101:2981-2988.

64. Prabhu SD, Frangogiannis NG. The Biological Basis for Cardiac Repair After Myocardial Infarction: From Inflammation to Fibrosis. Circulation Research. American Heart Association. 2016 Jun 24;119(1):91–112.

65. McKay RG, Pfeffer MA, Pasternak RC, Markis JE, Come PC, Nakao S, et al. Left ventricular remodeling after myocardial infarction: a corollary to infarct expansion. Circulation. 1986 Oct;74(4):693–702.

66. Konstam MA, Kramer DG, Patel AR, Maron MS, Udelson JE. Left ventricular remodeling in heart failure: current concepts in clinical significance and assessment. JACC Cardiovasc Imaging. 2011 Jan;4(1):98–108.

67. Savoye C, Equine O, Tricot O, Nugue O, Segrestin B, Sautière K, et al. Left ventricular remodeling after anterior wall acute myocardial infarction in modern clinical practice (from the REmodelage VEntriculaire [REVE] study group). The American Journal of Cardiology. 2006 Nov 1;98(9):1144–9.

68. Flachskampf FA, Schmid M, Rost C, Achenbach S, DeMaria AN, Daniel WG. Cardiac imaging after myocardial infarction. European Heart Journal. 2011 Feb;32(3):272–83.

69. Verma A, Meris A, Skali H, Ghali JK, Arnold JMO, Bourgoun M, et al. Prognostic implications of left ventricular mass and geometry following myocardial infarction: the VALIANT (VALsartan In Acute myocardial iNfarcTion) Echocardiographic Study. JACC Cardiovasc Imaging. 2008 Sep;1(5):582–91.

70. Lewis EF, Moye LA, Rouleau JL, Sacks FM, Arnold JMO, Warnica JW, et al. Predictors of

late development of heart failure in stable survivors of myocardial infarction: the CARE study. Journal of the American College of Cardiology. 2003 Oct 15;42(8):1446–53.

71. Bolognese L, Neskovic AN, Parodi G, Cerisano G, Buonamici P, Santoro GM, et al. Left ventricular remodeling after primary coronary angioplasty: patterns of left ventricular dilation and long-term prognostic implications. Circulation. 2002 Oct 29;106(18):2351–7.

72. Masci PG, Ganame J, Francone M, Desmet W, Lorenzoni V, Iacucci I, et al. Relationship between location and size of myocardial infarction and their reciprocal influences on post-infarction left ventricular remodelling. European Heart Journal. 2011 Jul;32(13):1640–8.

73. Frangogiannis NG. The mechanistic basis of infarct healing. Antioxid Redox Signal. 2006 Nov;8(11-12):1907–39.

74. van der Laan AM, Nahrendorf M, Piek JJ. Healing and adverse remodelling after acute myocardial infarction: role of the cellular immune response. Heart. 2012 Sep;98(18):1384–90.

75. BUJAK M, FRANGOGIANNIS N. The role of TGF-β signaling in myocardial infarction and cardiac remodeling. Cardiovascular Research. 2007 May 1;74(2):184–95.

76. van der Laan AM, Hirsch A, Robbers LFHJ, Nijveldt R, Lommerse I, Delewi R, et al. A proinflammatory monocyte response is associated with myocardial injury and impaired functional outcome in patients with ST-segment elevation myocardial infarction: monocytes and myocardial infarction. Am Heart J. 2012 Jan;163(1):57–65.e2.

77. Wojakowski W, Tendera M, Michałowska A, Majka M, Kucia M, Maślankiewicz K, et al. Mobilization of CD34/CXCR4+, CD34/CD117+, c-met+ stem cells, and mononuclear cells expressing early cardiac, muscle, and endothelial markers into peripheral blood in patients with acute myocardial infarction. Circulation. 2004 Nov 16;110(20):3213–20.

78. Maekawa Y, Anzai T, Yoshikawa T, Asakura Y, Takahashi T, Ishikawa S, et al. Prognostic significance of peripheral monocytosis after reperfused acute myocardial infarction:a possible role for left ventricular remodeling. Journal of the American College of Cardiology. 2002 Jan 16;39(2):241–6.

79. Takahashi T, Hiasa Y, Ohara Y, Miyazaki S-I, Ogura R, Suzuki N, et al. Relationship of admission neutrophil count to microvascular injury, left ventricular dilation, and long-term outcome in patients treated with primary angioplasty for acute myocardial infarction. Circ J. 2008 Jun;72(6):867–72.

80. Shinde AV, Frangogiannis NG. Fibroblasts in myocardial infarction: a role in inflammation and repair. J Mol Cell Cardiol. 2014 May;70:74–82.

81. Mann DL. Stress-activated cytokines and the heart: from adaptation to maladaptation. Annu Rev Physiol Annual Reviews 2003;65(1):81–101.

82. Nian M, Lee P, Khaper N, Liu P. Inflammatory cytokines and postmyocardial infarction remodeling. Circulation Research. 2004 Jun 25;94(12):1543–53.

83. Brooks PC, Clark RA, Cheresh DA. Requirement of vascular integrin alpha v beta 3 for angiogenesis. Science. 1994 Apr 22;264(5158):569–71.

84. Willems IE, Havenith MG, De Mey JG, Daemen MJ. The alpha-smooth muscle actin-positive cells in healing human myocardial scars. Am J Pathol. 1994 Oct;145(4):868–75.

85. Porter KE, Turner NA. Cardiac fibroblasts: at the heart of myocardial remodeling.

Pharmacol Ther. 2009 Aug;123(2):255–78.

86. van den Borne SWM, Diez J, Blankesteijn WM, Verjans J, Hofstra L, Narula J. Myocardial remodeling after infarction: the role of myofibroblasts. Nat Rev Cardiol. 2009 Dec 1;7(1):30–7.

87. Asano Y, Ihn H, Yamane K, Jinnin M, Mimura Y, Tamaki K. Increased expression of integrin alpha(v)beta3 contributes to the establishment of autocrine TGF-beta signaling in scleroderma fibroblasts. J Immunol. 2005 Dec 1;175(11):7708–18.

88. Hinz B. Masters and servants of the force: the role of matrix adhesions in myofibroblast force perception and transmission. European Journal of Cell Biology. 2006 Apr;85(3-4):175–81.

89. WIPFF P, HINZ B. Integrins and the activation of latent transforming growth factor β1 – An intimate relationship. European Journal of Cell Biology. 2008 Sep 4;87(8-9):601–15.

90. Okada H, Takemura G, Kosai K-I, Li Y, Takahashi T, Esaki M, et al. Postinfarction gene therapy against transforming growth factor-beta signal modulates infarct tissue dynamics and attenuates left ventricular remodeling and heart failure. Circulation 2005 May 17;111(19):2430–7.

91. Harsdorf von R. "Fas-ten" your seat belt: anti-apoptotic treatment in heart failure takes off. Circulation Research; 2004 Sep 17;95(6):554–6.

92. Li Y, Takemura G, Kosai K-I, Takahashi T, Okada H, Miyata S, et al. Critical roles for the Fas/Fas ligand system in postinfarction ventricular remodeling and heart failure. Circulation Research; 2004 Sep 17;95(6):627–36.

93. Hinz B, Phan SH, Thannickal VJ, Galli A, Bochaton-Piallat M-L, Gabbiani G. The myofibroblast: one function, multiple origins. Am J Pathol. 2007 Jun;170(6):1807–16.

94. Volders PG, Willems IE, Cleutjens JP, Arends JW, Havenith MG, Daemen MJ. Interstitial collagen is increased in the non-infarcted human myocardium after myocardial infarction. J Mol Cell Cardiol. 1993 Nov;25(11):1317–23.

95. Chan W, Duffy SJ, White DA, Gao X-M, Du X-J, Ellims AH, et al. Acute left ventricular remodeling following myocardial infarction: coupling of regional healing with remote extracellular matrix expansion. JACC Cardiovasc Imaging. 2012 Sep;5(9):884–93.

96. Carrick D, Haig C, Rauhalammi S, Ahmed N, Mordi I, McEntegart M, et al. Pathophysiology of LV Remodeling in Survivors of STEMI: Inflammation, Remote Myocardium, and Prognosis. JACC Cardiovasc Imaging. 2015 Jul;8(7):779–89.

97. Takada Y, Ye X, Simon S. The integrins. Genome Biol. 2007;8(5):215.

98. Max R, Gerritsen RR, Nooijen PT, Goodman SL, Sutter A, Keilholz U, et al. Immunohistochemical analysis of integrin alpha vbeta3 expression on tumor-associated vessels of human carcinomas. Int J Cancer. 1997 May 2;71(3):320–4.

99. Eliceiri BP, Cheresh DA. The role of alphav integrins during angiogenesis. Mol Med. 1998 Dec;4(12):741–50.

100. Cayrol F, Díaz Flaqué MC, Fernando T, Yang SN, Sterle HA, Bolontrade M, et al. Integrin αvβ3 acting as membrane receptor for thyroid hormones mediates angiogenesis in malignant T cells. Blood. American Society of Hematology; 2015 Jan 29;125(5):841–51.

101. Trajkovic-Arsic M, Mohajerani P, Sarantopoulos A, Kalideris E, Steiger K, Esposito I, et al. Multimodal molecular imaging of integrin αvβ3 for in vivo detection of pancreatic cancer. J Nucl Med. Society of Nuclear Medicine; 2014 Mar;55(3):446–51.

102. Yoshida T, Gong J, Xu Z, Wei Y, Duh EJ. Inhibition of pathological retinal angiogenesis by the integrin αvβ3 antagonist tetraiodothyroacetic acid (tetrac). Exp Eye Res. 2012 Jan;94(1):41–8.

103. Amann K, Haas CS, Schüssler J, Daniel C, Hartner A, Schöcklmann HO. Beneficial effects of integrin αvβ3-blocking RGD peptides in early but not late phase of experimental glomerulonephritis. Nephrol Dial Transplant. 2012 May;27(5):1755–68.

104. Gerber EE, Gallo EM, Fontana SC, Davis EC, Wigley FM, Huso DL, et al. Integrin-modulating therapy prevents fibrosis and autoimmunity in mouse models of scleroderma. Nature. 2014 Apr 9;503(7474):126–30.

105. Brooks PC, Montgomery AM, Rosenfeld M, Reisfeld RA, Hu T, Klier G, et al. Integrin alpha v beta 3 antagonists promote tumor regression by inducing apoptosis of angiogenic blood vessels. Cell. 1994 Dec 30;79(7):1157–64.

106. Taga T, Suzuki A, Gonzalez-Gomez I, Gilles FH, Stins M, Shimada H, et al. alpha v-Integrin antagonist EMD 121974 induces apoptosis in brain tumor cells growing on vitronectin and tenascin. Int J Cancer. 2002 Apr 10;98(5):690–7.

107. Indrevoll B, Kindberg GM, Solbakken M, Bjurgert E, Johansen JH, Karlsen H, et al. NC-100717: a versatile RGD peptide scaffold for angiogenesis imaging. Bioorg Med Chem Lett. 2006 Dec 15;16(24):6190–3.

108. Beer AJ, Haubner R, Sarbia M, Goebel M, Luderschmidt S, Grosu AL, et al. Positron emission tomography using [18F]Galacto-RGD identifies the level of integrin alpha(v)beta3 expression in man. Clin Cancer Res. 2006 Jul 1;12(13):3942–9.

109. Chen X, Park R, Tohme M, Shahinian AH, Bading JR, Conti PS. MicroPET and autoradiographic imaging of breast cancer alpha v-integrin expression using 18F- and 64Cu-labeled RGD peptide. Bioconjug Chem. 2004 Jan;15(1):41–9.

110. Haubner R, Weber WA, Beer AJ, Vabuliene E, Reim D, Sarbia M, et al. Noninvasive Visualization of the Activated αvβ3 Integrin in Cancer Patients by Positron Emission Tomography and [18F]Galacto-RGD. PLoS Med; 2005 Mar 29;2(3):e70.

111. Haubner R, Kuhnast B, Mang C, Weber WA, Kessler H, Wester H-J, et al. [18F]Galacto-RGD: synthesis, radiolabeling, metabolic stability, and radiation dose estimates. Bioconjug Chem; 2004 Jan;15(1):61–9.

112. Haubner R, Beer AJ, Wang H, Chen X. Positron emission tomography tracers for imaging angiogenesis. Eur J Nucl Med Mol Imaging. 2010 Jun 18;37(S1):86–103.

113. Liu S, Liu Z, Chen K, Yan Y, Watzlowik P, Wester H-J, et al. 18F-labeled galacto and PEGylated RGD dimers for PET imaging of αvβ3 integrin expression. Mol Imaging Biol; 2010 Oct;12(5):530–8.

114. Wadas TJ, Deng H, Sprague JE, Zheleznyak A, Weilbaecher KN, Anderson CJ. Targeting the alphavbeta3 integrin for small-animal PET/CT of osteolytic bone metastases. J Nucl Med. Society of Nuclear Medicine; 2009 Nov;50(11):1873–80.

115. Xiaoyuan Chen. Integrin αvβ3-Targeted Imaging of Lung Cancer. Neoplasia; 2005 Mar 1;7(3):271.

116. Kenny LM, Tomasi G, Turkheimer F, Larkin J. Preliminary clinical assessment of the relationship between tumor alphavbeta3 integrin and perfusion in patients studied with [18F] fluciclatide kinetics and [^{15}O]H_2O PET. EJNMMI Res;2014; 4: 30.

117. Morrison MS, Ricketts S-A, Barnett J, Cuthbertson A, Tessier J, Wedge SR. Use of a novel Arg-Gly-Asp radioligand, 18F-AH111585, to determine changes in tumor vascularity after antitumor therapy. Journal of Nuclear Medicine; 2009 Jan;50(1):116–22.

118. Sarrazy V, Koehler A, Chow ML, Zimina E, Li CX, Kato H, et al. Integrins αvβ5 and αvβ3 promote latent TGF-β1 activation by human cardiac fibroblast contraction. Cardiovascular Research. 2014 Jun 1;102(3):407–17.

119. Sun M. Temporal Response and Localization of Integrins beta1 and beta3 in the Heart After Myocardial Infarction: Regulation by Cytokines. Circulation. 2003 Feb 17;107(7):1046–52.

120. Antonov AS, Antonova GN, Munn DH, Mivechi N, Lucas R, Catravas JD, et al. αVβ3 integrin regulates macrophage inflammatory responses via PI3 kinase/Akt-dependent NF-κB activation. J Cell Physiol. 2011 Feb;226(2):469–76.

121. Higuchi T, Bengel FM, Seidl S, Watzlowik P, Kessler H, Hegenloh R, et al. Assessment of v 3 integrin expression after myocardial infarction by positron emission tomography. Cardiovascular Research. 2008 Feb 19;78(2):395–403.

122. Gao H, Lang L, Guo N, Cao F, Quan Q, Hu S, et al. PET imaging of angiogenesis after myocardial infarction/reperfusion using a one-step labeled integrin-targeted tracer 18F-AlF-NOTA-PRGD2. Eur J Nucl Med Mol Imaging. 2012 Apr;39(4):683–92.

123. Laitinen I, Notni J, Pohle K, Rudelius M, Farrell E, Nekolla SG, et al. Comparison of cyclic RGD peptides for αvβ3 integrin detection in a rat model of myocardial infarction. EJNMMI Res; 2013 May 11;3(1):38.

124. Menichetti L, Kusmic C, Panetta D, Arosio D, Petroni D, Matteucci M, et al. MicroPET/CT imaging of αvβ3 integrin via a novel 68Ga-NOTA-RGD peptidomimetic conjugate in rat myocardial infarction. Eur J Nucl Med Mol Imaging. 2013 May 15.

125. Lee MS, Park HS, Lee BC, Jung JH, Yoo JS, Kim SE. Identification of Angiogenesis Rich-Viable Myocardium using RGD Dimer based SPECT after Myocardial Infarction. Sci Rep. Nature Publishing Group; 2016 Jun 10;6:27520.

126. Meoli DF, Sadeghi MM, Krassilnikova S, Bourke BN, Giordano FJ, Dione DP, et al. Noninvasive imaging of myocardial angiogenesis following experimental myocardial infarction. J Clin Invest. 2004 Jun 15;113(12):1684–91.

127. Rasmussen T, Follin B, Kastrup J, Brandt-Larsen M, Madsen J, Emil Christensen T, et al. Angiogenesis PET Tracer Uptake ((68)Ga-NODAGA-E[(cRGDyK)]$_2$) in Induced Myocardial Infarction in Minipigs. Diagnostics. Multidisciplinary Digital Publishing Institute; 2016 Jun 17;6(2):26.

128. van den Borne SWM, Isobe S, Verjans JW, Petrov A, Lovhaug D, Li P, et al. Molecular Imaging of Interstitial Alterations in Remodeling Myocardium After Myocardial Infarction. Journal of the American College of Cardiology; 2008 Dec 9;52(24):2017–28.

129. Sherif HM, Saraste A, Nekolla SG, Weidl E, Reder S, Tapfer A, et al. Molecular imaging of early αvβ3 integrin expression predicts long-term left-ventricle remodeling after myocardial infarction in rats. J Nucl Med. Society of Nuclear Medicine; 2012 Feb;53(2):318–23.

130. Johnson LL, Schofield L, Donahay T, Bouchard M, Poppas A, Haubner R. Radiolabeled

arginine-glycine-aspartic acid peptides to image angiogenesis in swine model of hibernating myocardium. JACC Cardiovasc Imaging. 2008 Jul;1(4):500–10.

131. Eo JS, Paeng JC, Lee S, Lee Y-S, Jeong JM, Kang KW, et al. Angiogenesis imaging in myocardial infarction using 68Ga-NOTA-RGD PET: characterization and application to therapeutic efficacy monitoring in rats. Coron Artery Dis. 2013 Jun;24(4):303–11.

132. Hendrikx G, Vöö S, Bauwens M, Post MJ, Mottaghy FM. SPECT and PET imaging of angiogenesis and arteriogenesis in pre-clinical models of myocardial ischemia and peripheral vascular disease. Eur J Nucl Med Mol Imaging; 2016 Dec;43(13):2433–47.

133. Makowski MR, Ebersberger U, Nekolla S, Schwaiger M. In vivo molecular imaging of angiogenesis, targeting v 3 integrin expression, in a patient after acute myocardial infarction. European Heart Journal. 2008 Mar 13;29(18):2201–1.

134. Verjans J, Wolters S, Laufer W, Schellings M, Lax M, Lovhaug D, et al. Early molecular imaging of interstitial changes in patients after myocardial infarction: Comparison with delayed contrast-enhanced magnetic resonance imaging. Journal of Nuclear Cardiology. Springer-Verlag; 2010 Jul 24;17(6):1065–72.

135. Sun Y, Zeng Y, Zhu Y, Feng F, Xu W, Wu C, et al. Application of (68)Ga-PRGD2 PET/CT for αvβ3-integrin imaging of myocardial infarction and stroke. Theranostics. 2014;4(8):778–86.

136. Evans NR, Tarkin JM, Chowdhury MM, Warburton EA, Rudd JHF. PET Imaging of Atherosclerotic Disease: Advancing Plaque Assessment from Anatomy to Pathophysiology. Curr Atheroscler Rep; 2016 Jun;18(6):30.

137. Hansson GK, Libby P, Tabas I. Inflammation and plaque vulnerability. Journal of Internal Medicine. 2015 Nov;278(5):483–93.

138. Falk E. Pathogenesis of atherosclerosis. Journal of the American College of Cardiology. 2006 Apr 18;47(8 Suppl):C7–12.

139. Bentzon JF, Otsuka F, Virmani R, Falk E. Mechanisms of plaque formation and rupture. Circulation Research; 2014 Jun 6;114(12):1852–66.

140. Joshi FR, Lindsay AC, Obaid DR, Falk E, Rudd JHF. Non-invasive imaging of atherosclerosis. Eur Heart J Cardiovasc Imaging. 2012 Mar;13(3):205–18.

141. Chung J-W, Park SH, Kim N, Kim W-J, Park JH, Ko Y, et al. Trial of ORG 10172 in Acute Stroke Treatment (TOAST) classification and vascular territory of ischemic stroke lesions diagnosed by diffusion-weighted imaging. J Am Heart Assoc. American Heart Association, Inc; 2014 Aug 11;3(4):e001119–9.

142. Quillard T, Libby P. Molecular Imaging of Atherosclerosis for Improving Diagnostic and Therapeutic Development. Circulation Research. 2012 Jul 5;111(2):231–44.

143. Cho I, Chang H-J, Sung JM, Pencina MJ, Lin FY, Dunning AM, et al. Coronary computed tomographic angiography and risk of all-cause mortality and nonfatal myocardial infarction in subjects without chest pain syndrome from the CONFIRM Registry (coronary CT angiography evaluation for clinical outcomes: an international multicenter registry). Circulation. 2012 Jul 17;126(3):304–13.

144. Kolodgie FD. Pathologic assessment of the vulnerable human coronary plaque. Heart. 2004 Dec 1;90(12):1385–91.

145. Burke AP, Kolodgie FD, Farb A, Weber DK, Malcom GT, Smialek J, et al. Healed plaque ruptures and sudden coronary death: evidence that subclinical rupture has a role in plaque progression. Circulation. 2001 Feb 20;103(7):934–40.

146. Kubo T, Maehara A, Mintz GS, Doi H, Tsujita K, Choi S-Y, et al. The dynamic nature of coronary artery lesion morphology assessed by serial virtual histology intravascular ultrasound tissue characterization. Journal of the American College of Cardiology. 2010 Apr 13;55(15):1590–7.

147. Arbab-Zadeh A, Fuster V. The Myth of the "Vulnerable Plaque": Transitioning From a Focus on Individual Lesions to Atherosclerotic Disease Burden for Coronary Artery Disease Risk Assessment. Journal of the American College of Cardiology. 2015 Mar 3;65(8):846–55.

148. Iribarren C, Sidney S, Sternfeld B, Browner WS. Calcification of the aortic arch: risk factors and association with coronary heart disease, stroke, and peripheral vascular disease. JAMA. 2000 Jun 7;283(21):2810–5.

149. Yüce G, Türkvatan A, Yener Ö. Can aortic atherosclerosis or epicardial adipose tissue volume be used as a marker for predicting coronary artery disease? J Cardiol. 2015 Feb;65(2):143–9.

150. Kronzon I. Aortic Atherosclerotic Disease and Stroke. Circulation. 2006 Jun 26;114(1):63–75.

151. Peters SAE, Ruijter den HM, Bots ML, Moons KGM. Improvements in risk stratification for the occurrence of cardiovascular disease by imaging subclinical atherosclerosis: a systematic review. Heart. 2012 Feb;98(3):177–84.

152. Khoury Z, Schwartz R, Gottlieb S, Chenzbraun A, Stern S, Keren A. Relation of coronary artery disease to atherosclerotic disease in the aorta, carotid, and femoral arteries evaluated by ultrasound. The American Journal of Cardiology. 1997 Dec 1;80(11):1429–33.

153. Joshi NV, Vesey A, Newby DE, Dweck MR. Will 18F-sodium fluoride PET-CT imaging be the magic bullet for identifying vulnerable coronary atherosclerotic plaques? Curr Cardiol Rep. 2014 Sep;16(9):521.

154. Skålén K, Gustafsson M, Rydberg EK, Hultén LM, Wiklund O, Innerarity TL, et al. Subendothelial retention of atherogenic lipoproteins in early atherosclerosis. Nature; 2002 Jun 13;417(6890):750–4.

155. Virmani R, Kolodgie FD, Burke AP, Farb A, Schwartz SM. Lessons From Sudden Coronary Death : A Comprehensive Morphological Classification Scheme for Atherosclerotic Lesions. Arteriosclerosis, Thrombosis, and Vascular Biology. 2000 May 1;20(5):1262–75.

156. Antonov AS, Kolodgie FD, Munn DH, Gerrity RG. Regulation of macrophage foam cell formation by alphaVbeta3 integrin: potential role in human atherosclerosis. Am J Pathol. 2004 Jul;165(1):247–58.

157. Weerasinghe D, McHugh KP, Ross FP, Brown EJ, Gisler RH, Imhof BA. A role for the alphavbeta3 integrin in the transmigration of monocytes. J Cell Biol; 1998 Jul 27;142(2):595–607.

158. Moreno PR, Falk E, Palacios IF, Newell JB, Fuster V, Fallon JT. Macrophage infiltration in acute coronary syndromes. Implications for plaque rupture. Circulation. 1994 Aug;90(2):775–8.

159. Criqui MH, Denenberg JO, Ix JH, McClelland RL, Wassel CL, Rifkin DE, et al. Calcium density of coronary artery plaque and risk of incident cardiovascular events. JAMA. 2014 Jan 15;311(3):271–8.

160. New SE, Goettsch C, Aikawa M, Marchini JF, Shibasaki M, Yabusaki K, et al. Macrophage-Derived Matrix Vesicles: An Alternative Novel Mechanism for Microcalcification in Atherosclerotic Plaques. Circulation Research. 2013 Apr 24.

161. Joshi NV, Toor I, Shah ASV, Carruthers K, Vesey AT, Alam SR, et al. Systemic Atherosclerotic Inflammation Following Acute Myocardial Infarction: Myocardial Infarction Begets Myocardial Infarction. J Am Heart Assoc; 2015 Sep;4(9):e001956.

162. Tawakol A, Fayad ZA, Mogg R, Alon A, Klimas MT, Dansky H, et al. Intensification of statin therapy results in a rapid reduction in atherosclerotic inflammation: results of a multicenter fluorodeoxyglucose-positron emission tomography/computed tomography feasibility study. Journal of the American College of Cardiology. 2013 Sep 3;62(10):909–17.

163. Fayad ZA, Mani V, Woodward M, Kallend D, Abt M, Burgess T, et al. Safety and efficacy of dalcetrapib on atherosclerotic disease using novel non-invasive multimodality imaging (dal-PLAQUE): a randomised clinical trial. Lancet. 2011 Oct;378(9802):1547–59.

164. Dweck MR, Chow MWL, Joshi NV, Williams MC, Jones C, Fletcher AM, et al. Coronary Arterial 18F-Sodium Fluoride Uptake. Journal of the American College of Cardiology; 2012 Apr 24;59(17):1539–48.

165. Zemplenyi T, Crawford DW, Cole MA. Adaptation to arterial wall hypoxia demonstrated in vivo with oxygen microcathodes. Atherosclerosis. 1989 Apr;76(2-3):173–9.

166. Moss AJ, Adamson PD, Newby DE, Dweck MR. Positron emission tomography imaging of coronary atherosclerosis. Future Cardiology. 2016 Jul;12(4):483–96.

167. Pant S, Deshmukh A, Mehta JL. Angiogenesis in Atherosclerosis: An Overview. In: Biochemical Basis and Therapeutic Implications of Angiogenesis; 2013. pp. 209–24.

168. Koch S, Tugues S, Li X, Gualandi L, Claesson-Welsh L. Signal transduction by vascular endothelial growth factor receptors. Biochem J; 2011 Jul 15;437(2):169–83.

169. Virmani R. Atherosclerotic Plaque Progression and Vulnerability to Rupture: Angiogenesis as a Source of Intraplaque Hemorrhage. Arteriosclerosis, Thrombosis, and Vascular Biology. 2005 Oct 1;25(10):2054–61.

170. Sluimer JC, Gasc J-M, van Wanroij JL, Kisters N, Groeneweg M, Sollewijn Gelpke MD, et al. Hypoxia, Hypoxia-Inducible Transcription Factor, and Macrophages in Human Atherosclerotic Plaques Are Correlated With Intraplaque Angiogenesis. Journal of the American College of Cardiology. 2008 Apr;51(13):1258–65.

171. Sluimer JC, Kolodgie FD, Bijnens APJJ, Maxfield K, Pacheco E, Kutys B, et al. Thin-walled microvessels in human coronary atherosclerotic plaques show incomplete endothelial junctions relevance of compromised structural integrity for intraplaque microvascular leakage. Journal of the American College of Cardiology. 2009 Apr 28;53(17):1517–27.

172. Hiyama T, Tanaka T, Endo S, Komine K, Kudo T, Kobayashi H, et al. Angiogenesis in atherosclerotic plaque obtained from carotid endarterectomy: association between symptomatology and plaque morphology. Neurol Med Chir; 2010;50(12):1056–61.

173. Mofidi R, Crotty TB, McCarthy P, Sheehan SJ, Mehigan D, Keaveny TV. Association between plaque instability, angiogenesis and symptomatic carotid occlusive disease. Br J Surg; 2001 Jul;88(7):945–50.

174. Hoshiga M, Alpers CE, Smith LL, Giachelli CM, Schwartz SM. Alpha-v beta-3 integrin expression in normal and atherosclerotic artery. Circulation Research. 1995 Dec;77(6):1129–35.

175. Bishop GG, McPherson JA, Sanders JM, Hesselbacher SE, Feldman MJ, McNamara CA, et al. Selective alpha(v)beta(3)-receptor blockade reduces macrophage infiltration and restenosis after balloon angioplasty in the atherosclerotic rabbit. Circulation. 2001 Apr 10;103(14):1906–11.

176. Coleman KR, Braden GA, Willingham MC, Sane DC. Vitaxin, a humanized monoclonal antibody to the vitronectin receptor (alphavbeta3), reduces neointimal hyperplasia and total vessel area after balloon injury in hypercholesterolemic rabbits. Circulation Research. 1999 Jun 11;84(11):1268–76.

177. Maile LA, Busby WH, Nichols TC, Bellinger DA, Merricks EP, Rowland M, et al. A monoclonal antibody against alphaVbeta3 integrin inhibits development of atherosclerotic lesions in diabetic pigs. Sci Transl Med. 2010 Feb 10;2(18):18ra11–1.

178. Winter PM, Morawski AM, Caruthers SD, Fuhrhop RW, Zhang H, Williams TA, et al. Molecular Imaging of Angiogenesis in Early-Stage Atherosclerosis With αvβ3-Integrin–Targeted Nanoparticles. Circulation. 2003 Nov 4;108(18):2270-4.

179. Winter PM, Neubauer AM, Caruthers SD, Harris TD, Robertson JD, Williams TA, et al. Endothelial αvβ3 Integrin–Targeted Fumagillin Nanoparticles Inhibit Angiogenesis in Atherosclerosis. Arteriosclerosis, Thrombosis, and Vascular Biology. 2006;26:2103-2109

180. Laitinen I, Saraste A, Weidl E, Poethko T, Weber AW, Nekolla SG, et al. Evaluation of αvβ3 Integrin-Targeted Positron Emission Tomography Tracer 18F-Galacto-RGD for Imaging of Vascular Inflammation in Atherosclerotic Mice. Circulation. 2009 Jul;2(4):331-8.

181. Yoo JS, Lee J, Jung JH, Moon BS, Kim S, Lee BC, et al. SPECT/CT Imaging of High-Risk Atherosclerotic Plaques using Integrin-Binding RGD Dimer Peptides. Sci Rep; 2015 Jun 20;:1–11.

182. Su H, Gorodny N, Gomez LF, Gangadharmath UB, Mu F, Chen G, et al. Atherosclerotic plaque uptake of a novel integrin tracer 18F-Flotegatide in a mouse model of atherosclerosis. Journal of Nuclear Cardiology. 2014 Mar 14;21(3):553–62.

183. Razavian M, Marfatia R, Mongue-Din H, Tavakoli S, Sinusas AJ, Zhang J, et al. Integrin-targeted imaging of inflammation in vascular remodeling. Arteriosclerosis, Thrombosis, and Vascular Biology. 2011 Dec;31(12):2820–6.

184. Vancraeynest D, Roelants V, Bouzin C, Hanin F-X, Walrand S, Bol V, et al. αVβ3 integrin-targeted microSPECT/CT imaging of inflamed atherosclerotic plaques in mice. EJNMMI Res. EJNMMI Research; 2016 Mar 22;:1–9.

185. Saraste A, Laitinen I, Weidl E, Wildgruber M, Weber AW, Nekolla SG, et al. Diet intervention reduces uptake of αvβ3 integrin-targeted PET tracer 18F-galacto-RGD in mouse atherosclerotic plaques. J Nucl Cardiol. 2012 Aug;19(4):775–84.

186. Golestani R, Mirfeizi L, Zeebregts CJ, Westra J, de Haas HJ, Glaudemans AWJM, et al. Feasibility of [18F]-RGD for ex vivo imaging of atherosclerosis in detection of αvβ3

integrin expression. J Nucl Cardiol. 2015 Dec;22(6):1179-86.

187. Beer AJ, Pelisek J, Heider P, Saraste A, Reeps C, Metz S, et al. PET/CT Imaging of Integrin alpha v beta 3 Expression in Human Carotid Atherosclerosis. JACC: Cardiovascular Imaging, 7(2):178-187

188. Battle MR, Goggi JL, Allen L, Barnett J, Morrison MS. Monitoring Tumor Response to Antiangiogenic Sunitinib Therapy with 18F-Fluciclatide, an 18F-Labeled V 3-Integrin and V 5-Integrin Imaging Agent. Journal of Nuclear Medicine. 2011 Feb 22;52(3):424–30.

189. Maile LA, Busby WH, Xi G, Gollahan KP, Flowers W, Gafbacik N, et al. An anti-αVβ3 antibody inhibits coronary artery atherosclerosis in diabetic pigs. Atherosclerosis. 2017 Jan 27;258:40–50.

190. McParland BJ, Miller MP, Spinks TJ, Kenny LM, Osman S, Khela MK, et al. The biodistribution and radiation dosimetry of the Arg-Gly-Asp peptide 18F-AH111585 in healthy volunteers. Journal of Nuclear Medicine. 2008 Oct;49(10):1664–7.

191. Tomasi G, Kenny L, Mauri F, Turkheimer F, Aboagye EO. Quantification of receptor-ligand binding with [18F]fluciclatide in metastatic breast cancer patients. Eur J Nucl Med Mol Imaging. 2011 Sep 3;38(12):2186–97.

192. North American Symptomatic Carotid Endarterectomy Trial Collaborators. Beneficial effect of carotid endarterectomy in symptomatic patients with high-grade carotid stenosis. N Engl J Med. 1991 Aug 15;325(7):445–53.

193. Derlin T, Richter U, Bannas P, Begemann P, Buchert R, Mester J, et al. Feasibility of 18F-Sodium Fluoride PET/CT for Imaging of Atherosclerotic Plaque. Journal of Nuclear Medicine. 2010 May 25;51(6):862–5.

194. Blau M, Ganatra R, Bender MA. 18 F-fluoride for bone imaging. Seminars in Nuclear Medicine. 1972 Jan;2(1):31–7.

195. Cheng VY, Slomka PJ, Ahlen M, Thomson LEJ, Waxman AD, Berman DS. Impact of carbohydrate restriction with and without fatty acid loading on myocardial 18F-FDG uptake during PET: A randomized controlled trial. J Nucl Cardiol. 2010 Apr;17(2):286–91.

196. Shankar LK, Hoffman JM, Bacharach S, Graham MM, Karp J, Lammertsma AA, et al. Consensus recommendations for the use of 18F-FDG PET as an indicator of therapeutic response in patients in National Cancer Institute Trials. 2006. 1059–66.

197. Wykrzykowska J, Lehman S, Williams G, Parker JA, Palmer MR, Varkey S, et al. Imaging of inflamed and vulnerable plaque in coronary arteries with 18F-FDG PET/CT in patients with suppression of myocardial uptake using a low-carbohydrate, high-fat preparation. Journal of Nuclear Medicine. Society of Nuclear Medicine; 2009 Apr;50(4):563–8.

198. Glaser M, Morrison M, Solbakken M, Arukwe J, Karlsen H, Wiggen U, et al. Radiosynthesis and biodistribution of cyclic RGD peptides conjugated with novel [18F]fluorinated aldehyde-containing prosthetic groups. Bioconjug Chem. 2008 Apr;19(4):951–7.

199. Mena E, Owenius R, Turkbey B, Sherry R, Bratslavsky G, Macholl S, et al. [18F]Fluciclatide in the in vivo evaluation of human melanoma and renal tumors expressing αvβ3 and αvβ5 integrins. Eur J Nucl Med Mol Imaging. 2014 Jun 28;41(10):1879–88.

200. Demer LL, Tintut Y. Vascular calcification: pathobiology of a multifaceted disease. Circulation. 2008 Jun 3;117(22):2938–48.

201. Idelevich A, Rais Y, Monsonego-Ornan E. Bone Gla protein increases HIF-1alpha-dependent glucose metabolism and induces cartilage and vascular calcification. Arteriosclerosis, Thrombosis, and Vascular Biology. 2011 Sep;31(9):e55–71.

202. Kapustin AN, Shanahan CM. Osteocalcin: a novel vascular metabolic and osteoinductive factor? Arteriosclerosis, Thrombosis, and Vascular Biology. 2011 Oct;31(10):2169–71.

203. Aikawa E, Nahrendorf M, Figueiredo J-L, Swirski FK, Shtatland T, Kohler RH, et al. Osteogenesis associates with inflammation in early-stage atherosclerosis evaluated by molecular imaging in vivo. Circulation. 2007 Dec 11;116(24):2841–50.

204. Westman PC, Lipinski MJ, Luger D, Waksman R, Bonow RO, Wu E, et al. Inflammation as a Driver of Adverse Left Ventricular Remodeling After Acute Myocardial Infarction. Journal of the American College of Cardiology. 2016 May 3;67(17):2050–60.

205. Shinde AV, Humeres C, Frangogiannis NG. The role of α-smooth muscle actin in fibroblast-mediated matrix contraction and remodeling. Biochim Biophys Acta. 2017 Jan;1863(1):298–309.

206. Müller AM, Hermanns MI, Skrzynski C, Nesslinger M, Müller K-M, Kirkpatrick CJ. Expression of the endothelial markers PECAM-1, vWf, and CD34 in vivo and in vitro. Exp Mol Pathol. 2002 Jun;72(3):221–9.

207. McSweeney SJ, Hadoke PWF, Kozak AM, Small GR, Khaled H, Walker BR, et al. Improved heart function follows enhanced inflammatory cell recruitment and angiogenesis in 11betaHSD1-deficient mice post-MI. Cardiovascular Research. 2010 Oct 1;88(1):159–67.

208. Woodfin A, Voisin M-B, Nourshargh S. PECAM-1: a multi-functional molecule in inflammation and vascular biology. Arteriosclerosis, Thrombosis, and Vascular Biology. 2007 Dec;27(12):2514–23.

209. Kim RJ, Wu E, Rafael A, Chen EL, Parker MA, Simonetti O, et al. The use of contrast-enhanced magnetic resonance imaging to identify reversible myocardial dysfunction. N Engl J Med. 2000 Nov 16;343(20):1445–53.

210. Treibel TA, White SK, Moon JC. Myocardial Tissue Characterization: Histological and Pathophysiological Correlation. Curr Cardiovasc Imaging Rep. 2014;7(3):9254.

211. Chin CWL, Shah ASV, McAllister DA, Joanna Cowell S, Alam S, Langrish JP, et al. High-sensitivity troponin I concentrations are a marker of an advanced hypertrophic response and adverse outcomes in patients with aortic stenosis. European Heart Journal. 2014 Sep 7;35(34):2312–21.

212. Chin CWL, Semple S, Malley T, White AC, Mirsadraee S, Weale PJ, et al. Optimization and comparison of myocardial T1 techniques at 3T in patients with aortic stenosis. Eur Heart J Cardiovasc Imaging. 2013 Nov 25.

213. Messroghli DR, Greiser A, Fröhlich M, Dietz R, Schulz-Menger J. Optimization and validation of a fully-integrated pulse sequence for modified look-locker inversion-recovery (MOLLI) T1 mapping of the heart. J Magn Reson Imaging. 2007;26(4):1081–6.

214. Shah ASV, Chin CWL, Vassiliou V, Cowell SJ, Doris M, Kwok TC, et al. Left ventricular hypertrophy with strain and aortic stenosis. Circulation. 2014 Oct 28;130(18):1607–16.

215. Bland JM, Altman DG. Statistical methods for assessing agreement between two methods of clinical measurement. Lancet. 1986 Feb 8;1(8476):307–10.

216. Messika-Zeitoun D, Bielak LF, Peyser PA, Sheedy PF, Turner ST, Nkomo VT, et al. Aortic valve calcification: determinants and progression in the population. Arteriosclerosis, Thrombosis, and Vascular Biology. 2007 Mar;27(3):642–8.

217. Bonow RO, Chatterjee K, de Leon AC Jr, Faxon DP, Freed MD, Gaasch WH, et al. 2008 Focused Update Incorporated Into the ACC/AHA 2006 Guidelines for the Management of Patients With Valvular Heart Disease. Journal of the American College of Cardiology. 2008 Sep;52(13):e1–e142.

218. Derlin T, Tóth Z, Papp L, Wisotzki C, Apostolova I, Habermann CR, et al. Correlation of inflammation assessed by 18F-FDG PET, active mineral deposition assessed by 18F-fluoride PET, and vascular calcification in atherosclerotic plaque: a dual-tracer PET/CT study. J Nucl Med. Society of Nuclear Medicine; 2011 Jul;52(7):1020–7.

219. Derlin T, Wisotzki C, Richter U, Apostolova I, Bannas P, Weber C, et al. In vivo imaging of mineral deposition in carotid plaque using 18F-sodium fluoride PET/CT: correlation with atherogenic risk factors. J Nucl Med. 2011 Mar;52(3):362–8.

220. Narisawa S, Harmey D, Yadav MC, O'Neill WC, Hoylaerts MF, Millán JL. Novel inhibitors of alkaline phosphatase suppress vascular smooth muscle cell calcification. J Bone Miner Res. John Wiley and Sons and The American Society for Bone and Mineral Research (ASBMR); 2007 Nov;22(11):1700–10.

221. Utsunomiya H, Yamamoto H, Kitagawa T, Kunita E, Urabe Y, Tsushima H, et al. International Journal of Cardiology. International Journal of Cardiology. 2013 Oct 15;168(6):5205–11.

222. Ishimaru S, Tsujino I, Takei T, Tsukamoto E, Sakaue S, Kamigaki M, et al. Focal uptake on 18F-fluoro-2-deoxyglucose positron emission tomography images indicates cardiac involvement of sarcoidosis. European Heart Journal. 2005 Aug;26(15):1538–43.

223. Folco EJ, Sheikine Y, Rocha VZ, Christen T, Shvartz E, Sukhova GK, et al. Hypoxia But Not Inflammation Augments Glucose Uptake in Human Macrophages. Journal of the American College of Cardiology. 2011 Aug 2;58(6):603–14.

224. Osnabrugge RLJ, Mylotte D, Head SJ, Van Mieghem NM, Nkomo VT, LeReun CM, et al. Aortic stenosis in the elderly: disease prevalence and number of candidates for transcatheter aortic valve replacement: a meta-analysis and modeling study. Journal of the American College of Cardiology. 2013 Sep 10;62(11):1002–12.

225. Miller JD, Weiss RM, Heistad DD. Calcific Aortic Valve Stenosis: Methods, Models, and Mechanisms. Circulation Research. 2011 May 26;108(11):1392–412.

226. Dweck MR, Jenkins WSA, Vesey AT, Pringle MAH, Chin CWL, Malley TS, et al. 18F-NaF Uptake Is a Marker of Active Calcification and Disease Progression in Patients with Aortic Stenosis. Circulation: Cardiovascular Imaging. 2014 Feb 7.

227. Irkle A, Vesey AT, Lewis DY, Skepper JN, Bird JLE, Dweck MR, et al. Identifying active vascular microcalcification by (18)F-sodium fluoride positron emission tomography. Nat Commun. 2015 Jul 7;6:7495.

228. Bonow RO, Carabello BA, Chatterjee K, de Leon AC Jr, Faxon DP, Freed MD, et al. 2008 Focused Update Incorporated Into the ACC/AHA 2006 Guidelines for the Management of Patients With Valvular Heart Disease. Journal of the American College of Cardiology. 2008

Sep;52(13):e1–e142.

229. Cannon CP, Brindis RG, Chaitman BR, Cohen DJ, Cross JT, Drozda JP, et al. 2013 ACCF/AHA Key Data Elements and Definitions for Measuring the Clinical Management and Outcomes of Patients With Acute Coronary Syndromes and Coronary Artery Disease: A Report of the American College of Cardiology Foundation/American Heart Association Task Force on Clinical Data Standards (Writing Committee to Develop Acute Coronary Syndromes and Coronary Artery Disease Clinical Data Standards). Journal of the American College of Cardiology; 2013 Mar 5;61(9):992–1025.

230. Joint Task Force on the Management of Valvular Heart Disease of the European Society of Cardiology (ESC), European Association for Cardio-Thoracic Surgery (EACTS), Vahanian A, Alfieri O, Andreotti F, Antunes MJ, et al. Guidelines on the management of valvular heart disease European Heart Journal. 2012. 33;2451–96.

231. PhD M-ACD, PhD PPD, PhD DM-ZM, PhD RC, MD JM, MBBS SA, et al. Impact of Aortic Valve Calcification, as Measured by MDCT, on Survival in Patients With Aortic Stenosis. Journal of the American College of Cardiology. 2014 Sep 23;64(12):1202–13.

232. Clavel M-A, Messika-Zeitoun D, Pibarot P, Aggarwal SR, Malouf J, Araoz PA, et al. The complex nature of discordant severe calcified aortic valve disease grading: new insights from combined Doppler echocardiographic and computed tomographic study. Journal of the American College of Cardiology. 2013 Dec 17;62(24):2329–38.

233. Dweck MR, Chin C, Newby DE. Small valve area with low-gradient aortic stenosis: beware the hard hearted. Journal of the American College of Cardiology. 2013 Dec 17;62(24):2339–40.

234. Aikawa E, Otto CM. Look more closely at the valve: imaging calcific aortic valve disease. Circulation. 2012 Jan 3;125(1):9–11.

235. Sutton MG, Sharpe N. Left ventricular remodeling after myocardial infarction: pathophysiology and therapy. Circulation. 2000 Jun 27;101(25):2981–8.

236. Cerqueira MD, Weissman NJ, Dilsizian V, Jacobs AK, Kaul S, Laskey WK, et al. Standardized myocardial segmentation and nomenclature for tomographic imaging of the heart. A statement for healthcare professionals from the Cardiac Imaging Committee of the Council on Clinical Cardiology of the American Heart Association. 2002. pp. 539–42.

237. Verjans JWH, van de Borne SWM, Hofstra L, Narula J. Molecular imaging of myocardial remodeling after infarction. Methods Mol Biol. 2011;680:227–35.

238. Plein S, Kidambi A. Understanding LV Remodeling Following Myocardial Infarction. JACC: Cardiovascular Imaging. 2012 Sep 1;5(9):894–6.

239. Rubeaux M, Joshi N, Dweck MR, Fletcher A, Motwani M, Thomson LE, et al. Motion correction of 18F-sodium fluoride PET for imaging coronary atherosclerotic plaques. J Nucl Med. 2015 Oct 15;:jnumed.115.162990.

240. Dweck MR, Doris MK, Motwani M, Adamson PD, Slomka P, Dey D, et al. Imaging of coronary atherosclerosis - evolution towards new treatment strategies. Nat Rev Cardiol. 2016 Sep;13(9):533–48.

241. Dweck MR, Aikawa E, Newby DE, Tarkin JM, Rudd JHF, Narula J, et al. Noninvasive Molecular Imaging of Disease Activity in Atherosclerosis. Circulation Research. 2016 Jul 8;119(2):330–40.

242. Beer AJ, Pelisek J, Heider P, Saraste A, Reeps C, Metz S, et al. PET/CT imaging of integrin αvβ3 expression in human carotid atherosclerosis. JACC Cardiovasc Imaging. 2014 Feb;7(2):178–87.

243. Kate ten GL, Sijbrands EJG, Valkema R, Cate ten FJ, Feinstein SB, Steen AFW, et al. Molecular imaging of inflammation and intraplaque vasa vasorum: A step forward to identification of vulnerable plaques? J Nucl Cardiol. 2010 Jun 15;17(5):897–912.

244. Vancraeynest D, Roelants V, Bouzin C, Hanin F-X, Walrand S, Bol V, et al. αVβ3 integrin-targeted microSPECT/CT imaging of inflamed atherosclerotic plaques in mice. EJNMMI Res. 2016 Dec;6(1):29.

245. Laitinen I, Saraste A, Weidl E, Poethko T, Weber AW, Nekolla SG, et al. Evaluation of v 3 Integrin-Targeted Positron Emission Tomography Tracer 18F-Galacto-RGD for Imaging of Vascular Inflammation in Atherosclerotic Mice. Circulation: Cardiovascular Imaging. 2009 Jul 14;2(4):331–8.

246. Jenkins WSA, Vesey AT, Stirrat C, Connell M, Lucatelli C, Neale A, et al. Cardiac αVβ3 integrin expression following acute myocardial infarction in humans. Heart. 2016 Dec 7;:heartjnl–2016–310115.

247. Jenkins WS, Vesey AT, Stirrat C, Connell M, Lucatelli C, Neale A, et al. Cardiac αvβ3 integrin expression following acute myocardial infarction in humans. Heart.

248. Niccoli Asabella A, Ciccone MM, Cortese F, Scicchitano P, Gesualdo M, Zito A, et al. Higher reliability of 18F-FDG target background ratio compared to standardized uptake value in vulnerable carotid plaque detection: a pilot study. Ann Nucl Med. 2014 Jul;28(6):571–9.

249. Hong SN, Gona P, Fontes JD, Oyama N, Chan RH, Kenchaiah S, et al. Atherosclerotic biomarkers and aortic atherosclerosis by cardiovascular magnetic resonance imaging in the Framingham Heart Study. J Am Heart Assoc. 2013;2(6):e000307.

250. Witteman JC, Kannel WB, Wolf PA, Grobbee DE, Hofman A, D'Agostino RB, et al. Aortic calcified plaques and cardiovascular disease (the Framingham Study). The American Journal of Cardiology. 1990 Nov 1;66(15):1060–4.

251. Dutta P, Courties G, Wei Y, Leuschner F, Gorbatov R, Robbins CS, et al. Myocardial infarction accelerates atherosclerosis. Nature. 2012 Jun 27;487(7407):325–9.

252. Cannon CP, Blazing MA, Giugliano RP, McCagg A, White JA, Theroux P, et al. Ezetimibe Added to Statin Therapy after Acute Coronary Syndromes. N Engl J Med. 2015 Jun 18;372(25):2387–97.

253. Jenkins WS, Chin C, Rudd JH, Newby DE, Dweck MR. What can we learn about valvular heart disease from PET/CT? Future Cardiology. 2013 Sep;9(5):657–67.

254. Gerber Y, Weston SA, Enriquez-Sarano M, Berardi C, Chamberlain AM, Manemann SM, et al. Mortality Associated With Heart Failure After Myocardial Infarction: A Contemporary Community Perspective. Circ Heart Fail. American Heart Association, Inc; 2016 Jan;9(1):e002460.

255. Pawade TA, Cartlidge TRG, Jenkins WSA, Adamson PD, Robson P, Lucatelli C, et al. Optimization and Reproducibility of Aortic Valve 18F-Fluoride Positron Emission Tomography in Patients With Aortic Stenosis. Circulation: Cardiovascular Imaging. American Heart Association, Inc; 2016 Oct;9(10):e005131.

256. Hutcheson JD, Aikawa E, Merryman WD. Potential drug targets for calcific aortic valve disease. Nat Rev Cardiol. 2014 Apr;11(4):218–31.

257. Hung M-Y, Tsimikas S. What is the ultimate test that lowering lipoprotein(a) is beneficial for cardiovascular disease and aortic stenosis? Curr Opin Lipidol. 2014 Dec;25(6):423–30.

258. Thanassoulis G, Campbell CY, Owens DS, Smith JG, Smith AV, Peloso GM, et al. Genetic associations with valvular calcification and aortic stenosis. N Engl J Med. Massachusetts Medical Society; 2013 Feb 7;368(6):503–12.

259. Bull S, Loudon M, Francis JM, Joseph J, Gerry S, Karamitsos TD, et al. A prospective, double-blind, randomized controlled trial of the angiotensin-converting enzyme inhibitor Ramipril In Aortic Stenosis (RIAS trial). Eur Heart J Cardiovasc Imaging. 2015 Aug;16(8):834–41.

260. Aggarwal SR, Clavel M-A, Messika-Zeitoun D, Cueff C, Malouf J, Araoz PA, et al. Sex differences in aortic valve calcification measured by multidetector computed tomography in aortic stenosis. Circulation: Cardiovascular Imaging. Lippincott Williams & Wilkins; 2013 Jan 1;6(1):40–7.

261. Hein S, Arnon E, Kostin S, Schönburg M, Elsässer A, Polyakova V, et al. Progression from compensated hypertrophy to failure in the pressure-overloaded human heart: structural deterioration and compensatory mechanisms. Circulation. 2003 Feb 25;107(7):984–91.

262. Slomka PJ, Pan T, Germano G. Imaging moving heart structures with PET. J Nucl Cardiol. 2015 Mar 26.

263. Saraste A, Knuuti J. Cardiac PET, CT, and MR: what are the advantages of hybrid imaging? Curr Cardiol Rep. 2012 Feb;14(1):24–31.

264. Muzard J, Sarda-Mantel L, Loyau S, Meulemans A, Louedec L, Bantsimba-Malanda C, et al. Non-invasive molecular imaging of fibrosis using a collagen-targeted peptidomimetic of the platelet collagen receptor glycoprotein VI. PLoS ONE. 2009;4(5):e5585.

265. Zimny M, Klosterhalfen B, Conze J, Hamacher K, Fehler S, Schumpelick V, et al. Uptake of cis-4-[18 F]fluoro-L-proline in scar formation: a marker of collagen synthesis? Nucl Med Commun. 2002 Jul;23(7):695–8.

266. Skovgaard D, Kjaer A, Heinemeier KM, Brandt-Larsen M, Madsen J, Kjaer M. Use of cis-[18F]fluoro-proline for assessment of exercise-related collagen synthesis in musculoskeletal connective tissue. Gelovani J, editor. PLoS ONE. 2011 Feb 11;6(2):e16678.

267. Fukushima K, Bravo PE, Higuchi T, Schuleri KH, Lin X, Abraham MR, et al. Molecular hybrid positron emission tomography/computed tomography imaging of cardiac angiotensin II type 1 receptors. Journal of the American College of Cardiology. 2012 Dec 18;60(24):2527–34.

268. Rodriguez-Porcel MM, Cai WW, Gheysens OO, Willmann JKJ, Chen KK, Wang HH, et al. Imaging of VEGF receptor in a rat myocardial infarction model using PET. Journal of Nuclear Medicine. 2008 Mar 31;49(4):667–73.

269. Rötering S, Deuther-Conrad W, Cumming P, Donat CK, Scheunemann M, Fischer S, et al. Imaging of α7 nicotinic acetylcholine receptors in brain and cerebral vasculature of juvenile pigs with [(18)F]NS14490. EJNMMI Res. 2014;4(1):43.

270. Schulz-Menger J, Bluemke DA, Bremerich J, Flamm SDS, Fogel MA, Friedrich MGM, et al. Standardized image interpretation and post processing in cardiovascular magnetic

resonance: Society for Cardiovascular Magnetic Resonance (SCMR) board of trustees task force on standardized post processing. J Cardiovasc Magn Reson BioMed Central; 2013;15:35.

Appendix

1. Patient information sheets

i) Role of inflammation and calcification in the progression of aortic stenosis

ii) Identification of *in vivo* angioneogenesis and fibrosis in myocardial infarction using positron emission tomography.

iii) Identification of *in vivo* angioneogenesis and fibrosis in aortic stenosis using positron emission tomography.

2. Patient consent forms

i) Role of inflammation and calcification in the progression of aortic stenosis

ii) Identification of *in vivo* angioneogenesis and fibrosis in myocardial infarction using positron emission tomography

iii) Identification of *in vivo* angioneogenesis and fibrosis in aortic stenosis using positron emission tomography.

3. ARSAC licenses

i) Role of inflammation and calcification in the progression of aortic stenosis

ii) Identification of *in vivo* angioneogenesis and fibrosis in myocardial infarction using positron emission tomography

iii) Identification of *in vivo* angioneogenesis and fibrosis in aortic stenosis using positron emission tomography.

4. Published papers

i) Jenkins WS, Dweck MR, Vesey AT, *et al.* 18F-NaF uptake is a marker of active calcification and disease progression in patients with aortic stenosis. Circulation; Cardiovascular Imaging. 2014 Mar;7(2):371-8.

ii) Jenkins WS, Vesey AT, Shah AS, *et al*. Valvular 18F-fluoride and 18F-FDG uptake predict disease progression and clinical outcome in patients with aortic stenosis. Journal of the American College of Cardiology. 2015 Sep 8;66(10):1200-1.

iii) Jenkins WS, Vesey AT, Stirrat C, *et al.* Cardiac Alpha-V Beta-3 Integrin Expression Following Acute Myocardial Infarction in Humans. Heart. 2017;103(8):607-615.

Volunteer Information Sheet (Study Group)

ROLE OF INFLAMMATION IN THE PROGRESSION OF AORTIC STENOSIS

THE RING OF FIRE

You are being invited to take part in a research study. Before you decide whether or not to participate, it is important that you understand why the research is being done and what it will involve. Please read the following information and discuss it with others if you wish. If there is anything that you are still unclear about or any questions that you would like to ask you can contact us for further information. You can also contact Dr Bloomfield who is not directly involved with this study but can give you independent advice. He can be contacted through the Royal Infirmary switchboard (0131 242 1000) by asking for his secretary.

Thank you for taking the time to read this information sheet.

Why are we doing this study?

Aortic stenosis is a condition caused by narrowing of one the major valves within the heart. The reasons why this narrowing develops are poorly understood. As a result there are no treatments to stop the disease except major heart surgery when the valve becomes very seriously narrowed. Furthermore we have no means of predicting how quickly valve narrowing will progress. Sometimes the valve gets narrow quickly and in other patients it stays much the same for many years.

We want to study two processes, inflammation and calcification. These are thought to play a role in the development of aortic stenosis and why the valve gets narrower. We will use a special scan called PET CT to tell us whether these processes are indeed occurring in narrowed valves.

We hope that the information provided by this study will help identify new treatments that can then be targeted to stop the progression of aortic stenosis. In the future this may mean we are able to delay or even prevent the need for surgery.

Why have I been chosen to take part?
We are looking for patients with a range of aortic stenosis to study using these scans.
Using PET CT we will assess how much inflammation and calcification is occurring on your valve. We will then assess how quickly your valve narrowing worsens over a two year period. By doing the same thing in 120 patients we will develop a good understanding of how important these two process are, where on the valve they occur and when are they most important.

It is up to you to decide whether or not to take part. If you decide to take part you will be given this information sheet to keep and you will be asked to sign a consent form. Even once you have signed the form you can still withdraw at any time and you do not have to give a reason.
You will not benefit directly from this study. However, the information we get could help us to improve the way we treat patients with aortic stenosis in the future.

What will happen to me if I decide to take part?

We will need to perform three different assessments of you and your valve. The first will happen we you first agree to participate. The second after 1 year and the third after 2 years.

<u>Assessment when you register in the trial</u>
You will be invited to the clinic. The following will happen. We will talk about whether you have any symptoms; perform a full examination of your heart; take some blood tests; and organise an echo (ultrasound) scan of your heart. The echo test is not painful and involves no harmful affects to you. You will already have had one of these scans in the clinic.

We will call you back for a PET CT scan. For the 48 hours leading up to the scan we will ask that you eat an Atkins diet (high fat, low carbohydrate). When you arrive we will need to place a plastic tube (cannula) in one of your veins. We will inject you with a special tracer. After 90 minutes of sitting in a quiet room we will perform the PET CT scan. You will need to lie still on a bed for around 20 minutes whilst the scan takes place. It is not painful.

The next day we will ask you to return for another scan. This will involve exactly the same process but we will use a different tracer.

The molecules for inflammation and calcification have already been used frequently in humans and are not harmful.

<u>Assessment after 1 year</u>
This will involve the same assessment as your baseline assessment described above.

Assessment after 2 years
This will involve the same assessment as those performed above. However this time we will not be performing either of the PET CT scans.

What happens to the blood samples that are taken?
A proportion will be tested right away for various tests. A portion of the blood samples taken will be frozen, and stored in an anonymised manner so that further tests may be performed on them in the future. Any further tests would require future ethical approval

Is there anything else that I have to do?
There are no restrictions on your lifestyle through participating in this study.

Will taking part in this study affect my treatment?
No – you will still be followed up by your cardiologist as if you were not participating in the trial.

What are the side effects of taking part?
Performing PET CT scans will expose you to a dose of radiation. The amount of radiation varies but is around 8 times the amount you would normally receive in a year from background natural sources of radiation. The lifetime risk of developing cancer from the radiation used in the scan is small: less than 1 in 1000. To put this number in context in the average population 1 in 4 people will develop cancer. Therefore the risk to participants taking part in the trial increases from 250 per 1000, to 251 per 1000.

If you are female and there is a possibility you might be pregnant then we would like you to perform a pregnancy test. Radiation can cause damage to babies in the womb and so we want to ensure that no scans are performed on pregnant ladies.

The CT scanner takes detailed images of a small area of your chest so there is a small chance that we will find another abnormality in this area. Often these abnormalities turn out to be of no significance to your health. However, if this happens we will let you and your GP know and arrange for you to see a specialist for any further tests that are required.

What are the possible disadvantages of taking part?
Involvement in the trial will mean you attending for various appointments and scans. Whenever possible we will ensure that these occur during the same visit.

What are the possible benefits of taking part?
There will not be any direct benefit to you of taking part in the study, however it is hoped that the findings of this study will benefit other patients with aortic stenosis in the future. The information from the PET CT scans will provide us

with extra information about your heart and your aortic valve. We are unsure as to how useful this will prove. It is the purpose of this study to find that out.

Will my GP be informed?
As long as you agree we would like to inform your General Practitioner of your participation in this study.

What if something goes wrong?
If you are harmed by taking part in this research project, there are no special compensation arrangements, although in the case of negligent harm, subjects will be covered by the University of Edinburgh insurance policy. If you are harmed as a result of the study you may have grounds for legal action but you may have to pay for this. If you are not satisfied with any aspect of the way you were approached or your treatment during this study, please contact the Faculty of Medicine at the University of Edinburgh. This study has been reviewed by the Lothian Local Research and Ethics Committee.

Will my taking part in this study be kept confidential?
All the information collected about you during the course of the research will be kept strictly confidential. Any information about you which leaves the hospital will have your name and address removed so that you cannot be recognised from it.

What will happen to the results of the research study?
Once we have completed the study and analysed the results, we will write a paper which will be submitted for publication in one of the medical journals. We do not routinely contact participants to inform them of the outcome of the research but would be happy to do so if requested. If you would like a copy of the results please contact Dr Marc Dweck using the contact details listed below. You will not be personally identified in any report/publication.

Who is organising the research?
The study is being organised through the University of Edinburgh. Your doctors will not be paid for including you in this study.

Who has reviewed the study?
The study has been reviewed by the South East Scotland Research Ethics Committee 2.

Where can I obtain further information about the study?
You can get further information from Dr Marc Dweck or Prof Newby who will arrange to meet you.
You could also discuss the study with Dr Bloomfield who is another doctor working in this hospital who is not involved in the study and can therefore act as an independent advisor.
Dr Marc Dweck can be reached by contacting his mobile on 07813 619 208; his email marcdweck@hotmail.com: or by letter addressed to the Cardiovascular Research Unit, Chancellor's Building, 49 Little France

Crescent, Edinburgh EH16 SU4. Prof Newby can be contacted via the hospital switchboard (0131 536 1000).

To speak to Dr Bloomfield ask for to be put through to his secretary at the Royal Infirmary of Edinburgh.

Thank you once again for reading this information sheet.

Volunteer Information Sheet
(Post MI group - revascularised)

Identification of *In Vivo* Angioneogenesis and Fibrosis in Myocardial Infarction using Positron Emission Tomography.

You are being invited to take part in a research study. Before you decide whether or not to participate, it is important that you understand why the research is being done and what it will involve. Please read the following information and do discuss it with others if you wish. If there is anything that you are still unclear about, or any questions that you would like to ask, you can contact us for further information. We aim to re-contact you in 1 – 3 days from when you receive this form, to discuss whether you would like to proceed with the study.

Thank you for taking the time to read this information sheet.

Why are we doing this study?

Heart attacks are one of the commonest causes of ill health in the United Kingdom. Whilst the treatment immediately following a heart attack continues to improve, the repair mechanisms through which the heart heals itself are not fully understood, and we find it difficult to identify those patients who will go on to suffer from 'heart failure' at a later stage.

We would like to study two processes; new blood vessel growth (angiogenesis) and scar formation (fibrosis), in patients who have suffered a heart attack. These are essential for heart muscle repair, and we will use two special scans called **PET-CT** and **MRI** to tell us *where* and *when* these processes are happening in the heart.

We aim to help identify those patients who are at risk of developing further problems and help us identify new treatments that can aid heart muscle recovery.

MRI Scanner

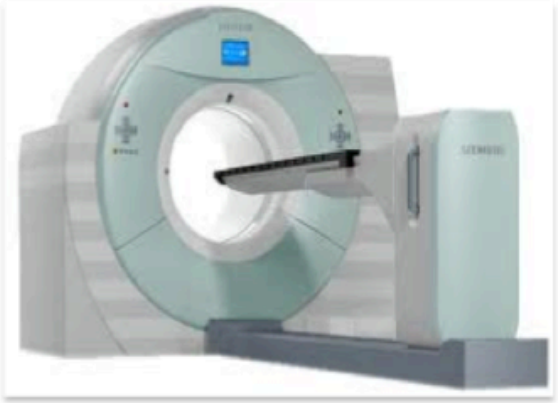

PET/CT Scanner

Why have I been chosen to take part?
We are looking for patients who have had a heart attack, and undergone an angiogram and 'stenting' (unblocking) of the blocked blood vessel. Using PET-CT we will assess how much new blood vessel formation and scarring is occurring in the heart. We would like to do this initially 2 weeks following your heart attack, and then again 7 weeks later. We will also perform an MRI scan soon after your heart attack, and 6 – 12 months later, to assess the impact of the heart attack and how well the heart is healing.

Do I have to take part?
No. It is up to you to decide whether you would like to take part. If you decide to take part you will be given this information sheet to keep and you will be asked to sign a consent form. Even once you have signed the form you can still withdraw at any time and you do not have to give a reason.

You will not benefit directly from this study. However, the information we get could help us to improve the way we treat patients with heart attacks in the future.

What will happen to me if I decide to take part?
Once you have been discharged from hospital you will be invited back **2 weeks after your heart attack** to our research department, which is immediately next to the Edinburgh Royal Infirmary. We will discuss the study again and Dr Will Jenkins will ask you to sign a consent form. We will talk about your symptoms, perform a full examination of your heart and place a plastic tube (cannula) in your vein. We will use this to take some blood tests (30 mls or 2 tablespoon of blood) and then inject you with an experimental imaging agent called '^{18}F-fluciclatide'. This contains a small amount of radiation which we can detect using a specialized camera called a PET scanner. Fluciclatide has previously been used safely in people but has not yet been approved for routine use. We will measure your blood pressure and heart rate, and will repeat this a number of times during your visit. After approximately 60 min of sitting in a quiet room we will perform the PET-CT scan. You will need to lie still on a bed for around 20 min whilst the scan takes place. It is not painful.

Towards the end of the scan we will inject a dye known as ‘contrast’ that will enable us to see the arteries supplying the heart in greater detail. This technique is known as a CT-coronary angiogram. If required we may slow your heart down slightly to around 60 beats per minute using a medication called metoprolol. It is similar to the 'beta-blocker' medication that is commonly started following a heart attack, and will be given through your cannula so will not be painful. We may also give you a tablet to dissolve underneath the tongue called 'GTN', which dilates the blood vessels around your heart so that we can see them clearer. These two medications are very commonly prescribed by GP's and Hospital Doctors and are safe. GTN can cause a brief headache in some patients. The medications enable us to obtain good quality scans to ensure that we can use all the information gained by our study in the best possible ways.

On the same day as your PET-CT scan, we will perform another scan called a cardiac MRI scan. We will inject a different type of dye called ‘gadobutrol’ into your vein for this scan. This will show us the size of the heart attack and will help us interpret the pictures we have from the CT-PET scan. In the other arm we will inject a medication called adenosine, which dilates your heart vessels. A small number of patients experience symptoms such as light-headedness, nausea, chest discomfort or mild breathlessness with this medication. These effects are short-lived and they usually resolve spontaneously with time. You will need to lie still on this bed inside the scanner for one hour, and we will give you headphones so that you can listen to music during this time. This will help block out any noise that the scanner makes. The scan is not painful.

Nine weeks after your heart attack we will ask you to return again for a second PET-CT scan. The process explained above will be repeated. We will again take some blood tests (30 mls or 2 tablespoon of blood) and insert a cannula.

Finally, **6 to 12 months after your heart attack** we will ask you to return for a final MRI scan. This will show us whether what we see on the first two scans predicts the amount of scar tissue in the heart at this later stage. We will need again to insert a cannula to give the dye.

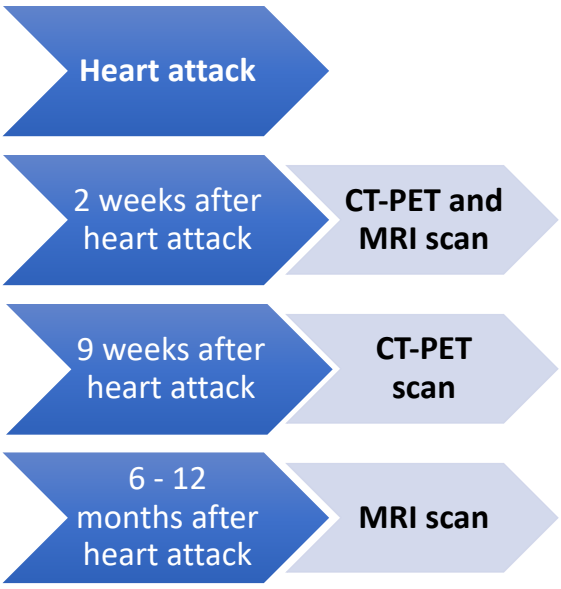

In a small group of patients, for the first CT-PET scan, we will need to have two cannulas (small plastic tubes) put in your arm – one in a vein, one in an artery (at your wrist). These cannulas will allow us to inject the tracer as well as take some extra blood samples during the scan. After the cannulas have been inserted we will inject the tracer and immediately start performing the scan. This scan will take 80 minutes and will include the CT-coronary angiogram. At the end of the scan, we will remove the cannulas and you will be free to leave.

What happens to the blood samples that are taken?
A proportion will be tested right away for various tests. A portion of the blood samples taken will be frozen, and stored in an anonymised manner so that further tests may be performed on them in the future (under NHS Lothian's Tissue Governance standards). We also intend to study your DNA using a process called 'genome-wide assessment' to help us understand if genes determine whether your body develops heart disease. Please note that we cannot use this data and information to test for other genetic conditions.

Is there anything else that I have to do?
There are no restrictions on your lifestyle through participating in this study. You should let your doctor know if you experience any symptom that you think may be related to this study.

Will taking part in this study affect my treatment?
No – you will still be followed up by your medical team (if required) as if you were not participating in the trial.

What are the side effects of taking part?
Performing PET CT and CT-coronary artery scans will expose you to a dose of radiation. The amount of radiation varies but is around 8 times the amount you would normally receive in a single year from background natural sources

of radiation. The lifetime risk of developing cancer from the radiation used in the scan is small: less than 1 in 750. To put this number in context in the average population 1 in 4 people will develop cancer in their lifetime. Therefore the risk to participants increases from 500 in 2000 to 501 in 2000

The MRI scanner uses powerful magnets but no radiation. Therefore any patients who have any metal in their bodies cannot take part in our study. This includes anyone with cochlear implants, aneurysm clips, pacemakers, or those who have ever had metal in their eyes.

The dyes used in our MRI and CT scans are used every day in hospitals throughout the world. They can affect the kidneys especially in patients with preexisting kidney problems. The contrast given in CT scans contains iodine and can occasionally have side effects ranging from headache and itch all the way to severe allergic reactions but these are extremely rare.

Fluciclatide is an experimental imaging agent that has limited experience to date but appears to be generally well tolerated. In three clinical trials, only two subjects have experienced any potential side effects (indigestion and headache). One further patient had a change in one of their blood counts that may have been related to fluciclatide. If you were found to be allergic to Fluciclatide or its components, you would be excluded from the study.

We will not include any female who has the potential to become pregnant. Radiation can cause damage to babies in the womb and so we want to ensure that no scans are performed on pregnant ladies.

The CT and MRI scanner takes detailed images of a small area of your chest so there is a small chance that we will find another abnormality in this area. Often these abnormalities turn out to be of no significance to your health. However, if this happens we will let you and your GP know and arrange for you to see a specialist for any further tests that are required.

What are the possible disadvantages of taking part?
Involvement in the trial will mean you attending for various appointments and scans. Whenever possible we will ensure that these occur during the same visit. If required we can also reimburse you for travel costs. Please discuss this at the time of your appointment.

What are the possible benefits of taking part?
There will not be any direct benefit to you in taking part in the study, however it is hoped that the findings of this study will benefit other patients with heart attacks in the future. The information from the PET CT and MRI scans will provide us with extra information about your heart, and some of the blood vessels in your body. We are unsure as to how useful this will prove. It is the purpose of this study to find that out.

Will my GP be informed?

As long as you agree we would like to inform your General Practitioner of your participation in this study.

Will my taking part in this study be kept confidential?
All the information collected about you during the course of the research will be kept strictly confidential. Any information about you that leaves the hospital will have your name and address removed so that you cannot be recognised from it.

What will happen to the results of the research study?
We will use the information that we will obtain from your scans in the best possible way, including analysing the other blood vessels and organs in your body to see if we can use this technique to benefit people with other medical conditions. Once we have completed the study and analysed the results, we will write a paper which will be submitted for publication in one of the medical journals. We do not routinely contact participants to inform them of the outcome of the research but would be happy to do so if requested. If you would like a copy of the results please contact Dr William Jenkins using the contact details listed below. You will not be personally identified in any report/publication. The data of the study will also be shared with General Electric Healthcare Medical Diagnostics.

Who is organising the research?
The study is being organised through the University of Edinburgh and NHS Lothian. Your doctors will not be paid for including you in this study.

Who has reviewed the study?
The study has been reviewed by the South East Scotland Research Ethics Review Service.

Where can I obtain further information about the study?
You can get further information from Dr William Jenkins or Professor Newby who will arrange to meet you. You can also contact Dr Henriksen who is not directly involved with this study but can act as an independent advisor. He can be contacted through the Royal Infirmary switchboard (0131 242 1000) by asking for his secretary.

Dr William Jenkins can be reached by contacting him on 0131 242 6428; his email williamjenkins@doctors.net.uk : or by letter addressed to the Cardiovascular Research Unit, Chancellor's Building, 49 Little France Crescent, Edinburgh EH16 SU4. Prof Newby can be contacted via the hospital switchboard (0131 536 1000).

What if I wish to make a complaint?
If you wish to make a complaint about the study please contact NHS Lothian:
NHS Lothian Complaints Team
2nd Floor, Waverley Gate
2-4 Waterloo Place

Edinburgh EH1 3EG
Tel: 0131 465 5708

Thank you once again for reading this information sheet.

Volunteer Information Sheet
(AS study group)

Identification of *In Vivo* Angioneogenesis and Fibrosis in Aortic Stenosis Using Positron Emission Tomography.

You are being invited to take part in a research study. Before you decide whether or not to participate, it is important that you understand why the research is being done and what it will involve. Please read the following information and do discuss it with others if you wish. If there is anything that you are still unclear about, or any questions that you would like to ask, you can contact us for further information. We aim to re-contact you in 1 – 3 days from when you receive this form, to discuss whether you would like to proceed with the study.

Thank you for taking the time to read this information sheet.

Why are we doing this study?

Aortic stenosis is a condition caused by narrowing of one the major valves within the heart. The reasons why this narrowing develops are poorly understood. As a result there are no treatments to stop the disease except major heart surgery when the valve becomes very seriously narrowed. Furthermore we have no means of predicting how quickly valve narrowing will progress.

We want to study two processes; new blood vessel growth (angiogenesis) and scar formation (fibrosis). These are thought to play a role in the development of aortic stenosis, why the valve gets narrower and how the heart compensates for it. We will use two special scans called PET-CT and MRI to tell us whether these processes are indeed occurring in narrowed valves.

We hope that the information provided by this study will help identify new treatments

MRI Scanner

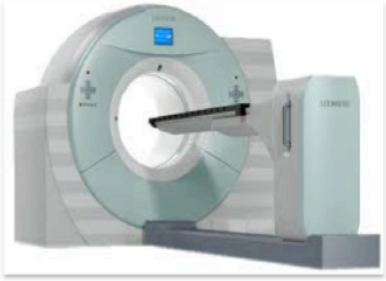

PET/CT Scanner

that can then be targeted to stop the progression of aortic stenosis. In the future this may mean we are able to delay or even prevent the need for surgery.

Why have I been chosen to take part?

We are looking for patients with aortic stenosis to study using these scans. Using PET CT we will assess how much new blood vessel growth and scar formation is occurring on your valve and in the surrounding heart muscle. From this we will get good understandings of how important these two processes are, where on the valve they occur and whether it varies with the severity of aortic stenosis. We will also perform an MRI scan to more accurately assess how well the heart is working.

You will not benefit directly from this study. However, the information we get could help us to improve the way we treat patients with aortic stenosis in the future.

Do I have to take part?

No. It is up to you to decide whether or not to take part. If you decide to take part you will be given this information sheet to keep and you will be asked to sign a consent form. Even once you have signed the form you can still withdraw at any time and you do not have to give a reason.

What will happen to me if I decide to take part?

If you are happy to participate in our study, we will ask you to attend the Royal Infirmary for a repeat echocardiogram scan of your heart. At that first meeting Dr William Jenkins will go through the information sheet again with you before asking you to sign a consent form. You will then be invited back to our research department, which is immediately next to the Edinburgh Royal Infirmary. We will talk about your symptoms, perform a full examination of your heart and place a plastic tube (cannula) in one of your veins. We will use this to take some blood tests (30 mls or 2 tablespoon of blood) and then inject you with an experimental imaging agent called '^{18}F-fluciclatide'. This contains a small amount of radiation which we can detect using a specialized camera called a PET scanner. Fluciclatide has previously been used safely in people but has not yet been approved for routine use. . We will measure your blood pressure and heart rate, and will repeat this a number of times during your visit. After approximately 60min of sitting in a quiet room we will perform the PET-CT scan. You will need to lie still on a bed for around 20 min whilst the scan takes place. It is not painful.

Towards the end of the scan we will inject a dye known as ‘contrast’ that will enable us to see the arteries supplying the heart in greater detail. This technique is known as a CT-coronary angiogram. We may be required slow your heart down slightly to around 60 beats per minute using a medication called metoprolol. This is a 'beta-blocker' and will be given through your cannula so will not be painful. We may also

give you a tablet to dissolve underneath the tongue called 'GTN', which dilates the blood vessels around your heart so that we can see them more clearly. These two medications are very commonly prescribed by GP's and Hospital Doctors. GTN can cause a brief transient headache in some patients. The medications enable us to obtain good quality pictures to ensure that we can use all the information gained by our study in the best possible ways.

Around the same time as your PET-CT scan, we will perform another scan called a cardiac MRI scan. This will help us interpret the pictures we have from the PET-CT scan. We will inject a different type of dye called 'gadobutrol' into your vein for this scan. You will need to lie still on a bed inside the scanner for one hour, but we will give you headphones so that you can listen to music during this time. This will also help block out any noise that the scanner makes. The scan is not painful.

Finally, 1 to 2 years after your initial scan, we will ask you to return for a final echocardiogram, an MRI scan and more blood samples (approximately 30mls or two tablespoons). With this information we can establish whether the amount of new blood vessel formation and scar tissue formation seen on your initial scan can predict the function of the heart and the overall amount of scar tissue within the heart at this later point in time.

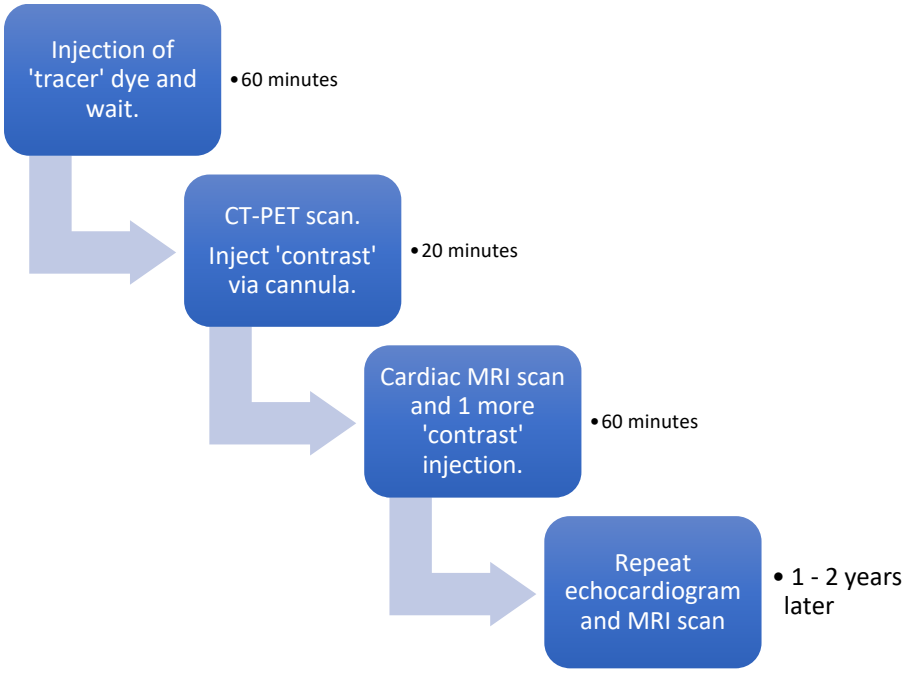

In a small group of patients, for the first CT-PET scan, we will need to have two cannulas (small plastic tubes) put in your arm – one in a vein, one in an artery (at your wrist). These cannulas will allow us to inject the tracer as well as take some extra blood samples during the scan (approximately 100mls / 7 tablespoons of blood). After the cannulas have been inserted we will inject the tracer and immediately start

performing the scan. This scan will take 80 minutes and will include the CT-coronary angiogram. At the end of the scan, we will remove the cannulas and you will be free to leave.

What happens to the blood samples that are taken?

A proportion will be tested right away for various tests. A portion of the blood samples taken will be frozen, and stored in an anonymised manner so that further tests may be performed on them in the future (under NHS Lothian's Tissue Governance standards). We also intend to study your DNA using a process called 'genome-wide assessment' to help us understand if genes determine how your body responds to the heart valve disease. Please note that we cannot use this data and information to test for other genetic conditions.

Is there anything else that I have to do?

There are no restrictions on your lifestyle through participating in this study. You should let your doctor know if you experience any symptom that you think may be related to this study.

Will taking part in this study affect my treatment?

No – you will still be followed up by your medical team (if required) as if you were not participating in the trial.

What are the side effects of taking part?

Performing PET CT and CT-coronary artery scans will expose you to a dose of radiation. The amount of radiation varies but is around 8 times the amount you would normally receive in a single year from background natural sources of radiation. The lifetime risk of developing cancer from the radiation used in the scan is small: less than 1 in 750. To put this number in context in the average population 1 in 4 people will develop cancer in their lifetime. Therefore the risk to participants increases from 500 in 2000 to 501 in 2000.

The MRI scanner uses powerful magnets but no radiation. Therefore any patients who have any metal in their bodies cannot take part in our study. This includes anyone with cochlear implants, aneurysm clips, pacemakers, or those who have ever had metal in their eyes.

The dyes used in our MRI and CT scans are used every day in hospitals throughout the world. They both affect the kidneys especially in patients with preexisting kidney problems. The contrast given in CT scans contain iodine and can occasionally have side effects ranging from headache and itch all the way to severe allergic reactions but these are extremely rare.

Fluciclatide is an experimental imaging agent that has limited experience to date but appears to be generally well tolerated. In three clinical trials, only two subjects have experienced any potential side effects (indigestion and headache). One further patient

had a change in one of their blood counts that may have been related to fluciclatide. If you were found to be allergic to Fluciclatide or its components, you would be excluded from the study.

We will not include any female who has the potential to become pregnant. Radiation can cause damage to babies in the womb and so we want to ensure that no scans are performed on pregnant ladies.

The CT and MRI scanner takes detailed images of a small area of your chest so there is a small chance that we will find another abnormality in this area. Often these abnormalities turn out to be of no significance to your health. However, if this happens we will let you and your GP know and arrange for you to see a specialist for any further tests that are required.

What are the possible disadvantages of taking part?

Involvement in the trial will mean you attending for various appointments and scans. Whenever possible we will ensure that these occur during the same visit. If required we can also reimburse you for travel costs. Please discuss this at the time of your appointment.

What are the possible benefits of taking part?

There will not be any direct benefit to you in taking part in the study, however it is hoped that the findings of this study will benefit other patients with heart attacks in the future. The information from the PET CT scans will provide us with extra information about your heart, your heart valves, and some of the blood vessels in your body. We are unsure as to how useful this will prove. It is the purpose of this study to find that out.

Will my GP be informed?

As long as you agree we would like to inform your General Practitioner of your participation in this study.

Will my taking part in this study be kept confidential?

All the information collected about you during the course of the research will be kept strictly confidential. Any information about you which leaves the hospital will have your name and address removed so that you cannot be recognised from it.

What will happen to the results of the research study?

We will use the information that we will obtain from your scans in the best possible way, including analysing the other blood vessels and organs in your body to see if we can use this technique to benefit people with other medical conditions. Once we have completed the study and analysed the results, we will write a paper which will be submitted for publication in one of the medical journals. We do not routinely contact participants to inform them of the outcome of the research but would be happy to do so if requested. If you would like a copy of the results please contact Dr William Jenkins

using the contact details listed below. You will not be personally identified in any report/publication. The data of the study will also be shared with General Electric Healthcare Medical Diagnostics.

Who is organising the research?

The study is being organised through the University of Edinburgh and NHS Lothian. Your doctors will not be paid for including you in this study.

Who has reviewed the study?

The study has been reviewed by the South East Scotland Research Ethics Review Service.

Where can I obtain further information about the study?

You can get further information from Dr William Jenkins or Professor Newby who will arrange to meet you. You can also contact Dr Henriksen who is not directly involved with this study but can act as an independent advisor. He can be contacted through the Royal Infirmary switchboard (0131 242 1000) by asking for his secretary.

Dr William Jenkins can be reached by contacting him on 0131 242 6428; his email williamjenkins@doctors.net.uk: or by letter addressed to the Cardiovascular Research Unit, Chancellor's Building, 49 Little France Crescent, Edinburgh EH16 SU4. Prof Newby can be contacted via the hospital switchboard (0131 536 1000).

If you wish to make a complaint about the study please contact NHS Lothian:

NHS Lothian Complaints Team
2nd Floor
Waverley Gate
2-4 Waterloo Place
Edinburgh, EH1 3EG
Tel: 0131 465 5708

Thank you once again for reading this information sheet.

Volunteer Consent Form

(Study Group)

ROLE OF INFLAMMATION IN THE PROGRESSION OF AORTIC STENOSIS: *THE RING OF FIRE*

Participant Name	
Participant DOB	
Participant identification No for this trial	

☐ I confirm that I have read and understood the accompanying information sheet.

☐ I agree to take part in the above research project as described in the information sheet.

☐ I understand that this will not influence the medical treatment that is planned for me in any way.

☐ I understand that I am under no obligation to participate in this research, that I may withdraw from the study at any stage and that doing so will not influence my treatment in any way.

☐ I understand that each of the CTPET scans performed will be associated with exposure to a dose of radiation.

☐ I understand that any information related to my case will be stored in an anonymised manner

☐ I understand that blood samples will be stored for future use. I agree to them being used in future studies subject to ethical approval

☐ I consent to my GP being informed as to my participation in the trial.

Signed…… Date ……..

Name of patient……

I confirm that the nature of the research, and the voluntary nature of the study have been explained in terms understandable to the patient

Signed …….. Date……..

Name of investigator ……..

Patient Name:

Patient DoB:

Patient Identification Number for this trial:

CONSENT FORM

Identification of *In Vivo* Angioneogenesis and Fibrosis in Myocardial Infarction using Positron Emission Tomography.

Myocardial Infarction Group
(re-vascularised / non-revascularised)

Name of Researcher: Professor David E. Newby

Please initial all boxes

1. I confirm that I have read and understand the information sheet dated 15/01/13 (Post MI group - revascularised, version 1.5, or Post MI group – non-revascularised, version 1.5) for the above study. I have had the opportunity to consider the information, ask questions and have had these answered satisfactorily. ☐
2. I agree to participate, understand that my participation is voluntary and that I am free to withdraw at any time without giving any reason, without my medical care or legal rights being affected. ☐
3. I understand that this will not influence the medical treatment that is planned for me in any way. ☐
4. I understand that the CTPET scan performed will be associated with exposure to a dose of radiation. ☐
5. I understand that the CT, PET and MRI scans will require the administration of drugs. ☐
6. I understand that any information related to my case will be stored in an anonymised manner. ☐
7. I understand that anonymised blood samples and anonymised DNA will be stored (under NHS Lothian's Tissue Governance standards) for future research studies. ☐

8. I understand that relevant sections of my medical notes and data collected during the trial may be looked at by the trial researchers and individuals from the Sponsor, regulatory authorities, the NHS organization or from General Electric Healthcare, where it is relevant to my taking part in this research. I give permission for these individuals to have access to my records. ☐

9. I agree to my GP being informed of my participation in the study, and that he will be informed of any incidental findings on my scans. ☐

10. I agree to the further use of identifiable data/tissue in the event of a loss of capacity. ☐

11. I agree that blood and tissue samples may be used for genetic analysis. ☐

Name of Participant	Date	Signature
Name of Person taking consent.	Date	Signature

Patient Name:

Patient DoB:

Patient Identification Number for this trial:

CONSENT FORM

Identification of *In Vivo* Angioneogenesis and Fibrosis in Aortic Stenosis using Positron Emission Tomography.

Aortic Stenosis Study Group

Name of Researcher: Professor David E. Newby

Please initial all boxes

12. I confirm that I have read and understand the information sheet dated 15/01/2013 (AS Study Group version 1.5) for the above study. I have had the opportunity to consider the information, ask questions and have had these answered satisfactorily. ☐
13. I agree to participate, understand that my participation is voluntary and that I am free to withdraw at any time without giving any reason, without my medical care or legal rights being affected. ☐
14. I understand that this will not influence the medical treatment that is planned for me in any way. ☐
15. I understand that the CTPET scan performed will be associated with exposure to a dose of radiation. ☐
16. I understand that the CT, PET and MRI scans will require the administration of drugs. ☐
17. I understand that any information related to my case will be stored in an anonymised manner. ☐
18. I understand that anonymised blood samples and anonymised DNA will be stored (under NHS Lothian's Tissue Governance standards) for future research studies. ☐
19. I understand that relevant sections of my medical notes and data collected during the trial may be looked at by the trial researchers and individuals from the Sponsor, regulatory authorities, ☐

the NHS organisation or from General Electric Healthcare, where it is relevant to my taking part in this research. I give permission for these individuals to have access to my records.

20. I agree to my GP being informed of my participation in the study, and that he will be informed of any incidental findings on my scans. ☐

21. I agree to the further use of identifiable data/tissue in the event of a loss of capacity. ☐

22. I agree that blood and tissue samples may be used for genetic analysis. ☐

Name of Participant	Date	Signature
Name of Person taking consent.	Date	Signature

CERTIFICATE

FOR THE

ADMINISTRATION OF RADIOACTIVE MEDICINAL PRODUCTS

Certificate Reference Number RPC 577 / 3258 / 25995

It is hereby certified for the purposes of the Medicines (Administration of Radioactive Substances) Regulations 1978, amended by the Medicines (Administration of Radioactive Substances) Amendment Regulations 1995, that

Prof Edwin Jacques Rudolph van BEEK
Royal Infirmary of Edinburgh
51 Little France Crescent
Edinburgh
EH16 4SA

may administer until ***11-Jul-2015*** *the radioactive medicinal products specified in the Schedule to this certificate for the purpose(s) there specified.*

For The Secretary of State for Health

.....

Health Protection
Toxicology and Radiation
Department of Health

12-July-2010

Prof Edwin Jacques Rudolph van BEEK
Royal Infirmary of Edinburgh
51 Little France Crescent
Edinburgh
EH16 4SA

Date of Certificate 12-July-2010

Schedule to Research Certificate Number RPC 577 / 3258 / 25995

Research Project

ROLE OF INFLAMMATION IN THE PROGRESS OF AORTIC STENOSIS "THE RING OF FIRE"

Serial	Nuclide	Chemical Form
9a21vii	18F	FDG
9a31	18F	NaF

Edwin Jacques Rud van BEEK

Research Certificates Held At : Royal Infirmary of Edinburgh

Certificate : RPC 577 / 3258 / 25995

Research Title : ROLE OF INFLAMMATION IN THE PROGRESS OF AORTIC STENOSIS "THE RING OF FIRE"

Expiry Date : 11/07/2015

Serial	Nuclide	Chemical Form
9a21vii	18F	FDG
9a31	18F	NaF

Administration of Radioactive Substances Advisory Committee (ARSAC)

ARSAC Support Unit

Centre for Radiation, Chemical and
Environmental Hazards.
Public Health England
Chilton, Didcot, Oxon OX11 0RQ
Tel: **01235 825007 (administration)**
01235 825006 (administration)
01235 825004/825001 (scientific)
Fax: 01235 834925
E-mail:ARSAC@phe.gov.uk

NHS LOTHIAN
CHIEF EXECUTIVE'S OFFICE
23 OCT 2013

Chief Executive
NHS Lothian
University Hospitals Division
51 Little France Crescent
Edinburgh
EH16 4SA

Our Ref : RPC 577 / 3258 / 30463
Date 08 October 2013

Administration of Radioactive Medicinal Products to Persons
The Medicines (Administration of Radioactive Substances) Regulations 1978, Amended By
The Medicines (Administration Of Radioactive Substances) Regulations 1995
Certificate for the Administration of Radioactive Medicinal Products

In accordance with the process described in paragraph B3.5.1 of Health Circular HC(95)3 of January 1995, I enclose for information two copies of the certificates and revised schedules granted to the following clinician within your employing authority under the above Regulations:

RPC 577 / 3258 / 30463 Edwin Jacques Rudolph van BEEK

The original certificate has been sent to the applicant.

Please note that the relevant Radiation Protection Adviser should also have a copy and I would be grateful if you would pass one on.

Copies of the "Notes for Guidance on the Clinical Administration of Radiopharmaceuticals and the Use of Sealed Radioactive Sources" are available from this office if required and the website www.ARSAC.org.uk.

If you should have any queries then please do not hesitate to contact me at the above address, quoting the above RPC number on all correspondence.

Yours sincerely

Miss K Burton
ARSAC Support Unit

CERTIFICATE

FOR THE

ADMINISTRATION OF RADIOACTIVE MEDICINAL PRODUCTS

Certificate Reference Number RPC 577 / 3258 / 30463

It is hereby certified for the purposes of the Medicines (Administration of Radioactive Substances) Regulations 1978, amended by the Medicines (Administration of Radioactive Substances) Amendment Regulations 1995, that

Prof Edwin Jacques Rudolph van BEEK
Royal Infirmary of Edinburgh
51 Little France Crescent
Edinburgh
EH16 4SA

may administer until ***07-Oct-2018*** *the radioactive medicinal products specified in the Schedule to this certificate for the purpose(s) there specified.*

For The Secretary of State for Health

.....

Health Protection
Toxicology and Radiation
Department of Health

08-October-2013

Prof Edwin Jacques Rudolph van BEEK
Royal Infirmary of Edinburgh
51 Little France Crescent
Edinburgh
EH16 4SA

Date of Certificate 08-October-2013

Schedule to Research Certificate Number RPC 577 / 3258 / 30463

Research Project

THE IDENTIFICATION OF MYOCARDIAL FIBROSIS BY POSITRON EMISSION TOMOGRAPHY IN PATIENTS WITH CARDIOMYOPATHIES

Serial	Nuclide	Chemical Form
9a39	18F	AH-111585 (fluciclatide)

End of Certificate Schedule

CERTIFICATE

FOR THE

ADMINISTRATION OF RADIOACTIVE MEDICINAL PRODUCTS

Certificate Reference Number RPC 577 / 3258 / 29379

It is hereby certified for the purposes of the Medicines (Administration of Radioactive Substances) Regulations 1978, amended by the Medicines (Administration of Radioactive Substances) Amendment Regulations 1995, that

Prof Edwin Jacques Rudolph van BEEK
Royal Infirmary of Edinburgh
51 Little France Crescent
Edinburgh
EH16 4SA

may administer until ***03-Dec-2017*** *the radioactive medicinal products specified in the Schedule to this certificate for the purpose(s) there specified.*

For The Secretary of State for Health

Health Protection
Toxicology and Radiation
Department of Health

04-December-2012

Prof Edwin Jacques Rudolph van BEEK
Royal Infirmary of Edinburgh
51 Little France Crescent
Edinburgh
EH16 4SA

Date of Certificate 04-December-2012

Schedule to Research Certificate Number RPC 577 / 3258 / 29379

Research Project

Identification of In Vivo Angioneogenesis and Fibrosis in Aortic Stenosis using Positron Emission Tomography.

Serial	Nuclide	Chemical Form
9a39	18F	AH-111585 (fluciclatide)

End of Certificate Schedule

18F-Sodium Fluoride Uptake Is a Marker of Active Calcification and Disease Progression in Patients With Aortic Stenosis

Marc R. Dweck, MD, PhD*; William S.A. Jenkins, MD*; Alex T. Vesey, MD; Mark A.H. Pringle, BSc; Calvin W.L. Chin, MD; Tamir S. Malley, MD; William J.A. Cowie, BSc; Vasiliki Tsampasian, MD; Hamish Richardson, BSc; Alison Fletcher, PhD; William A. Wallace, MD, PhD; Renzo Pessotto, MD; Edwin J.R. van Beek, MD, PhD; Nicholas A. Boon, MD; James H.F. Rudd, MD, PhD; David E. Newby, MD, PhD

Background—18F-Sodium fluoride (18F-NaF) and 18F-fluorodeoxyglucose (18F-FDG) are promising novel biomarkers of disease activity in aortic stenosis. We compared 18F-NaF and 18F-FDG uptake with histological characterization of the aortic valve and assessed whether they predicted disease progression.

Methods and Results—Thirty patients with aortic stenosis underwent combined positron emission and computed tomography using 18F-NaF and 18F-FDG radiotracers. In 12 patients undergoing aortic valve replacement surgery (10 for each tracer), radiotracer uptake (mean tissue/background ratio) was compared with CD68 (inflammation), alkaline phosphatase, and osteocalcin (calcification) immunohistochemistry of the excised valve. In 18 patients (6 aortic sclerosis, 5 mild, and 7 moderate), aortic valve computed tomography calcium scoring was performed at baseline and after 1 year. Aortic valve 18F-NaF uptake correlated with both alkaline phosphatase (r=0.65; P=0.04) and osteocalcin (r=0.68; P=0.03) immunohistochemistry. There was no significant correlation between 18F-FDG uptake and CD68 staining (r=−0.43; P=0.22). After 1 year, aortic valve calcification increased from 314 (193–540) to 365 (207–934) AU (P<0.01). Baseline 18F-NaF uptake correlated closely with the change in calcium score (r=0.66; P<0.01), and this improved further (r=0.75; P<0.01) when 18F-NaF uptake overlying computed tomography–defined macrocalcification was excluded. No significant correlation was noted between valvular 18F-FDG uptake and change in calcium score (r=−0.11; P=0.66).

Conclusions—18F-NaF uptake identifies active tissue calcification and predicts disease progression in patients with calcific aortic stenosis.

Clinical Trial Registration—URL: http://www.clinicaltrials.gov. Unique identifier: NCT01358513.

(*Circ Cardiovasc Imaging*. 2014;7:371-378.)

Key Words: aortic valve stenosis ■ calcification, physiologic ■ fluorodeoxyglucose F18 ■ inflammation ■ positron-emission tomography

Downloaded from http://circimaging.ahajournals.org/ by guest on February 1, 2018

The mechanisms underlying aortic stenosis (AS) remain incompletely understood, and the accurate prediction of disease progression remains a challenge.[1] Calcification and inflammation are thought to play key pathophysiological roles. Indeed, the amount of established calcium in the valve correlates with disease severity and predicts future adverse cardiovascular events.[2,3] Although computed tomography (CT) and echocardiography can provide measures of established valvular calcification, they cannot directly assess ongoing calcification activity, which is considered to be the main driver of disease progression.

Clinical Perspective on p 378

Recent reports have investigated 2 positron emission tomography (PET) radiotracers, 18F-sodium fluoride (18F-NaF) and 18F-fluorodeoxyglucose (18F-FDG), as measures of calcification activity and inflammation, respectively, in the aortic valve,[4] coronary arteries,[5,6] and major vessels.[7] 18F-FDG PET has become a widely used tool for the assessment of inflammation in the aorta and carotid arteries, with uptake correlating with macrophage burden.[8] Several studies have investigated its uptake in AS, although histological validation

Received September 27, 2013; accepted February 5, 2014.

From the Centre for Cardiovascular Science (M.R.D., W.S.A.J., A.T.V., M.A.H.P., C.W.L.C., T.S.M., W.J.A.C., V.T., R.P., N.A.B., D.E.N.) and Clinical Research Imaging Centre (M.R.D., W.S.A.J., A.T.V., C.W.L.C., H.R., A.F., E.J.R.v.B., D.E.N.), University of Edinburgh, Edinburgh, UK; Department of Pathology, Royal Infirmary of Edinburgh, Edinburgh, UK (W.A.W.); and Division of Cardiovascular Medicine, University of Cambridge, Cambridge, UK (J.H.F.R.).

*Drs Dweck and Jenkins contributed equally to this work.

Correspondence to Marc R. Dweck, MD, PhD, Centre for Cardiovascular Science, University of Edinburgh, 47 Little France Crescent, Edinburgh, UK, EH16 4TJ. E-mail MDweck@staffmail.ed.ac.uk

© 2014 American Heart Association, Inc.

Circ Cardiovasc Imaging **is available at http://circimaging.ahajournals.org** **DOI: 10.1161/CIRCIMAGING.113.001508**

is lacking.[4,9] 18F-NaF has been used as a bone tracer for >40 years, displaying increased activity in conditions associated with increased bone metabolism such as Paget disease. In bone, it is thought to bind and then incorporate into exposed hydroxyapatite crystals via an exchange mechanism with hydroxyl groups to form fluoroapatite. Given that hydroxyapatite is also a key structural component of calcification in the aortic valve and vascular atheroma, it is presumed that similar mechanisms explain its accumulation in these tissues. However, this remains hypothetical. The principal aims of the present study were, therefore, to validate the use of 18F-NaF and 18F-FDG in AS by comparing in vivo radiotracer uptake with immunohistochemistry of calcification and inflammation in excised valvular tissue and to investigate whether either of these agents predicts disease progression at 1 year.

Methods

Patient Populations

Two cohorts of patients with AS were recruited into this study: (1) 12 patients undergoing valve replacement surgery, and (2) 18 patients with asymptomatic disease under surveillance at the Edinburgh Heart Center. The latter cohort was randomly selected for repeat scanning from a larger, previously described population who underwent baseline PET imaging.[4,5,10]

All patients were >50 years of age, and exclusion criteria included a normal aortic valve, insulin-dependent diabetes mellitus, end-stage renal failure, life expectancy of <2 years, and metastatic malignancy. Patients with severe AS were excluded from the cohort of patients under surveillance because of the potential for disease progression and symptom development before the follow-up 1-year scan. The study was performed in accordance with the Declaration of Helsinki and after local research ethics committee approval. All patients provided written informed consent before participating.

Baseline Assessment

All patients underwent full clinical assessment at baseline, and AS severity was assessed using Doppler and 2-dimensional echocardiography by means of the peak transvalvular velocity, mean gradient, and aortic valve area according to American Heart Association/American College of Cardiology guidelines.[11] Aortic sclerosis was defined as thickening of the aortic valve cusps in the absence of accelerated flow (<2 m/s) through the valve. Combined PET and CT scans of the aortic valve were performed using a hybrid scanner (Biograph mCT; Siemens Medical Systems, Erlangen, Germany) 60 minutes after administration of 125 MBq of 18F-NaF. Subsequently, a second PET/CT scan was performed using the same hybrid scanner 90 minutes after administration of 200 MBq of 18F-FDG. Glucose is a major energy source of the myocardium, so that intense 18F-FDG uptake frequently occurs, spilling over and contaminating the signal in the valve. We attempted to reduce myocardial uptake by asking patients to avoid carbohydrates for 24 hours before their 18F-FDG scan, thereby switching the myocardium from glucose to free fatty-acid metabolism. Myocardial 18F-FDG uptake was assessed within regions of interest (ROIs) placed in the basal septum of the left ventricle and classified as being adequately suppressed if mean standard uptake values were <5.0.[4] An ECG-gated breath-hold CT scan (noncontrast enhanced, 40 mA/rot [CareDose]; 100 kV) was performed for calculation of the aortic valve calcium score using dedicated analysis software (VScore; Vital Images, Minnetonka, MN) on axial scans.[12] Particular care was taken to differentiate valvular calcium from that in the aortic root and mitral valve annulus.[6] At 1-year follow-up, patients in the surveillance cohort underwent repeat clinical assessment and CT calcium scoring using the same protocol.

Quantification of Aortic Valve PET Activity

18F-NaF and 18F-FDG uptake in the aortic valve was quantified using an Osirix workstation (OsiriX version 3.5.1 64-bit; OsiriX Imaging Software, Geneva, Switzerland) as reported previously.[4,5] Briefly, fused PET-CT images were reoriented into the plane of the valve and circular ROIs drawn on adjacent 3-mm slices until the entire valve had been examined. For 18F-NaF, ROIs were placed around the perimeter of the valve while excluding the aortic root (whole-valve technique). To reduce the potential for myocardial 18F-FDG activity contaminating the aortic valve signal, ROIs for this tracer were drawn in the center of the valve as previously described (center-valve technique).[4,9] Within these ROIs, mean standard uptake values were calculated for each slice, averaged, and corrected for blood pool activity to provide mean tissue/background ratios. Mean tissue/background ratios were selected prospectively for subsequent comparisons with histology and disease progression because this measure was felt to best represent tracer uptake across the valve as a whole.

Distribution of 18F-NaF in the Aortic Valve Relative to Calcium Scoring

We undertook a voxel-by-voxel analysis comparing the distribution of calcium on CT with 18F-NaF uptake. ROIs were drawn around the valve, and each voxel was assessed for the presence of calcium (>130 HU) and increased 18F-NaF uptake (tissue/background ratio max >1.97 based on the highest uptake in the control cohort of our previous study)[4] using dedicated software MATLAB (Mathworks Inc, Natick, MA). We hypothesized that regions of completely novel calcium development might have an even more important effect on disease progression, and therefore we calculated the percentage of the valve with increased radiotracer uptake in the absence of underlying calcium on CT (% of PET-positive but CT-negative pixels).

Histological Assessment

In the patients undergoing aortic valve replacement, the aortic valve was removed at the time of operation, with care taken to preserve the integrity of the valve architecture. Samples were then fixed in 4% paraformaldehyde for 24 hours. Plaques were decalcified in EDTA for 10 days and embedded in paraffin, and 5-μm sections were prepared. Immunohistochemical staining for osteocalcin (antihuman mouse mAb ab13418; Abcam), CD68 (antihuman mouse clone PG-M1 m0876, DAKO), and tissue nonspecific alkaline phosphatase (TNAP; antihuman rabbit pAb CAT#LF PA50004; Abfrontier) was then undertaken after heat-induced epitope retrieval using a Citrate Buffer pH 6 (Novocastra Leica microsystems) in a decloaking chamber. Osteocalcin staining required no heat-induced epitope retrieval. Sections were stained using a Leica Vision Biosystems Bond×immunostaining robot. After blocking in peroxide for 10 minutes, sections were incubated with the specific antihuman antibodies for 2 hours at room temperature at the following dilutions: osteocalcin 1:200, TNAP 1:100, and CD68 1:100. All incubation steps were followed by washing in TBS/Tween. Sections for osteocalcin and CD68 were incubated for 15 minutes with prepolymer/postprimary followed by 15 minutes with polymer (HRP) for all antibodies before 3,3′-diaminobenzidine visualization and hematoxylin counterstain. Sections were dehydrated in graded ethanol and cleared in xylene before cover slipping in Pertex.

Images were taken on a Zeiss Axioskop2 fitted with an Axiocam MRc digital camera using Axiovision software. Tissue cross-sectional area on each section was manually delineated using Image Pro Plus 5 (Rockville, MD). Immunohistochemical staining for osteocalcin and TNAP was identified by visual assessment and quantified using automated color-based segmentation by a trained observer blinded to the PET data. Staining was expressed as a percentage of the total valve area. Macrophage infiltration using CD68 was assessed using a similar approach but with an object size set threshold applied at 20×10 pixels to limit counting to cell-sized objects. The density of cell staining in the valve tissue was expressed as cells per square millimeter. This technique was also used to identify cellular staining for TNAP and osteocalcin.

Reproducibility Studies

Interobserver reproducibility of the immunohistochemical data was investigated. Tissue staining with alkaline phosphatase, CD68, and

Downloaded from http://circimaging.ahajournals.org/ by guest on February 1, 2018

osteocalcin was quantified in 5 valves independently by 2 trained observers (W.S.A.J. and A.T.V.).

Autoradiography

Clinical PET systems have limited resolution. To gain further information about the precise localization of the 18F-NaF signal in aortic valve tissue, we undertook autoradiography. Nondecalcified valvular tissue was rapidly cooled in dry ice and then sectioned at 7-μm thickness using a cryostat (CM1520; Wetzlar, Germany). Sections for autoradiography were mounted on Superfrost slides (Gerhard Menzel, Braunschweig, Germany) before treatment with spray fixative. Sections were bathed in a solution of 18F-NaF at a concentration close to in vivo imaging concentrations (1 kBq/mL) for 60 minutes and then rinsed with PBS. A freshly blanked phosphor screen was then placed over the slides and an overnight exposure undertaken. The screen was then read using a FujiFilm FLA-5100 Fluorescent Image Analyser (Raytek Scientific Limited, Sheffield, UK). Sections adjacent to those used for autoradiography were stained for elemental phosphate (ie, calcium orthophosphate) using Von Kossa stain, and after surface decalcification in situ with Von Ebner solution, for TNAP and osteocalcin. Sections were then manually registered and examined for colocalization with 18F-NaF signal.

Statistical Methods

Continuous variables were assessed for normality both visually and using the D'Agostino-Pearson test. Variables were expressed as either mean±SD or median with interquartile ranges (IQRs) subject to whether they approximated a normal distribution. Categorical data were presented as n (%). The 95% normal range for differences between sets of immunohistochemical measurements (the limits of agreement) were estimated using Bland–Altman analysis by multiplying the SD of the mean difference by 1.96.[13] Intraclass correlation coefficients with 95% confidence intervals were calculated for interobserver variation. Baseline and follow-up calcium scores approximated a normal distribution and were compared using a paired *t* test. However, despite attempts at data transformation, the changes in calcium scores were not normally distributed, and correlations with CT progression data were assessed using Spearman correlation and linear regression analysis. We acknowledge the limitations in using linear regression in the context of a non-normal distribution. A 2-sided $P<0.05$ was regarded as statistically significant. Statistical analysis was performed with the use of Graph Pad Prism version 6.0 (GraphPad Software Inc, San Diego, CA).

Results

Histology Cohort

Twelve patients with symptomatic AS were recruited into the histology cohort (8 men; 76±6 years of age; peak aortic valve velocity, 4.6±0.9 m/s). Patients underwent PET scanning a median of 92 days before surgical aortic valve replacement. Eight patients received both 18F-NaF and 18F-FDG PET scans. In addition, 2 had a single 18F-NaF scan, whereas 2 more had a single 18F-FDG scan. Thus, 10 valves were available for the histological validation of each tracer. No patient had a significant perioperative complication (Table 1). Effective myocardial suppression of 18F-FDG activity was achieved in 40% (median myocardial standard uptake value, 5.4; IQR, 1.9–10.4).

Immunohistochemistry and Autoradiography

All valve samples displayed positive cellular staining for TNAP (225 cells/mm^2 valve tissue; IQR, 143–328), osteocalcin (130 cells/mm^2 valve tissue; IQR, 85–274), and CD68 (172 cells/mm^2 valve tissue; IQR, 73–271; Figure 1). Extensive TNAP and osteocalcin staining was also observed in the extracellular matrix, occupying approximately a sixth of the valve area sampled (17±5% and 17±7%, respectively).

On autoradiography, 18F-NaF uptake was observed to colocalize closely with staining for structural calcium phosphate, TNAP, and osteocalcin (Figure 1). However, signal was also clearly apparent in areas free of macroscopically visible calcium, thus highlighting the sensitivity of 18F-NaF in the detection of newly evolving calcification.

Reproducibility of Immunohistochemistry

Interobserver reproducibility was good for the quantification of osteocalcin and TNAP staining, as well as CD68 cell

Table 1. Baseline Characteristics of Progression Cohort

	Total	Aortic Sclerosis	Mild Aortic Stenosis	Moderate Aortic Stenosis
No.	18	6 (33)	7 (39)	5 (28)
Age, y	75 (71–79)	74 (70–78)	74 (69–80)	79 (70–83)
Men	15 (83)	4 (66)	7 (100)	4 (80)
Hypertension	13 (72)	3 (50)	5 (71)	5 (100)
Hyperlipidemia	12 (67)	4 (66)	5 (71)	3 (60)
Diabetes mellitus	5 (28)	1 (16)	4 (57)	0 (0)
Ischemic heart disease	13 (72)	4 (66)	6 (86)	3 (60)
Serum creatinine, μmol/L	92±29	85 (72–92)	91 (67–125)	84 (69–133)
Cigarette smoking	0 (0)	0 (0)	0 (0)	0 (0)
Peak aortic valve velocity, m/s	2.6 (1.8–3.1)	1.7 (1.6–1.8)	2.4 (2.1–2.6)	3.4 (3.2–3.6)
Aortic valve area, cm^2	1.68 (1.26–2.28)	1.92 (1.8–2.1)	1.63 (1.42–1.87)	1.03 (0.78–1.18)
Mean gradient, mm Hg	10.8 (7.0–16.5)	6.2 (4.8–7.0)	11.0 (9.3–14.0)	22.0 (18.8–27.2)
Aortic valve calcium score, AU	314 (193–540)	106 (13–204)	355 (211–536)	1167 (436–1472)
Time between CT scans, d	386 (377–409)	390 (375–408)	394 (376–426)	183 (360–399)
18F-FDG dose injected, MBq	193 (188–196)	193 (185–205)	191(185–194)	194 (190–206)
18F-NaF dose injected, MBq	123 (120–126)	124 (117–127)	123 (117–128)	123 (120–126)

Categorical displayed as total number (%). Median (interquartile range). CT indicates computed tomography; 18F-FDG, 18F-fluorodeoxyglucose; and 18F-NaF, 18F-sodium fluoride.

Downloaded from http://circimaging.ahajournals.org/ by guest on February 1, 2018

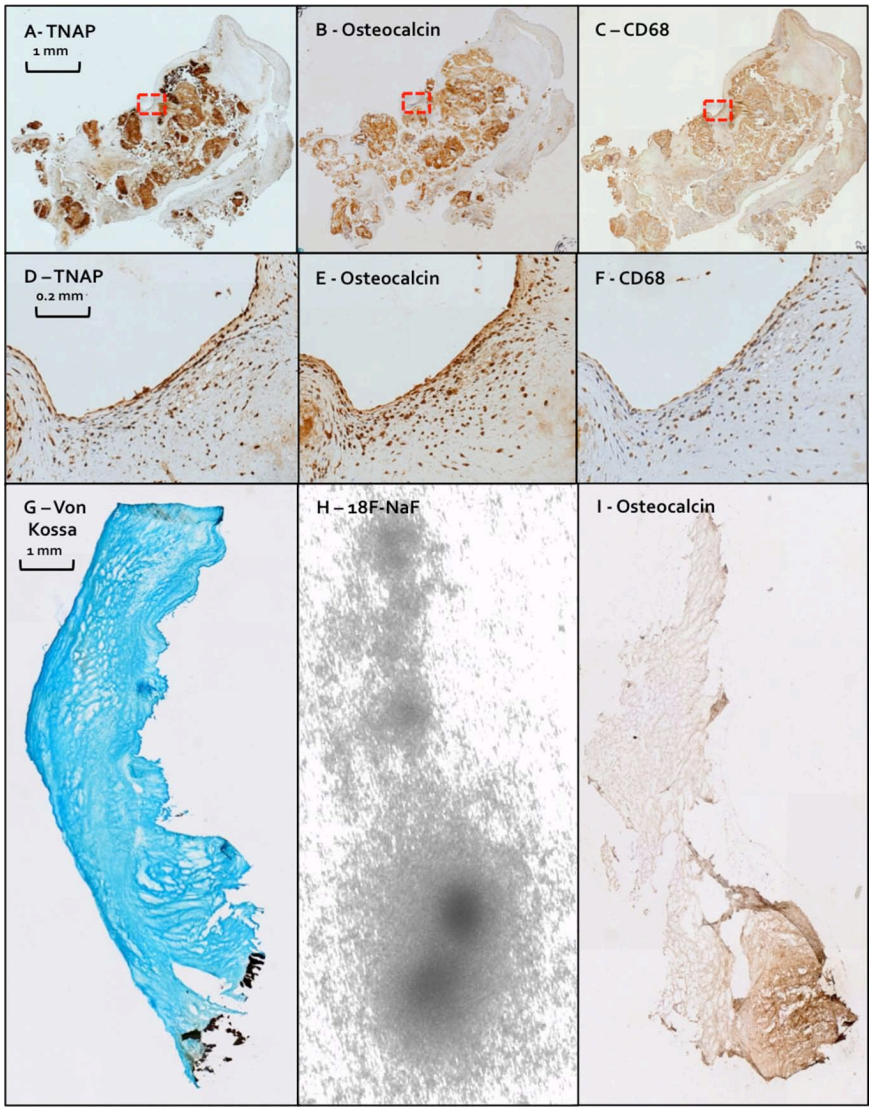

Figure 1. Histology and 18F-sodium fluoride (NaF) autoradiography of excised aortic valve tissue from patients with aortic stenosis. **A**–**F**, Fixed, decalcified, and paraffin-embedded aortic valve tissue after exposure to tissue nonspecific alkaline phosphatase (TNAP), osteocalcin, and CD68 antibodies. **A**–**C**, Widespread positive staining for TNAP, osteocalcin, and CD68 (magnification ×4) in the extracellular matrix, which is also observed on an individual cellular level (**D**–**F**, magnification ×20), respectively. **G**-**I**, Three adjacent and consecutive aortic valve leaflet sections displaying positive immunohistochemical staining for osteocalcin (**I**, magnification ×4) that colocalizes to areas of maximal 18F-NaF uptake on autoradiography (**H**). These likely represent areas of ongoing calcification activity, which extend beyond the areas of established calcium identified in black by Von Kossa stain (**G**, magnification ×4).

counting. All observations were characterized by an absence of fixed or proportional biases, narrow limits of agreement (−13.4% to 9.3%, −8.0% to 5.0%, and −7.9% to 9.6%, respectively), and interclass correlation coefficient values of 0.90 (0.35–0.99), 0.88 (0.60–0.97), and 0.99 (0.99–1.00), respectively (Tables 2 and 3).

Correlation With Radiotracer Uptake

There was a good correlation between in vivo valvular 18F-NaF uptake and both alkaline phosphatase (r=0.65 [95% confidence interval, 0.03–0.90]; P=0.04) and osteocalcin (r=0.68 [0.10–0.91]; P=0.03; Figure 2) staining of the excised tissue. In comparison, there was no association between 18F-FDG uptake and CD68 staining in the valve (r=–0.43; P=0.22).

Disease Progression

Of the 18 patients (75±6 years of age; 17 men; peak aortic-jet velocity, 2.6±0.9 m/s) reassessed at a median interval of 386 days (Table 1), 6 had aortic sclerosis, 7 had mild AS, and 5 had moderate AS. Effective myocardial suppression of 18F-FDG uptake was achieved in 66% (median myocardial standard uptake value, 3.6; IQR, 2.0–5.4).

A correlation was observed between baseline aortic valve calcium scores on CT and 18F-NaF activity on PET (r=0.74 [0.42–0.90]; P≤0.001). However, as described previously, the pattern of 18F-NaF uptake was distinct from the distribution of established calcium.[4,5,14] Indeed 18F-NaF uptake in the absence of underlying calcium occupied a median of 8.3% (IQR 1.6–23.4) of the total valve area, emphasizing that 18F-NaF provides distinct and complementary information to CT calcium scoring (Figure 1).

At 1 year, aortic valve calcium scores increased from 314 (193–540) to 365 (207–934) AU (P<0.01). Interestingly, these regions of novel calcium developed in much the same distribution as the observed baseline 18F-NaF uptake (Figure 3A and 3B). Indeed, we observed an excellent correlation between baseline valvular 18F-NaF PET uptake and the change in calcium score after 1 year (r=0.66 [0.27–0.86]; P=0.003; Figure 3C). This was similar to that observed for the current gold standard method of prediction: the baseline calcium score (r=0.58 [0.15–0.82]; P=0.01; Figure 3D) improved further when only increased 18F-NaF uptake in the absence of underlying CT macrocalcification was considered (r=0.75 [0.42–0.90];

Downloaded from http://circimaging.ahajournals.org/ by guest on February 1, 2018

Table 2. Histology Cohort Data

Baseline characteristics	
No.	12
Age, y	76±6
Men	9 (75)
Hypertension	8 (66)
Hyperlipidemia	5 (42)
Ischemic heart disease	4 (33)
Cigarette smoking	1 (8)
Diabetes mellitus	0 (0)
Serum creatinine, μmol/L	87±26
Peak aortic valve velocity (m/s)	4.6±0.9
Aortic valve area, cm^2	0.70 (0.53–0.97)
Mean gradient, mm Hg	48 (44–65)
Aortic valve calcium score, AU	5343 (3114–6292)
Aortic sclerosis	0 (0%)
Mild aortic stenosis	0 (0%)
Moderate aortic stenosis	3 (25%)
Severe aortic stenosis	9 (75%)
Time between 18F-NaF scan and AVR, d	92 (24–345)
Time between 18F-FDG scan and AVR, d	96 (23–331)
18F-FDG dose injected, MBq	200 (193–209)
18F-NaF dose injected, MBq	129 (119–132)
In vivo aortic valve PET data	
18F-NaF uptake (mean TBR)	2.15 (1.98–2.48)
18F-FDG uptake (mean TBR)	1.40 (1.31–1.76)

Categorical data are displayed as n (%). Normally distributed data are displayed as mean±SD. Non-normally distributed data are distributed as median (interquartile range). AVR indicates aortic valve replacement; FDG, fluorodeoxyglucose; NaF, sodium fluoride; PET, positron emission tomography; and TBR, tissue/background ratio.

P=0.01). No statistically significant correlation was observed between 18F-FDG uptake and the subsequent change in CT calcium score (*r*=–0.11 [–0.56 to 0.39]; *P*=0.66; Figure 3E).

Discussion

We provide the first preliminary evidence that valvular 18F-NaF uptake acts as a marker of calcification activity in patients with AS. Not only did uptake values demonstrate a correlation with histological markers of active calcification (TNAP and osteocalcin), but they were also a good predictor of the subsequent progression in aortic valve CT calcium scores at 1 year. In contrast, 18F-FDG uptake did not correlate with CD68 staining on histology or the progression in calcium scores. Our data indicate that 18F-NaF holds promise as a biomarker of disease activity in patients with AS.

The pathophysiology of AS is incompletely understood, delaying the development of biomarkers and effective medical therapies. Calcification and inflammation are thought to play a key pathological role,[1] so that noninvasive markers of their activity are of interest in better understanding the cause of this condition and in predicting disease progression.

Recent studies have investigated 18F-NaF PET as a marker of vascular calcification in AS[3] and atherosclerosis affecting the aorta,[7] coronary,[5,6] and carotid arteries.[15] However, this is the first study to provide histological validation of 18F-NaF uptake in vascular tissue. In bone, 18F-NaF is thought to incorporate onto the surface of hydroxyapatite crystal.[14] Given that hydroxyapatite is also a key component of vascular calcification, it too has been the presumed radiotracer target in AS and atherosclerosis. This hypothesis is supported by our autoradiography and immunohistochemical data, demonstrating a good correlation between 18F-NaF activity and osteocalcin staining: a well-recognized osteogenic protein that itself binds to hydroxyapatite.

Given that 18F-NaF binds to a structural component of vascular calcification, why then does it not simply label all regions of macrocalcification identified by CT? Indeed it is common for regions of dense calcium on CT to show no 18F-NaF uptake. This phenomenon is likely related to the available surface area of exposed hydroxyapatite crystal to which the 18F-fluoride ion can adsorb and the inactivity of established areas of calcification. 18F-NaF uptake is much greater at sites of evolving powdery microcalcification than established regions of field calcification in which the core of hydroxyapatite is internalized and, therefore, hidden from the 18F-NaF tracer. Thus, 18F-NaF binds more readily to regions of developing calcium and acts as a marker of calcification activity, providing distinct information to calcium scoring. In contrast, the latter quantifies regions of established macroscopic calcium in the valve but cannot

Table 3. Immunohistochemical Analysis

Histology	Osteocalcin	TNAP	CD68
No.	10	10	10
Mean valve area analyzed, mm^2	234±152	253±116	190±86
% staining of the valve	17±7	17±5	n/a
Positive cellular staining, cells/mm^2	130 (85–274)	225 (143–328)	172 (73–271)
Interobserver reproducibility			
Mean difference	–2.1%	–1.5%	0.8%
Limits of agreement	–13.4% to 9.3%	–8.0% to 5.0%	–7.9% to 9.6%
ICC	0.88 (0.60–0.97)	0.90 (0.35–0.99)	0.99 (0.99–1.00)

Categorical data are displayed as n (%). Normally distributed data are displayed as mean±SD. Non-normally distributed data are distributed as median (interquartile range). ICC as value (95% confidence interval). ICC indicates interclass correlation coefficient; n/a, not applicable; and TNAP, tissue nonspecific alkaline phosphatase.

Downloaded from http://circimaging.ahajournals.org/ by guest on February 1, 2018

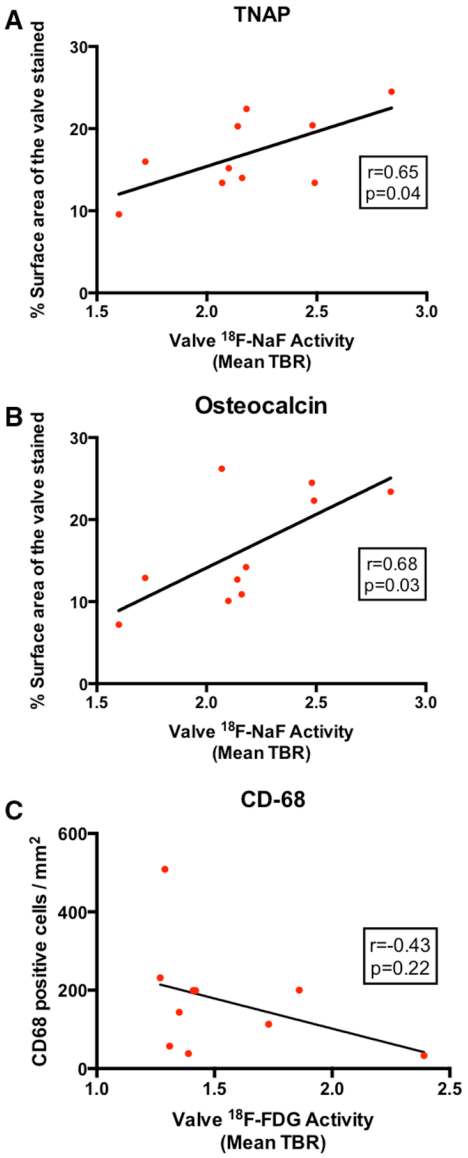

Figure 2. Correlations between in vivo aortic valve positron emission tomography (PET) activity and histological markers of calcification and inflammation. **A**, 18F-Sodium fluoride (NaF) vs tissue nonspecific alkaline phosphatase (TNAP). A good correlation was observed between the percentage aortic valve tissue staining for TNAP and the valvular 18F-NaF activity (mean tissue to background ratio [TBR]); r=0.65, P=0.04. **B**, 18F-NaF vs osteocalcin. Again a strong correlation was observed between the percentage surface area of the valve stained with osteocalcin and the aortic valve 18F-NaF PET activity (mean TBR); r=0.68, P=0.03. **C**, 18F-fluorodeoxyglucose (FDG) vs CD68. A poor correlation was observed between CD68 staining on immunohistochemistry and 18F-FDG PET activity in the aortic valve (mean TBR); r=–0.43, P=0.22.

inform whether the process of calcification is quiescent or active. Again this hypothesis is supported by our data. We have demonstrated a strong correlation between in vivo 18F-NaF uptake and staining for 1 of the key enzymes regulating mineralization: TNAP. This enzyme is expressed in the early stages of new calcium formation and is known to work by breaking down pyrophosphate: a potent inhibitor of mineralization.[16] Furthermore, as one would expect from a measure of activity, baseline 18F-NaF uptake closely correlated with the subsequent change in calcium score at 1 year. Indeed, 18F-NaF uptake performed as well as the current gold standard method of prediction, the degree of established calcium in the valve at baseline.[2,3] However, larger studies are now required to compare these 2 techniques, whereas calcium scoring may be easier to obtain; changes in the 18F-NaF PET signal are likely to occur more quickly, making it a more attractive technique with which to assess the early and more immediate effects of novel treatment strategies.

Interestingly, the pattern of 18F-NaF uptake may be important, with 18F-NaF uptake remote from established macrocalcification on CT offering the best prediction of calcium score progression in our cohort. The spatial resolution of PET/CT is ≈4 mm, and we acknowledge that the voxel-by-voxel analysis used to establish this observation is at the limit of resolution for PET imaging. Nevertheless, the strong correlation with progression is of interest and indicates that further investigation of the spatial distribution of 18F-NaF uptake is warranted.

The results of valvular 18F-FDG imaging were somewhat disappointing and surprising given previous data suggesting an important role for inflammation in AS.[17] Although correlations between 18F-FDG uptake and macrophage burden have previously been demonstrated in regions of aortic and carotid atheroma,[8] we were unable to replicate this with respect to the valve. There are several explanations for this discrepancy. The first is the close proximity of the valve to the myocardium. As discussed, avid uptake of 18F-FDG by the left ventricular myocardium can spill over into the aortic valve contaminating its signal. Unfortunately, despite the stringent dietary restrictions and center-valve analysis technique, it remains possible that myocardial contamination occurred, confounding the correlation with CD68 immunohistochemistry. Indeed poor myocardial suppression was achieved in the histology group, perhaps reflecting their advanced disease and symptomatic status. Alternative methods have been used to reduce further this myocardial uptake, including administration of heparin[18] and a high-fat drink before scanning.[19] However, these make the practicalities of scanning more difficult and have yet to show a clear advantage over dietary restrictions. An alternative explanation for the poor correlation with histology is that the aortic valve 18F-FDG signal relates to uptake by nonmacrophage cell types within the valve, such as osteoblasts, or is governed by external factors, such as hypoxia.[20] In this scenario, one might still expect 18F-FDG to predict disease progression, but once again this was not evident in our cohort. It would, therefore, seem that 18F-FDG holds less potential as a predictor of disease progression than 18F-NaF does, although it remains possible that longer periods of follow-up are required to detect such an association. Indeed on occasion, we also observed 18F-NaF activity that did not translate into a detectable change in calcium score at 1 year. AS is a slowly developing condition, so it is likely to take time for relatively low levels of 18F-NaF or 18F-FDG uptake to translate into new areas of macrocalcification detectable on CT imaging. Larger studies with longer follow-up are, therefore, required to address this issue, confirm our preliminary data, and assess whether 18F-NaF PET can predict disease progression with respect to echocardiographic parameters of valvular stenosis.

Downloaded from http://circimaging.ahajournals.org/ by guest on February 1, 2018

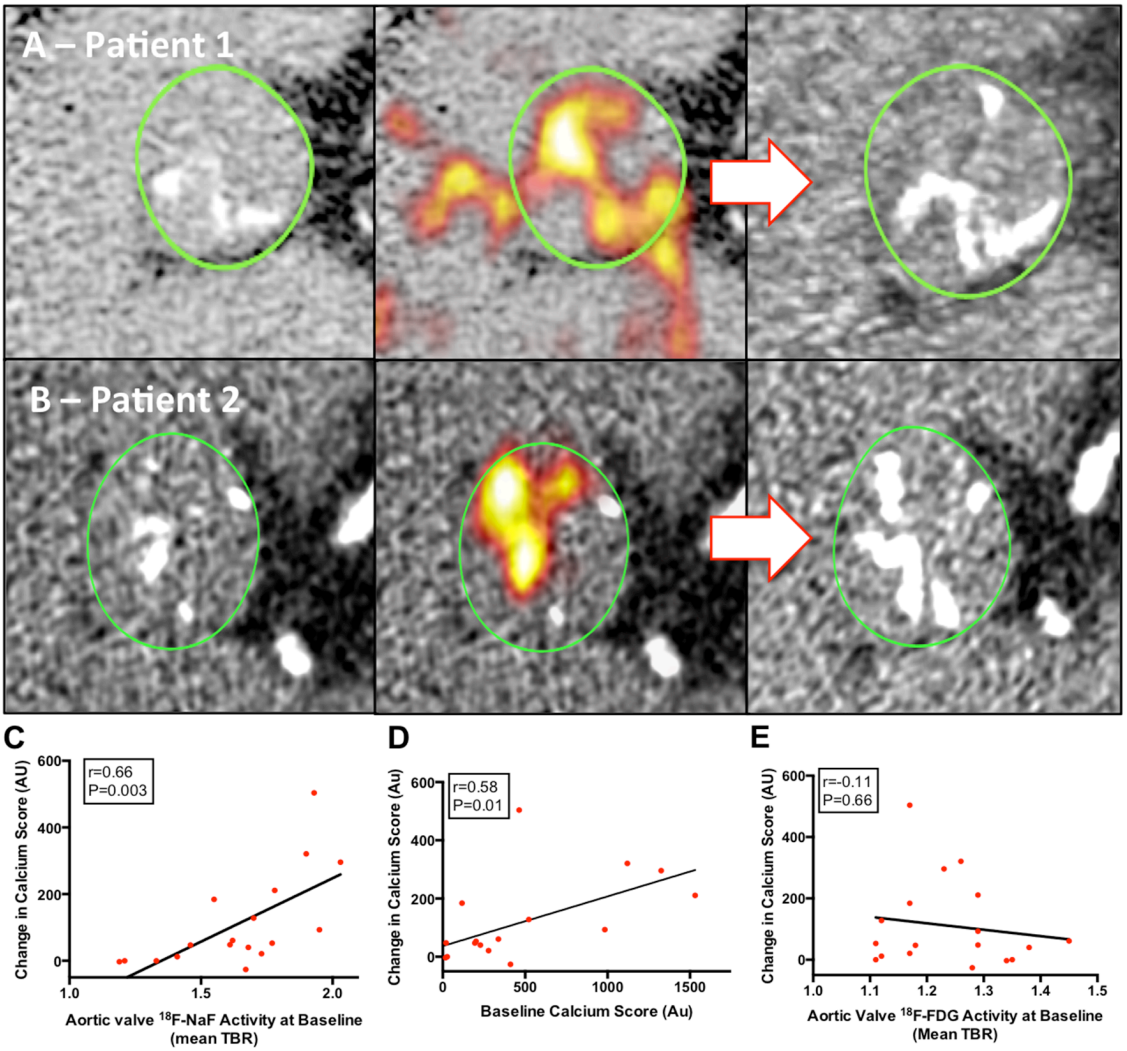

Figure 3. Change in aortic valve computed tomography (CT) calcium score and 18F-sodium fluoride (NaF) positron emission tomography (PET) activity after 1 year. **A** and **B**, Coaxial short axis views of the aortic valve from 2 patients with mild aortic stenosis (**top** and **bottom**). On baseline CT scans (**left**) established regions of macrocalcification appear white. Baseline fused 18F-NaF PET and CT scans (**middle**) show intense 18F-NaF uptake (red, yellow regions) both overlying and adjacent to existing calcium deposits on the CT. One-year follow-up CT scans (**right**) demonstrate increased calcium accumulation in much the same distribution as the baseline PET activity. **C**–**E**, Predictors of progression in aortic valve calcium score. An excellent correlation was observed between baseline 18F-NaF activity in the aortic valve and the subsequent change in calcium score at 1 year r=0.66, P<0.01 (**A**). This matched the current gold standard predictor of disease progression the baseline calcium score r=0.58, P=0.01 (**B**). By contrast, there was a poor correlation with 18F-fluorodeoxyglucose (FDG) activity in the valve r=–0.11, P=0.66 (**C**).

Conclusions

We provide the first preliminary data to support 18F-NaF as a marker of valve calcification activity in AS and as a potential method for predicting disease progression.

Acknowledgments

We acknowledge the support of staff at the Edinburgh Heart Centre at the Royal Infirmary of Edinburgh, the radiography and radiochemistry staff of the Clinical Research Imaging Centre, and the histology staff at the Queens Medical Research Institute.

Sources of Funding

The study was funded by the British Heart Foundation (PG/12/8/29371). Dr Dweck was supported by a fellowship and project grant from the British Heart Foundation (FS/10/026 & PG/12/8/29371). Dr Jenkins was supported by a British Heart Foundation scholarship scheme and fellowship grant (SS/CH/09/002/2636 and FS/12/84/29814). Drs Dweck, Jenkins, and Newby were supported by the British Heart Foundation (CH/09/002, FS/12/84/29814, SS/CH/09/002/2636, and FS/10/026). The work of Dr Rudd was supported by the Higher Education Funding Council for England, the British Heart Foundation, and the Cambridge National Institute for Health Research Biomedical Research Centre. Dr van Beek was supported by the Scottish Imaging Network—a Platform of Scientific Excellence. The Wellcome Trust Clinical Research Facility and the Clinical Research Imaging Centre are supported by the National Health Service Research Scotland through NHS Lothian.

Disclosures

None.

References

1. Quarto C, Dweck MR, Murigu T, Joshi S, Melina G, Angeloni E, Prasad SK, Pepper JR. Late gadolinium enhancement as a potential marker of increased perioperative risk in aortic valve replacement. *Interact Cardiovasc Thorac Surg*. 2012;15:45–50.

Downloaded from http://circimaging.ahajournals.org/ by guest on February 1, 2018

2. Messika-Zeitoun D, Bielak LF, Peyser PA, Sheedy PF, Turner ST, Nkomo VT, Breen JF, Maalouf J, Scott C, Tajik AJ, Enriquez-Sarano M. Aortic valve calcification: determinants and progression in the population. *Arterioscler Thromb Vasc Biol*. 2007;27:642–648.
3. Rosenhek R, Binder T, Porenta G, Lang I, Christ G, Schemper M, Maurer G, Baumgartner H. Predictors of outcome in severe, asymptomatic aortic stenosis. *N Engl J Med*. 2000;343:611–617.
4. Dweck MR, Jones C, Joshi NV, Fletcher AM, Richardson H, White A, Marsden M, Pessotto R, Clark JC, Wallace WA, Salter DM, McKillop G, van Beek EJ, Boon NA, Rudd JH, Newby DE. Assessment of valvular calcification and inflammation by positron emission tomography in patients with aortic stenosis. *Circulation*. 2012;125:76–86.
5. Dweck MR, Chow MW, Joshi NV, Williams MC, Jones C, Fletcher AM, Richardson H, White A, McKillop G, van Beek EJ, Boon NA, Rudd JH, Newby DE. Coronary arterial 18F-sodium fluoride uptake: a novel marker of plaque biology. *J Am Coll Cardiol*. 2012;59:1539–1548.
6. Joshi NVVA, Williams MC, Shah ASV, Calvert PA, Craighead FHM, Yeoh SE, Wallace WA, Salter D, Fletcher AM, van Beek EJR, Flapan AD, Uren NG, Behan MWH, Cruden NLM, Mills NL, Fox KAA, Rudd JHF, Dweck MR, Newby DE. 18F-Fluoride positron emission tomography identifies ruptured and high-risk coronary atherosclerotic plaques. *Lancet*. 2013;13:61754–61757.
7. Derlin T, Tóth Z, Papp L, Wisotzki C, Apostolova I, Habermann CR, Mester J, Klutmann S. Correlation of inflammation assessed by 18F-FDG PET, active mineral deposition assessed by 18F-fluoride PET, and vascular calcification in atherosclerotic plaque: a dual-tracer PET/CT study. *J Nucl Med*. 2011;52:1020–1027.
8. Tawakol A, Migrino RQ, Bashian GG, Bedri S, Vermylen D, Cury RC, Yates D, LaMuraglia GM, Furie K, Houser S, Gewirtz H, Muller JE, Brady TJ, Fischman AJ. *In vivo* 18F-fluorodeoxyglucose positron emission tomography imaging provides a noninvasive measure of carotid plaque inflammation in patients. *J Am Coll Cardiol*. 2006;48:1818–1824.
9. Marincheva-Savcheva G, Subramanian S, Qadir S, Figueroa A, Truong Q, Vijayakumar J, Brady TJ, Hoffmann U, Tawakol A. Imaging of the aortic valve using fluorodeoxyglucose positron emission tomography increased valvular fluorodeoxyglucose uptake in aortic stenosis. *J Am Coll Cardiol*. 2011;57:2507–2515.
10. Dweck MR, Khaw HJ, Sng GK, Luo EL, Baird A, Williams MC, Makiello P, Mirsadraee S, Joshi NV, van Beek EJ, Boon NA, Rudd JH, Newby DE. Aortic stenosis, atherosclerosis, and skeletal bone: is there a common link with calcification and inflammation? *Eur Heart J*. 2013;34:1567–1574.
11. Bonow RO, Carabello BA, Chatterjee K, de Leon AC Jr, Faxon DP, Freed MD, Gaasch WH, Lytle BW, Nishimura RA, O'Gara PT, O'Rourke RA, Otto CM, Shah PM, Shanewise JS, Smith SC Jr, Jacobs AK, Adams CD, Anderson JL, Antman EM, Fuster V, Halperin JL, Hiratzka LF, Hunt SA, Nishimura R, Page RL, Riegel B. ACC/AHA 2006 guidelines for the management of patients with valvular heart disease: a report of the American College of Cardiology/American Heart Association Task Force on Practice Guidelines (writing Committee to Revise the 1998 guidelines for the management of patients with valvular heart disease) developed in collaboration with the Society of Cardiovascular Anesthesiologists endorsed by the Society for Cardiovascular Angiography and Interventions and the Society of Thoracic Surgeons. *J Am Coll Cardiol*. 2006;48:e1–e148.
12. Cowell SJ, Newby DE, Burton J, White A, Northridge DB, Boon NA, Reid J. Aortic valve calcification on computed tomography predicts the severity of aortic stenosis. *Clin Radiol*. 2003;58:712–716.
13. Bland JM, Altman DG. Statistical methods for assessing agreement between two methods of clinical measurement. *Lancet*. 1986;1:307–310.
14. Derlin T, Richter U, Bannas P, Begemann P, Buchert R, Mester J, Klutmann S. Feasibility of 18F-sodium fluoride PET/CT for imaging of atherosclerotic plaque. *J Nucl Med*. 2010;51:862–865.
15. Derlin T, Wisotzki C, Richter U, Apostolova I, Bannas P, Weber C, Mester J, Klutmann S. *In vivo* imaging of mineral deposition in carotid plaque using 18F-sodium fluoride PET/CT: correlation with atherogenic risk factors. *J Nucl Med*. 2011;52:362–368.
16. Narisawa S, Harmey D, Yadav MC, O'Neill WC, Hoylaerts MF, Millán JL. Novel inhibitors of alkaline phosphatase suppress vascular smooth muscle cell calcification. *J Bone Miner Res*. 2007;22:1700–1710.
17. Toutouzas K, Drakopoulou M, Synetos A, Tsiamis E, Agrogiannis G, Kavantzas N, Patsouris E, Iliopoulos D, Theodoropoulos S, Yacoub M, Stefanadis C. *In vivo* aortic valve thermal heterogeneity in patients with nonrheumatic aortic valve stenosis the: first *in vivo* experience in humans. *J Am Coll Cardiol*. 2008;52:758–763.
18. Ishimaru S, Tsujino I, Takei T, Tsukamoto E, Sakaue S, Kamigaki M, Ito N, Ohira H, Ikeda D, Tamaki N, Nishimura M. Focal uptake on 18F-fluoro-2-deoxyglucose positron emission tomography images indicates cardiac involvement of sarcoidosis. *Eur Heart J*. 2005;26:1538–1543.
19. Cheng VY SP, Ahlen M, Thomson LEJ, Waxman AD, Berman DS. Impact of carbohydrate restriction with and without fatty acid loading on myocardial 18F-FDG uptake during PET: a randomized controlled trial. *J Nucl Cardiol*. 2010;17:286–291.
20. Folco EJ, Sheikine Y, Rocha VZ, Christen T, Shvartz E, Sukhova GK, Di Carli MF, Libby P. Hypoxia but not inflammation augments glucose uptake in human macrophages: implications for imaging atherosclerosis with 18fluorine-labeled 2-deoxy-D-glucose positron emission tomography. *J Am Coll Cardiol*. 2011;58:603–614.

CLINICAL PERSPECTIVE

Aortic stenosis is the most common form of valvular heart disease in the developed world; however, its rate of progression can vary greatly between patients, and as yet we lack effective medical therapies. Progressive valvular calcification is a key pathophysiological process driving aortic stenosis. Recent studies have suggested that the positron emission tomography (PET) tracer 18F-sodium fluoride (18F-NaF) can measure vascular calcification activity, although validation of this technique has previously been lacking. In this study, we sought to provide such validation, comparing aortic valve 18F-NaF uptake with both histological measures of calcification activity and the progression of aortic valve calcium scores on computed tomography. Ten patients scheduled for aortic valve replacement underwent 18F-NaF PET before their operation with valvular PET uptake, demonstrating a significant correlation with histological markers of calcification activity on the excised aortic valve tissue. In a separate cohort, we assessed 18 patients with calcific aortic valve disease who underwent 18F-NaF PET and computed tomography calcium scoring of the aortic valve both at baseline and after 1 year. Once again a good correlation was observed between the baseline PET uptake and change in calcium score. Our results are promising, providing the first preliminary validation of 18F-NaF as a marker of calcification activity in the aortic valve. More studies are now required to investigate 18F-NaF PET as a method for predicting disease progression in aortic stenosis and assessing the early efficacy of novel treatments aimed at reducing calcification activity in this condition.

Downloaded from http://circimaging.ahajournals.org/ by guest on February 1, 2018

JACC VOL. 66, NO. 10, 2015
SEPTEMBER 8, 2015:1198–205

Valvular ^{18}F-Fluoride and ^{18}F-Fluorodeoxyglucose Uptake Predict Disease Progression and Clinical Outcome in Patients With Aortic Stenosis

^{18}F-Fluoride is a positron emission tomography (PET) radiotracer that preferentially binds to regions of newly forming vascular microcalcifications beyond the resolution of computed tomography (CT) (1). ^{18}F-Fluorodeoxyglucose (^{18}F-FDG) has been widely used to measure vascular inflammation (2). This is the first prospective longitudinal study to investigate whether these tracers predict disease progression and clinical outcomes in aortic stenosis.

Patients age >50 years attending the outpatient department of the Edinburgh Heart Centre were approached for recruitment in this prospective cohort study alongside age- and sex-matched controls, as described previously (2). PET and CT were performed in 121 volunteers (age 72 ± 8 years; 68% men) with and without aortic valve disease (20 controls, 20 with aortic sclerosis, and 25 with mild, 33 with moderate, and 23 with severe aortic stenosis) using ^{18}F-fluoride (125 MBq) and ^{18}F-FDG (200 MBq). Uptake in the valve was measured using the most diseased segment tissue: background ratio, based upon averaging the mean standard uptake values in the 2 adjacent valve slices with the highest signal, corrected for blood-pool activity. Disease progression was assessed at 1 and 2 years using CT aortic valve calcium scoring and echocardiography. The primary clinical outcome endpoint was a composite of cardiovascular death and aortic valve replacement.

FIGURE 1 Valvular ^{18}F-Fluoride Uptake Predicts the Progression of Calcification in Aortic Stenosis

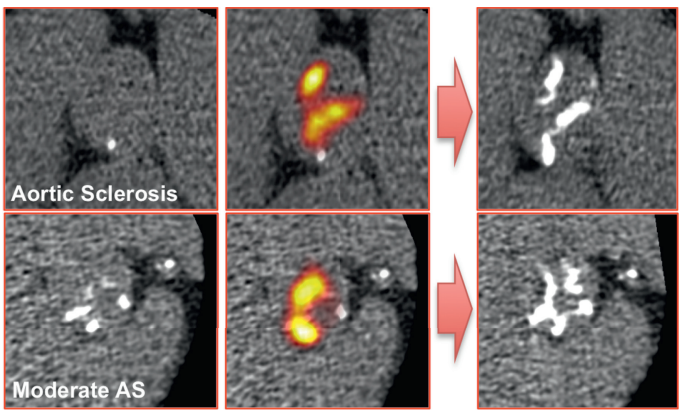

Two patients with calcific aortic valve disease. **(Left)** Baseline computed tomography (CT) images. **(Middle)** Fused positron emission tomography (PET)/CT images showing increased ^{18}F-fluoride valvular uptake **(red/yellow areas)**. **(Right)** Repeat CT scans after 2 years with new areas of macroscopic calcium **(white areas)** in a similar distribution to that of baseline PET uptake.

Ninety-nine participants (81%) returned for repeat clinical assessment and echocardiography at the 2-year time point (median 736 [interquartile range (IQR): 722 to 760] days from enrollment). Ninety-seven patients returned for repeat CT calcium scoring (10 scans were uninterpretable). Aortic valve calcium score increased by 61 (IQR: 5 to 226) AU/year, and aortic valve mean gradient increased by 0.7 (IQR: −0.2 to 2.9) mm Hg/year. After a median of 1,526 (IQR: 1,475 to 1,615) days, 29 patients had undergone aortic valve replacement, whereas 7 experienced cardiovascular death.

After 2 years, new valvular calcium on CT was visible in a similar distribution as the ^{18}F-fluoride activity on baseline PET imaging (**Figure 1**). Indeed, baseline ^{18}F-fluoride uptake correlated strongly with the subsequent rate of progression in aortic valve calcium score (Spearman $r = 0.80$; $p < 0.001$) and with echocardiographic measures of hemodynamic progression (mean gradient $r = 0.32$; $p = 0.001$). In an exploratory analysis, ^{18}F-fluoride emerged as an independent predictor of clinical outcome after age and sex adjustments (hazard ratio: 1.55; 95% CI: 1.33 to 1.81; $p < 0.001$). ^{18}F-FDG demonstrated moderate correlations with disease progression assessed by CT (Spearman $r = 0.43$; $p = 0.001$) and echocardiography (^{18}F-FDG $r = 0.30$; $p = 0.001$) and predicted clinical outcomes independently of age and sex (hazard ratio: 1.35; 95% CI: 1.16 to 1.58; $p < 0.001$).

There were strong associations between the baseline CT valvular calcium score and rate of change in calcium score (Spearman $r = 0.88$; 95% CI: 0.82 to 0.92; $p < 0.001$). Given the degree of collinearity between CT calcium scoring and ^{18}F-fluoride uptake in the valve (2), assessing whether ^{18}F-fluoride uptake provided incremental predictive information to CT was challenging. However, in a retrospective analysis using the regression line between the CT calcium score and ^{18}F-fluoride uptake as a cutoff, patients with aortic stenosis and higher than expected ^{18}F-fluoride uptake for a given CT calcium score progressed 3 times faster than participants with lower than expected uptake (median change in calcium score 315 [IQR: 127 to 492] AU/year vs. 99 [IQR: 51 to 290] AU/year, respectively; $p = 0.003$) **Figures 1** and **2**. When a similar analysis was performed for ^{18}F-FDG, no

significant difference was observed (median change in calcium score: 231 [IQR: 79 to 446] AU/year vs. 124 [IQR: 61 to 321] AU/year; p = 0.14). Neither tracer offered independent prediction of clinical outcomes after correction for CT calcium scoring, perhaps reflecting the small number of events and again the collinearity between imaging parameters.

In conclusion we demonstrated that both ^{18}F-fluoride and ^{18}F-FDG predicted disease progression and adverse clinical outcomes in aortic stenosis. In particular, ^{18}F-fluoride provided excellent prediction of the change in CT calcium score, appearing to be of incremental value to baseline CT imaging. Larger studies are required to confirm the incremental predictive value of PET compared with CT. However, our data would support PET/CT as a novel method for measuring disease activity in aortic stenosis, with the ability to predict its natural history. This may be of particular value in studies investigating novel therapies, in which beneficial treatment effects are likely to be detected rapidly without the need for protracted follow-up. (Role of Active Valvular Calcification and Inflammation in Patients With Aortic Stenosis; NCT01358513)

*William S.A. Jenkins, MD
Alex T. Vesey, MD
Anoop S.V. Shah, MD, PhD
Tania A. Pawade, MD
Calvin W.L. Chin, MD
Audrey C. White, CRCS-AE
Alison Fletcher, PhD
Timothy R.G. Cartlidge, MD
Andrew J. Mitchell, MD
Mark A.H. Pringle, MD
Oliver S. Brown, BSc
Renzo Pessotto, MD
Graham McKillop, MD
Edwin J.R. Van Beek, MD, PhD
Nicholas A. Boon, MD
James H.F. Rudd, MD, PhD
*David E. Newby, MD, PhD
Marc R. Dweck, MD, PhD

*British Heart Foundation/University Centre for Cardiovascular Science
Room SU 305, Chancellor's Building
University of Edinburgh
49 Little France Crescent
Edinburgh EH16 4SB
Scotland
E-mail: williamjenkins@doctors.net.uk

http://dx.doi.org/10.1016/j.jacc.2015.06.1325

Please note: The authors have reported that they have no relationships relevant to the contents of this paper to disclose. Drs. Jenkins and Vesey contributed equally to this work. Drs. Newby and Dweck are joint senior authors.

FIGURE 2 ^{18}F-Flouride Uptake for a Given CT Calcium Score

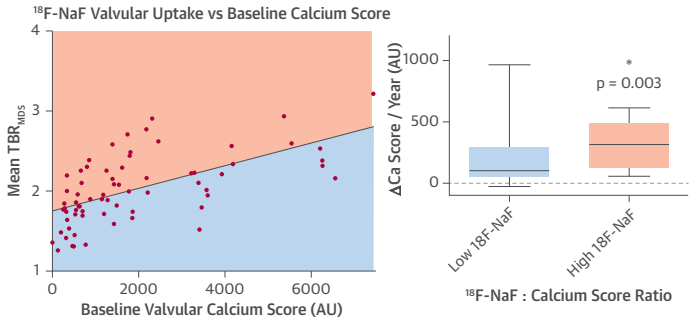

Patients with higher than expected ^{18}F-fluoride uptake for a given CT calcium score **(dots in red above regression line)** demonstrated disease progression rates 3-fold greater than those with lower than expected uptake **(dots in blue below regression line)**. The same was not true for ^{18}F-fluorodeoxyglucose. AS = aortic stenosis; TBR_{MDS} = most diseased segment tissue: background ratio; ^{18}F-NaF = ^{18}F-fluoride.

REFERENCES

1. Irkle A, Vesey AT, Lewis DY, et al. Identifying active vascular microcalcification by ^{18}F-sodium fluoride positron emission tomography. Nature Commun 2015;6:7495.

2. Dweck MR, Jones C, Joshi NV, et al. Assessment of valvular calcification and inflammation by positron emission tomography in patients with aortic stenosis. Circulation 2012;125:76–86.

Trends in Infective Endocarditis Incidence, Microbiology, and Valve Replacement in the United States From 2000 to 2011

The Devil Is in the Details

We read with great interest the paper by Pant et al. (1) regarding trends in infective endocarditis (IE) incidence using the Nationwide Inpatient Sample (NIS) database to address a nagging question that has rightfully garnered much attention and gravity: have recent changes in IE prophylaxis guidelines for dental procedures in this country and abroad resulted in an increase in IE incidence caused by viridans group streptococci (VGS)? As investigators who have previously used the NIS database (2,3), we pose 2 concerns to Pant et al. First, they unfortunately used ICD-9-CM codes that included enterococcal (04104) and non-VGS (038.2 *Streptococcus pneumoniae* septicemia, and

Downloaded from http://heart.bmj.com/ on February 1, 2018 - Published by group.bmj.com

OPEN ACCESS

ORIGINAL ARTICLE

Cardiac $\alpha_V\beta_3$ integrin expression following acute myocardial infarction in humans

William S A Jenkins,[1] Alex T Vesey,[1] Colin Stirrat,[1] Martin Connell,[2] Christophe Lucatelli,[2] Anoushka Neale,[1] Catriona Moles,[1] Anna Vickers,[1] Alison Fletcher,[2] Tania Pawade,[1] Ian Wilson,[3] James H F Rudd,[4] Edwin J R van Beek,[2] Saeed Mirsadraee,[2] Marc R Dweck,[1] David E Newby[1]

► Additional material is published online only. To view please visit the journal online (http://dx.doi.org/10.1136/heartjnl-2016-310115).

[1]British Heart Foundation Centre for Cardiovascular Science, University of Edinburgh, Edinburgh, UK
[2]Clinical Research Imaging Center, University of Edinburgh, Edinburgh, UK
[3]Edinburgh Molecular Imaging Ltd, Edinburgh, UK
[4]Division of Cardiovascular Medicine, University of Cambridge, Cambridge, Cambridgeshire, UK

Correspondence to
Dr William S A Jenkins, British Heart Foundation Centre for Cardiovascular Science, Chancellors Building, 49 Little France Crescent, University of Edinburgh, Edinburgh EH16 4SB, UK; williamjenkins@doctors.net.uk

MRD and DEN contributed equally.

Received 6 June 2016
Revised 16 September 2016
Accepted 20 September 2016
Published Online First 7 December 2016

ABSTRACT

Objective Maladaptive repair contributes towards the development of heart failure following myocardial infarction (MI). The $\alpha_v\beta_3$ integrin receptor is a key mediator and determinant of cardiac repair. We aimed to establish whether $\alpha_v\beta_3$ integrin expression determines myocardial recovery following MI.

Methods ^{18}F-Fluciclatide (a novel $\alpha_v\beta_3$-selective radiotracer) positron emission tomography (PET) and CT imaging and gadolinium-enhanced MRI (CMR) were performed in 21 patients 2 weeks after ST-segment elevation MI (anterior, n=16; lateral, n=4; inferior, n=1). CMR was repeated 9 months after MI. 7 stable patients with chronic total occlusion (CTO) of a major coronary vessel and nine healthy volunteers underwent a single PET/CT and CMR.

Results ^{18}F-Fluciclatide uptake was increased at sites of acute infarction compared with remote myocardium (tissue-to-background ratio (TBR_{mean}) 1.34±0.22 vs 0.85±0.17; p<0.001) and myocardium of healthy volunteers (TBR_{mean} 1.34±0.22 vs 0.70±0.03; p<0.001). There was no ^{18}F-fluciclatide uptake at sites of established prior infarction in patients with CTO, with activity similar to the myocardium of healthy volunteers (TBR_{mean} 0.71±0.06 vs 0.70±0.03, p=0.83). ^{18}F-Fluciclatide uptake occurred at sites of regional wall hypokinesia (wall motion index≥1 vs 0; TBR_{mean} 0.93±0.31 vs 0.80±0.26 respectively, p<0.001) and subendocardial infarction. Importantly, although there was no correlation with infarct size (r=0.03, p=0.90) or inflammation (C reactive protein, r=−0.20, p=0.38), ^{18}F-fluciclatide uptake was increased in segments displaying functional recovery (TBR_{mean} 0.95±0.33 vs 0.81±0.27, p=0.002) and associated with increase in probability of regional recovery.

Conclusion ^{18}F-Fluciclatide uptake is increased at sites of recent MI acting as a biomarker of cardiac repair and predicting regions of recovery.

Trial registration number NCT01813045; Post-results.

INTRODUCTION

Ischaemic heart disease remains the leading cause of death globally, with over 1 million people suffering acute myocardial infarction (MI) per year in the USA alone. As the acute management of MI improves, the number of patients surviving acute myocardial injury is higher than ever before. In this population, adverse cardiac remodelling and the syndrome of delayed heart failure represent the major cause of morbidity.[1] Understanding reparative mechanisms following infarction is becoming increasingly important.

Repair following MI is triggered by a complex interaction of neurohormonal activation and upregulation of angiogenic and pro-fibrotic transcription factors that initiate the restoration of a capillary network through angiogenesis and re-endothelialisation, as well as extracellular matrix (ECM) remodelling through macrophage accumulation and fibroblast activation. This interplay of angiogenesis, inflammation and fibrosis determines the extent of preservation and restoration of myocardial integrity.[2] In some circumstances, maladaptive persistent processes may encourage remodelling and scarring to extend into the myocardium long after the initial causative injury. This may lead to progressive ventricular dilatation, ventricular dysfunction and heart failure.

The $\alpha_v\beta_3$ integrin is a transmembrane cell surface receptor that facilitates migration, proliferation and interaction with the ECM, thereby allowing cells to respond to, and in turn modify, their extracellular environment. Expressed at low levels by quiescent endothelial cells, $\alpha_v\beta_3$ integrin is markedly upregulated in states of angiogenesis within the myocardium after infarction.[3 4] In addition, preclinical and clinical studies document $\alpha_v\beta_3$ integrin expression by both activated cardiac myofibroblasts and macrophages during margination and chemotaxis. Thus, $\alpha_v\beta_3$ integrin expression appears central to the coordination of repair following MI.

In this study, we investigated the expression of $\alpha_v\beta_3$ integrin following MI using the novel $\alpha_v\beta_3$ integrin-selective radiotracer, ^{18}F-fluciclatide, combined with cardiac positron emission tomography (PET), CT and cardiovascular MRI (CMR). The study aims to describe and characterise the uptake of this radiotracer and to correlate it with clinical markers of disease severity and functional recovery in patients with recent MI.

METHODS

PET/CT scanning with ^{18}F-fluciclatide and CMR were performed in three groups of participants recruited from Royal Infirmary of Edinburgh between July 2013 and February 2015. Exclusion criteria were age <40 years, women of childbearing potential not taking contraception, severe renal failure (serum creatinine >2.8 mg/dL) or hepatic failure (Child-Pugh grade B or grade C), atrial

To cite: Jenkins WSA, Vesey AT, Stirrat C, *et al*. *Heart* 2017;**103**:607–615.